

NASA CR-172,508

NASA Contractor Report 172508

NASA-CR-172508
19850012866

OPTIMAL SYMMETRIC FLIGHT STUDIES

A. R. Weston, P. K. A. Menon,
K. D. Bilimoria, E. M. Cliff,
and H. J. Kelley

VIRGINIA POLYTECHNIC INSTITUTE
AND STATE UNIVERSITY
Blacksburg, Virginia

Grant NAG1-203
February 1985

LIBRARY COPY

1985

LANGLEY RESEARCH CENTER
LIBRARY, NASA
HAMPTON, VIRGINIA

NASA

National Aeronautics and
Space Administration

Langley Research Center
Hampton, Virginia 23665



NASA Contractor Report 172508

Optimal Symmetric Flight Studies

A. R. Weston

P. K. A. Menon

K. D. Bilimoria

E. M. Cliff

H. J. Kelley

Virginia Polytechnic Institute and State University
Blacksburg, Virginia 24061

Prepared for

Langley Research Center
under grant NAG 1-203

N85-21176 #



TABLE OF CONTENTS

	<u>Page</u>
ACKNOWLEDGMENTS	vi
LIST OF FIGURES AND TABLES	vii
SYMBOLS	xii
SUMMARY	xiv
 <u>Chapter</u>	
1 INTRODUCTION	1
2 ON-BOARD NEAR-OPTIMAL CLIMB-DASH ENERGY MANAGEMENT ..	3
2.1 Preface	4
Problem Formulation	7
Symmetric Flight	8
Aerodynamic Modelling	9
2.2 Optimal Control: Reduced-Order Modelling	10
Rectilinear-Motion Model	12
Energy-State Models	13
Energy Climbs	14
Method of Matched Asymptotic Expansions ...	17
Conclusions	18
2.3 On-Board Guidance	19
Nominal Path	19
Feedback Law	20
Feedback Coefficients	21
On-Board Use	22
2.4 Optimal Solutions for the Point-Mass Model	23
Method of Solution	25
2.5 Initial Exposure to OPTSQL	26
Aircraft Data Manipulation	26
Initial Flight-Mechanics Problem	28
First Trajectories to the Dash Point.....	29
Eigenvalue Analysis	30
Backwards Integration of Stable Eigen-	
vectors	31
Conclusions	31
2.6 Modifications to OPTSQL	32
Splined Aircraft Data	32
Family of Trajectories to the Dash Point ..	33
2.7 Optimal-Reference-Path Calculations	33
Final Load Factor	34
One Panel Integration	35
Energy-Model/Point-Mass-Model Comparisons .	36

Table of Contents (cont.)

<u>Chapter</u>		<u>Page</u>
	2.8 Feedback Coefficients - Calculations	36
	Method of Evaluation	37
	Pilot Scheme	38
	Logarithmic Splining	40
	2.9 Simulation and Testing	42
	2.10 Extension to 3-D Flight	43
	Cross-Range Considerations	43
	Computational Considerations	44
	Selection of the Initial Path-Angle	45
	2.11 Implementation and Conclusions	46
	Implementation	46
	Conclusions	47
	Future Work	47
3	OPTIMAL SYMMETRIC FLIGHT WITH AN INTERMEDIATE VEHICLE MODEL	97
	3.1 Preface	98
	3.2 Intermediate Vehicle Model	99
	3.3 Legendre-Clebsch Necessary Condition	110
	3.4 Conjugate-Point Test	114
	3.5 Numerical Solution of the Time-Range Problem ...	121
	3.6 Discussion and Conclusions	123
4	ENERGY STATE REVISITED	138
	4.1 Preface	139
	4.2 Climb Equations	140
	4.3 Choice of Variables	140
	4.4 Climb-Dash Problem	143
5	CLASSICAL AND NEO-CLASSICAL CRUISE-DASH OPTIMIZATION.	149
	5.1 Preface	150
	5.2 Problem Formulation	150
	5.3 Cruise-Dash Analysis	155
	5.4 Computations and Results	157
	5.5 Modelling	160
	Atmosphere	160
	Aerodynamics	160
	Propulsion	160
	5.6 Computation of $Q^*(V)$	161
	5.7 Conclusions	163

Appendix

Page

A	ENERGY-MODELLED CLIMB AND CLIMB-DASH - THE KAISER TECHNIQUE	178
A.1	Preface	179
A.2	Quasi-Steady Climb Analysis and Corrections	180
A.3	Energy Height and Energy Modelling	181
A.4	Energy Interchange	184
A.5	Climb-Dash	185
A.7	Conclusions	186
B	SINGULAR OPTIMAL CONTROL AND THE IDENTICALLY NON- REGULAR PROBLEM IN THE CALCULUS OF VARIATIONS	192
B.1	Preface	193
B.2	Identically Non-Regular Problem	194
B.3	The Problem in an Optimal-Control Format	197
B.4	Transformation to Canonical Form	198
B.5	Illustrative Examples	200
B.6	Smoothness Difficulties and their Impact	205
B.7	Concluding Remarks	206
	References	207

ACKNOWLEDGMENTS

The support of NASA Langley Research Center under grant NAG 1-203, Dr. Christopher Gracey and Dr. Douglas Price serving as Technical Monitors, is gratefully acknowledged.

We wish to thank Dr. Klaus Well and Mr. Eugen Berger of DFVLR, Oberpfaffenhofen, West Germany, for their extensive help in the use of the Multiple-shooting program (OPTSOL), which they kindly supplied.

Thanks are due to Mr. Philip Reed of the Imperial War Museum, London, and to Dr. Wolfgang Herbst of MBB-Flugzeuge, Munich, for supplying copies of the Kaiser report in English and German, respectively, and to Dr. Klaus Well of DFVLR for an independent translation of the German version. Special thanks to Mr. Fritz Kaiser for his comments illuminating his pioneering investigations.

Thanks are due to Dr. David Hull and Dr. Jason Speyer of the University of Texas, Austin, for stimulating discussions of state-variable choice.

LIST OF ILLUSTRATIONS

<u>Figure</u>		<u>Page</u>
2.1	Energy Climb Schedule in h-v plane	55
2.2	Energy-Range-Climb to the Dash Point	56
2.3	Terminal Energy Transient	57
2.4	Terminal Transient with Mach and q Limits	58
2.5	C_{D_0} (M) Smooth Data	59
2.6	$C_{D_{CL2}}$ (M) Smooth Data	59
2.7	Unlimited Flight Envelope, Smooth Data	60
2.8	Envelope with Mach Limit, Smooth Data	60
2.9	Envelope with q and Mach Limits	61
2.10	Speed vs Time	62
2.11	Path-Angle vs Time	63
2.12	Altitude vs Time	64
2.13	Eigenvalues at the Dash Point	65
2.14	Eigenvalues at Reduced Throttle	65
2.15	Flight Envelope Spline Data	66
2.16	Initial Load Factor	67
2.17	Final Load Factor	67
2.18	Load Factor vs Energy	68
2.19	Path-Angle vs Energy	69
2.20	Altitude vs Energy	69
2.21	Load Factor vs Energy	70
2.22	Lift Coefficient vs Energy	70
2.23	Path-Angle vs Energy	71

List of Illustrations (cont.)

<u>Figure</u>		<u>Page</u>
2.24	Altitude vs Energy	71
2.25	Load Factor vs Energy	72
2.26	Lift Coefficient vs Energy	72
2.27	Range-Energy-Climb and Point Mass Solution	73
2.28	Altitude Gain vs Energy	74
2.29	Path-Angle Gain vs Energy	75
2.30	Altitude Gain vs Energy	76
2.31	Path-Angle Gain vs Energy	77
2.32	Altitude Gain vs Energy	78
2.33	Path-Angle Gain vs Energy	79
2.34	Altitude Gain vs Log(E)	80
2.35	Path-Angle Gain vs Log(E)	81
2.36	Altitude Gain vs Energy	82
2.37	Path-Angle vs Energy	83
2.38	Altitude Gain vs Log(E)	84
2.39	Path-Angle Gain vs Log(E)	85
2.40	Altitude vs Energy	86
2.41	Altitude Error vs Time	87
2.42	Altitude vs Energy	88
2.43	Altitude vs Energy	89
2.44	Altitude vs Energy	90
2.45	Altitude vs Energy	91
2.46	Altitude vs Energy	92
2.47	Interceptor Path with y as Running Variable	93

List of Illustrations (cont.)

<u>Figure</u>		<u>Page</u>
2.48	Interceptor Path without y as Running Variable	94
2.49	Heading vs Energy	95
2.50	Heading vs Time	96
3.1	Flight-Path Angle vs Acceleration variable for the Range Problem	126
3.2	Flight-Path Angle vs Airspeed in Gliding Flight for the Range Problem	127
3.3	Flight-Path Angle vs Airspeed in Powered Flight for the Range Problem	128
3.4	(H/λ_x) vs Airspeed for Equilibrium Flight - Parabolic $(T - D)/W$ Distribution	129
3.5	$(T - D)/W$ vs Airspeed - A Typical Parabolic Distribution	130
3.6	Representative Analytical Solution for (H/λ_x) in the First Equilibrium Regime	131
3.7	Representative Analytical Solution for (H/λ_x) in the Second Equilibrium Regime	132
3.8	Representative Analytical Solution for (H/λ_x) in the Third Equilibrium Regime	133
3.9	A Parabolic Distribution of Specific Excess Power vs Airspeed	134
3.10	(H/λ_x) vs Airspeed at Constant Specific Energy for F-4 Aircraft for Unaccelerated Flight.....	135
3.11	Flight Envelope, Energy-Climb Schedule, Equilibrium Locus and a Climb-Dash Euler Solution	136
3.12	Euler Solutions for the Climb-Dash Problem	137
4.1	Contours in the Altitude-Velocity Chart	145
4.2	Flight-Path Angle vs Energy - Energy Climb	146

List of Illustrations (cont.)

<u>Figure</u>	<u>Page</u>
4.3	Altitude vs Velocity - Climb-Dash 147
4.4	Flight-Path Angle vs Energy - Climb-Dash 148
5.1	Lines of Constant $J = (\lambda_F Q - \lambda_R V)$ and $Q^*(V)$ 164
5.2	Minimum Fuel-flow $Q^*(V)$ vs Velocity 165
5.3	Minimum Fuel-flow $Q^*(V)$ vs Velocity (high-speed region) 166
5.4	Fuel-minimizing altitude h_0 vs Velocity 167
5.5	Fuel-minimizing throttle-setting η_0 vs Velocity 168
5.6	Candidate minima of $J = (\lambda_V Q - \lambda_R V)$ 169
5.7	Cruise-Dash Points and Flight Envelopes in the (h,V) plane 170
5.8	Constant fuel-flow contours for level unaccelerated flight 171
5.9	A Non-convex Region of $Q^*(V)$ vs Velocity 172
5.10	Fuel Savings for Time-Shared Operation 173
5.11	Zero-lift Drag Coefficient C_{D_0} vs Mach Number 174
5.12	Induced Drag Coefficient $C_{D_{CL2}}$ vs Mach Number 175
5.13	Maximum Afterburning Thrust vs Mach Number and Altitude 176
5.14	Maximum Afterburning Fuel-Flow vs Mach Number and Altitude 177
A.1	ME 262 Minimum-Time Climb (Kaiser)..... 188
A.2	ME 262 Distance Climb (Kaiser) 189
A.3	ME 262 Distance Climb Family (Constant Multiplier) .. 190
A.4	ME 262 Climb-Dash Family (Energy-Modelled Euler Solutions)..... 191

LIST OF TABLES

	<u>Page</u>
2.1	Representation of Aerodynamic Data 49
2.2	C_{D_0} Data 51
2.3	$C_{D_{CL2}}$ Data 52
2.4	$C_{L_{max}}$ Data 53
2.5	Thrust Data 54

SYMBOLS

a	= Velocity of Sound
C_D	= Drag Coefficient
C_{D_0}	= Zero-Lift Drag Coefficient
$C_{D_{CL^2}}$	= Induced Drag Coefficient
C_L	= Lift Coefficient
D	= Drag
E	= Specific Energy, $(h + V^2/2g)$
E_d	= Dash Energy
E_f	= Final Energy
E_{max}	= Maximum Sustainable Energy
g	= Acceleration due to Gravity
H	= Hamiltonian
h	= Altitude
J	= Performance Index
L	= Lift
M	= Mach Number
m	= Mass of Aircraft
n	= Load Factor
Q	= Fuel-flow Rate
q	= Dynamic Pressure
S	= Wing Surface Area
T	= Thrust
V	= Airspeed

List of Symbols (cont.)

V_d	= Dash Velocity
W	= Weight of Aircraft
\tilde{W}	= Weight of Fuel Consumed
x	= Downrange
y	= Crossrange

Greek Symbols

α	= Angle of Attack
γ	= Flight-path Angle
ϵ^1	= Fast Interpolation Parameter
ϵ^2	= Intermediate Interpolation Parameter
η	= Throttle Setting
λ_E	= Energy Multiplier
λ_h	= Altitude Multiplier
λ_m	= Mass Multiplier
λ_v	= Velocity Multiplier
$\lambda_{\tilde{W}}$	= Fuel-weight Multiplier
λ_x	= Down-Range Multiplier
λ_y	= Cross-Range Multiplier
λ_γ	= Path-Angle Multiplier
μ	= Bank Angle
ρ	= Density of Air
χ	= Heading Angle

SUMMARY

Several topics in optimal symmetric flight of airbreathing vehicles are examined. In one study an approximation scheme designed for on-board real-time energy management of climb-dash is developed and calculations for a high-performance aircraft presented. In another a vehicle model intermediate in complexity between energy and point-mass models is explored and some quirks in optimal-flight characteristics peculiar to the model uncovered. In yet another study, energy-modelling procedures are re-examined with a view to stretching the range of validity of zeroth-order approximation by special choice of state variables. In a final study time-fuel tradeoffs in cruise-dash are examined for the consequences of nonconvexities appearing in the classical steady cruise-dash model. Two appendices provide retrospective looks at two early publications on energy modelling (Ref. 22) and related optimal-control theory (Ref. 58).

CHAPTER 1

INTRODUCTION

The present report brings together four studies of optimal symmetric flight which have order-reduction as a common feature. The research started out as an effort to implement a singular-perturbation approach to optimal flight, that of Ref. 25, in closed-loop form along the lines of a concept put forth in Ref. 20. The effort stayed on track during a minimum-time climb-dash phase which appears as Chapter 2. It wandered off down an interesting by-way offered by a vehicle model intermediate in complexity between the familiar point-mass and "energy" models, which had been previously employed in the literature but not thoroughly researched. The quirks discovered in this vehicle model are reported in Chapter 3 and are of considerable research interest; however, the intermediate vehicle model does not appear to have sufficient merit for use in the applications work of main interest.

In the course of the minimum-time climb-dash research it became evident that a need exists to stretch the zeroth-order asymptotic theory as far as possible and that there is freedom in choice of state variables which recommends itself for this purpose. Chapter 4 reports the synthesis of two "fast" state variables potentially useful in this connection. Although further research along these lines appears worthwhile, it is already clear that possible improvements make the scheme attractive for applications.

The fourth study, that of Chapter 5, began as a seemingly straightforward exercise to incorporate a fuel constraint. Analysis of the "slowest" motions, cruise-dash, encountered complications due to the appearance of nonconvexity phenomena, with resulting ambiguities. This matter deserves further study; even more so, perhaps, does the related "chattering" phenomenon which appears in energy approximation, and which is related to oscillatory behavior in point-mass approximation.

An excursion into the origin of the "energy-climb" technique, which traces back to WWII Messerschmitt, appears as Appendix A. A look at a mathematical technique for treating optimal-control problems of small dimension linear in a scalar control (Ref. 57) appears as Appendix B. The technique lends itself to the energy-climb problem and one of Mancill's results is recognizable as the generalized Legendre-Clebsch condition for the special low-dimensional problem.

CHAPTER 2

ON-BOARD NEAR-OPTIMAL CLIMB-DASH ENERGY MANAGEMENT

A. R. Weston

E. M. Cliff

H. J. Kelley

SECTION 2.1

PREFACE

On-board flight control and guidance is a subject which has had varying reception in different fields of Aerospace Engineering. In the area of unmanned missiles there has been extensive research, with many resulting applications, in developing on-board guidance systems, as reported in the survey papers, Refs. 1 and 2. These studies have encompassed many new optimal control and even differential gaming ideas (Ref. 3): in this field the on-board flight computer is an accepted and usually necessary part of the guidance system. While conventional homing and proportional navigation guidance laws are simple, and require minimal computation, more complex guidance schemes may be implemented on-board by the use of singular perturbation methodology, as in Ref. 4.

The willingness to apply state-of-the-art theoretical developments to manned aircraft is not as evident. This may be the result of a more conservative approach in applying new technology to machines which are responsible for peoples' lives, machines which are also extremely expensive, generally larger and more complex than many missiles. However one of the greatest obstacles may be the threatened removal of authority from the pilot; despite the existence of sophisticated autopilots on many expensive aircraft, there is an aversion to total automation, particularly on the part of the pilot. As a result there is a significant gap between the flight-path optimization and differential gaming results which have been achieved in the last twenty years, and their applications in on-board use. A part of this is due to the limited computational resources

available, particularly on fighter and small general aviation aircraft, where weight and space are at a premium. Some of the latest developments relating to the latter case are given in Ref. 5. On the other hand in the area of large transport aircraft the cost, weight and complexity of a small main-frame computer is justified, but this has yet to be implemented. In civil aviation much research has been done in the area of trajectory optimization, with particular emphasis on efficient fuel usage and minimizing the direct operating cost. Attention has focused on the calculation of sub-optimal flight paths, using order-reduction to simplify the problem, as in Refs. 6-9. Burrows (Ref. 6) used singular perturbations and order reduction to derive sub-optimal short and long haul trajectories, with on-board corrections to speed and energy errors based on expanding the performance index to second order, which he found to be more effective than simple linear feedback. Sorenson and Waters (Ref. 7) used an assumed constant energy cruise (as did Erzberger and Lee, Ref. 8), and pointed out that the on-board flight control needs to be coordinated with the ATC system, so that fuel saved during the flight is not wasted due to traffic congestion at the terminal area. Chakravarty and Vagners (Ref. 9) attempted to provide justification for their state variable selection through the use of non-dimensionalization. Transitions onto fuel-optimal climbs and descents are studied in Ref. 10, where they are used to derive a near-optimal feedback control law. Sub-optimal terminal guidance is examined by Erzberger, Ref. 11, for a fixed-wing aircraft, and by Beser, Ref. 12, for a tilt-rotor aircraft. Optimal shipboard terminal guidance is studied in Refs. 13-15.

Despite the active interest and work, as described above, in this area the applications have lagged behind. A description, for example, is given in Ref. 16 of the DC-9-80 Digital Flight Guidance System; here the emphasis is on establishing reliability and safety criteria for the engine and flight control systems. It seems safe to say that in this area applications efforts have focused on feasibility and reliability rather than optimality. As mentioned earlier, the computational resources on a fighter aircraft are even more limited than on a transport, for obvious reasons of space and weight constraints. In contrast with large transports there is a much greater range of applications for on-board optimal control for fighter aircraft. This is because a fighter can and often has to perform a much wider range of maneuvers (in terms of flight path angles and bank angles for instance) as studied in Refs. 17-19. In many missions there is less, if any, a priori knowledge of the flight path. Also it is often desirable for security to minimize the communication with the ground, which eliminates the possibility of solving flight-control problems on the ground and relaying commands to the air.

With this background it is the objective of this study to investigate on-board real-time flight control, with the intention of developing algorithms which are simple enough to be used in practice, for a variety of missions involving three-dimensional (3-D) flight. Initially an approach is developed which is restricted to the intercept mission in symmetric flight, based on Ref. 20. Extensive computation

is required on the ground prior to the mission but the ensuing on-board exploitation is extremely simple. The scheme takes advantage of the boundary-layer structure common in singular perturbations, studied in Ref. 21, arising with the multiple time scales appropriate to aircraft dynamics. Energy modelling of aircraft, as first examined in Refs. 22-24 and extensively developed in Refs. 25-27 is used as the starting point for the analysis. In the symmetric case, a nominal path is generated which fairns into the dash or cruise state. Feedback coefficients are found as functions of the remaining energy-to-go (dash energy less current energy), along the nominal path. These serve to generate transitions towards the nominal path, closed loop and to counter disturbances. In this situation the guidance method is similar to the neighboring-optimal guidance methods of Refs. 28-32; these have been applied to space shuttle re-entry problems, Refs. 33-35, and orbital transfer guidance, Refs. 36-37. However there are two significant differences between this study and these references. In the present work the gain indexing is done in terms of the current energy; this avoids the problems encountered in estimating the index time, as in the time-to-go or min-distance methods. Also, for the extension to 3-D flight, families of reference paths are used instead of a single trajectory, with heading-to-go as the additional running variable.

2.1.1 Problem Formulation

The overall problem is to develop an on-board, real-time flight control system, which is near-optimal, for an aircraft flying an

intercept mission, with arbitrary initial conditions. The equations of motion for a point-mass model of an aircraft can be written:

$$\dot{E} = V(\eta T - D)/W \quad (2-1)$$

$$\dot{h} = V \sin \gamma \quad (2-2)$$

$$\dot{\gamma} = (L \cos \mu - W \cos \gamma)/mV \quad (2-3)$$

$$\dot{\chi} = L \sin \mu / mV \cos \gamma \quad (2-4)$$

$$\dot{x} = V \cos \gamma \cos \chi \quad (2-5)$$

$$\dot{y} = V \cos \gamma \sin \chi \quad (2-6)$$

$$\dot{m} = -\eta Q \quad (2-7)$$

These equations embody the assumptions of thrust along the path, zero side-force, and flight over a flat earth with constant gravity. Also winds aloft are assumed to be zero, and the atmospheric properties standard.

2.1.2 Symmetric Flight

The first approach was to restrict the problem and simplify the model considerably, to reduce the analytical and computational burden, during the initial research and development of the guidance scheme. The restrictions in the problem are the following: to consider only symmetric flight, with fuel open, i.e. fuel optimization is not examined, which leads to maximum thrust in most maneuvers of practical interest.

The target is assumed to be at a sufficient distance from the interceptor that a climb-dash is required: in other words a range-optimal climb to the dash point on the level flight envelope, blending into a steady-state dash. This sequence ends with a terminal transient, which is considered briefly in the next chapter. The time spent during the climb is assumed to be much smaller than the time spent at the dash state. The restriction in the aircraft model is that the variation in mass due to the fuel expenditure is ignored. Under these limitations, the equations of motion are reduced to:

$$\dot{E} = V(\eta T - D)/W \quad (2-8)$$

$$\dot{h} = V \sin \gamma \quad (2-9)$$

$$\dot{\gamma} = (L - W \cos \gamma)/mV \quad (2-10)$$

$$\dot{x} = V \cos \gamma \quad (2-11)$$

2.1.3 Aerodynamic Modelling

The aircraft which is used as an example to perform numerical calculations is a high-performance interceptor. The drag is modelled as a parabolic function of the control:

$$C_D = C_{D_0} + C_{D_{CL2}} C_L^2 \quad (2-12)$$

The coefficients C_{D_0} and $C_{D_{CL2}}$ are functions of Mach Number:

$$C_{D_0} = C_{D_0}(M) \quad (2-13)$$

and

$$C_{D_{CL2}} = C_{D_{CL2}}(M) \quad (2-14)$$

The thrust is a function of Mach Number and altitude:

$$T = T(M,h)$$

The way in which these three functions are represented is important in the computational work undertaken in this study. The reasons for this are discussed, and the different methods which were used are described in Section 2.5 and Section 2.6.

SECTION 2.2

OPTIMAL CONTROL: REDUCED-ORDER MODELLING

Reduced order modelling, based on time-scale separations observed in vehicle dynamics, is particularly attractive to the analyst in solving problems for lifting atmospheric flight. Numerical computations are simplified by the reduction in the system order and as a result the number of initial conditions which may have to be guessed or iterated upon is also reduced. Further, an improvement in the conditioning of the differential equations results from the confinement of the more unstable dynamics to boundary-layer corrections, which are relatively short in time. It has been appreciated since Kaiser's early work (Ref. 22) that the h and γ variables can be changed much more rapidly than the specific energy, E , which explains the introduction of this new variable. Also

the energy can be thought of as a 'fast' variable in comparison to the range, at least in cases where the climb is a transient which fades into a steady-state cruise or dash condition, i.e. when the time spent in the steady state is much greater than that spent on the climb, as assumed here. This leads to the reformulating of the equations of motion, following the development of Ref. 25, with the inclusion of the interpolation parameters, ϵ^2 on the left hand sides of the differential equations for h and γ , and ϵ^1 on the left hand side of the differential equation for E :

$$\epsilon^2 \dot{h} = V \sin \gamma \quad (2-15)$$

$$\epsilon^2 \dot{\gamma} = (L - W \cos \gamma) / MV \quad (2-16)$$

$$\epsilon^1 \dot{E} = V (\eta T - D) / W \quad (2-17)$$

$$\dot{x} = V \cos \gamma \quad (2-18)$$

To solve the problems of time-optimal control the variational Hamiltonian is formed:

$$H = \lambda_E \dot{E} + \lambda_h \dot{h} + \lambda_\gamma \dot{\gamma} + \lambda_x \dot{x}$$

and the Maximum Principle (Refs. 38 and 39) is applied. The resulting Euler differential equations are:

$$\epsilon^2 \dot{\lambda}_h = - \frac{\partial H}{\partial h} \quad (2-19)$$

$$\epsilon^2 \dot{\lambda}_\gamma = - \frac{\partial H}{\partial \gamma} \quad (2-20)$$

$$\epsilon^1 \dot{\lambda}_E = - \frac{\partial H}{\partial E} \quad (2-21)$$

$$\dot{\lambda}_x = - \frac{\partial H}{\partial x} \quad (2-22)$$

The introduction of three separate time scales in the state system must conform to the requirement of the Tihonov theory (Ref. 40) that the ratio $(\epsilon^2/\epsilon^1) \rightarrow 0$ as $\epsilon^1 \rightarrow 0$, as shown in Ref. 25. When both ϵ^2 and ϵ^1 are equal to 1 the original point-mass model is recovered.

2.2.1 Rectilinear-Motion Model

The simplest model possible is obtained when both ϵ^1 and ϵ^2 are taken 0. By examination of the differential equations, the following consequences of these assumptions may be noted:

$$\epsilon^1 = 0 \longrightarrow \begin{bmatrix} \dot{h} = 0 \\ \dot{\gamma} = 0 \end{bmatrix} \longrightarrow \begin{bmatrix} \gamma = 0 \\ L = W \end{bmatrix} \quad (2-23)$$

$$\epsilon^2 = 0 \longrightarrow \dot{E} = 0 \longrightarrow \eta T = D \quad (2-24)$$

These equations embody the assumptions that the altitude, h , the path angle, γ , and the energy, E , can all be varied instantaneously in a control-like fashion subject to the constraints. In this slow rectilinear-motion model the path-angle is, however, fixed at a value of zero, and the lift coefficient is chosen at any energy/altitude combination so that the lift equals the weight. Further, the throttle is constrained so that the horizontal forces are balanced. The energy and

altitude are chosen to minimize the Hamiltonian. This consists only of the range rate and the associated multiplier, which is constant because the Hamiltonian is not an explicit function of range in this, or any other modelling in this study. As a result the min-H operation leads to the high speed point on the level flight envelope. In the language of singular perturbation theory this is the zeroth-order 'outer solution', into which the solutions from the other time scales must fair asymptotically. The matching of different solutions and the composite generation are discussed in a later sub-section. The next time-scale is now examined.

2.2.2 Energy-State Models

The next level of order reduction is generally referred to in the literature as energy modelling. In this case ϵ^1 is set to 1, and ϵ^2 to zero. Again the altitude and path-angle are assumed to be 'fast' and 'control-like', but the energy change is analyzed and E assumes the role of a 'slow' variable. Again the path-angle is fixed at zero, and the lift coefficient chosen so that the lift equals the weight; but the only remaining 'control-like' variable (apart from the throttle, η) is the altitude: at any energy the altitude must be picked so as to minimize the Hamiltonian, which is now defined as:

$$H = \lambda_X \dot{X} + \lambda_E \dot{E} = \lambda_X V + \lambda_E \dot{E} \quad (2-25)$$

where the differential equation for E is given by:

$$\dot{E} = V(\eta T - D)/W \quad (2-26)$$

$$\dot{\lambda}_E = - \frac{\partial H}{\partial E} \quad (2-27)$$

The altitude which minimizes the Hamiltonian is therefore going to be determined, at any energy, by the relative values of λ_E and λ_x and their signs: their ratio determines the relative importance of range rate and energy rate, and their signs determine the sense of the optimization. For example, if λ_E is small enough the altitude picked will correspond to the maximum possible instantaneous range rate possible at that energy, if λ_x is negative. This is the lowest altitude (and highest speed) which is allowed by the terrain limit, dynamic-pressure limit or Mach limit, whichever is greatest. On the other hand if the range multiplier is set to zero the altitude chosen will maximize the instantaneous excess power or energy rate, if λ_E is negative. This special case is the so-called 'energy-climb', and is discussed in the following subsection. Note that if either multiplier is positive the rate of change of the associated state will tend to be minimized.

2.2.3 Energy Climbs

Of the possible energy-state results the energy-climb is the simplest to calculate: as the Hamiltonian only contains one term, only one differential equation needs to be integrated assuming that λ_E remains negative. The initial value of the multiplier does not in general have to be determined: so long as it is negative the same path will result.

Indeed if time histories are not required none of the differential equations need to be integrated at all: the altitude-energy path may be found simply by maximizing the level-flight energy rate at any energy. The energy climb for the aircraft studied is shown in Fig. 2.1. It is interesting to note that this schedule shows multiple jumps in altitude, arising from realistic variations in the thrust data. This is somewhat different from other examples which have been examined, for example the F-4, where the altitude discontinuities in the energy-climb are primarily due to the transonic drag-rise (Ref. 41).

2.2.4 Energy-Range Climbs

When the range multiplier, λ_x , is not assumed to be zero, i.e., 'energy-range climbs' are examined, the analysis and resulting computations are slightly more complex than the 'energy-climb' discussed above. First of all the λ_E equation must be integrated, as the relative magnitude of λ_E to λ_x at any time or energy is important in choosing the altitude. Secondly, as a result of this, the initial ratio of λ_E to λ_x , r^0 , must be carefully picked: different values of r^0 will result in different paths with different terminal states. As the value of r^0 is increased from zero the resulting trajectories move downward in the flight envelope, with the terminal energy moving from the maximum energy, E_{\max} , towards the dash energy, E_d . At a certain value of $r^0 = R^0$ a path results which fairs gracefully into the dash-point. This is the range-optimal 'energy-range climb' which is desired and is shown in comparison to the energy climb found earlier in Fig. 2.2, with the level flight

envelope also shown. Determining the correct value of r^0 is an initial-value problem, but limited to only one dimension, and the usual one-dimensional search techniques, (i.e. golden-section, cubic and parabolic fits) may be employed. For values of r^0 which are greater than R^0 the resulting trajectories are range-optimal for terminal energies which are lower than E_d , over different time spans. These paths are characterized by a climb which approaches the dash point, a dash, and finally a terminal transient which takes the energy down to the desired level. This transient begins with an instantaneous dive to the maximum range rate (speed) at E_d , as allowed by the terrain, dynamic-pressure, or Mach limit, whichever is the most severe restriction at the current energy level. In the case studied, no Mach limit and dynamic-pressure limits were applied; rather the thrust data was faired off to limit the level-flight envelope from exceeding such limits, as explained in Section 2.6. As a result the terminal maneuver takes the aircraft down to the terrain limit, (outside the flight envelope), where it remains, losing energy. This situation is unchanged until the energy is reached corresponding to the dash speed at the terrain limit. At this point the engine is switched off (λ_E changes sign) and were speed brakes included in the model they would be applied: the instantaneous energy rate is made most negative. This sequence is shown in Fig. 2.3 for the aircraft being studied. For the case where Mach and dynamic-pressure limits are applied the equivalent maneuver is shown in Fig. 2.4.

This process needs some explanation: when E_f is less than E_d , the aircraft must perform some terminal transient which loses energy in

the most range-optimal way. There are two choices, or ways in which it can lose energy: at speeds below or speeds above the dash speed. Obviously the range-optimal strategy is to spend as much time in the latter region and as little in the former as is possible. This is done by switching off the engine when the speed drops below the dash speed, and if possible extending the drag brakes. The problem of the terminal-maneuver transient is not pursued here; it is of research interest.

2.2.5 Method of Matched Asymptotic Expansions

By the use of singular-perturbation theory, boundary-layer type corrections can be used to overcome the energy-modelling weakness, i.e. initial and final jumps in altitude, as in Refs. 25 and 42, and transonic or internal jumps, as in Ref. 41. While the altitude discontinuities are eliminated by expansion to the zeroth order, realistic path-angle values are obtained, in the Ref. 25 approach, only by continuing the expansion to the first order or higher. This is a nontrivial problem in the case where the altitude transitions occur at the beginning or the end of a trajectory, and is even more complex in the case of the internal jump. As a result, even the corrected energy model loses its attraction when realistic path-angles are required for onboard use as commands. A scheme for providing more realistic path-angle results in the zeroth order is explored in Ref. 43.

2.2.6 Conclusions

To conclude this section, some of the results of the reduced-order modelling are summarized below.

First of all energy-state modelling, while attractive in its simplicity, is inappropriate and unsuitable for on-board guidance use on its own, i.e. uncorrected, for the intercept mission contemplated. This is because it generates significant initial and terminal discontinuities in altitude and path-angle, which the aircraft is supposed to follow instantaneously. Secondly, multiple instantaneous jumps are also possible along the optimal path, and lastly the path-angle is obtained as zero, in the usual approximation, which is again a big disadvantage as the actual path-angles can be quite large.

Corrections to the energy-state model which overcome these weaknesses are possible and have been demonstrated in the literature (Refs. 41,42). However this additional complexity is extremely unwelcome for on-board calculations due to limited storage and, more importantly, execution time available on-board; indeed solutions are not guaranteed due to the instabilities of the state-Euler system which need to be suppressed. In this context it is questionable whether this approach is in fact easier or quicker than solving the optimal control problem for the full system.

However, certain ideas from the energy-state model are undeniably attractive. The solutions suggest a hierarchical structure of states in optimal control solutions. This is exhibited in the following way: altitude and path-angle 'command' values are determined by the current

energy, and in this sense the energy is the dominant state. If the current values h and γ do not coincide with these predetermined values, a rapid transition can be made which brings them to their 'correct' values. These ideas form the basis of the guidance scheme which is presented in the next section.

SECTION 2.3

ON-BOARD GUIDANCE

An alternative to using order reduction, suggested in Ref. 20, which is simple enough to lend itself to onboard implementation is now developed, for the case of symmetric flight. The scheme has roots in the hierarchical structure of optimal-control solutions of the energy model, in which the specific energy is a relatively 'slow' variable and its value determines the control-like 'fast' variables, h and γ .

2.3.1 Nominal Path

The phenomenon described above suggests that trajectories of the point-mass model funnel rapidly, (rather than instantaneously as in the energy model), into the vicinity of a single path, which leads to the dash-point. The idea pursued in this Chapter, and Ref. 20, which is based upon an antecedent memorandum, is to determine this 'skeletal path' for the point-mass model, for as wide a range of energies as possible. This is the nominal, or reference trajectory and the altitude and path-angle histories are recorded as functions of the energy or energy-to-go, rather than time or time-to-go, as is common in other neighboring optimal guidance schemes (Refs. 28-37). The advantage of

this approach in an on-board context is the approximations to the final time are not necessary, and implementation of the scheme is greatly simplified as a result.

2.3.2 Feedback Law

The next step is to generate a neighboring-optimal feedback guidance law which will control the aircraft so as to follow a neighbor of the nominal optimal path. There are two basic reasons for doing this. First of all the reference path is of little use open loop: even if the aircraft is at any time on the reference path, the control commands which are stored along this trajectory will be insufficient to keep the aircraft close to it. This is because disturbances and errors inevitably arise both in the actual flight (i.e. variable winds etc.) and in representing the control history using a cubic spline (Ref. 44). Secondly, even if this first problem could be ignored, the reference path is of little, if any, use when the aircraft has initial conditions which are far removed from the nominal: for instance if the aircraft is initially loitering at high altitudes and subsonic speeds, on combat patrol, for example. Linear-feedback coefficients are proposed to generate the necessary transients to bring the aircraft to the neighborhood of the nominal optimal and stabilize the subsequent path. The guidance law is a linear feedback control based on the difference between the nominal and actual altitude and path-angle values.

2.3.3 Feedback Coefficients

The feedback coefficients, which correspond to minimizing the second-variational approximation to the performance index, as in Refs. 28-37, are found by perturbing the altitude and path-angle separately from their nominal values along the reference trajectory. The optimal-control problem is re-solved and the partial derivative of the control with respect to the states (at fixed energy) is estimated by difference quotient approximation. The partial derivatives which are mentioned here are the variations in the parameters of an initial value problem; they should not be confused with the variations of the control along the trajectory. They are defined for an arbitrary value of energy = E^1 in the following way:

let $C_L^*(t)$ be the control which takes the aircraft from an initial point at low energy, E^0 , (altitude and path-angle zero), along the nominal path up to the dash point on the level flight envelope, while optimizing range;

the resultant state time histories are given by

$$h^*(t), \gamma^*(t), \text{ and } E^*(t)$$

let the energy of the aircraft reach the value E^1 , while travelling along the nominal path, at a time t^1 :

$$E^1 = E^*(t^1)$$

Then at E^1 the 'correct' altitude and path-angle are given by $h^*(t^1)$

and $\gamma^*(t^1)$. To find the altitude feedback coefficient at this energy level the procedure is as follows:

find the range-optimal path which has the same terminal conditions, and terminal time as before but use the nominal state at t^1 as the initial conditions, with a perturbation, Δh , introduced in the initial altitude:

$$\gamma(0) = \gamma^*(t^1) \quad (2-28)$$

$$E(0) = E^1 \quad (2-29)$$

$$h(0) = h^*(t^1) + \Delta h \quad (2-30)$$

The solution of this problem results in a new control time history, $C_{L_{new}}(t)$. The altitude feedback coefficient is found by the following secant approximation:

$$\frac{\partial C_L(E^1)}{\partial h} = \frac{C_{L_{new}}(0) - C_L^*(t^1)}{\Delta h} \quad (2-31)$$

2.3.4 On-Board Use

The C_L commands to the autopilot are taken from the nominal path with linear corrections for the variation of the altitude and path-angle from their nominal values. On-board use requires only the storage of the states (h and γ), control (lift coefficient or load factor), and the two feedback coefficients, each as functions of

energy, or energy-to-go. The feedback guidance law with the appropriate functional dependencies is shown below:

$$C_L = C_L^*(E) + \frac{\partial C_L}{\partial h}(E) (h-h^*(E)) + \frac{\partial C_L}{\partial \gamma}(E) (\gamma-\gamma^*(E)) \quad (2-32)$$

To summarize, the only variables required to be stored on-board in the symmetric problem are:

$$C_L^*(E)$$

$$h^*(E)$$

$$\gamma^*(E)$$

$$\frac{\partial C_L}{\partial h}(E)$$

$$\frac{\partial C_L}{\partial \gamma}(E)$$

SECTION 2.4

OPTIMAL SOLUTIONS FOR THE POINT-MASS MODEL

A requirement of the proposed idea is a large number of optimal-control solutions to the point-mass-modelled problem. Optimal control solutions can be found in many different ways. They can be found by the use of direct methods, such as gradient methods, where the control history is parameterized in sectionally-linear or spline approximation and the terminal conditions are met by either penalty or projection

techniques. Alternatively, the problem can be resolved into a two-point boundary value problem, with split boundary conditions. Half are known at the initial time and the other half at the final time. This can be solved by the use of indirect methods such as simple or multiple shooting (Refs. 22, 23). To solve the problem of time-optimal control the variational Hamiltonian is formed:

$$H = \lambda_E \dot{E} + \lambda_h \dot{h} + \lambda_\gamma \dot{\gamma} + \lambda_x \dot{x} \quad (2-33)$$

and the Maximum Principle (Refs. 38, 39) is applied.

The resulting Euler differential equations are:

$$\dot{\lambda}_E = - \frac{\partial H}{\partial E} \quad (2-34)$$

$$\dot{\lambda}_h = - \frac{\partial H}{\partial h} \quad (2-35)$$

$$\dot{\lambda}_\gamma = - \frac{\partial H}{\partial \gamma} \quad (2-36)$$

$$\dot{\lambda}_x = - \frac{\partial H}{\partial x} \quad (2-37)$$

The lift and the throttle setting must be chosen to minimize the Hamiltonian, which requires that:

$$\frac{\partial H}{\partial C_L} = 0 \quad (2-38)$$

and

$$\eta = 1$$

(2-39)

$$(\lambda_E < 0)$$

2.4.1 Method of Solution

Euler solutions were found in the present work by the method of multiple shooting, using the algorithm and computer program of Refs. 33, 45-47 kindly supplied by DFVLR, Oberpfaffenhofen, West Germany. In this method, the interval of integration is broken up into many sub-intervals. This is preferable to 'simple shooting', where the initial-value problem is attempted directly, as optimization problems of lifting atmospheric flight are ill-conditioned, the state-Euler system being violently unstable. Partitioning the time interval has the effect of suppressing error growth. This method was used primarily for reasons of accuracy. This need arises, for example, in the calculation of the feedback gains, found by the difference of the control at the beginning of two optimal solutions. Typically to find the gains to 5 figures the control must be known to about 8 figures. The multiple-shooting method has greater accuracy than the other methods available, and although it is often difficult to generate the initial reference trajectory, the subsequent calculation of the feedback gains is relatively easy as the method has good convergence properties in the vicinity of a solution. Further discussion on these topics is found in Section 2.8.

SECTION 2.5

INITIAL EXPOSURE TO OPTSOL

The first use of the multiple shooting program OPTSOL obtained from DFVLR was to solve a very simple optimal control problem. This, taken from Bryson and Ho (Ref. 48) page 121, is similar to the brachistochrone, and was solved numerically both with and without a constrained arc, to test the user-supplied software required for the program.

2.5.1 Aircraft Data Manipulation

The program OPTSOL had been brought to VPI&SU with subroutines already created to enable the solution of aircraft flight mechanics problems and, rather than try to start from the beginning, attempts were made to use the existing computational tools, at least until familiarity had been gained with the program. In particular, the data which was used to model the aircraft under study was extensively modified so that the integration subroutine in OPTSOL, known as DIFSYS, was able to function. This proved to be a problem, as DIFSYS, as received, was extremely sensitive to the degree of smoothness of the right hand sides of the differential equations. In fact if discontinuities are encountered in any derivative up to the eighth, the stepsize of integration shrinks to zero. As all data of the point-mass model had been represented by cubic splines and spline lattices to facilitate interpolation, considerable effort was spent on the generation of an analytical representation which would reproduce both the values and the

shapes of the data with consistency. This had been done at DFVLR by using polynomial expressions, and this method was examined for the aircraft data on hand and abandoned. While a polynomial of sufficiently high order will fit any number of consistent data points exactly, there is an increasing distortion of shape with increasing order of polynomial. In fact even low order polynomials did not match the data at all well. The approach taken was to use a combination of polynomials, exponentials and arctangent functions to accomplish this. In the case of the single valued functions, i.e. $C_{D_0}(M)$, $C_{D_{CL2}}(M)$, this was not too difficult. The arctangent functions can be used as 'soft' switches, separating different portions of the data, which can be represented by a simple function locally (i.e. by a straight line or a parabola). However in the case of multivariable functions such as thrust and fuel flow this is definitely a nontrivial problem (however only thrust was attempted). In the case of thrust, the representation was achieved by fitting against Mach number, using coefficients which were functions of altitude. 19 variables were optimized using a conjugate gradient process which minimized the sum of the square of the errors at the grid points. The functions developed for Thrust, C_{D_0} and $C_{D_{CL2}}$ are shown in Table 2.1, and the aerodynamic data are shown graphically in Figs. 2.5 and 2.6.

After construction of the smooth data, the flight envelope was calculated and drawn (Fig. 2.7). As in the case of some high-performance jet-fighter aircraft the envelope turns out not to be performance limited, i.e. the level flight maximum sustainable speed is much higher than the

Mach limit. In this case $M = 2.4$ is the Mach limit and the high speed point occurred at roughly $M = 3.0$. It should be mentioned that aerodynamic and thrust data are not actually available for $M = 2.4$ and the flight envelope found by extrapolation is essentially a conjecture. The important thing is that the excess power at level flight is greater than zero for a range of altitudes along the Mach limit, for which both thrust and aerodynamic data are reliable. This problem, which in general requires treatment of state-inequality constraints, was dealt with in the following way: the thrust was faired off sharply against Mach Number, near the Mach limit so that the flight envelope no longer exceeded it. This was done by multiplying the thrust by a switching arctangent function which rapidly (but smoothly) brought the thrust to zero while leaving it unaffected elsewhere. The dynamic-pressure limit was treated in the same way. The analytical formulation for these two limits are included in Table 2.1. The flight envelope with the Mach-number limit is shown in Fig. 2.8; the effect of both of the limits is shown in Fig. 2.9.

2.5.2 Initial Flight-Mechanics Problem

Once the dataset had been finalized, OPTSOL was used to generate some optimal trajectories for a simple atmospheric flight problem: maximize final speed, from a given initial state, with final path angle zero and final altitude free. This was solved for several different time intervals, using simple shooting (initially), and also multiple shooting, to gain familiarity with the use of multiple shooting and to

investigate the methods of finding families of trajectories, for instance by time stretching. The time-histories for a family of four different trajectories are shown in Fig. 2.10 - 2.12. These are, respectively, speed, path-angle, and altitude plots.

2.5.3 First Trajectories to the Dash Point

The next step was to attempt to find paths which went to the high speed point, over a fixed time interval and to try to decrease the initial energy while lengthening the overall flight time. This was done by starting at an altitude and speed combination, (path-angle zero), just below the dash point, guessing the values of the costates. A total integration time of 5 seconds was used, and as can be imagined, the first guess was far from the targeted final conditions; however by requiring OPTSOL to satisfy boundary conditions by successive proximity rather than in one jump, a trajectory which reached the specified altitude and path angle combination was found. However, it was not possible to get the final speed to the desired value in the 5 second interval, because the time was not long enough to reach it. To achieve the desired final speed and to observe the manner in which the system approaches the equilibrium point (the possibility of an oscillatory solution near the high speed point, analogous to oscillatory cruise solutions was considered a possibility), attempts were made to lengthen the time of integration, by stretching the sub-intervals in the multiple-shooting scheme. Initially it was found to be very difficult to extend the trajectory at all - OPTSOL would not converge for even extremely small increases in the final time. Eventually

the interval was increased to 6 seconds. The final speed also increased but still did not reach the value at the dash point. It became virtually impossible to increase the final time any further due to numerical integration difficulties. For this reason and computational expense, the approach was reassessed at this point.

2.5.4 Eigenvalue Analysis

The system was linearized about the high speed point to examine the dynamics of the system in the vicinity of the equilibrium point. The analysis revealed that the stability eigenvalues were all placed along the real axis. At first the absence of complex roots akin to phugoid oscillation suggested that the linearization had been incorrect. After this had been checked and rechecked, the analysis was repeated at a point removed from the vicinity of the sharp arctangent functions which had been used to limit the flight envelope, as it was conjectured that the switching functions may have introduced large gradients affecting the dynamics of the closed-loop system. The throttle coefficient was reduced to 0.68, reducing the speed of the dash point by about 100 ft/sec, well away from the arctangent switch region, and the linearized analysis was repeated. The eigenvalues were found to have both real and imaginary parts, as expected, showing that the steps taken to limit the flight envelope had engendered significant effect on the dynamics of the state-Euler system. The s-plane positions of the two cases are shown in Fig. 2.13 and 2.14.

2.5.5 Backwards Integration of Stable Eigenvectors

It was thought that a useful starting trajectory could be found by the stable eigenvectors of the linearized system. If the equilibrium state is disturbed in proportion to a stable eigenvector the disturbance will die out in the linear case and should fair in towards the equilibrium point, for some finite time at least, in the nonlinear case, if the disturbance is small enough. So if such a trajectory is integrated backwards in time (using the full nonlinear system) a series of points will be generated which will fair in towards the dash point, at least for some time. Only one of the three eigenvectors approached the dash point from the desired direction, i.e. from points lower in altitude and slower in speed. This was integrated for 22 seconds and used as an initial guess for OPTSOL. The path-angle at the initial time was non-zero and attempts were made to reduce it to zero. Again convergence troubles were encountered: OPTSOL could not tolerate large changes in the initial values and the effort was finally abandoned. Apart from the cost of computing and poor convergence behavior, the system also displayed an alarming instability to small changes: on occasions the speed in the final seconds dropped from its maximum value (about 2300 ft/sec) to 1 ft/sec.

2.5.6 Conclusions

It was concluded that the thrust-tailoring approach taken to make the problem easier had instead probably made it worse. The integration subroutine DIFSYS is very sensitive to small changes in derivatives of the right hand sides. By using a multiplicity of sharp arctangent

functions the computational burden became large, as every time DIFSYS encountered an arctangent transition the stepsize of integration automatically became very small, increasing the computer time required. Further it was evident the system was overly sensitive to small changes in initial values. As a result it was decided to use a simpler integration subroutine and to return to splined data.

SECTION 2.6

MODIFICATIONS TO OPTSOL

The first step to modify the operation of the program OPTSOL was to change the integration routine. The variable step, eighth order Runge-Kutta package DIFSYS seemed to be a primary source of the numerical difficulties and computational expense experienced in the early use of OPTSOL. It was removed in favor of a much simpler fixed step-size fourth order Runge-Kutta-Gill subroutine.

2.6.1 Splined Aircraft Data

This substitution enabled the use of cubic splines and spline lattices of Ref. 44 for representation of the aircraft thrust and aerodynamic data. The problem of the Mach-limit violation was handled by fairing off the thrust data gently over four-tenths of a Mach Number and increasing the drag by adding more missiles. The aerodynamic and thrust data are included in Tables 2.2-2.5. The new flight envelope was calculated and is shown in Fig. 2.15. The coordinates of the dash point were found by a Newton iteration applied to the usual necessary conditions.

2.6.2 Family of Trajectories to the Dash Point

The new data were used to calculate an 'energy-climb' schedule (Ref. 25); this was used as a guide for guesses of initial altitude, energy and trajectory time combinations. A thirty-panel division of the trajectory was employed to find trajectories starting at lower altitudes, over longer times. This procedure was successful in finding optimal-range histories starting from an initial energy of 30,000 ft. After this point it became difficult and expensive to progress any further down in altitude and energy. It was thought that a smaller stepsize might be necessary to evaluate partials with sufficient accuracy for the method to converge. However, this did not improve matters significantly. But when the program was brought to Langley Research Center the situation improved. The CDC computer has a word-length which is approximately double that of the IBM 370, so with double precision at Langley about 28 decimal digits were obtainable compared to 14 or 15 digits at VPI. This had a significant effect on the program's operation. Much smaller step-sizes were used to evaluate the Jacobian without a penalty in round-off error, and it is conjectured that the resulting improvement in the accuracy of the Jacobian helped the convergence of OPTSOL. The trajectory extension continued until zero altitude was reached over a trajectory of 282 seconds.

SECTION 2.7

OPTIMAL-REFERENCE-PATH CALCULATIONS

The first objective is to generate a reference optimal path using point-mass-model dynamics, over the widest possible energy range. In

the climb-dash problem, the highest energy of interest corresponds to that of the high-speed point on the aircraft envelope, the dash 'outer' solution. The lowest energy corresponds to the trajectory which just kisses the terrain limit, i.e. below this energy, optimal solutions which start at zero altitude would dive below the terrain limit if it were absent. This lower energy is found by examining the initial load factor of a family starting from level flight at the terrain limit altitude: when the initial load factor is unity the lower energy is determined. This is shown in Fig. 2.16, where the initial load factor is plotted for several different initial energies.

2.7.1 Final Load Factor

Once the energy had been found for which the aircraft pulled off the ground with an initial load factor of 1, the effect of the flight time was investigated. To satisfy the final conditions in a finite time requires that the aircraft perform some maneuvering near the terminal energy: the longer the time allowed to approach the equilibrium point, the more gradual the approach should be. The effect of flight time on the final load factor was studied (for the same initial and final conditions) and results are shown in Fig. 2.17. This clearly demonstrates how the optimal path tends to fair in asymptotically as the flight time is increased. The load factor dropped to 1.001 after the flight time had been increased to 360 seconds. This time was chosen for the nominal path adopted in guidance-scheme development, and the altitude and path-angle (state variables) as well as the lift-coefficient (control variable) have been splined as a function of the energy. The load factor is

shown in Fig. 2.18, drawn against energy, showing the grid points used in the spline. Figs. 2.19-2.22 show the energy histories for path-angle, altitude, load factor and lift coefficient respectively for $t_{\max} = 360$ secs. The other paths from the same initial energy, but over longer times, showed identical state and control energy histories over almost all the energy range. However, at the terminal energies the effect of different flight times is most evident. Comparisons of the trajectories which result for different flight times are shown in Figs. 2.23-2.26 for path-angle, altitude, load factor and lift coefficient respectively. These variables are plotted versus energy for the last 2000 ft of energy, for $t_{\max} = 300$ seconds and $t_{\max} = 360$ seconds. The dramatic effect that the flight time has on the final state and control behavior is obvious from these pictures.

2.7.2 One Panel Integration

After each converged solution was obtained a trajectory was performed for the entire time, from the initial conditions. At higher energies and over shorter times this would ordinarily generate final states which were close to those specified in OPTSOL, but owing to the error propagation of the mismatched paths at each grid point, there is a difference between a one-panel integration and a 30-panel integration. However, at energies with zero initial altitude the error propagation was such the final conditions were not nearly met. After about 150 to 200 seconds the instabilities in the state-Euler system would produce extreme results. This raised the question as to whether the solution generated by OPTSOL is optimal or even near optimal. To this end the number of panels was

reduced first to 10, then to 6. Attempts to drive the number smaller than this were not successful as it appeared that the computer was 'running out of digits', despite the fact that 28 were being used. However, the difference between the solution for 6 panels and for 30 panels lies beyond the 9th digit and so it was assumed that no benefit would be gained by trying to reduce the number of panels.

2.7.3 Energy-Model/Point-Mass-Model Comparisons

Having established the nominal optimal path which takes the aircraft up to the dash point, it is of interest to stop and consider the two different models which have been used to study the problem, in particular it is of interest to compare the two different paths which climb up to the high-speed point. These are shown in the h-V plane in Fig. 2.27, surrounded by the level-flight envelope. The energy-range-climb model is indeed close to the point-mass model particularly at higher energies.

SECTION 2.8

FEEDBACK COEFFICIENTS - CALCULATIONS

This section describes the numerical work done to evaluate and represent the feedback coefficients used in the guidance law for the case of symmetric flight. In this case the coefficients are the partials of the lift coefficient with respect to the altitude and path-angle, at a fixed energy.

2.8.1 Method of Evaluation

The calculation of the variation in the control due to errors in the altitude and path-angle is treated as an initial-value problem, and has been extensively discussed in Section 2.3. To improve the accuracy of the feedback coefficients, each one was evaluated twice, by introducing positive and negative perturbations, and taking the average of the two difference-quotient values. This method also allowed the determination of the optimal size of disturbance (in terms of the resulting accuracy) by varying the size of the disturbance, examining the degree of agreement between the two values until the 'best' stepsize has been found for both altitude and path-angle. While it is true that the optimal stepsize will in general vary along the reference path, it was found that this change was negligible and one value was effective in evaluating the entire range for either coefficient. As the stepsize is reduced the errors due to nonlinearities shrink, but those due to a finite word-length grow: hence a compromise defines the optimal disturbance. It has been noted that a multiple shooting method such as OPTSOL is well suited to these kinds of calculations: although it was an arduous task to establish the nominal path, once this had been achieved, the neighboring solutions were found rapidly (within 3 or 4 iterations) and with high accuracy. This last point is important, as the use of numerical differentiation of the initial control to find the feedback gains required high precision control information. Typically it was found that 8-9 decimal digits of information were required for 4-6 figure accuracy in the gains.

2.8.2 Pilot Scheme

Feedback coefficients were initially found over a small range of energies, to evaluate the usefulness of the scheme before committing the computational resources needed for the full-scale operation. The last fifth of the energy range was chosen for this purpose as the integration times are the shortest and this minimizes the CPU time required to find optimal control solutions. The energies and corresponding times were taken from the reference trajectory (of 360 seconds) in the following manner: the total energy change was divided into twenty. The reference path was then integrated again and whenever the energy at the end of an integration step exceeded an integer number of divisions of the total energy change, the time and energy were recorded. The disturbance sizes were varied so as to maximize the agreement in between the two values obtained for each coefficient. The optimal perturbation in altitude was found to be 0.05 feet; in path-angle it was found to be 0.0000001 radians. Agreement between the values of both of the coefficients was found to vary in between 4 and 6 figures. In addition to the energy levels already chosen for feedback coefficient evaluation, it was necessary to find values close to the final energy as well. This is because spline representations are very unreliable when used to extrapolate data. The energy at the beginning of the last panel in the multiple-shooting method, i.e. at 348 seconds, was chosen as the upper limit for this purpose. The gains at this energy, which is just 0.11 feet below the maximum value, turn out to be an order of magnitude larger than the gains at lower energies. This sensitivity of neighboring-optimal-guidance schemes close to the terminal state has been noted in the

literature (Refs. 28-37). It is worth commenting, however, that the apparent unboundedness in the gains near the final state could have been a result of the method by which they were calculated; it is quite possible that a finite integration time, which is shorter as the terminal state is approached, was responsible. In other words if a longer time of integration had been allowed for the paths which were close to the final state, a different behavior might have been observed. However, this effect is highly local, and due to limitations of time and money this topic was not pursued. Any actual implementation of the scheme would, of course, have to take this into account, possibly by setting an upper limit on the magnitudes of the gains, to avoid control saturation with small errors. To examine the transition in the feedback coefficients near the terminal state, the analysis was repeated for three more energies close to the final time, at 336, 324 and 300 seconds. This is an inexpensive set of calculations as the integration times are extremely short. Also the coefficients were evaluated at the energy corresponding to the trajectory time of 188.7 seconds, as it was felt that they were needed for accurate spline representation.

The next problem was to spline the coefficients as functions of the energy-to-go. Difficulties were encountered at first when the splining was attempted. Cubic splines are not suited in general to represent functions where large variations in the gradient exist. In this case the gradient changes by six orders of magnitude in the vicinity of the end-point, resulting in large extraneous oscillations appearing throughout the spline representation, which render the interpolation useless. One way (not very satisfactory) is to ignore the spurious points which

are causing the trouble. This was done in this case, and the plots of the coefficients are shown Figs. 2.28-2.29.

To overcome these difficulties the splines-under-tension of Ref. 49 were used. These are similar in character to the cubic splines of Ref. 44 which had been used so far; the additional feature of the splines-under-tension package is the ability to minimize spurious wiggles near regions of rapidly changing gradient by the use of a tension factor, σ . By increasing σ the anomalies can be reduced but not eliminated, at least in the vicinity of the end point. The problem is that as the tension factor is increased the oscillations near the end point die down but the rest of the representation becomes essentially polygonal, i.e. linear interpolation between the data points.

2.8.3 Logarithmic Splining

It became apparent that the normal or ordinary method of splining was inadequate and a different approach was needed to continue. Essentially this is a boundary-layer type problem: there is a region where the coefficients vary rapidly. It seemed to be appropriate to separate the two regions and, using different methods, spline each one separately. The only requirement would be that the two representations fair into each other smoothly. One possibility is to use the normal splines in the 'outer' region, and spline the terminal coefficients in terms of the logarithm of the energy-to-go, matching the slopes at the junction between the two regions. (Another possibility is to use the inverse of energy-to-go in the terminal region, but this was not used for reasons as the large variations in the gradients, which are the roots of this problem, still exist.) The logarithmic method was used to

spline the coefficients for the range of energies considered in this pilot section. The results are shown in Figs. 2.30-2.31. These show the gains using 10 grid points for interpolation. These show a dramatic improvement over the previous attempts to spline the data: these earlier efforts had been so bad that they would only be visible on the same graphs as a series of vertical lines passing through the grid points. It was considered likely that with a few additional points the small remaining anomalies would be eliminated. An additional 16 points were evaluated in the vicinity of these outstanding 'wiggles' and finally a usable representation was generated, shown in Figs. 2.32-2.33, as functions of energy. They are shown as functions of the logarithm of energy-to-go in Figs. 2.34-2.35.

When the decision was made to carry on and evaluate the coefficients over the rest of the energy range, the same method was used to spline the data: the logarithm of the energy-to-go was used, and there was no need to go to a boundary layer type of approximation after all. The coefficients as they were represented over the entire energy range are shown as functions of the energy in Figs. 2.36-2.37. The corresponding plots versus the logarithm of energy-to-go are shown in Figs. 2.38-2.39.

SECTION 2.9

SIMULATION AND TESTING

Following the satisfactory splining of the nominal states, controls and feedback coefficients as functions of the energy-to-go, the guidance scheme was tested by running a simulation of the point-mass-model, using the feedback law, and comparing the resulting trajectory with an Euler solution which started from the same initial conditions. Before the entire range of feedback coefficients had been worked out a pilot scheme tested out the idea on a small range of energy near the dash-point. This test was performed with an initial disturbance of 1000 ft; the trajectory which resulted from the guidance law is compared with the Euler solution from the same initial conditions and the nominal path in Fig. 2.40 where the altitude is plotted as a function of energy. The guidance law is so close to the optimal path from the same starting point that it is almost impossible to discern the difference between them on this Figure. The difference in altitude between the two is shown as a function of time in Fig. 2.41 it can be seen that the difference is always less than 11 ft. With zero disturbance the autopilot was able to follow the nominal path more than satisfactorily, over the entire range of energies, despite the inevitable errors which arise in the spline representations. Tests were performed with the initial altitude disturbed from that of the nominal path at different energies by 1000, 5000, 10000 and 15000 feet above and by 5000, 10000 feet below the nominal path. The resulting trajectories are shown in Figs. 2.42-2.46. These show that the feedback law follows the optimal solution closely, even when the initial disturbance is far

outside of the range of linearity of the feedback gains. The cost was calculated for the situation with an initial altitude of 15000 ft above the nominal value, at the point where the two trajectories faired into the dash point. The difference between the ranges was less than 600 ft, an extremely small number considering that the dash speed is 2400 ft/sec.

SECTION 2.10

EXTENSION TO 3-D FLIGHT

This section describes the work done to extend the analysis to three dimensional flight, and suggests what direction future efforts might take.

2.10.1 Cross-Range Considerations

The problem of extending the analysis to 3-D flight is now considered. The state system is augmented to include y , the cross range, and χ , the heading angle. The addition of the corresponding multipliers to the full state-Euler system raises the order of the problem to twelve. For the intercept problem the final value of y must be zero; the value of the final heading, relative to the initial heading, must either be calculated on-board, or be supplied by the GCI. This will in general vary, for a maneuvering target, and the value stored on-board must be periodically or continuously updated.

The boundary condition on y leads to a dependence of the optimal solution on the cross range: for the same heading-to-go and energy-to-go there will exist many different possible values of y . As a result, if this formulation is used, cross range-to-go is an additional running

variable: this increases the order of the nominal paths required, which means a large increase in the computations on the ground, as well as an increase in the storage requirements on-board.

To get around this situation it is proposed to avoid using an additional running variable by letting the final value of y be free: this can be accounted for in the computation of the final heading needed for intercept, as specified by the on-board flight computer or the GCI. The intercept paths which result from the two different methods are compared in Figs. 2.47-2.48, for a target which is initially far away from the interceptor.

2.10.2 Computational Considerations

The first approach considered to generate a family of paths to the dash point was to use the symmetric flight reference path as a starting point for the augmented system, and introduce a small heading-to-go at the initial time. The argument for doing this is that for very small headings the state-Euler system should not be changed very much: the paths are close to each other. However, this method is only useful for a small number of combinations of heading-to-go and energy-to-go. This is because the turning rate at the energy at which the aircraft lifts off the ground is so high that all the heading-to-go disappears in a short time, and over a very small energy range. In general a method must be found which generates the part of the family of reference paths which combines moderate and large headings-to-go and moderate to small energies-to-go. The difficulty lies in knowing what initial conditions to pick for the altitude and the path-angle: when the aircraft is

lifting off the ground, these variables are specified, but in the general case, starting from an arbitrary energy-to-go and heading-to-go combination, the selection is a problem. Letting them be free is not acceptable as it can lead to an initial lift coefficient of zero (i.e. in the symmetric case): the optimization algorithm takes advantage of the freedom to choose the initial conditions in a way which maximizes the short term benefit. This does not fit in with the concept of a nominal reference path, where the altitude and path-angle are the same at the same combination of energy and heading-to-go.

The solution that is recommended is to use the altitude that comes out of the energy-turn model, as in Ref. 25. Here the heading is assumed to be a 'slow' variable, and has the same status as energy. However, instead of having to choose one variable, (such as the ratio of the initial energy multiplier to the range multiplier, as in Section 2.2), the initial heading multiplier must also be iterated upon. This is done using a Davidon-Fletcher-Powell algorithm, to find the path which fairs into the dash point with zero heading. An example of such a path over a small range of energy and heading-to-go is shown in Fig. 2.49, where the heading is shown against energy, and in Fig. 2.50, where the heading vs time plot for the same initial conditions is shown.

2.10.3 Selection of the Initial Path-Angle

The energy-state model produces altitude predictions which are fairly accurate as a function of the current energy, (away from altitude jumps), as can be seen from Fig. 2.27 where the Euler solution to the climb-dash is compared to the energy-range solution. However, the same

can not be said for the path-angle, which is predicted to be zero along the path. As a result a modification is considered, (Ref. 43), which produces realistic values along the path. The difference lies in the selection of the fast and slow variables: if altitude is chosen, zero path-angle results, if velocity is chosen, a value of the path-angle results which is too high. A new fast variable is examined in Ref. 43 which picks path-angle values in between these two values, and which may be used as initial conditions for the problem at hand.

SECTION 2.11

IMPLEMENTATION AND CONCLUSIONS

2.11.1 Implementation

Before the scheme may be used on a real aircraft there are some important simplifications and restrictions which have been applied in the interest of reducing the initial workload which must be accounted for.

First, the weight variation of the aircraft must be included in the modelling as a substantial percentage of the total weight may be used up during a mission. This is perhaps the easiest or at least the most straight-forward problem: the required action is to increase the order of the system, i.e. the mass is added as another variable and the resulting boundary conditions are simply that the initial mass is known, initial mass multiplier is unknown, and the final mass is unknown resulting in the mass multiplier being zero at the final time.

Fuel optimization is a problem which will no doubt be of interest, with different combinations of fuel and range being optimized. Problems

can occur here with a nonconvex hodograph, i.e. leading to the possibility of chattering controls, in this case the throttle. Other problems of the real world which have not been addressed are variations in atmospheric conditions, i.e. winds aloft and non-standard temperature distribution against altitude. Possibly these could be dealt with by analysing the effect of small perturbations, finding an approximation to the first order changes in the variables which are stored on-board and using simple linear corrections. Certainly this is the simplest way of tackling such difficulties and it would be interesting to examine how effective this approach would be.

Another problem of interest is that of variable configuration, i.e. the effect on the guidance scheme of changes in the aircraft's characteristics due to battle damage, releasing external stores, etc.

The biggest problem that must be looked at is the extension to 3-D, discussed in the last section.

2.11.2 Conclusions

The numerical results bear out the following conclusions: first, that all trajectories which fair into the high-speed point consist of a rapid transition onto a reference or skeletal path if they do not originate on it. Secondly, the linear-feedback scheme proposed is able to control the aircraft so that it closely follows the appropriate neighbor of the nominal path for large perturbations of initial conditions.

2.11.3 Future Work

A 3-D extension of the computational scheme is of interest in which

there are two dominant states, i.e. heading-to-go in addition to energy-to-go. As a result, families of optimal paths which fair into the dash-point will be needed, and the feedback coefficients will be functions of two variables (represented via a spline lattice) instead of one.

Table 2.1 Representation of Aerodynamic Data

$$C_{D_0} = 0.0242 + \arctan(50(M-1.0))(1.0+0.35 \exp(-4.5(M-1.8)^2))(0.012/\pi) \\ + 0.08 \exp(-55(M-1.1)^2) + 0.0096 \exp(-20(M-1.35)^2) \\ + 0.003 \exp(-20(M-1.6)^2)$$

$$C_{D_{CL2}} = (0.5+0.2026 \arctan(50(M-1.23))) \arctan(50(2.25-M)(0.39M-0.475)) \\ + 0.075 + 0.05 \exp(-150(M-0.985)^2) + 0.4(0.5+\arctan(50(M-2.25)))$$

$$C_{L_{max}} = 0.82 + (0.72/\pi) \arctan(50(M-0.9-M) + \\ (1.23-0.6M)(0.5+0.2026 \arctan(50(M-0.9))) \arctan(50(2.05-M))$$

Thrust(M,h) =

$$(0.5+(1/\pi) \arctan(40(M-XM2)))(H2-H1) + H1 + \\ (0.5+(2/\pi^2) \arctan(40(M-XM1))) \arctan(40(XM2-M))(H2-H1/XM2-XM1)(M-XM1)$$

$XM1, XM2, H1, H2$ are functions of altitude:

$$XM1 = (3.84 (\exp(0.165(h+1.74)))) - 4.82$$

$$XM2 = 0.0156h^2 + 2.83h + 1.1$$

$$H1 = (f1.g1 + f2.2g2) f3 (41000)$$

$$H2 = (f11.g1+f22.g2)(0.5+(1/\pi) \arctan(40(0.91-h)))40405$$

$$f1 = -2.43h^2 - 1.59h + 0.974$$

$$f2 = 2.38h^2 - 3.24h + 1.24$$

$$g1 = (0.5 + (1/\pi) \arctan(40(0.3-h)))$$

$$g2 = (0.5 + (1/\pi) \arctan(40(h-0.3)))$$

$$f11 = 1.35h^2 - 1.53h + 1.56$$

$$f22 = 3.25h^2 - 6.25h + 2.98$$

$$f3 = (0.5 + (1/\pi) \arctan(40(0.75-M)))$$

$$h = \text{altitude}/10^5$$

Mach Limit Fairing

The thrust is multiplied by the factor given by:

$$f = (0.5 + (1/\pi) \arctan (150(2.4-M)))$$

Dynamic Pressure Limit Fairing

The thrust is multiplied by the factor given by:

$$f = (0.5 + (1/\pi) \arctan (150(M^* - M)))$$

$$M^* = \sqrt{(4000/\rho)/ss}$$

ρ = density

ss = speed of sound

Table 2.2 C_{D0} Data

Mach Number	C_{D0}
0.00	0.01950
0.50	0.01950
0.80	0.01950
0.88	0.02097
0.90	0.02134
1.00	0.03533
1.10	0.04095
1.20	0.04656
1.30	0.04570
1.40	0.04950
1.50	0.04934
1.60	0.04918
1.70	0.04744
1.80	0.04570
1.90	0.04450
2.00	0.04330
2.10	0.04166
2.20	0.04001
2.30	0.03801
2.50	0.03451

Table 2.3 C_{DCL2} Data

Mach Number	C_{DCL2}
0.00	0.07500
0.40	0.07500
0.60	0.07500
0.77	0.07500
0.80	0.07500
0.90	0.10000
1.00	0.12500
1.10	0.07500
1.20	0.10000
1.40	0.15000
1.60	0.22500
1.80	0.30000
2.00	0.38750
2.15	0.45000
2.20	0.47500
2.25	0.47500
2.40	0.47500

Table 2.4 C_{Lmax} Data

Mach Number	C_{Lmax}
0.00	1.180
0.40	1.180
0.60	1.180
0.80	1.160
1.00	1.080
1.20	0.930
1.40	0.810
1.60	0.700
1.80	0.630
2.00	0.570
2.20	0.500
2.40	0.460
2.50	0.460

Alt (kft)	Mach Number														
	0	0.2	0.4	0.6	0.8	1.0	1.2	1.4	1.6	1.8	2.0	2.2	2.4	2.6	3.0
0	38580	41110	44270	49630	54390	62170	65600	65600	65600	65600	65600	65600	59040	29520	0
10	33070	33070	33070	37160	42370	49950	54230	59930	59930	59930	59930	59930	53940	29520	0
20	23240	23240	23240	26830	30900	37630	43520	48070	54770	54770	54770	54770	49290	24645	0
30	15540	15540	15540	17950	21210	26450	32120	38070	42600	48010	52430	55810	50230	25115	0
40	12000	12000	12000	12000	14400	18400	22400	26800	30200	34000	37200	40000	36000	18000	0
50	6648	6648	6648	6648	7978	10230	12800	15110	17220	20150	21960	24020	22580	11290	0
60	5660	5660	5660	5660	5660	5660	6540	8200	9800	11200	12760	14000	13320	6660	0
70	4400	4400	4400	4400	4400	4400	4400	4400	4400	5400	6400	7200	6930	3465	0
80	2200	2200	2200	2200	2200	2200	2200	2200	2200	2700	3200	3600	3460	1730	0
100	0	0	0	0	0	0	0	0	0	0	0	0	0	0	0

Table 2.5 Thrust Data (lbs)

Fig. 2.1Energy Climb Schedule on h-v plane

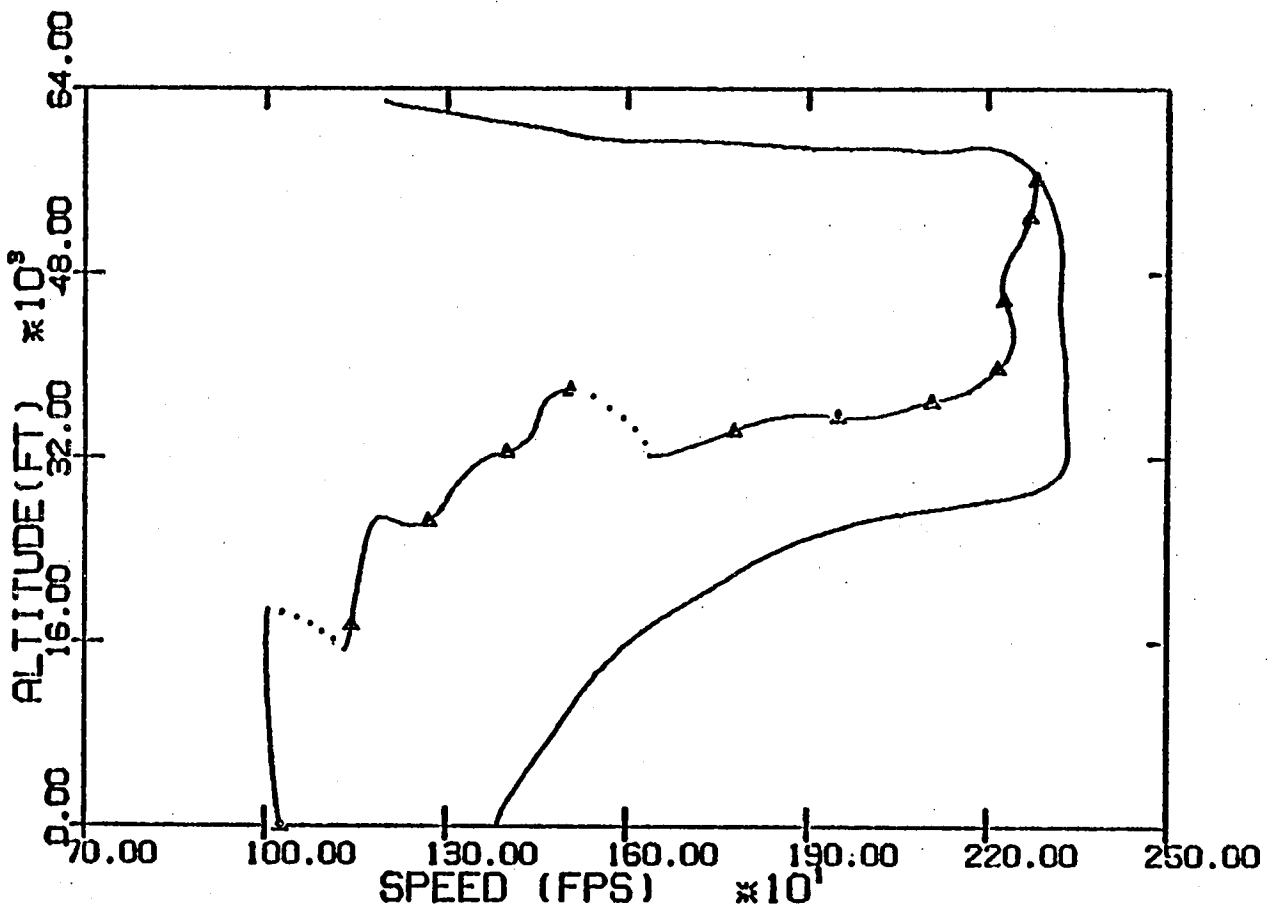


Fig. 2.2 Energy-Range-Climb to the Dash Point

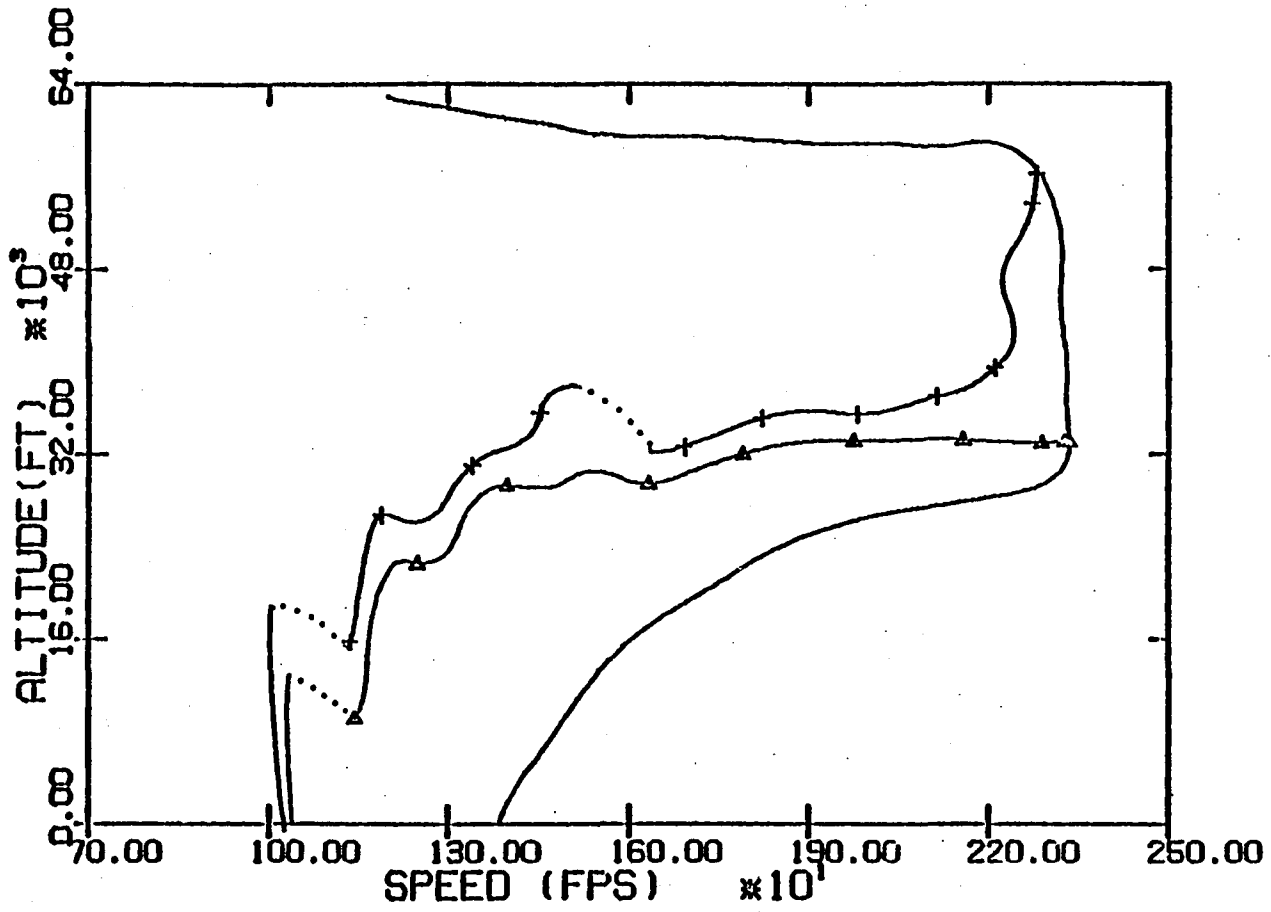


Fig. 2.3 Terminal Energy Transient

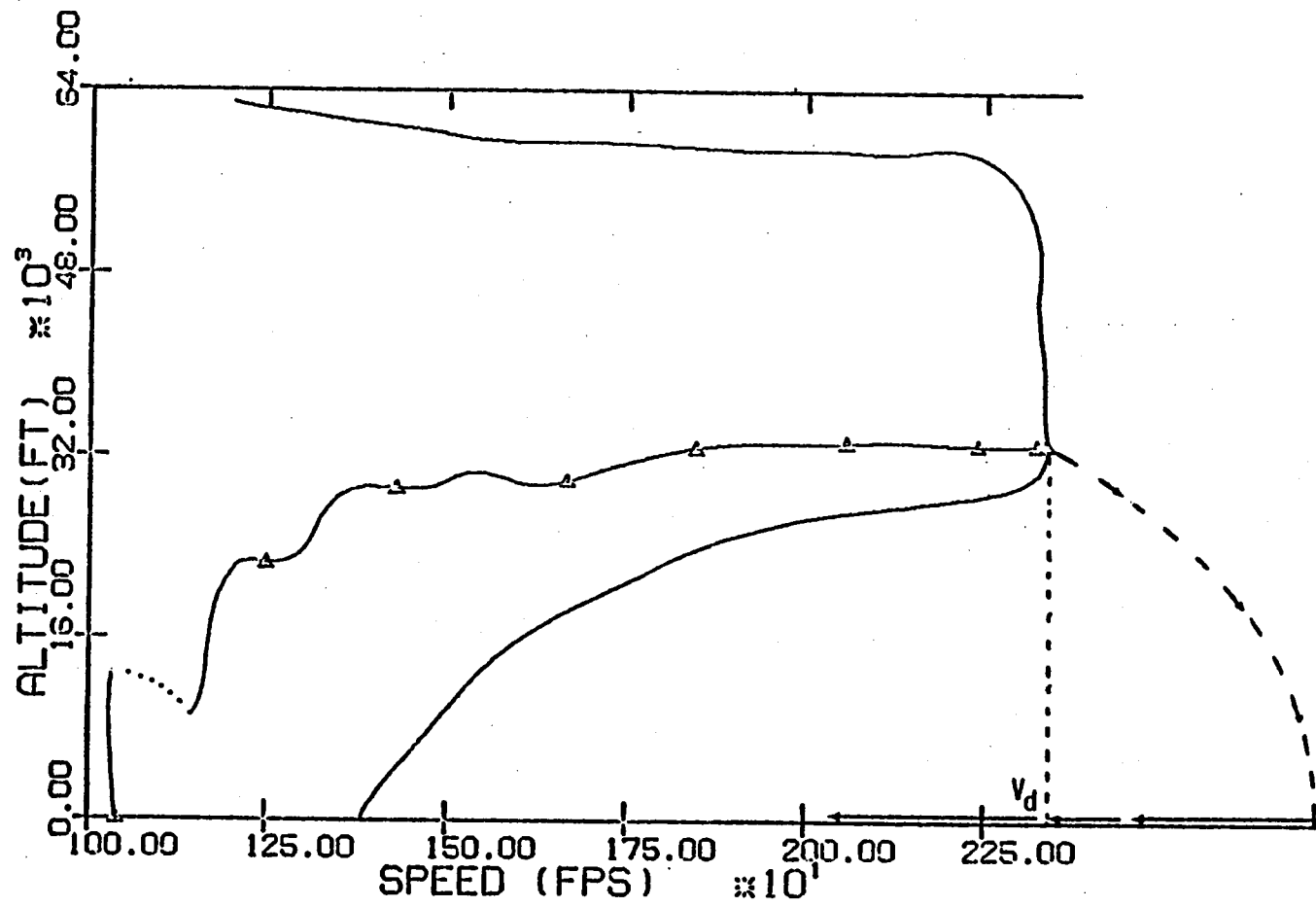
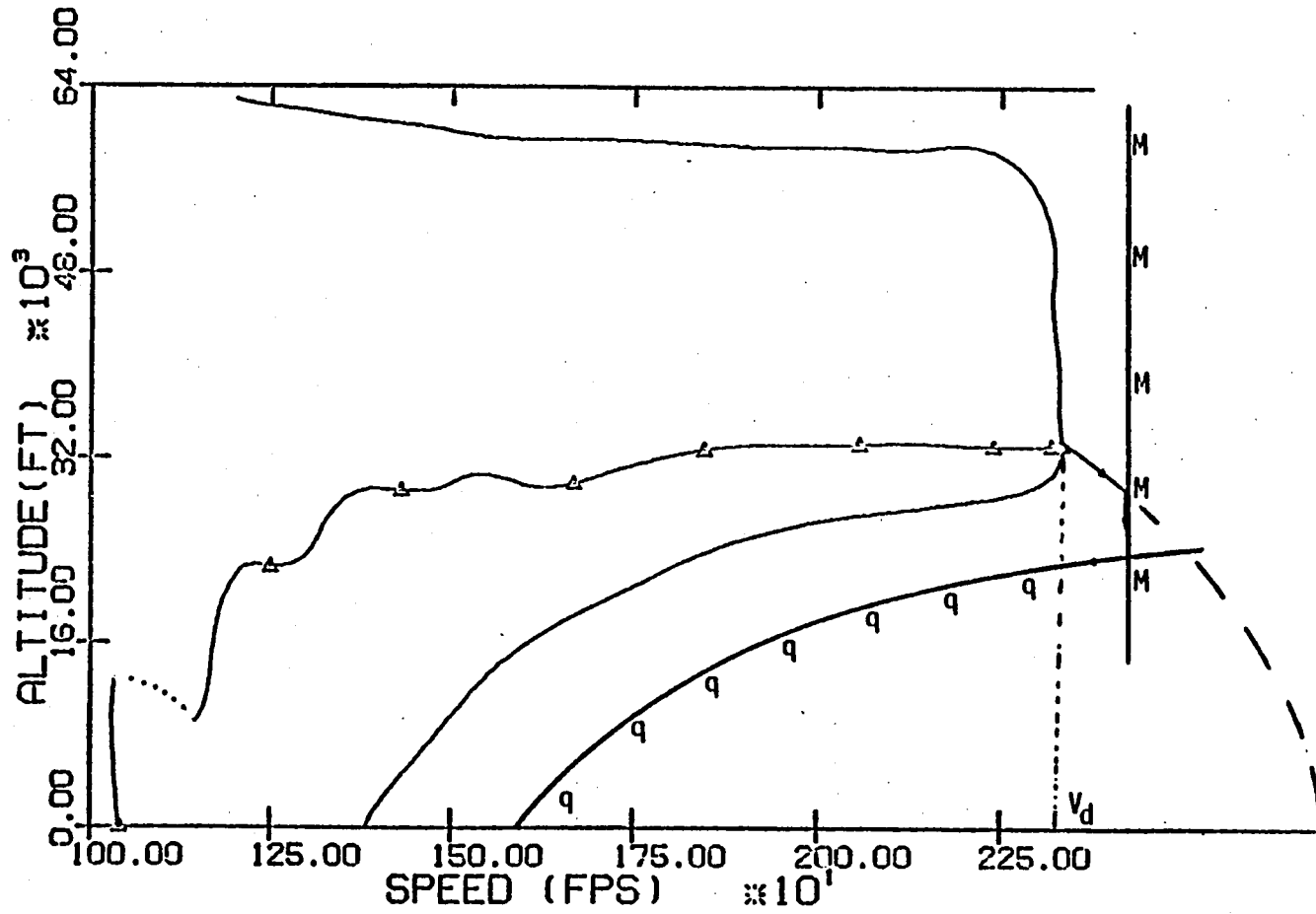


Fig. 2.4 Terminal Transient



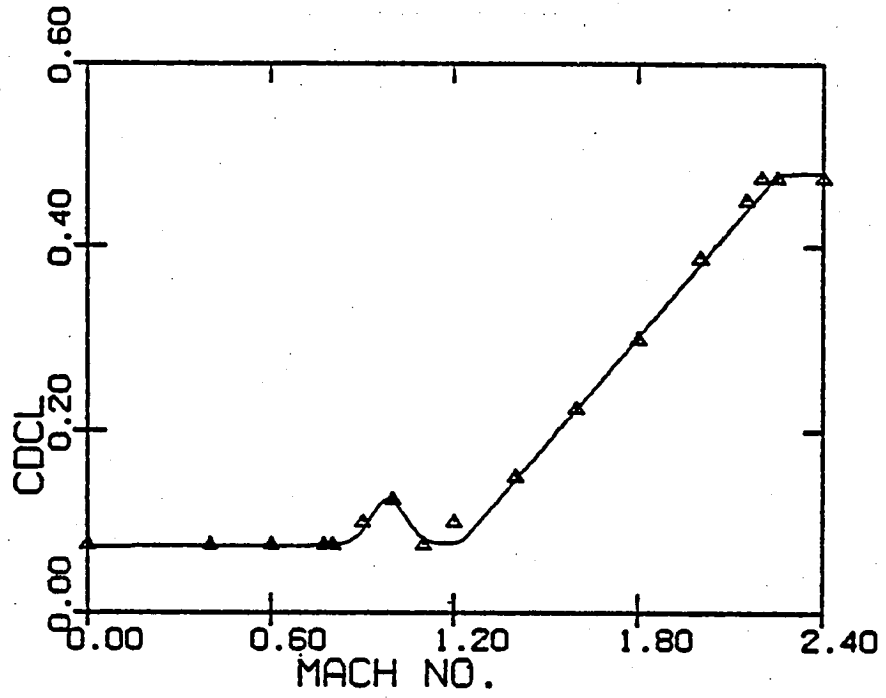


Fig. 2.6 C_{DCL2} (M) Smooth Data

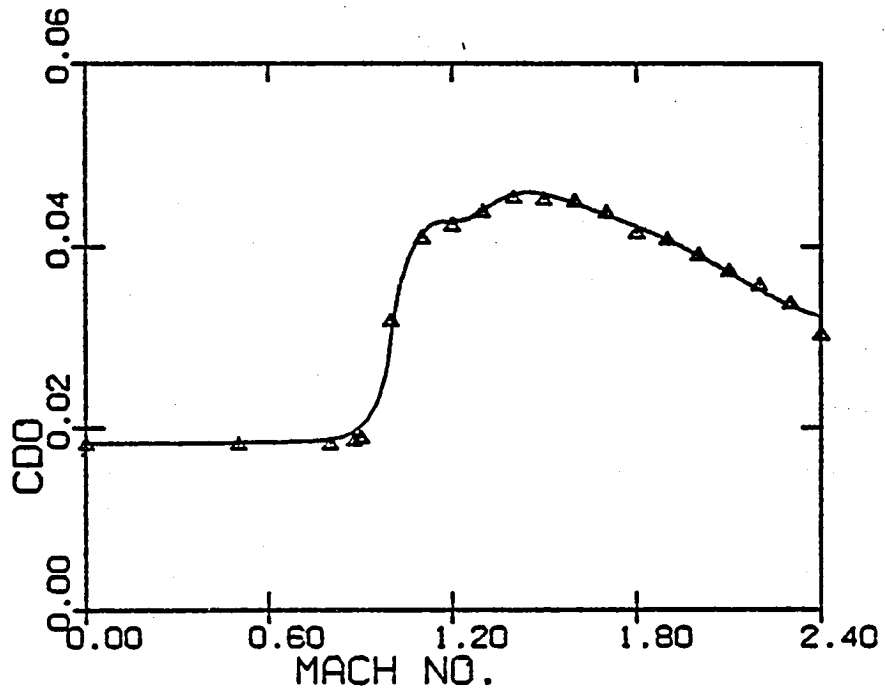


Fig. 2.5 C_{D0} (M) Smooth Data

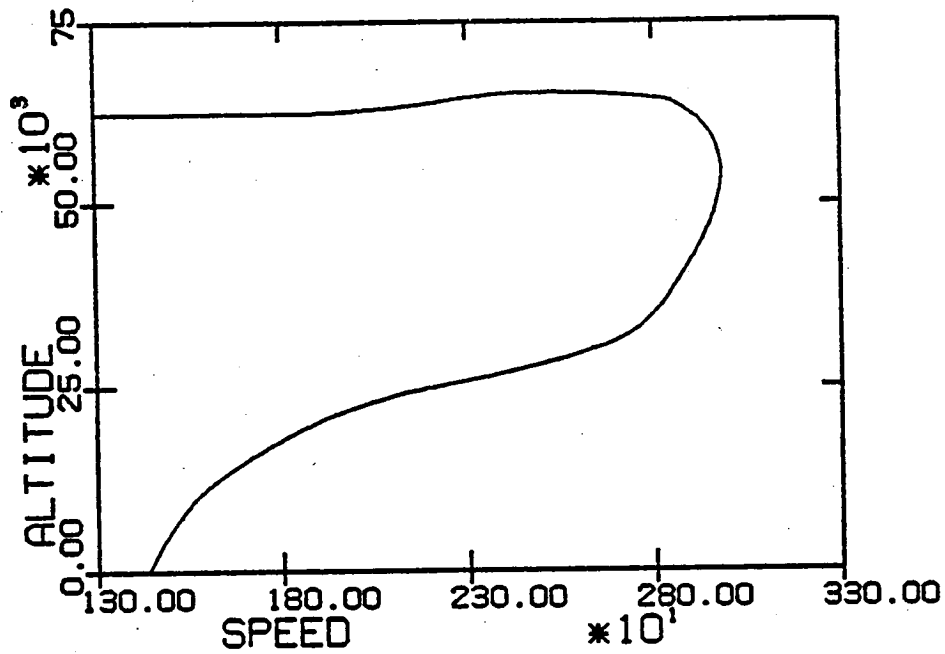


Fig. 2.7.....Unlimited Flight Envelope, Smooth Data

FLIGHT ENVELOPE

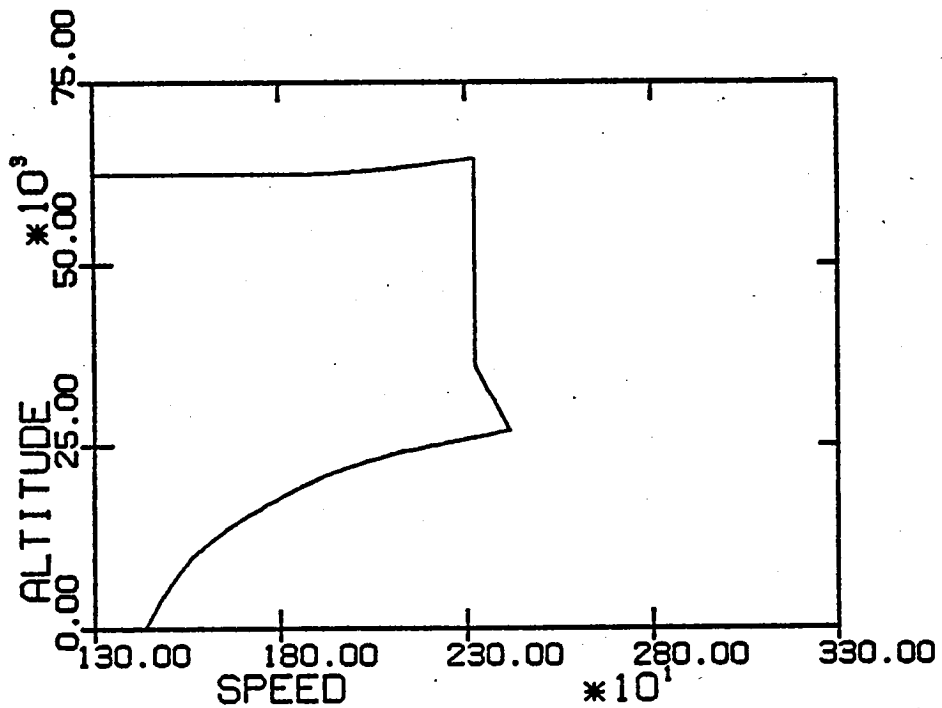


Fig. 2.8Envelope with Mach Limit, Smooth Data

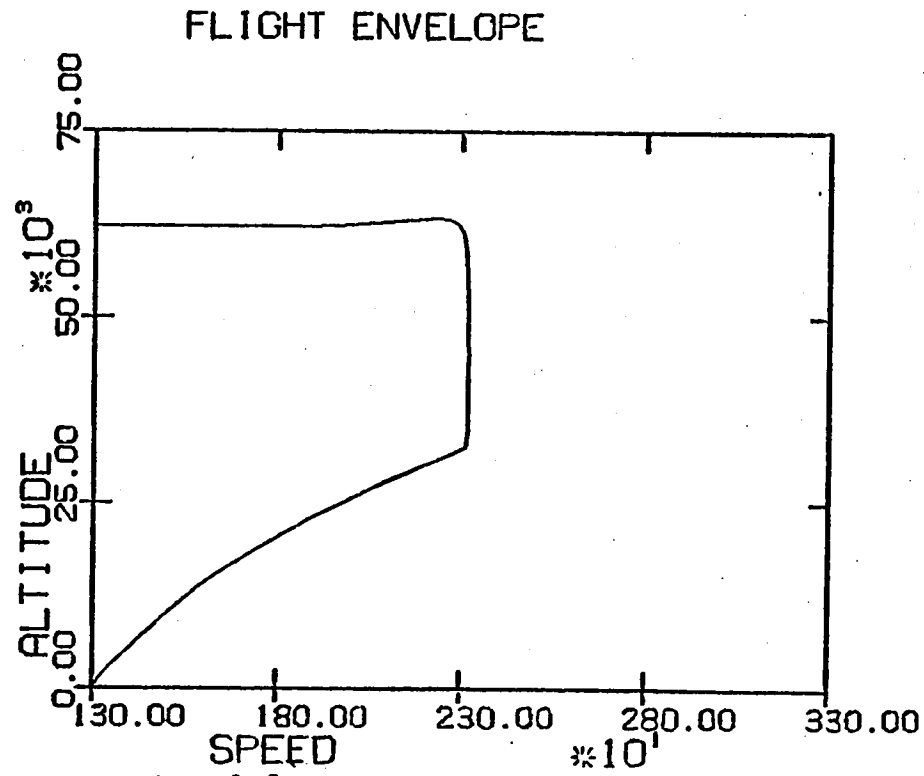


Fig. 2.9Envelope with q and Mach Limits

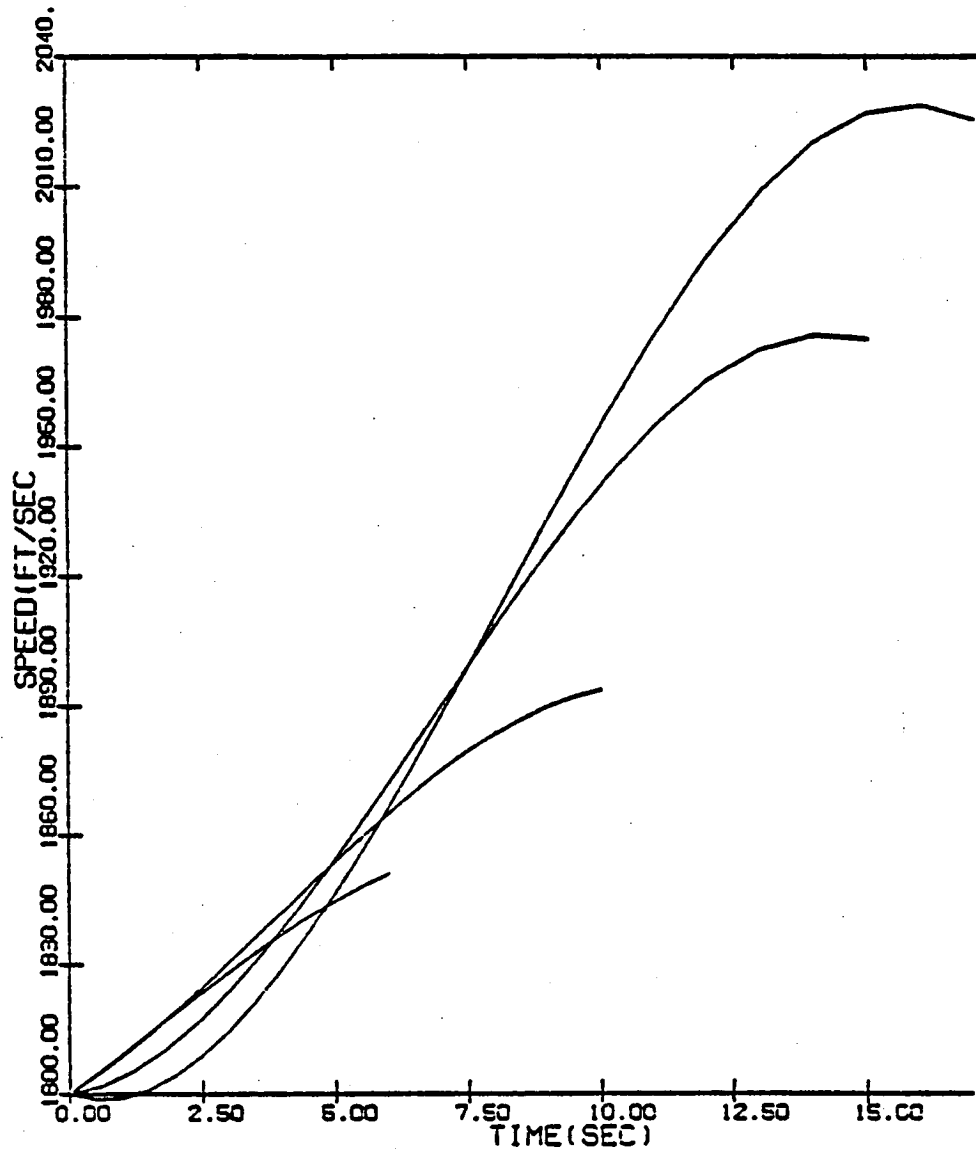


Fig. 2.10Speed vs Time

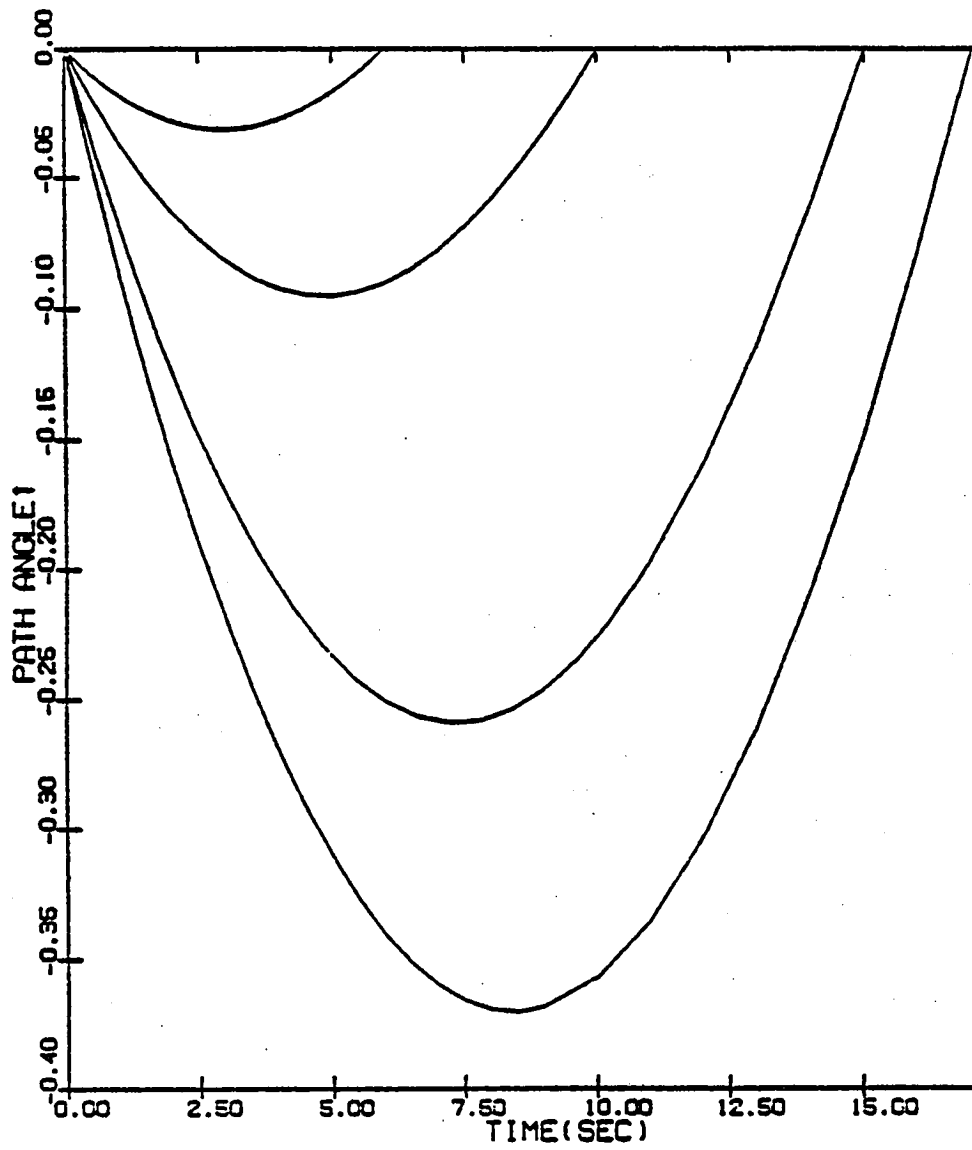


Fig. 2.11.....Path-Angle vs Time

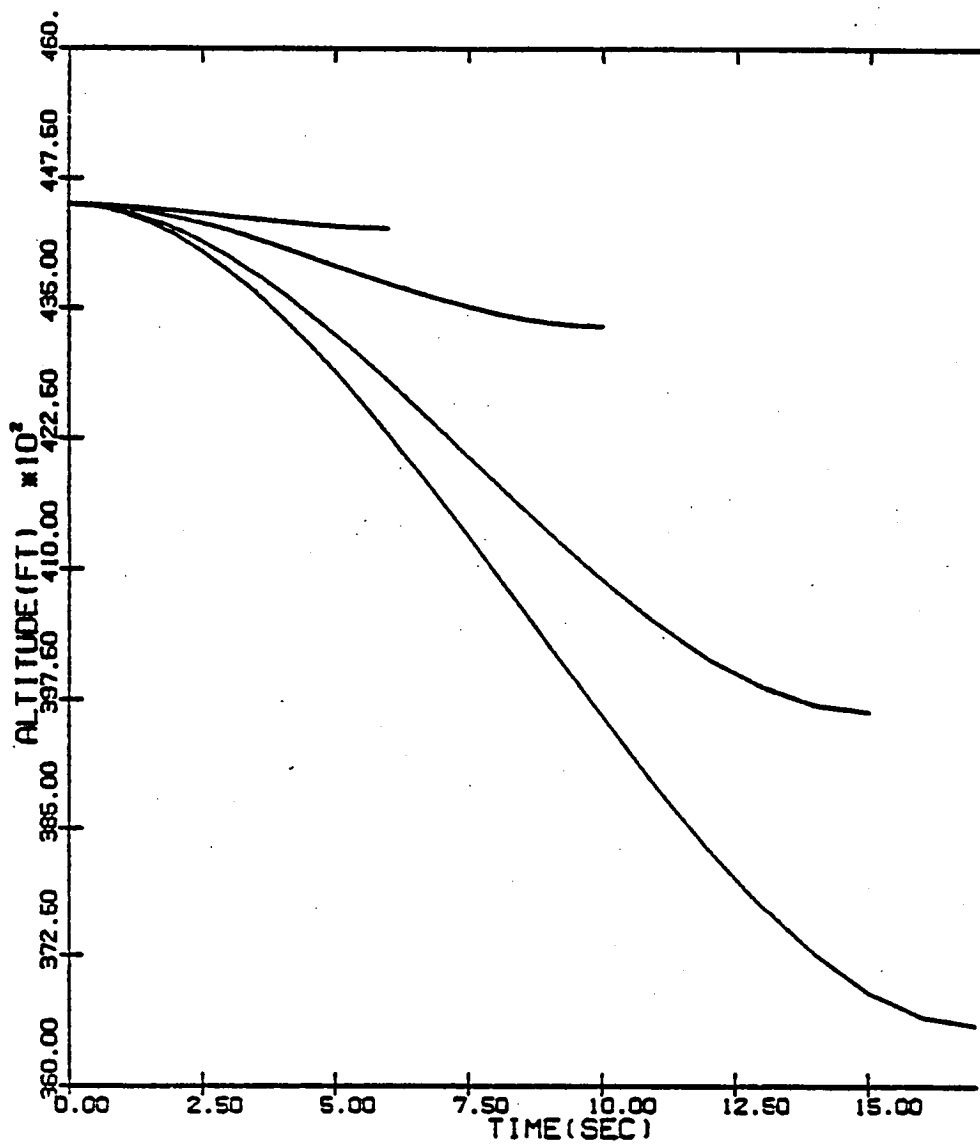


Fig. 2.12Altitude vs Time

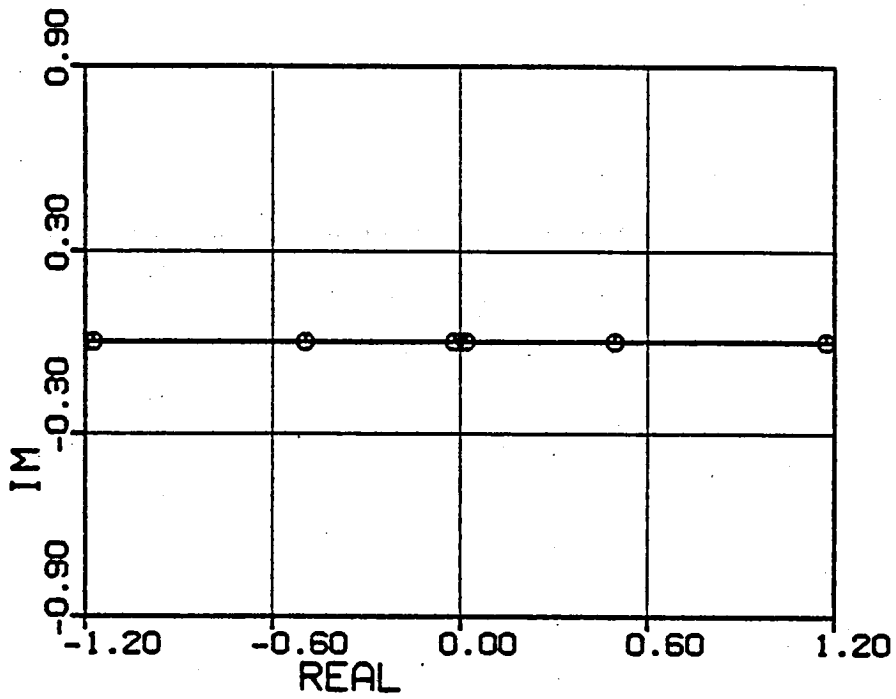


Fig. 2.13Eigenvalues at the Dash Point

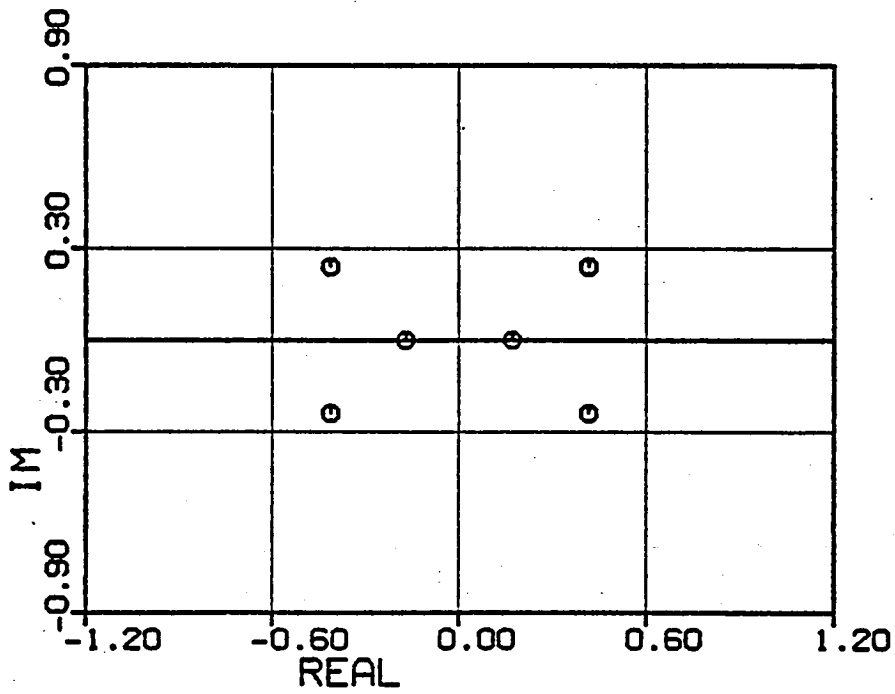
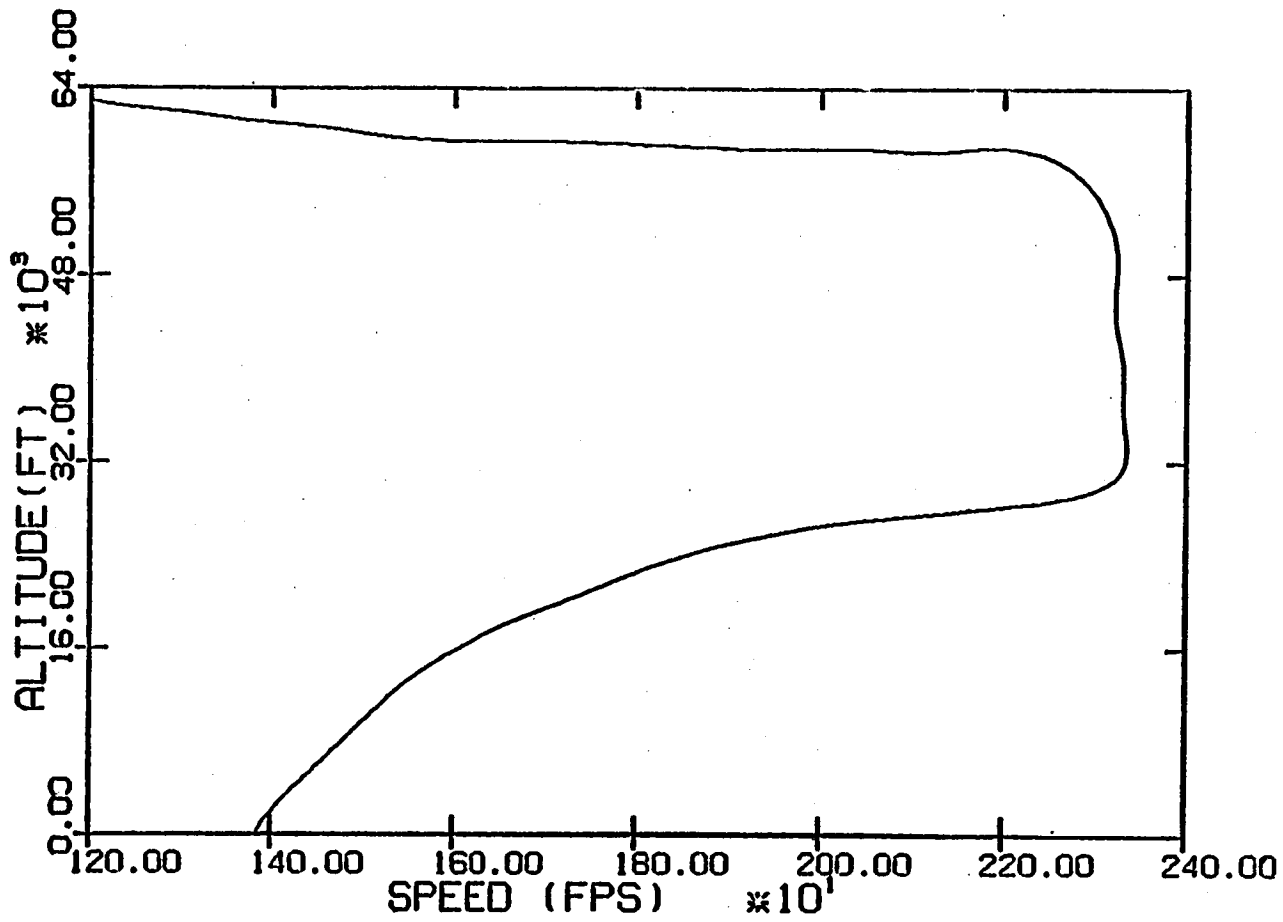


Fig. 2.14Eigenvalues at Reduced Throttle

Fig. 2.15 Flight Envelope Spline Data



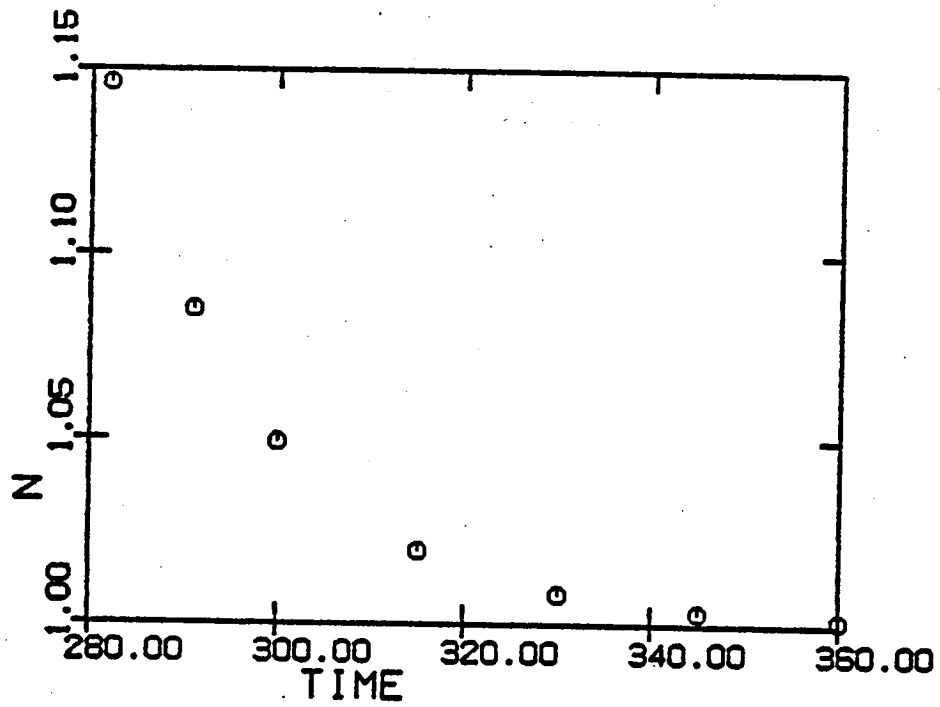


Fig. 2.17.....Final Load Factor

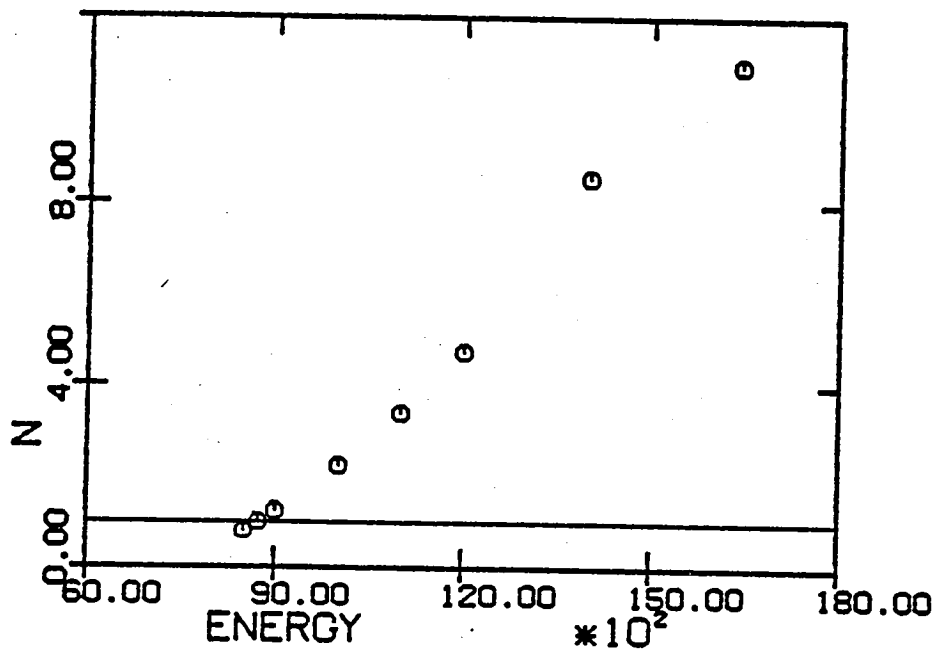
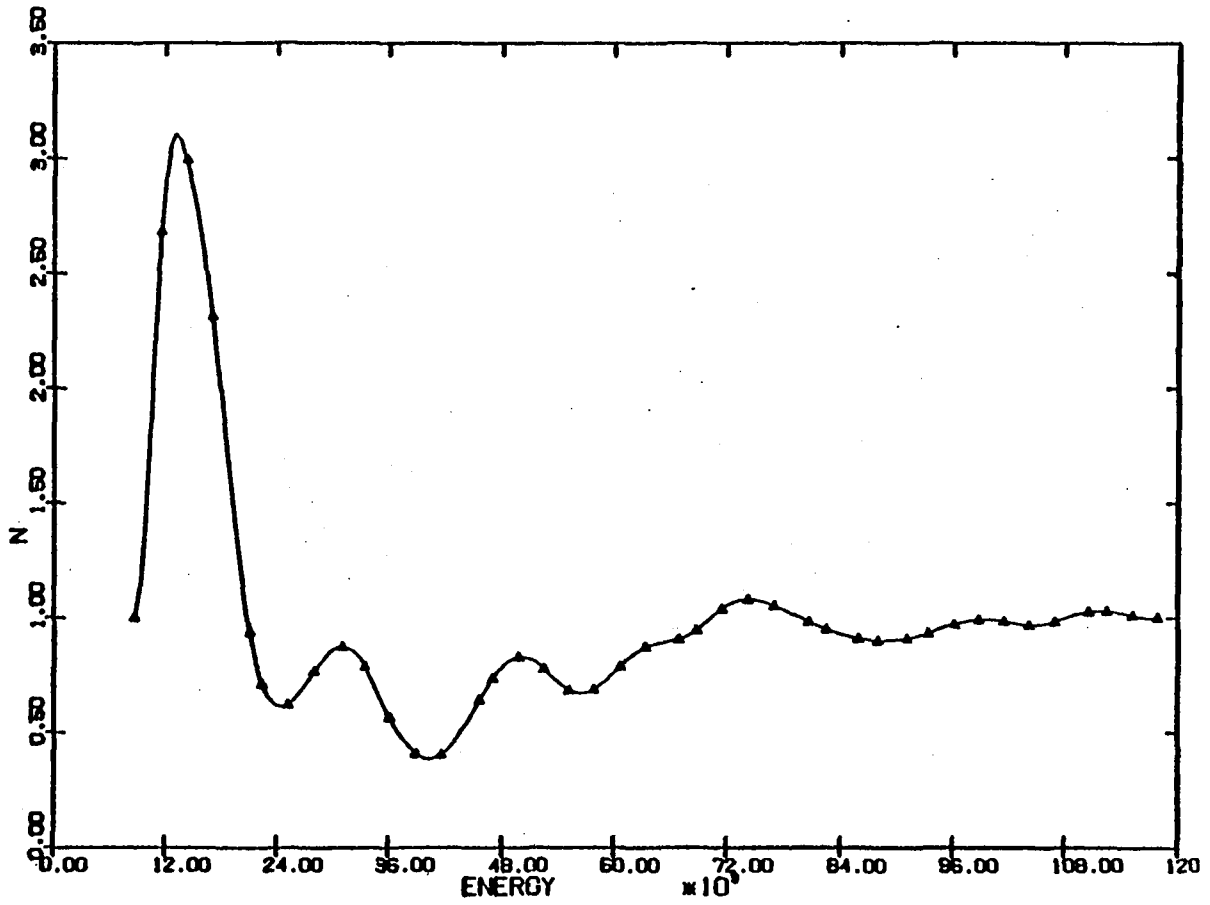


Fig. 2.16Initial Load Factor

Fig. 2.18....Load Factor vs Energy



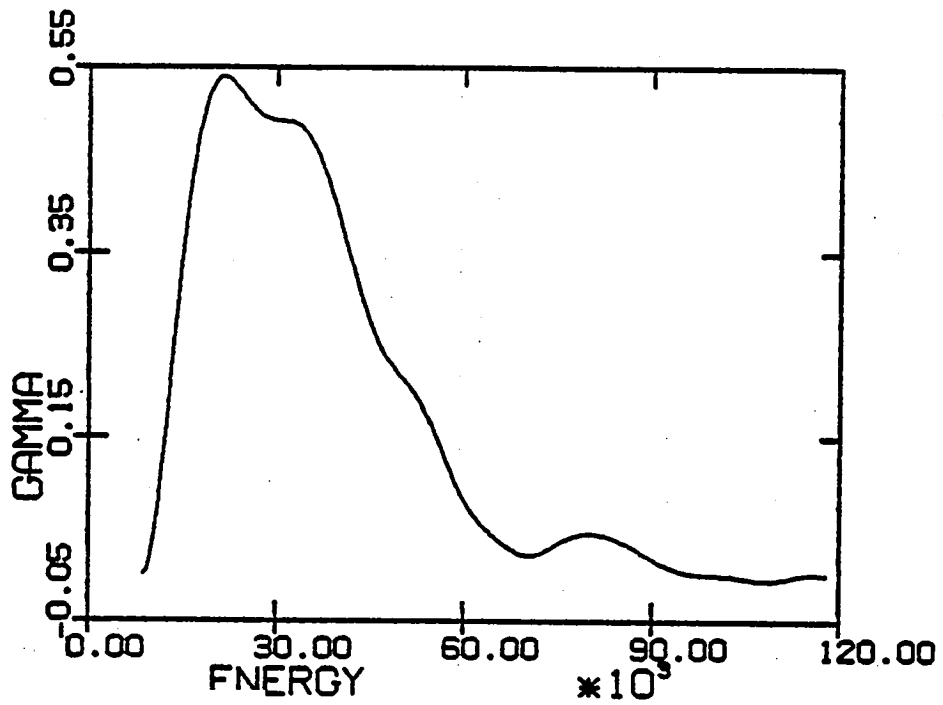


Fig. 2.19Path-Angle vs Energy

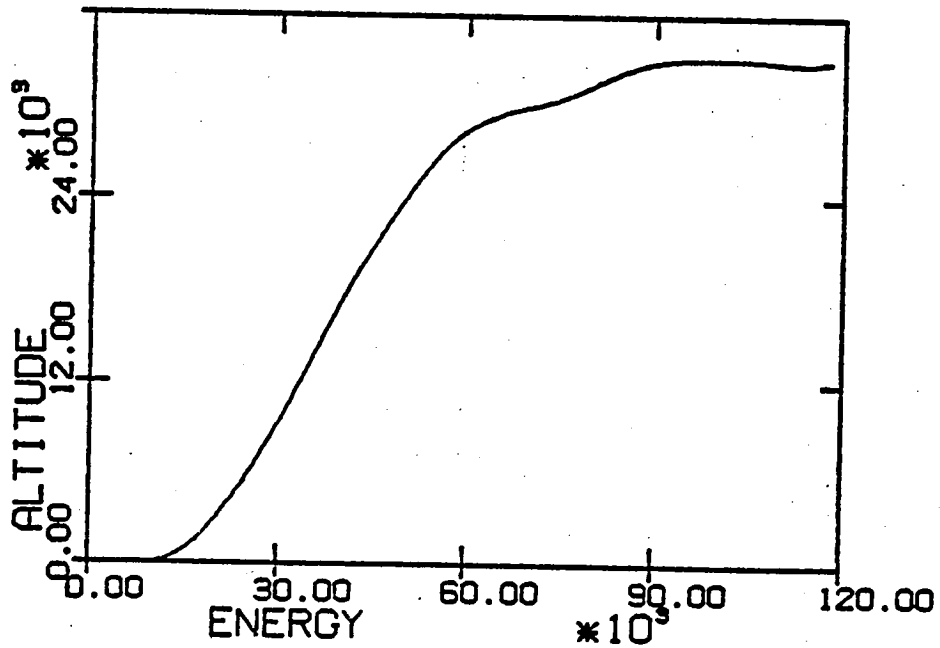


Fig. 2.20Altitude vs Energy

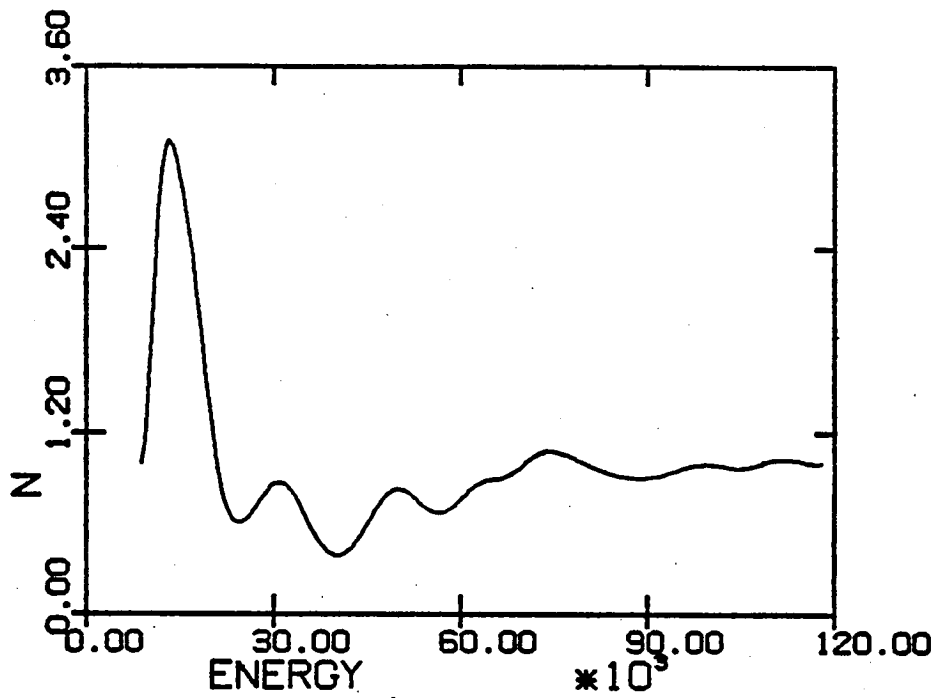


Fig. 2.21Load Factor vs Energy

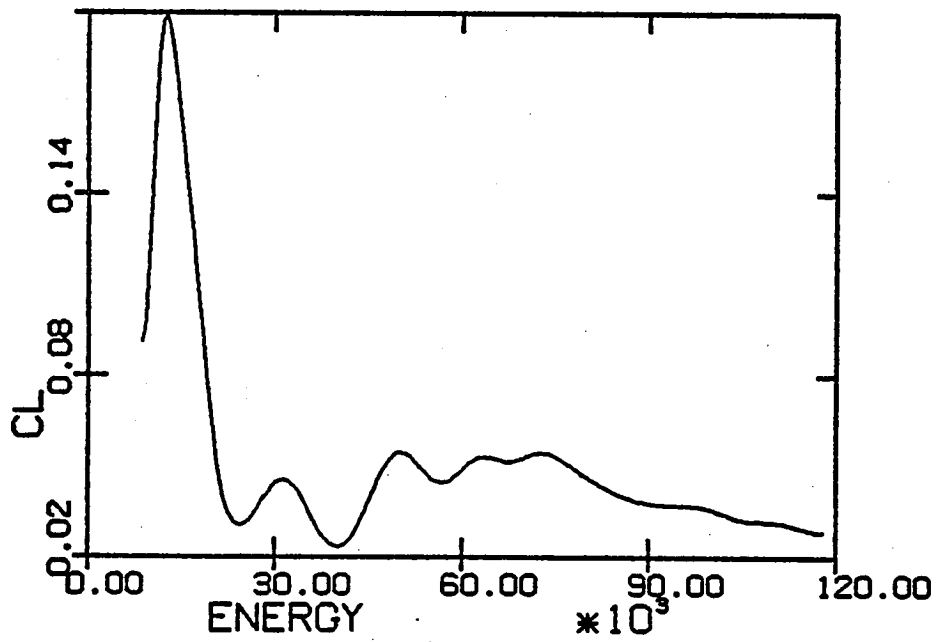


Fig. 2.22Lift Coefficient vs Energy

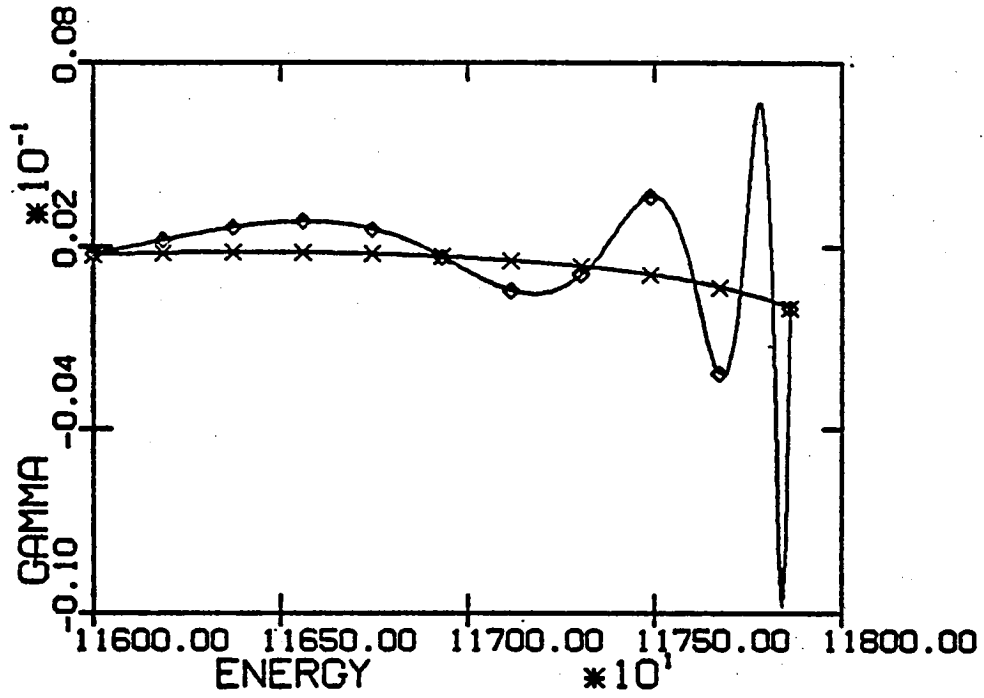


Fig. 2.23Path-Angle vs Energy 300,360 seconds

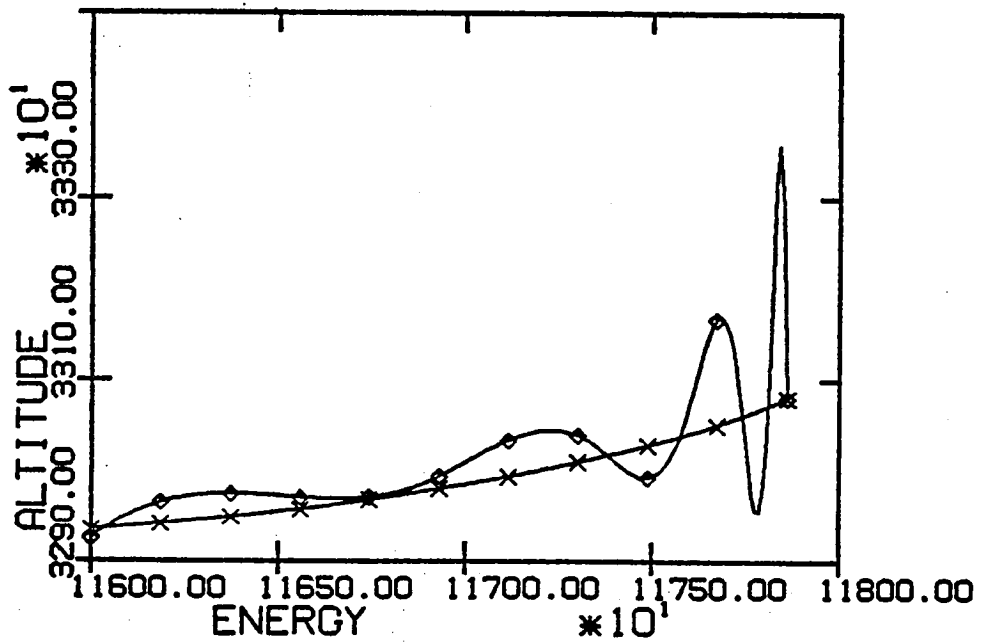


Fig. 2.24Altitude vs Energy 300,360 seconds

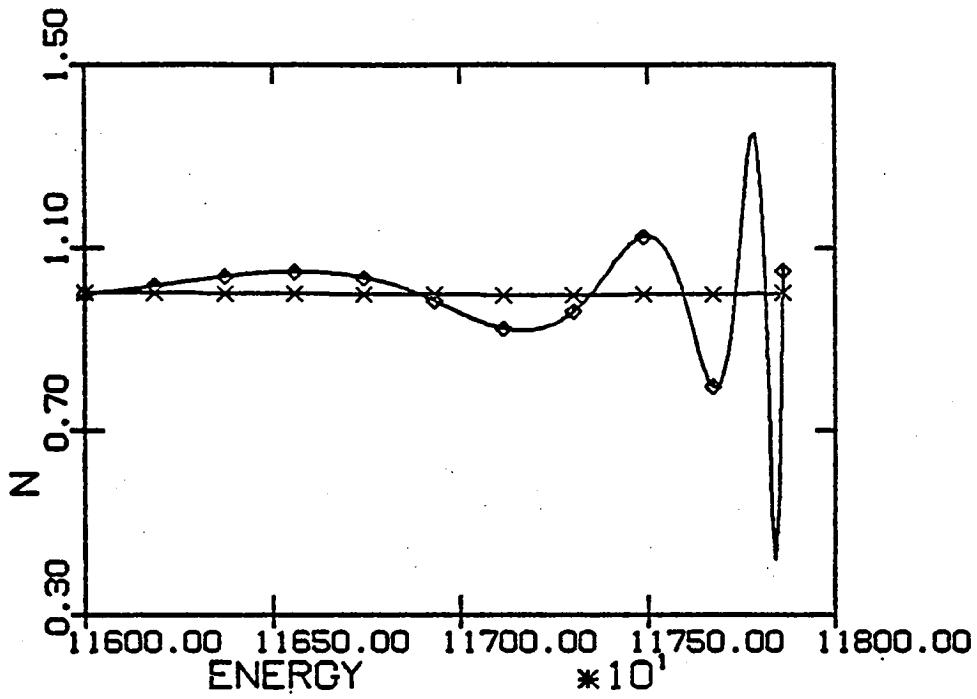


Fig. 2.25.....Load Factor vs Energy 300,360 seconds

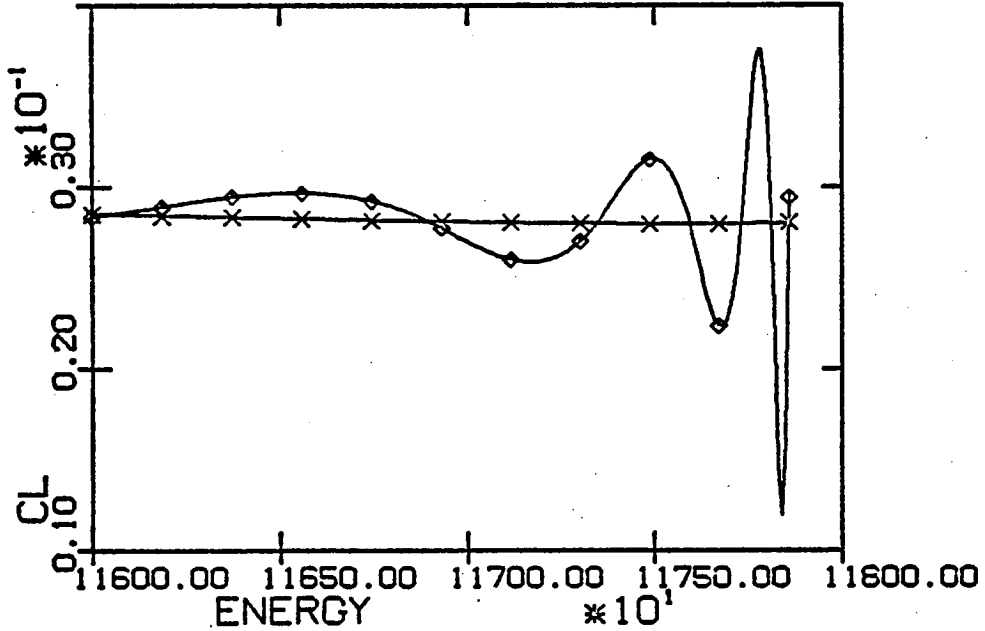


Fig. 2.26.....Lift Coefficient vs Energy 300,360 seconds

Fig. 2.27Range-Energy-Climb and Point Mass Solution

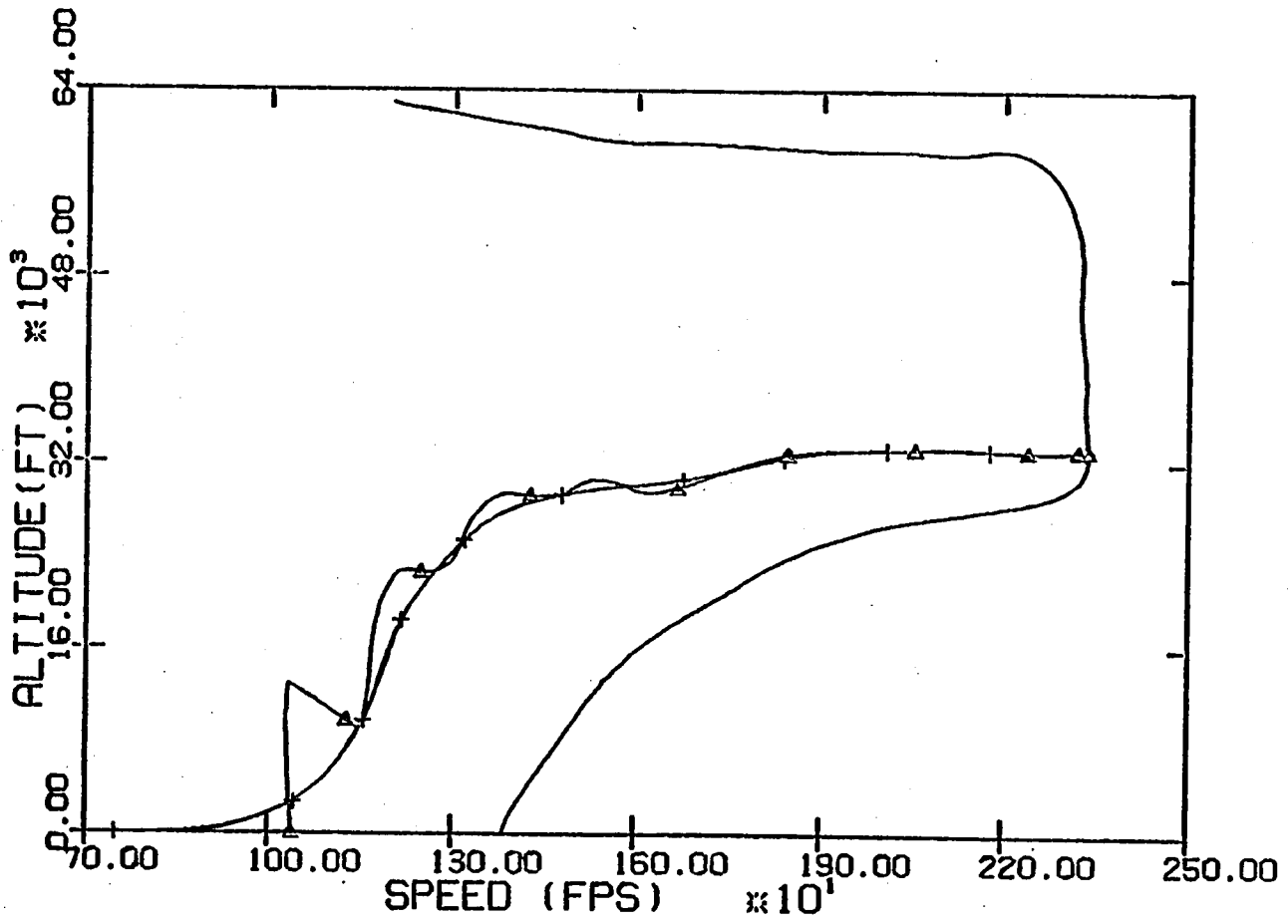


Fig. 2.28Altitude Gain vs Energy

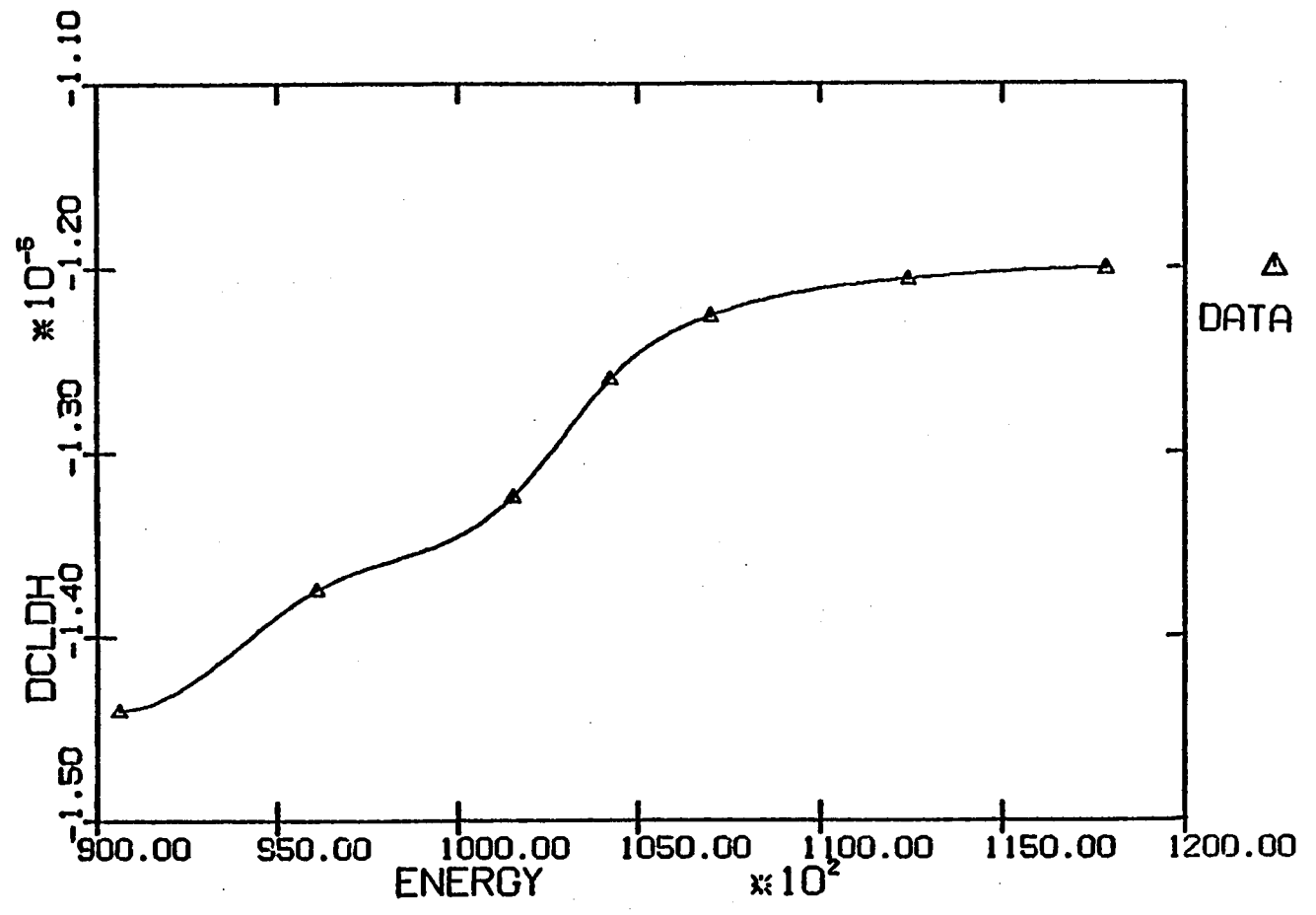


Fig. 2.29.....Path-Angle Gain vs Energy

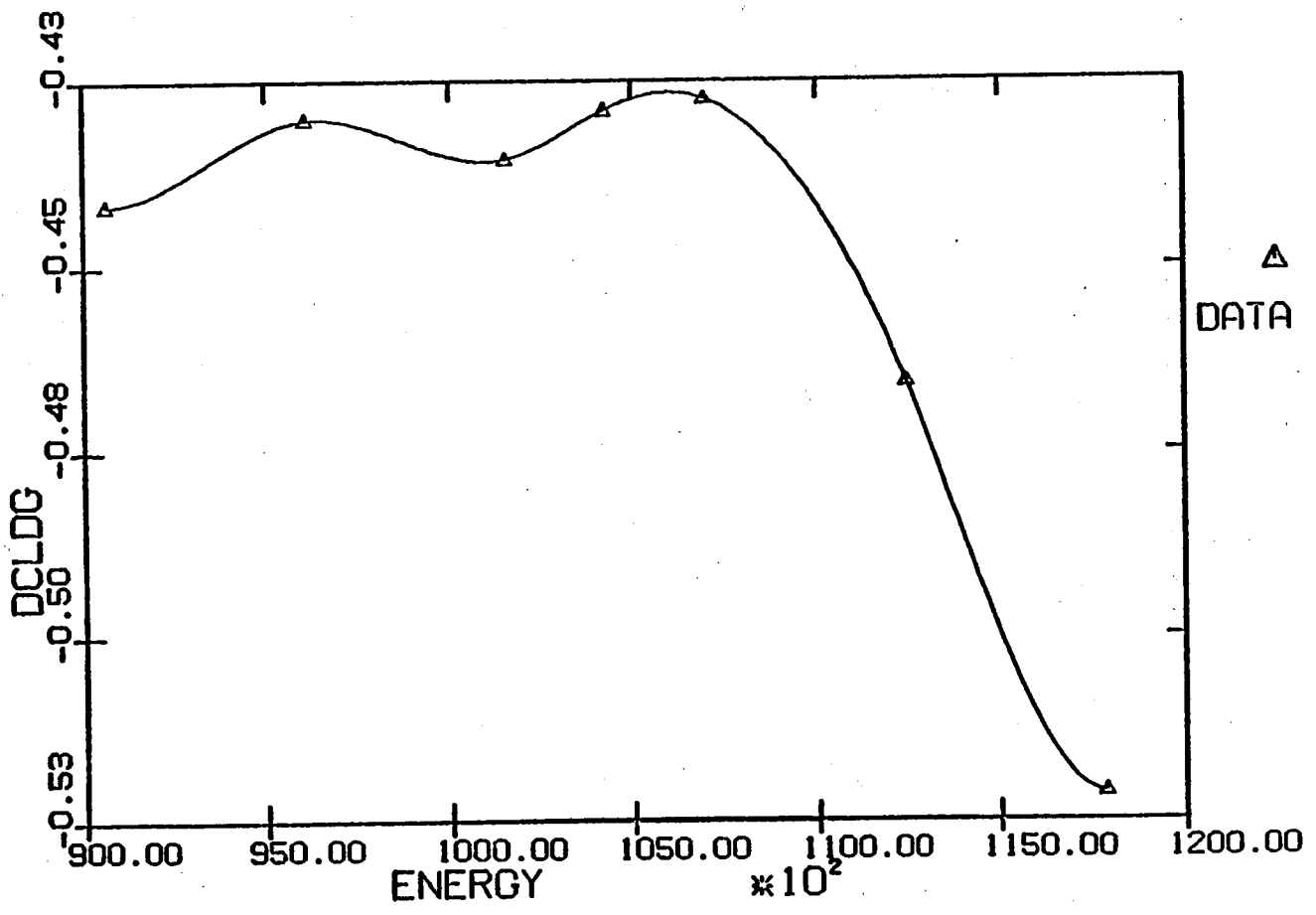


Fig. 2.30 Altitude Gain vs Energy

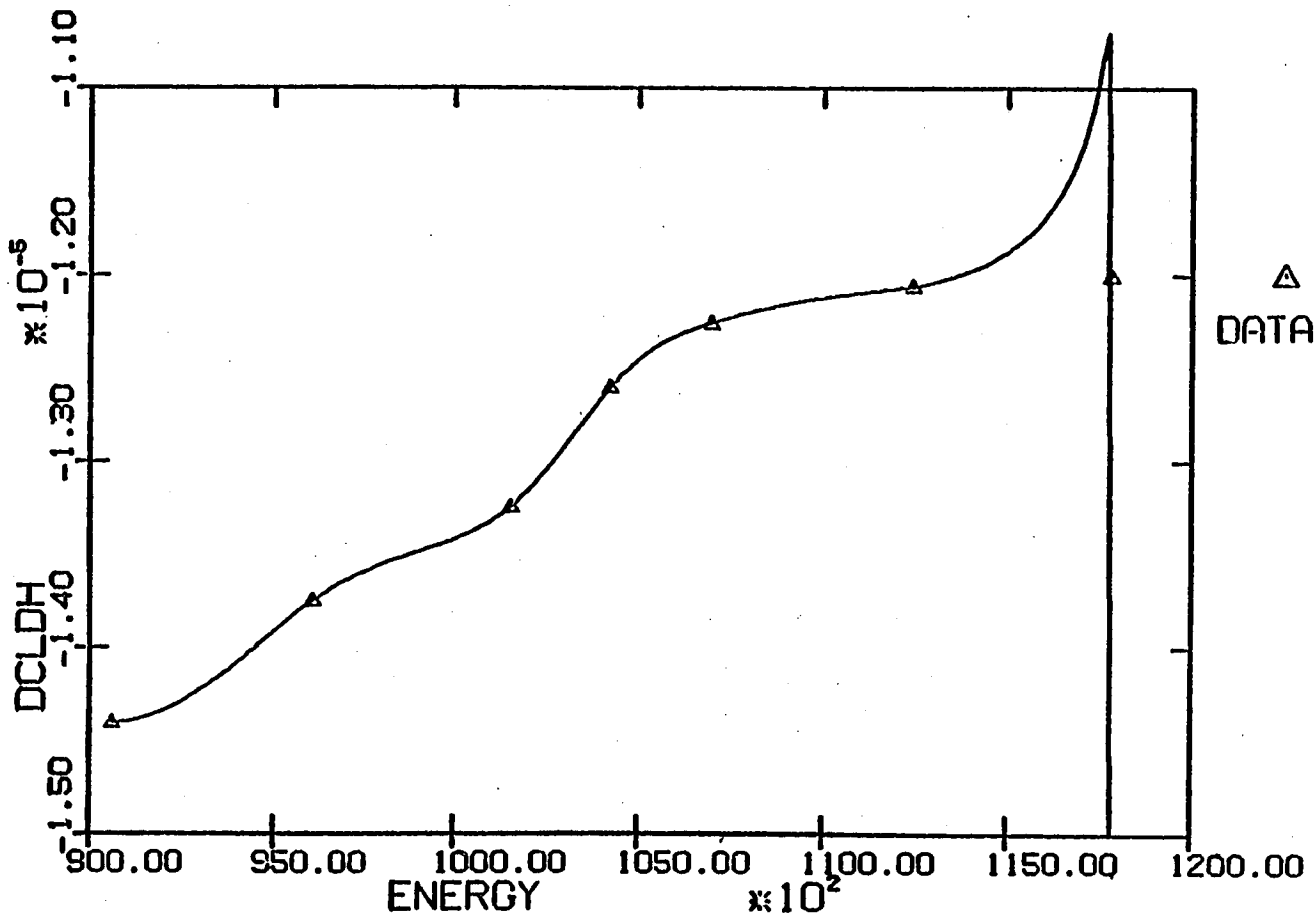


Fig. 2.31 Path-angle Gain vs Energy

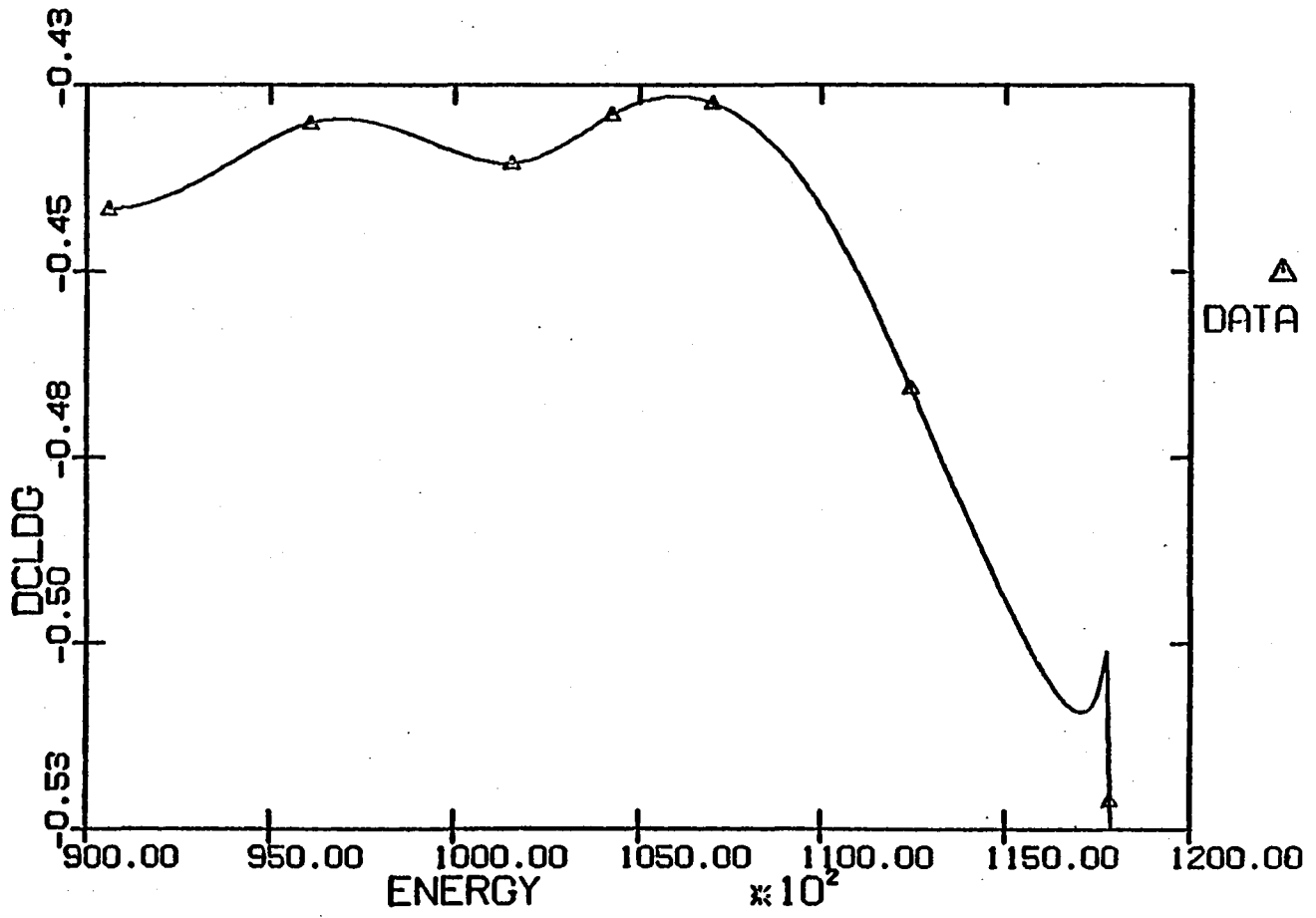


Fig. 2.32Altitude Gain vs Energy

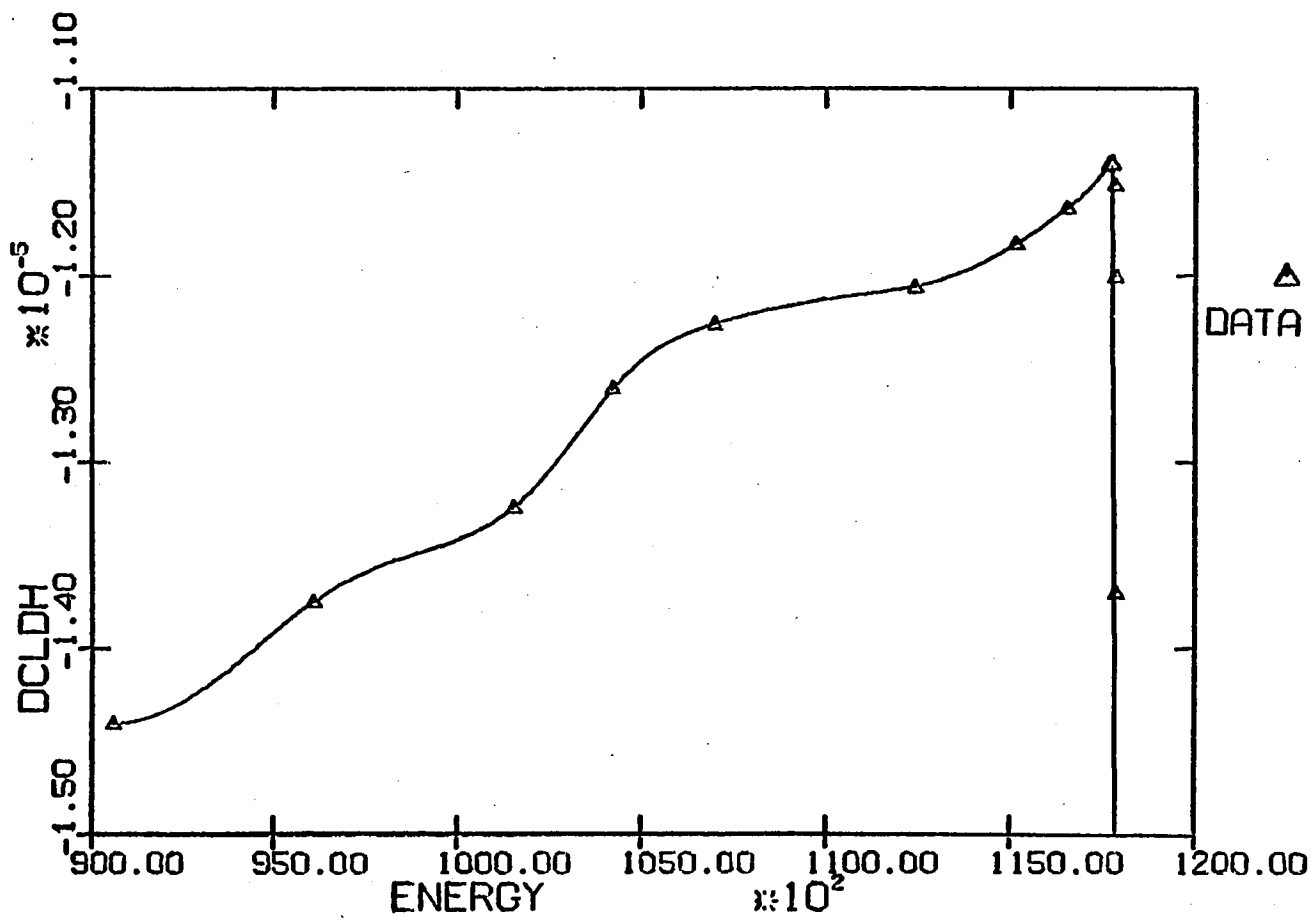


Fig. 2.33 Path-Angle Gain vs Energy

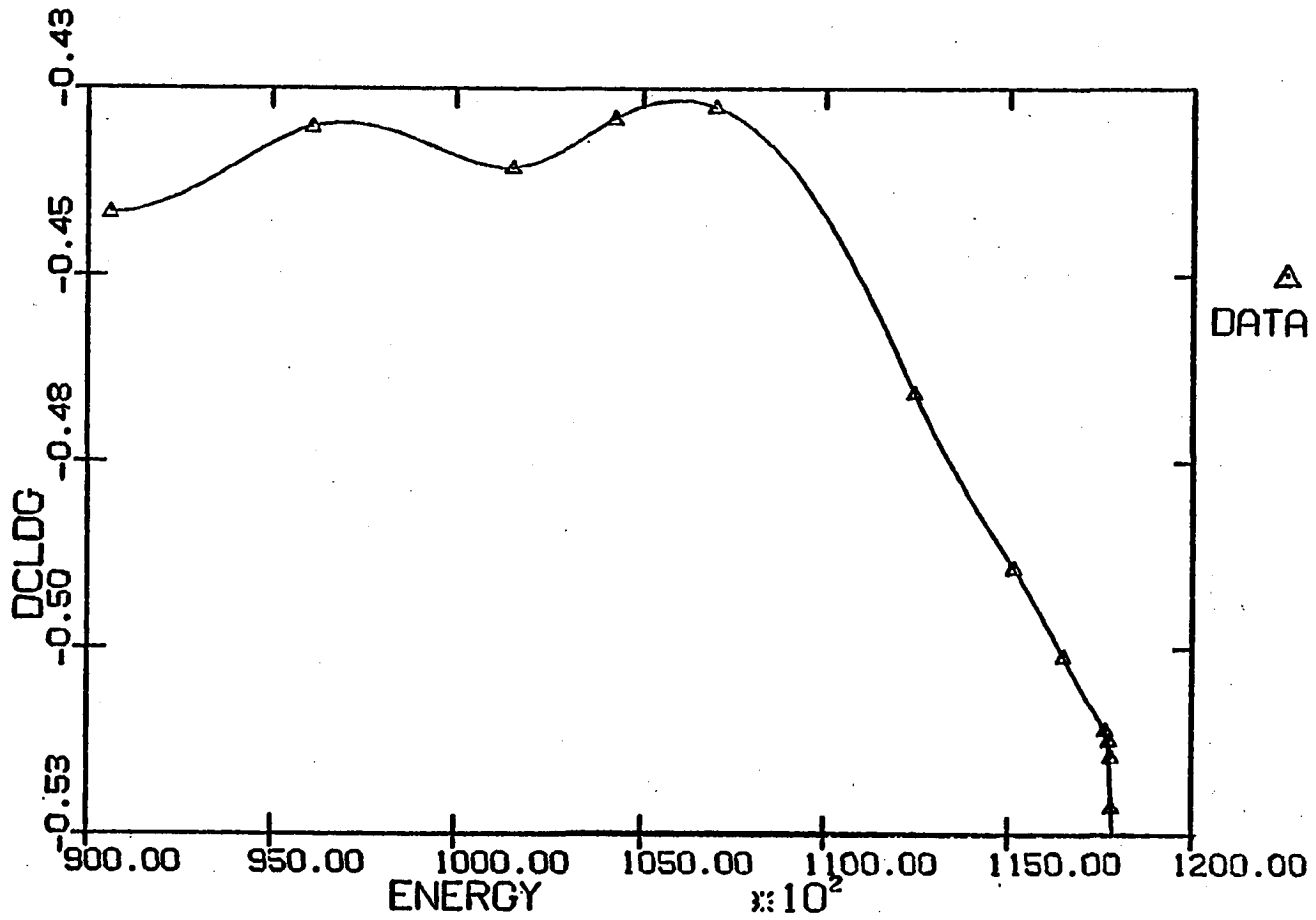


Fig. 2.34Altitude Gain vs Log(E)

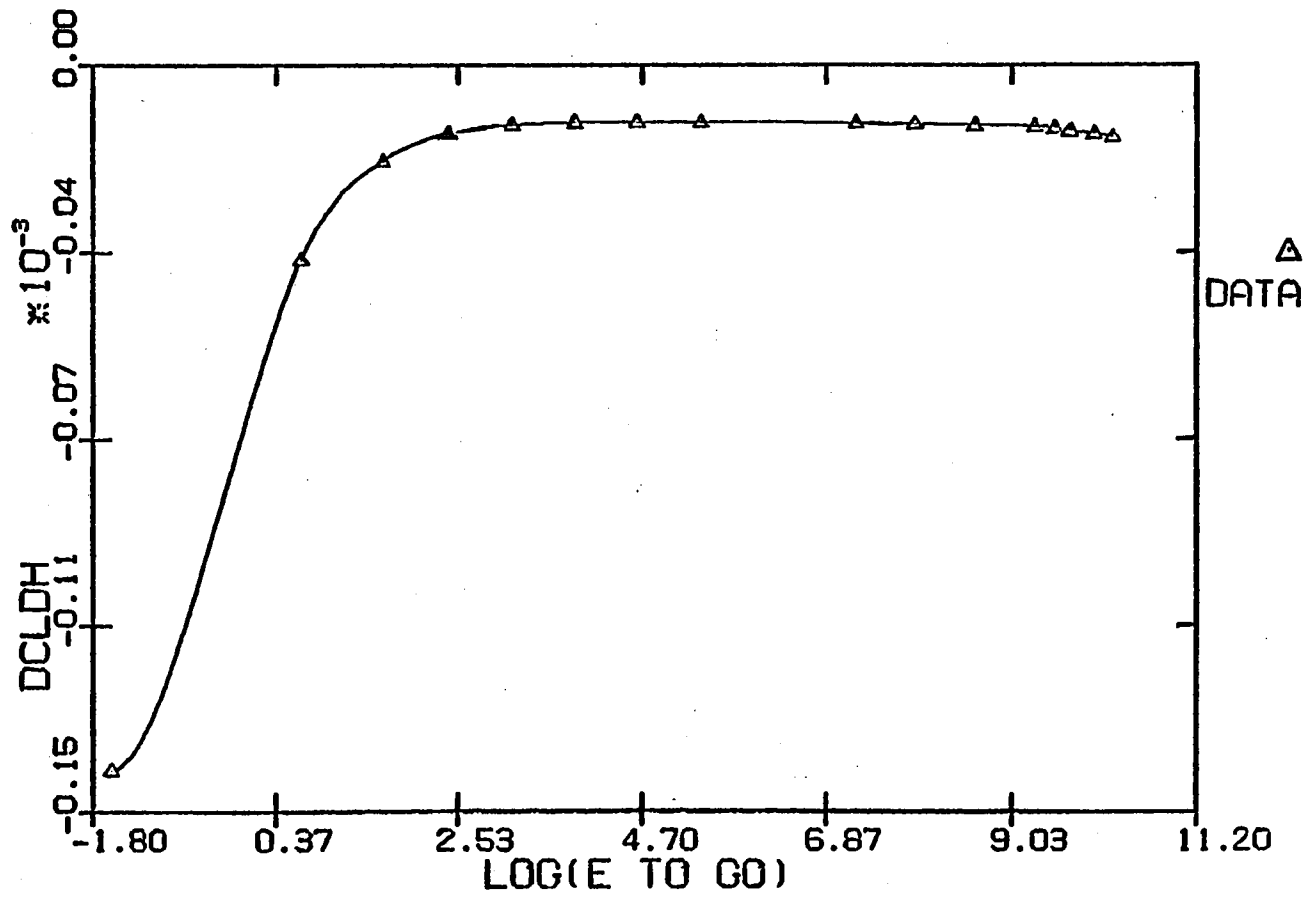


Fig. 2.35 Path-Angle Gain vs Log(E)

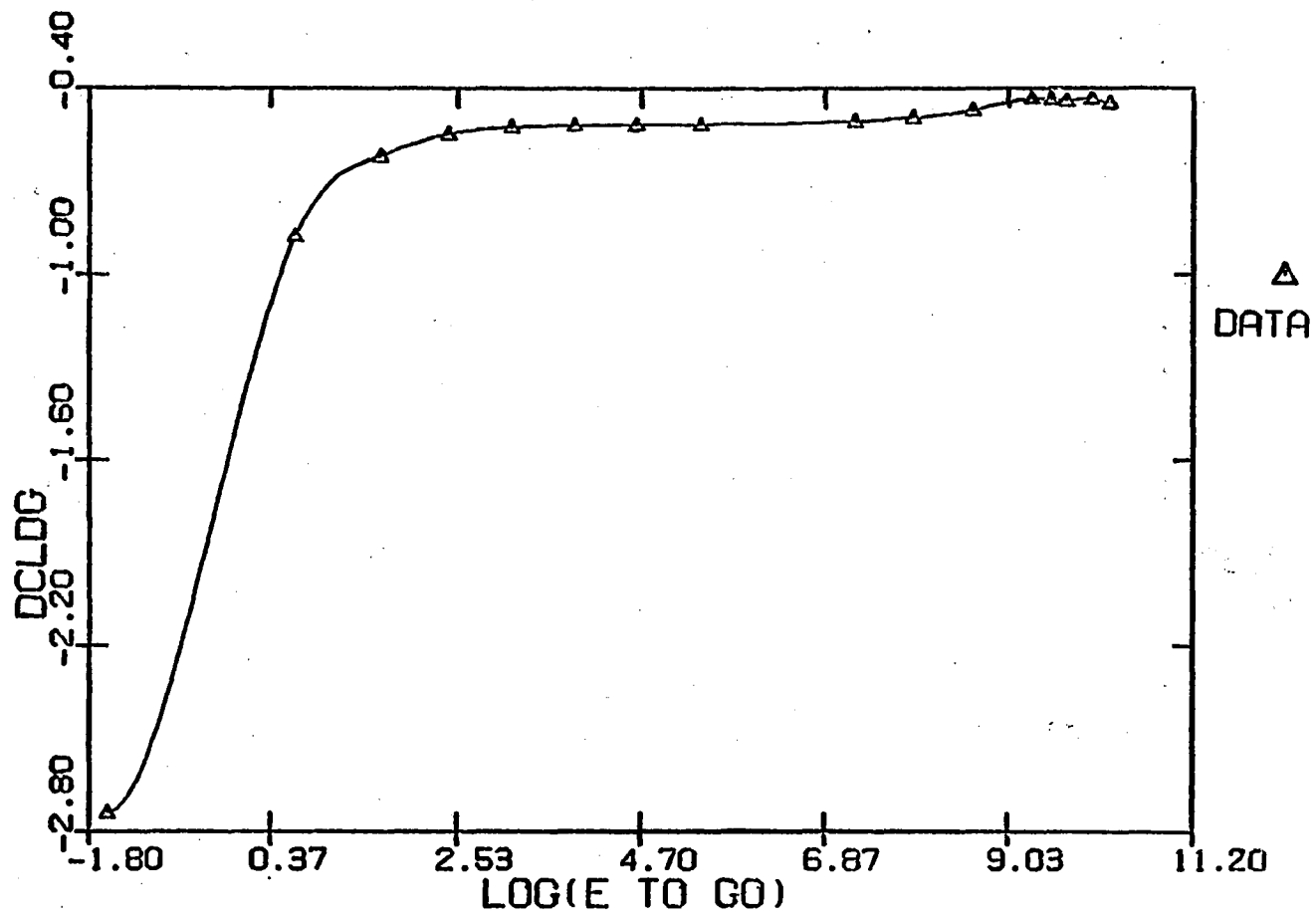
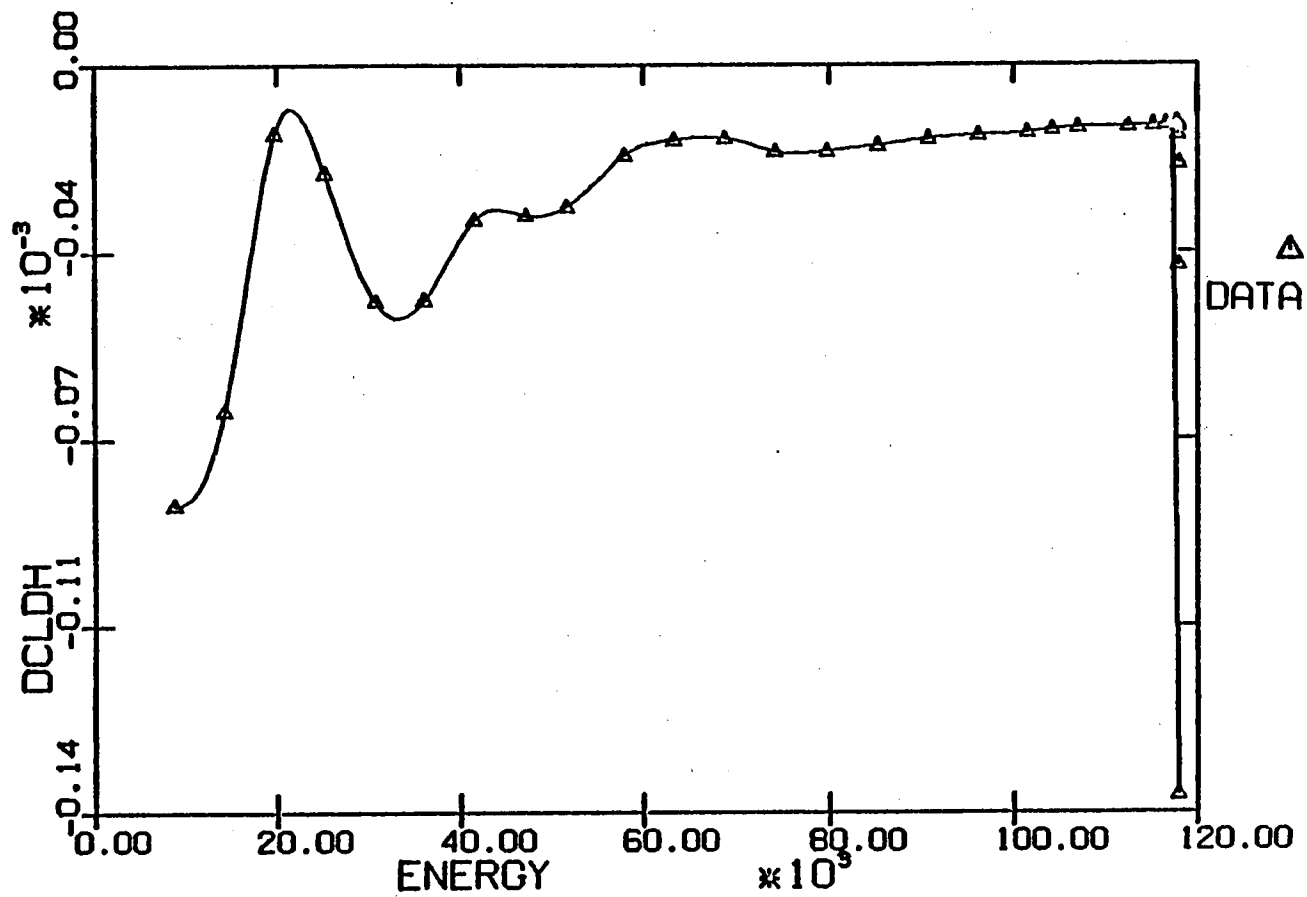


Fig. 2.36.....Altitude Gain vs Energy



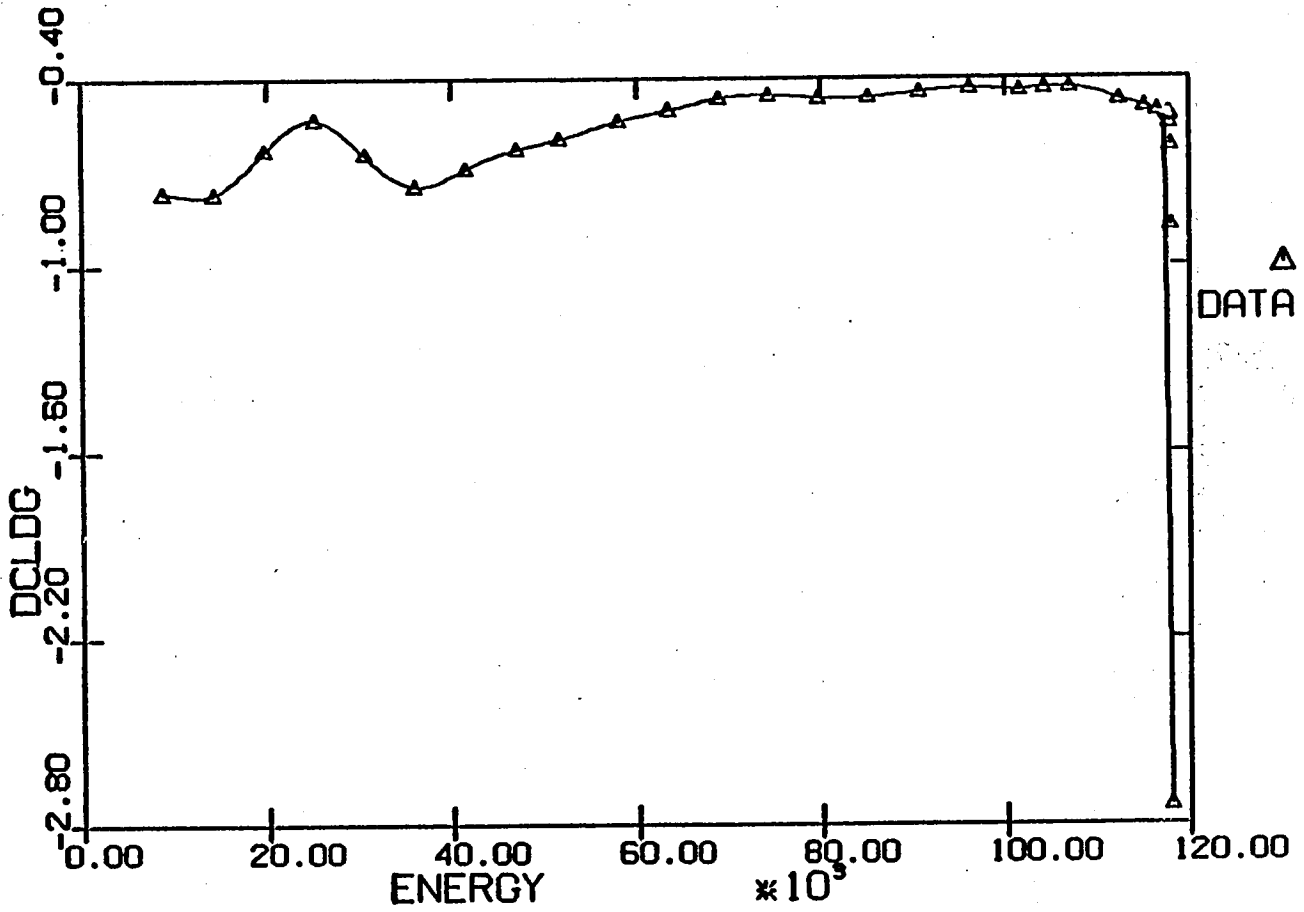


Fig. 2.37Path-Angle vs Energy

Fig. 2.38Altitude Gain vs Log(E)

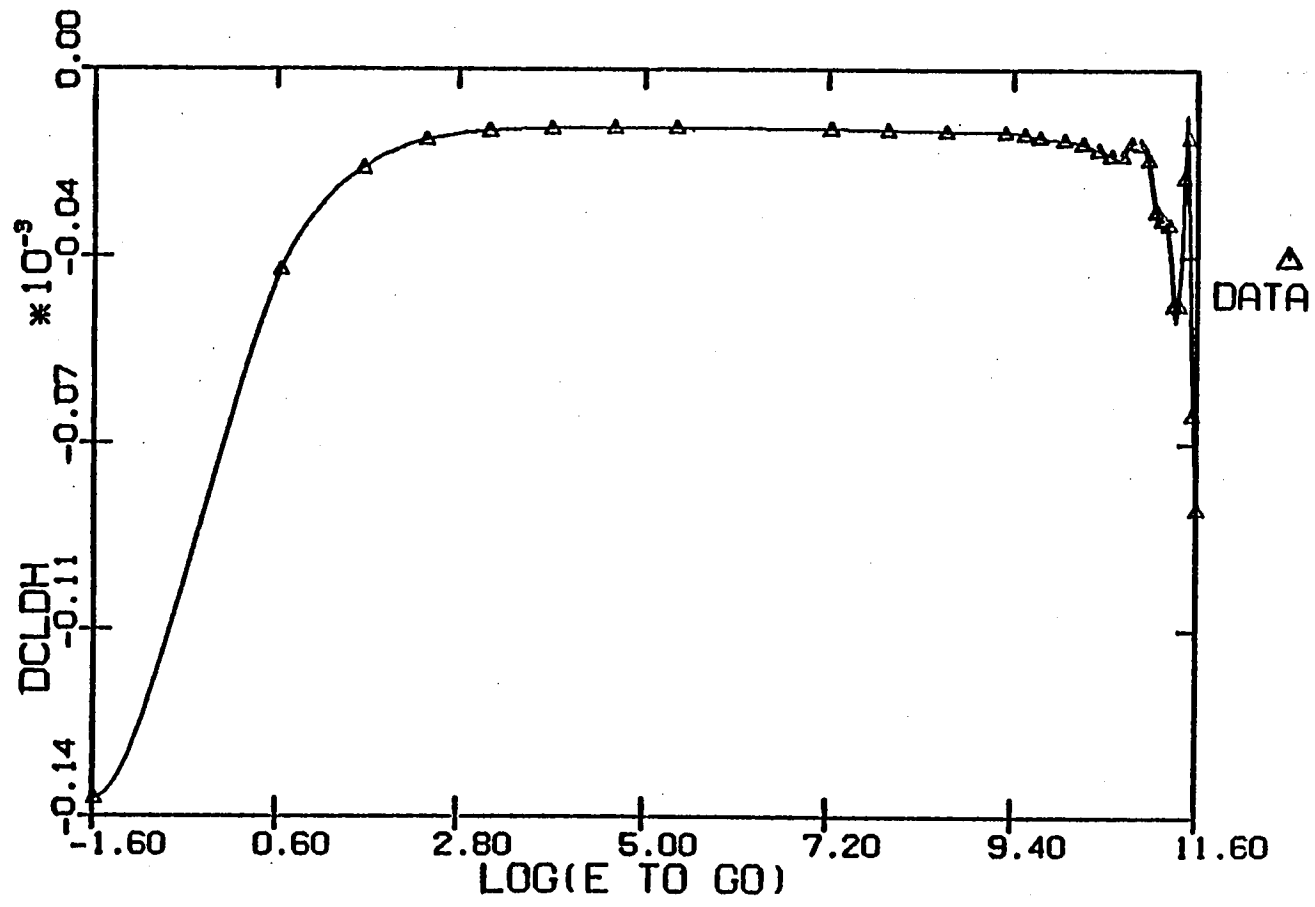


Fig. 2.39.....Path-Angle Gain vs Log(E)

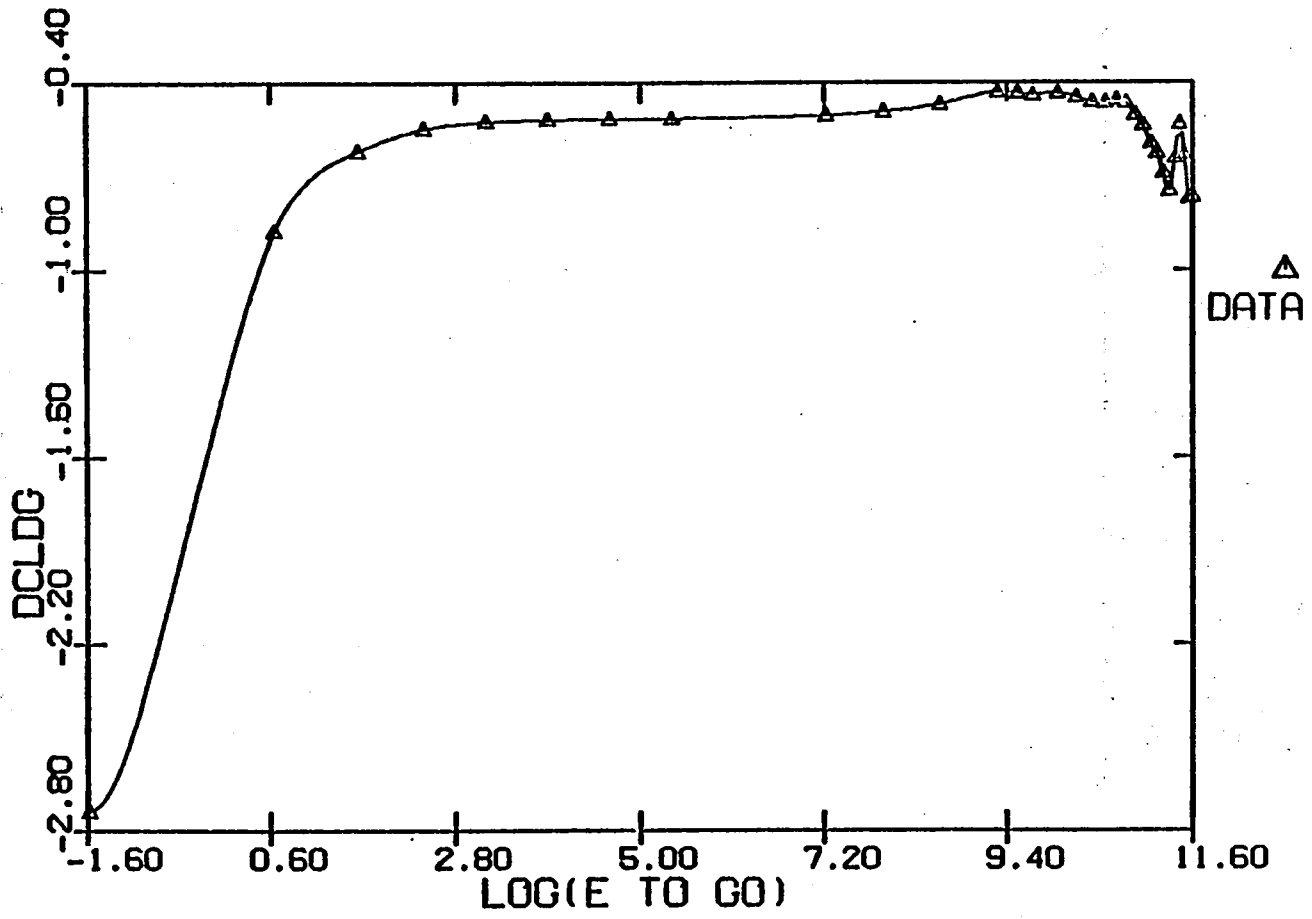
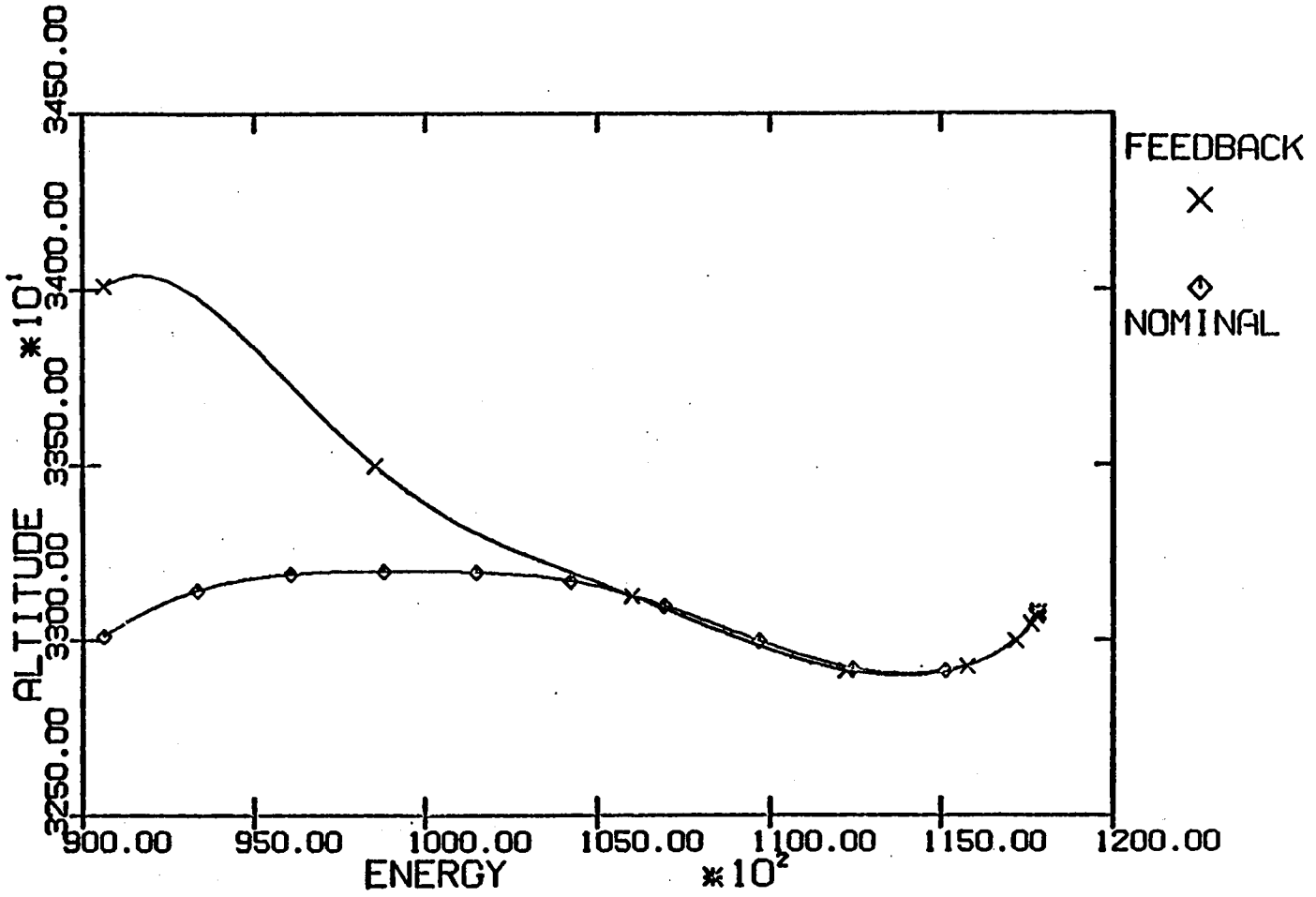


Fig. 2.40.....Altitude vs Energy, 1000 ft above



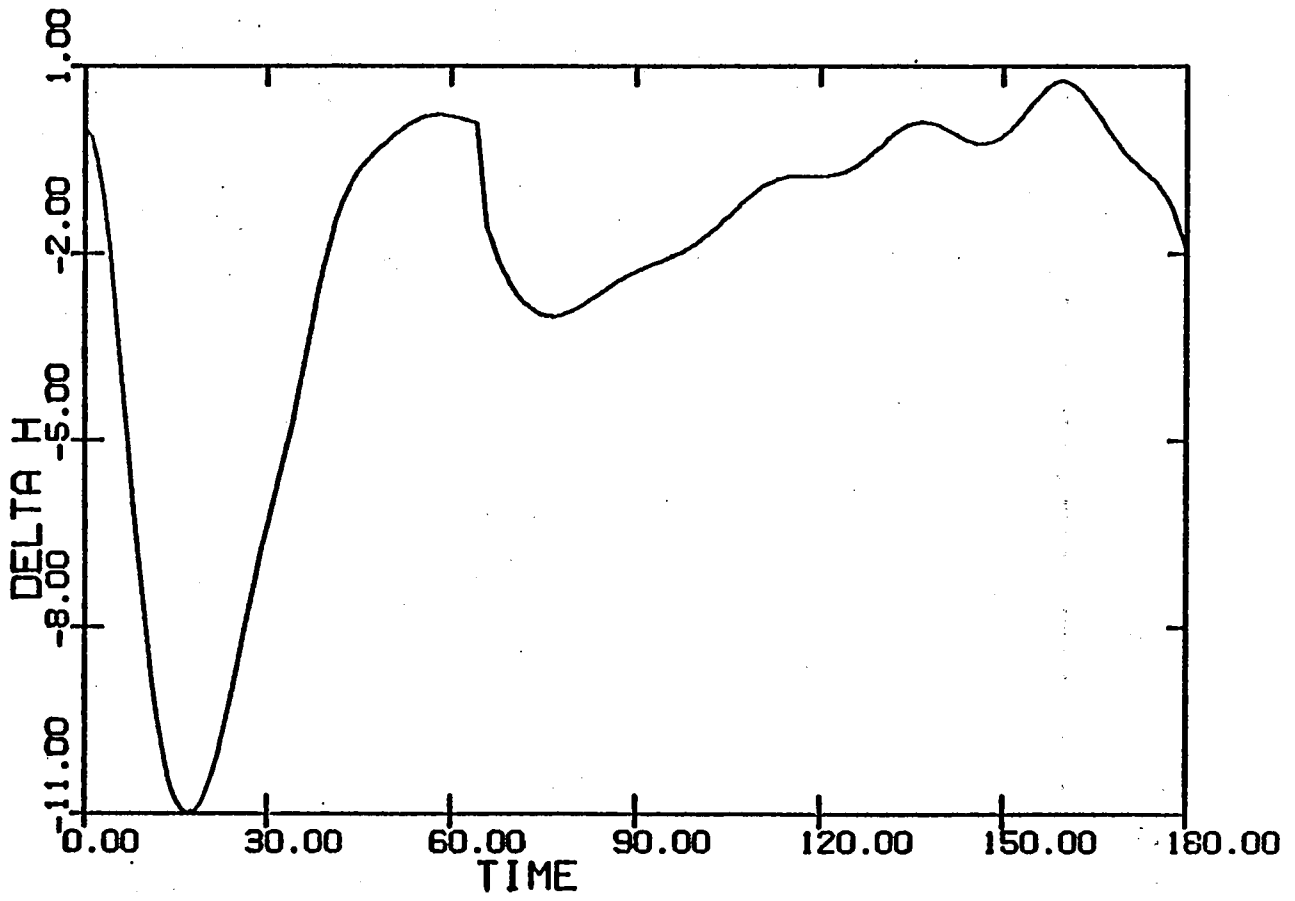


Fig. 2.41Altitude Error vs Time

Fig. 2.42.....Altitude vs Energy, 5000 ft above

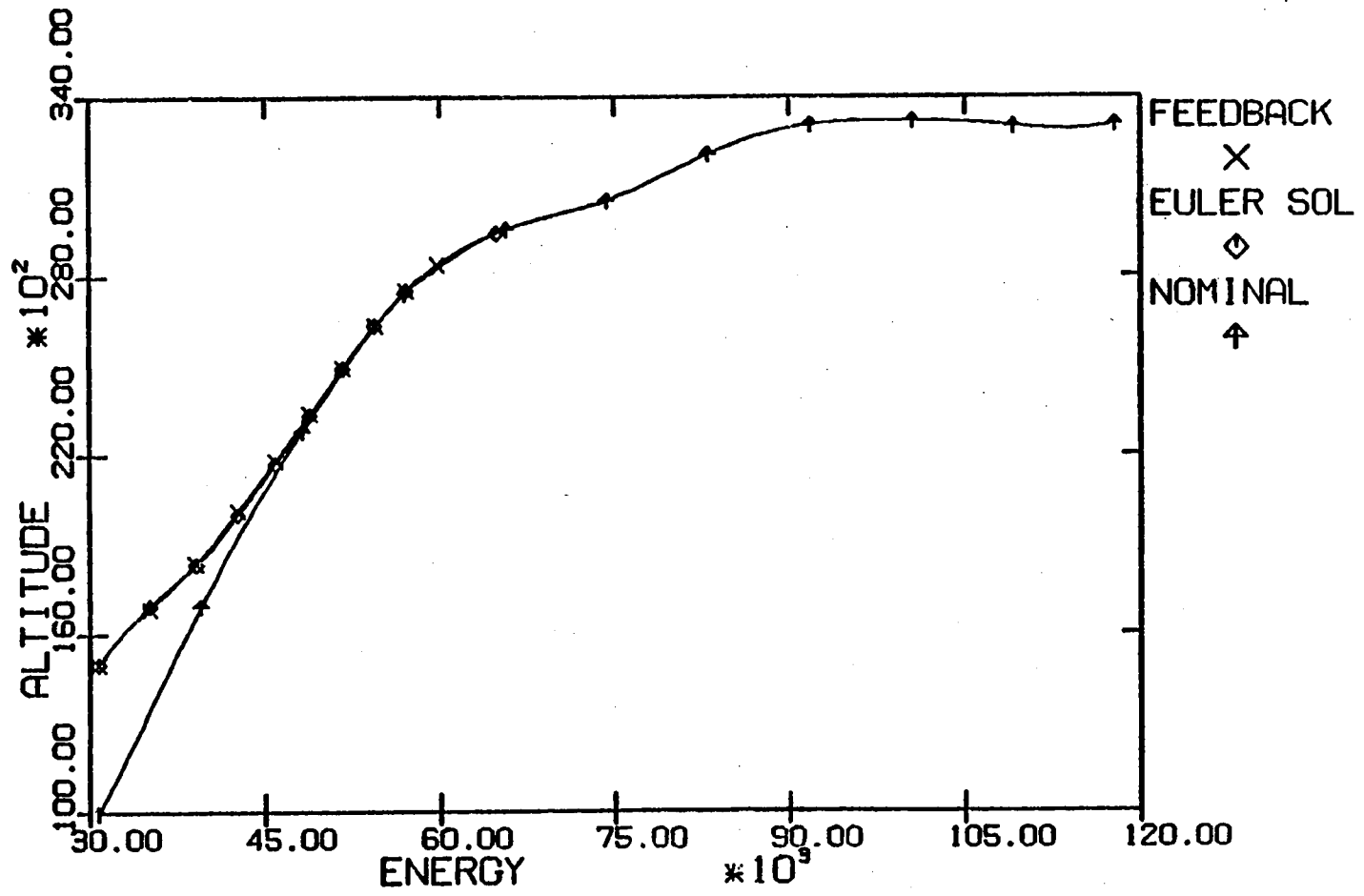


Fig. 2.43.....Altitude vs Energy, 10000 ft above

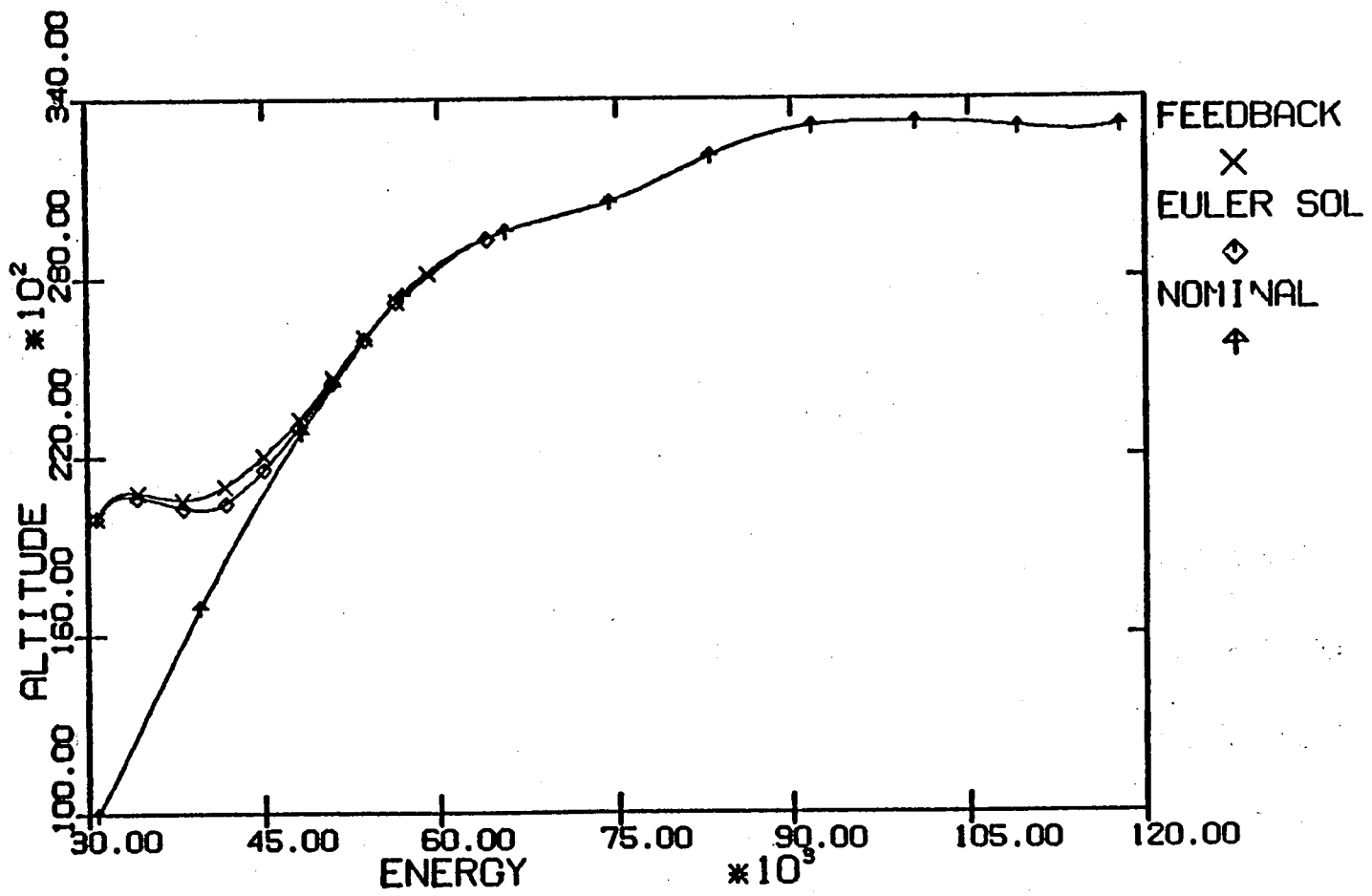


Fig. 2.44.....Altitude vs Energy, 15000 ft above

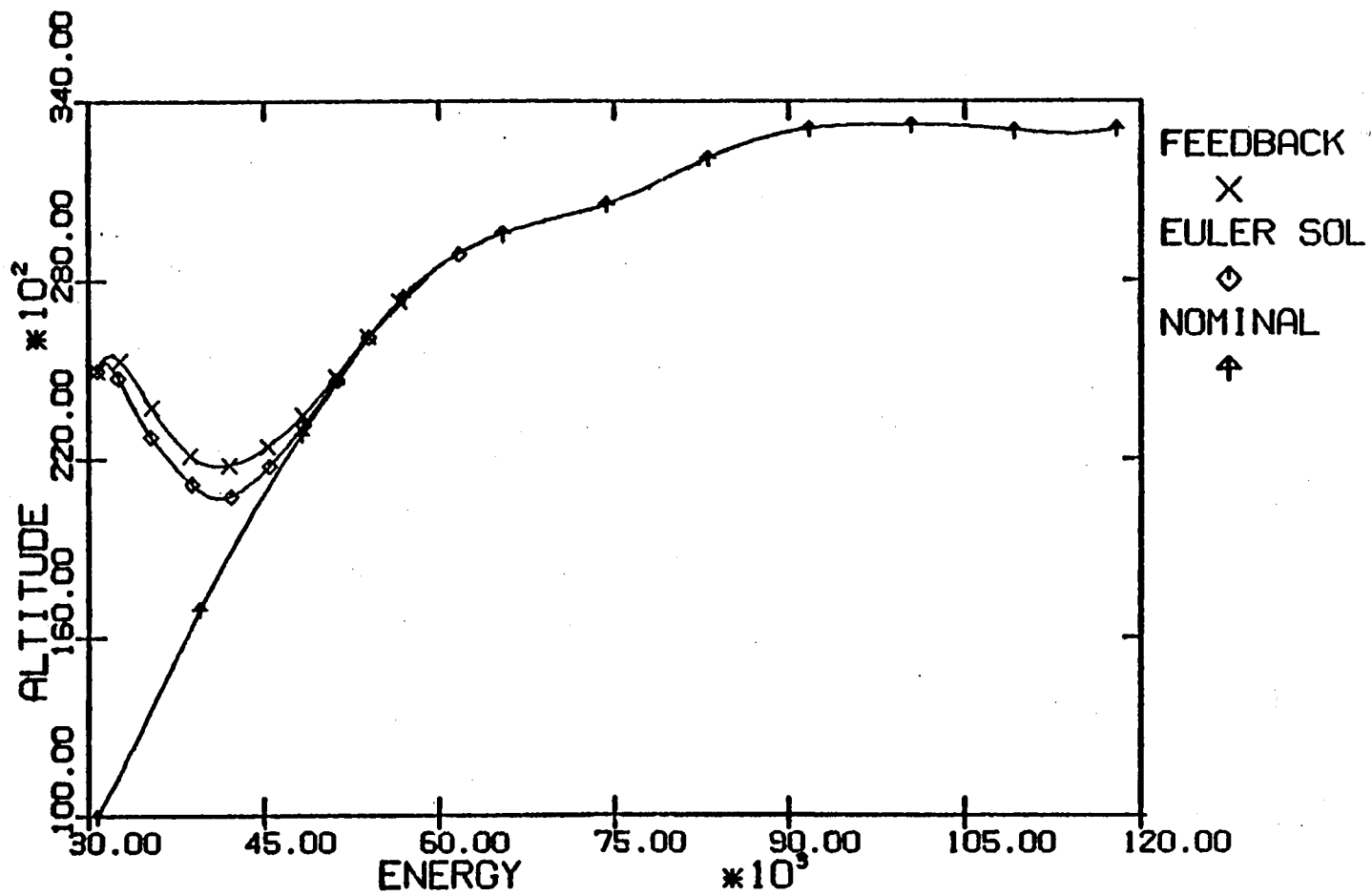


Fig. 2.45.....Altitude vs Energy, 5000 ft below

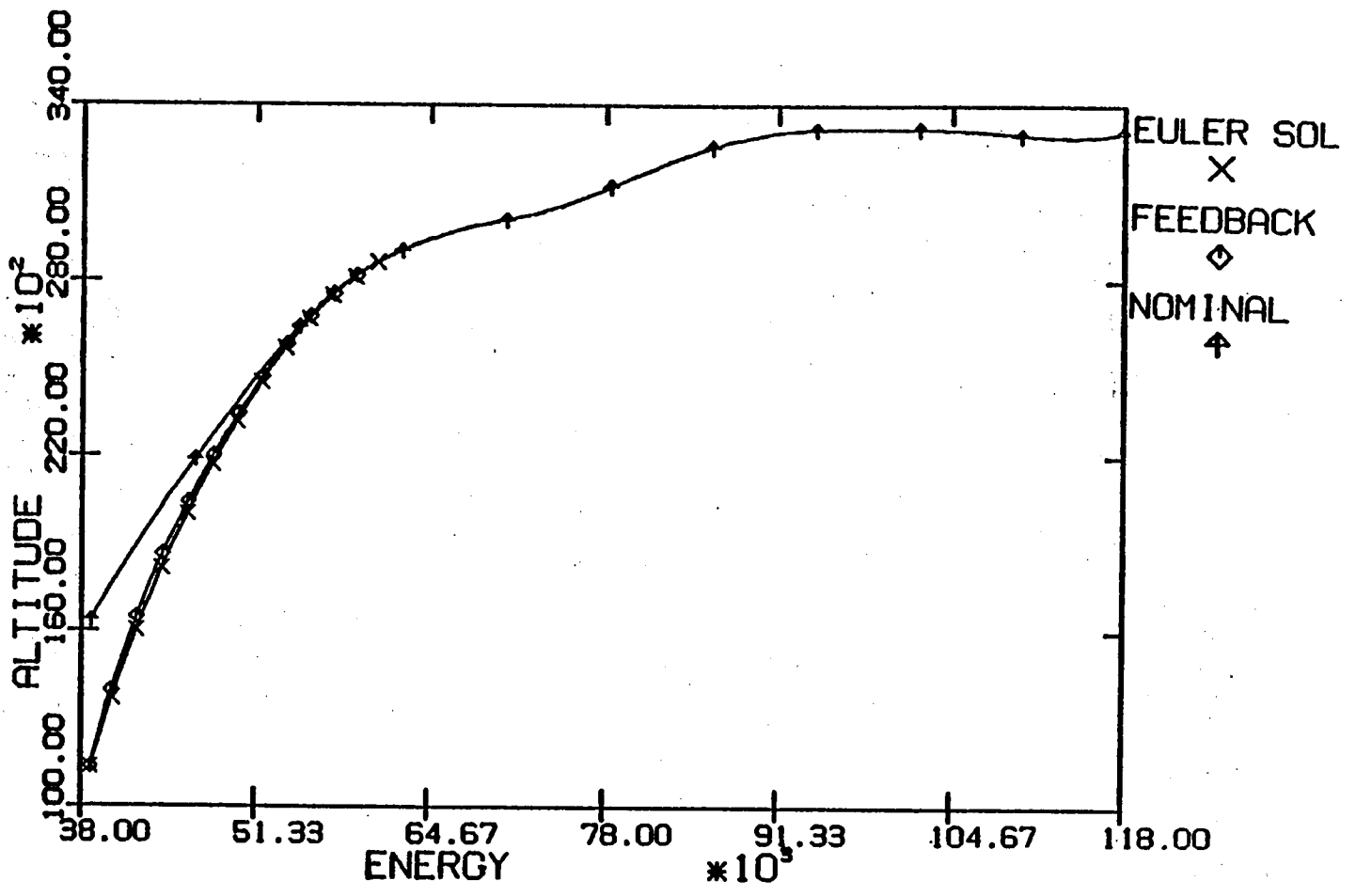
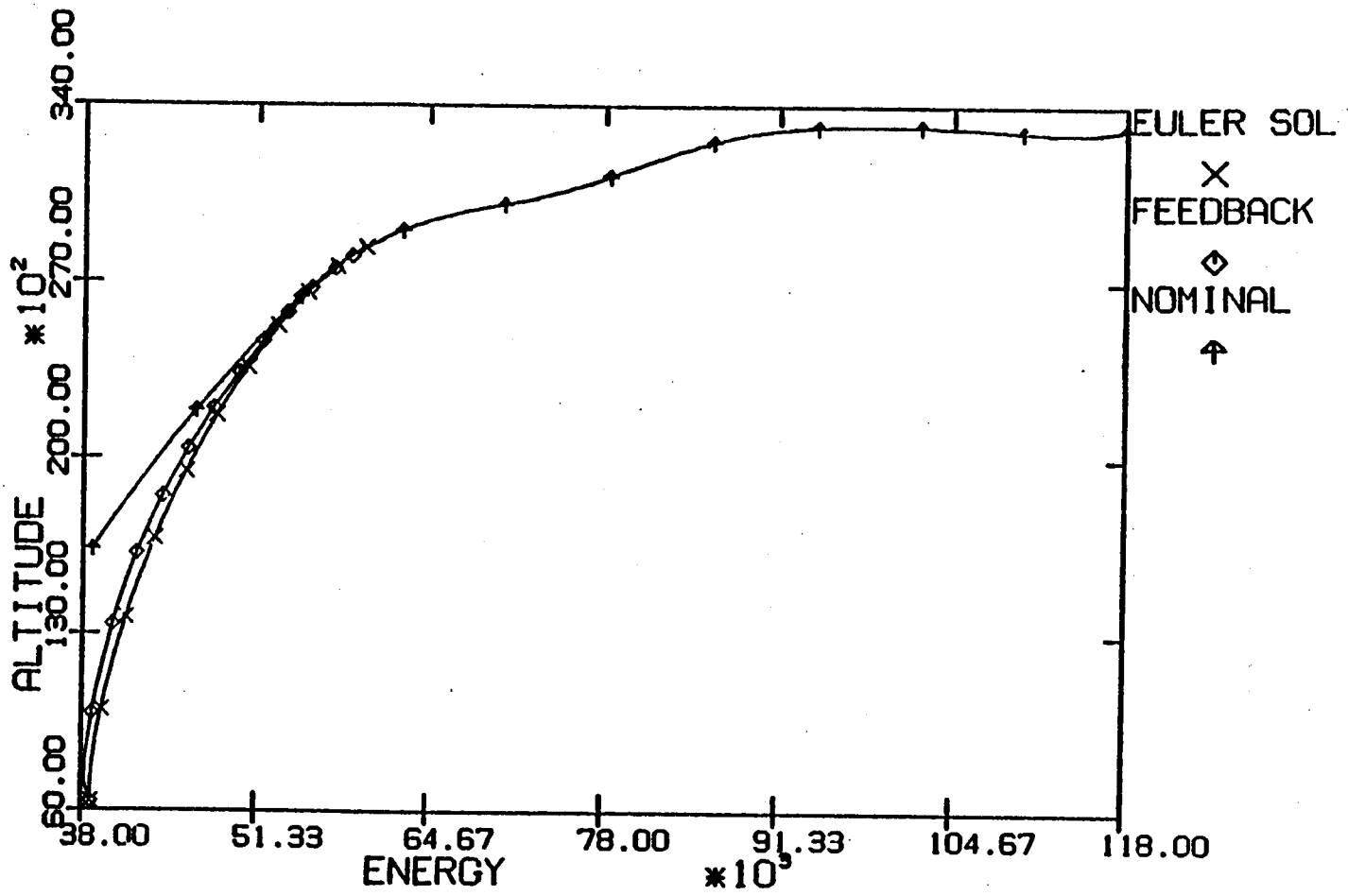


Fig. 2.46Altitude vs Energy, 10000 ft below



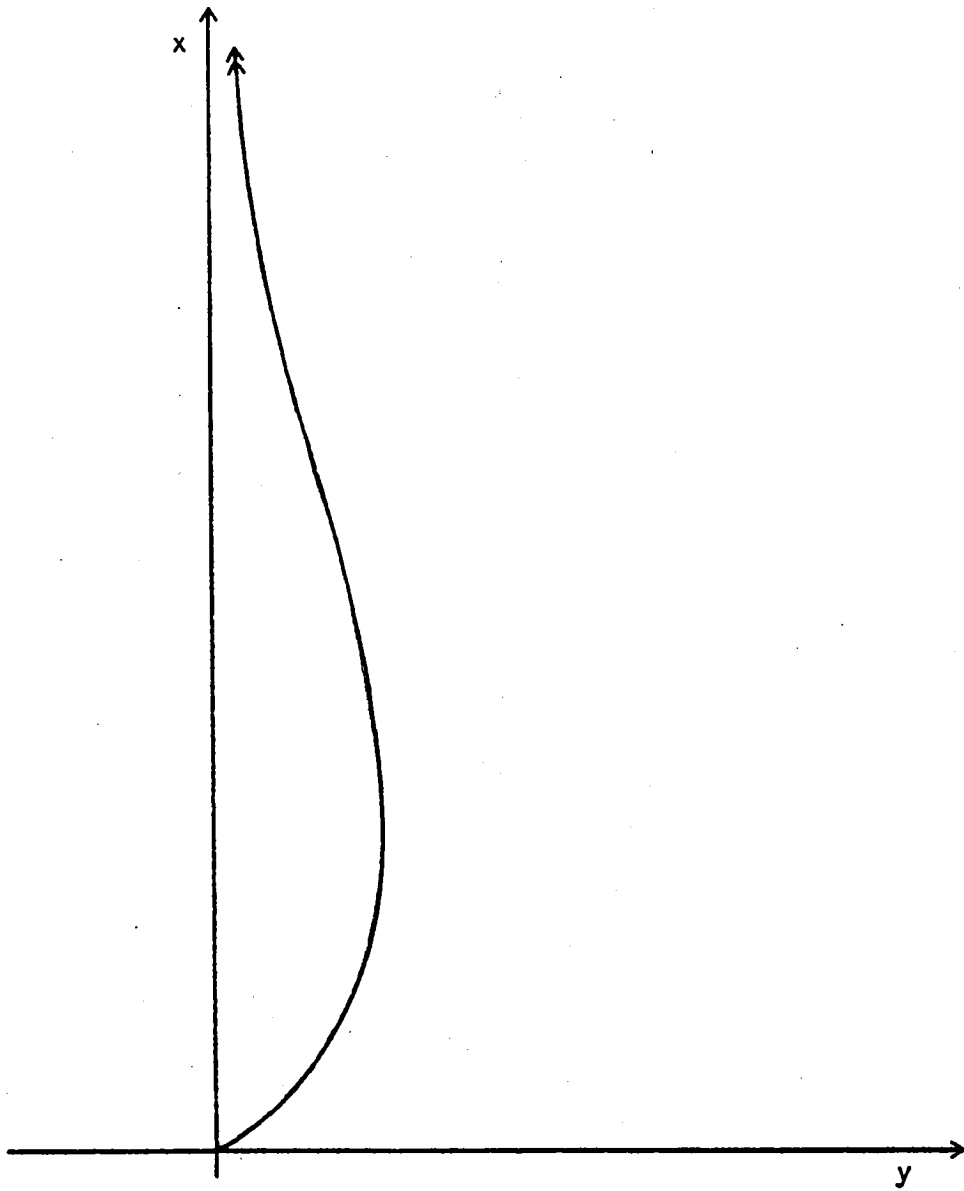


Fig. 2.47 Interceptor Path with y as Running Variable

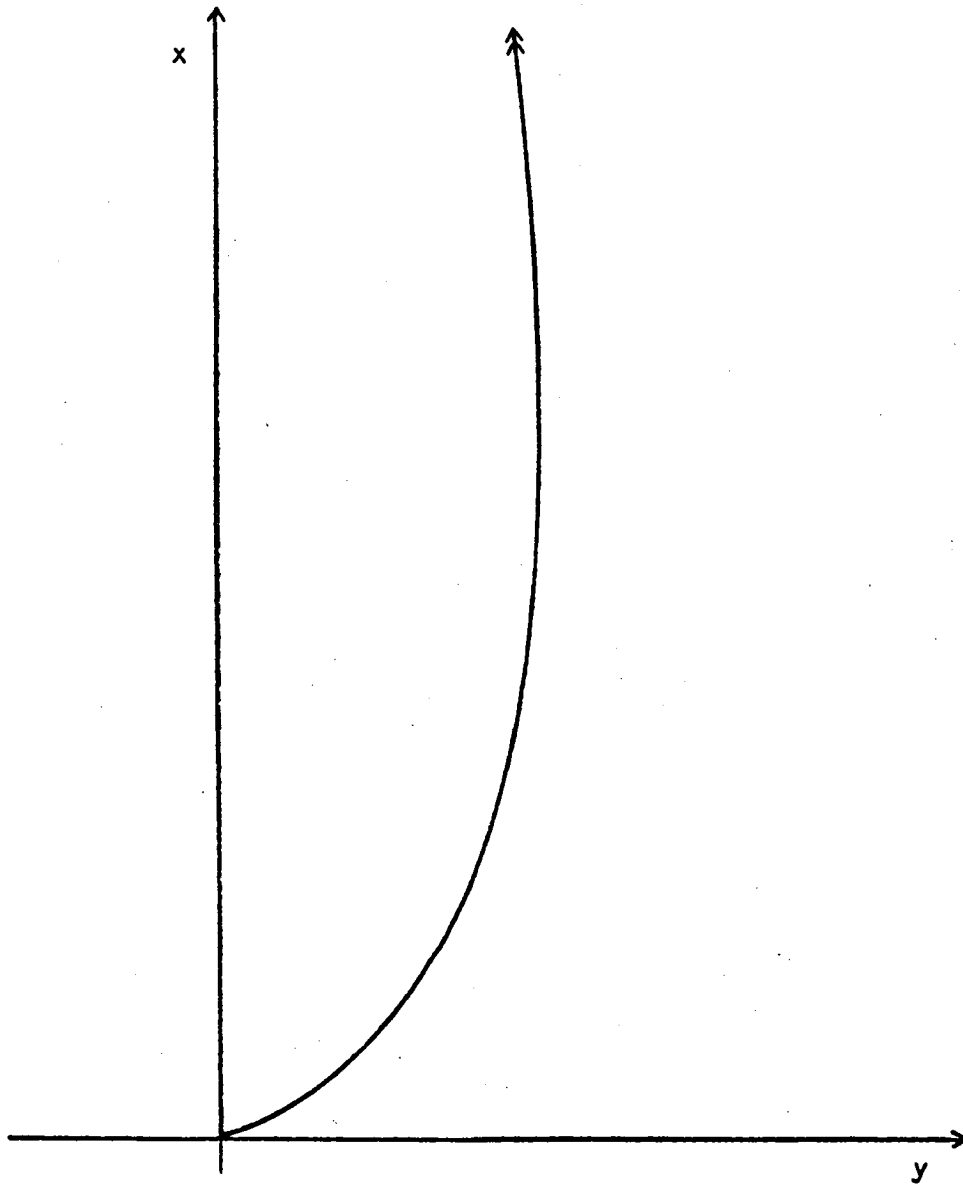
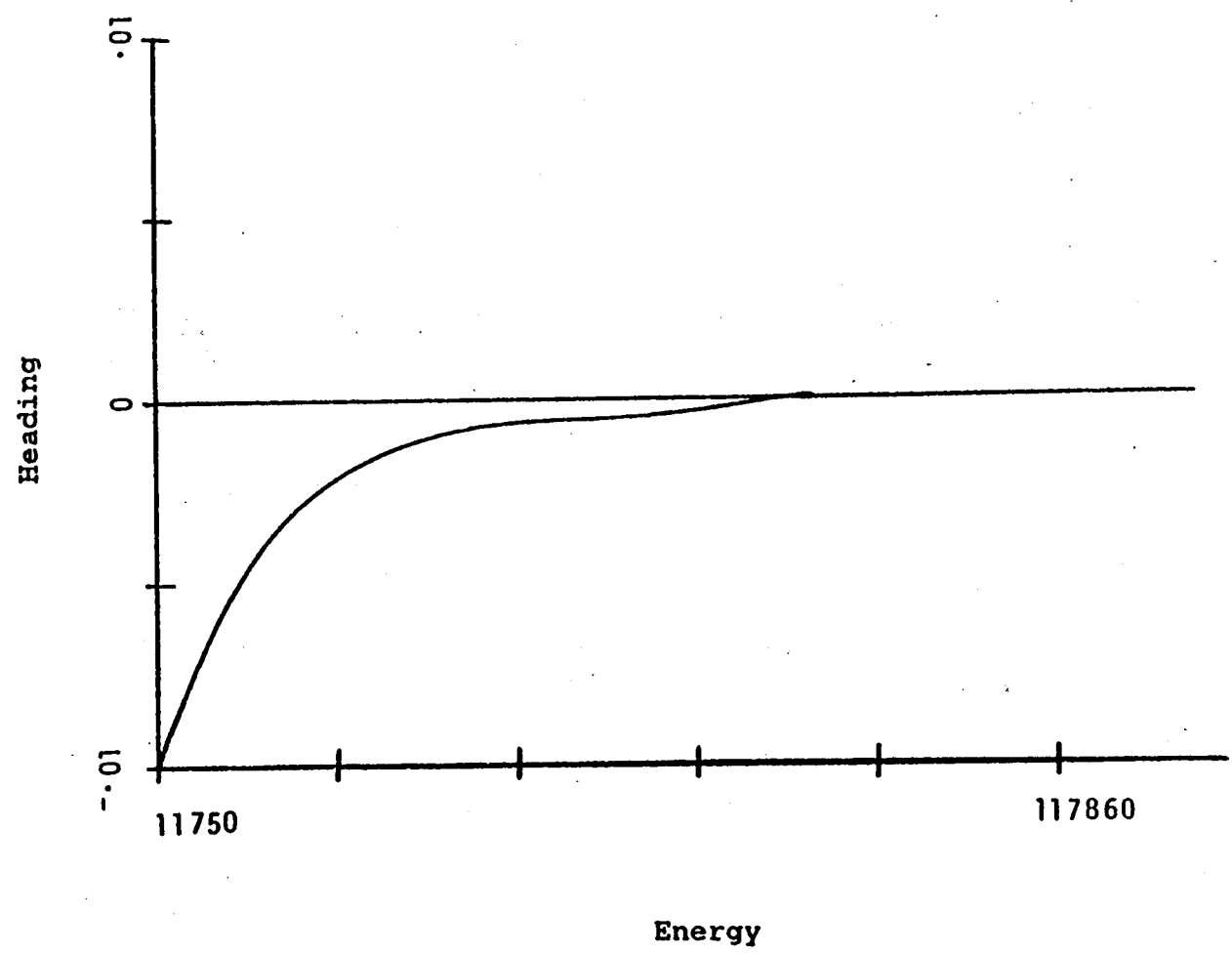


Fig. 2.48 Interceptor Path without y as Running Variable

Fig. 2.49 Heading vs Energy



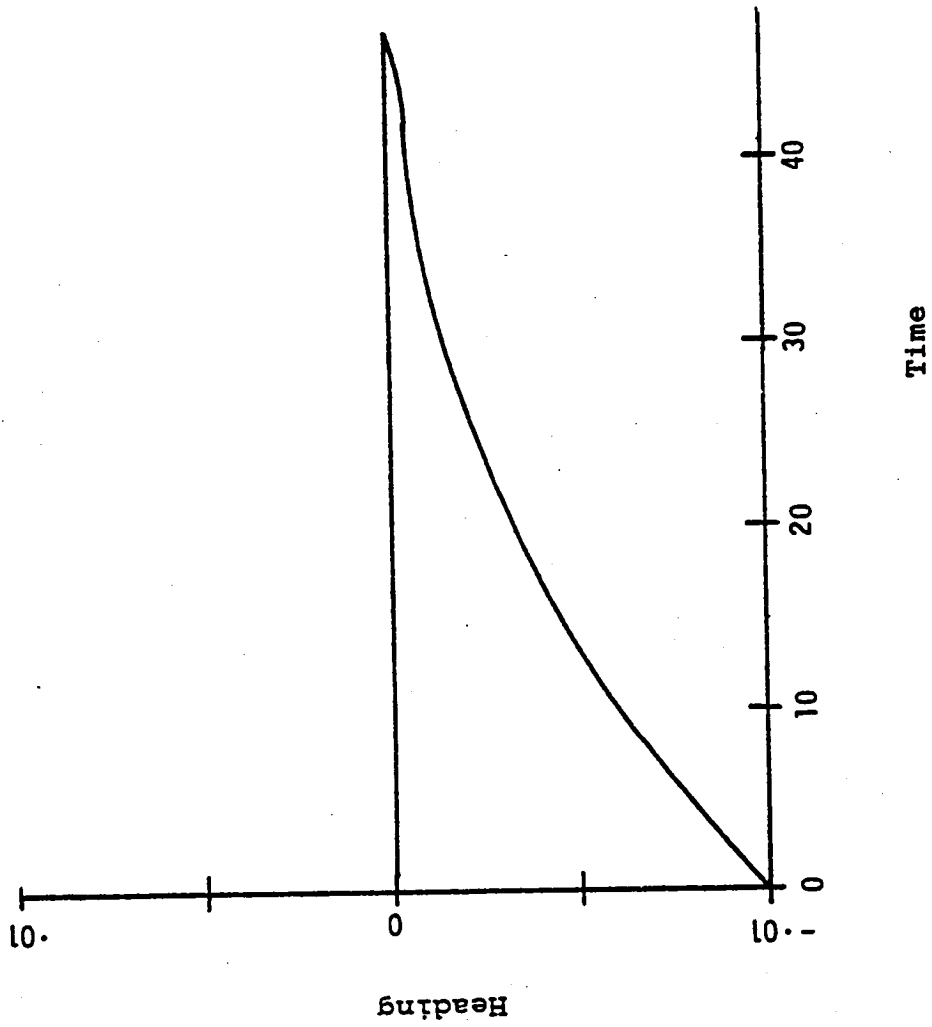


Fig. 2.50 Heading vs Time

CHAPTER 3

OPTIMAL SYMMETRIC FLIGHT WITH AN INTERMEDIATE VEHICLE MODEL

P. K. A. Menon

H. J. Kelley

E. M. Cliff

SECTION 3.1

PREFACE

There has been interest from the beginning of optimal-flight studies in approximations featuring simplified vehicle models. Representation of drag as the drag for level flight leads to an intermediate vehicle model in which path angle γ takes on the rôle of a control variable and the order of the system is reduced by one. An additional order-reduction leads to an "energy-state" model with altitude or speed as a control variable (Refs. 22, 23 and 24). This is reviewed in Ref. 43 which appears as Chapter 4. The present Chapter examines optimal symmetric flight with the intermediate vehicle model. Optimal flight in the vertical plane with a vehicle model intermediate in complexity between point-mass and energy models is studied. Flight-path angle takes on the rôle of a control variable. Range-open problems feature subarcs of vertical flight and singular subarcs as previously studied.

The analysis is based in part upon an exploration of Euler solutions for the path-angle-as-control model carried out in Ref. 50. The present analysis examines higher-order optimality conditions and "chattering-control" phenomena. The weaknesses of the model will be seen as more extensive than previously noted. The class of altitude-speed-range-time optimization problems with fuel expenditure unspecified is investigated and some interesting phenomena uncovered. The maximum-lift-to-drag glide appears as part of the family, final-time-open, with

appropriate initial and terminal transient maneuvers. A family of climb-range paths appears for thrust exceeding level-flight drag, some members exhibiting oscillations. Oscillatory paths generally fail the Jacobi test for durations exceeding a period and furnish a minimum only for short-duration problems.

Minimizing paths of long duration follow a certain corridor in the V-h chart. The features of the family sharpen for the special case of thrust and drag independent of altitude, and considerable analytical attention is accorded to this for the insight it provides to the more general model. The problem of "steepest climb" is found to be ill-posed with the vehicle model under consideration, straight-vertically-upward maneuver sequences being furnished by a family of paths alternating between upward and downward vertical flight and including a limiting "chattering" member.

SECTION 3.2

INTERMEDIATE VEHICLE MODEL

The point-mass dynamical model of aircraft flight incorporating the assumption of thrust-along-the-path is given by

$$\dot{V} = g \left[\frac{(T-D)}{W} - \sin\gamma \right] \quad (3-1)$$

$$\dot{h} = V \sin\gamma \quad (3-2)$$

$$\dot{x} = V \cos\gamma \quad (3-3)$$

$$\dot{W} = Q \quad (3-4)$$

$$\dot{\gamma} = \frac{g}{V} \left(\frac{L}{W} - \cos\gamma \right) \quad (3-5)$$

Here V is airspeed, h altitude, x down-range, \tilde{W} weight of fuel consumed, γ flight-path angle, T thrust, D drag, g the acceleration due to gravity, L lift and Q the fuel-consumption rate.

The sweeping assumption that drag can be approximated by its level-flight value is next invoked. This permits the deletion of equation (3-5) and the elevation of path-angle γ to control status. Lift coefficient, C_L , or angle-of-attack, α , previously a control variable, is correspondingly assumed to be such as to satisfy (3-5). There is obviously trouble ahead with this modelling should $\dot{\gamma}$ turn out to be large in optimized maneuvering or, worse yet, should γ exhibit jump behavior.

The optimal-control problem to be treated, then, is the minimization of a function of the final values of the state variables and final time.

The Hamiltonian function is

$$H = \lambda_V g \left\{ \frac{(T-D)}{W} - \sin\gamma \right\} + \lambda_h V \sin\gamma + \lambda_x V \cos\gamma + \lambda_{\tilde{W}} Q \quad (3-6)$$

and the Euler-Lagrange equations are

$$\dot{\lambda}_V = -\lambda_V \frac{g}{W} \frac{\partial}{\partial V} (T-D) - \lambda_h \sin\gamma - \lambda_x \cos\gamma - \lambda_{\tilde{W}} \frac{\partial Q}{\partial V} \quad (3-7)$$

$$\dot{\lambda}_h = -\lambda_V \frac{g}{W} \frac{\partial}{\partial h} (T-D) - \lambda_{\tilde{W}} \frac{\partial Q}{\partial h} \quad (3-8)$$

$$\dot{\lambda}_x = 0 \quad (3-9)$$

$$\dot{\lambda}_{\tilde{W}} = 0 \quad (3-10)$$

and

$$-\lambda_V g \cos\gamma + \lambda_h V \cos\gamma - \lambda_x V \sin\gamma = 0 \quad (3-11)$$

In the following, the time derivatives of (3-11) will be used to eliminate the time-varying costates in favor of the control γ and derivatives. Note that this is somewhat formal since $\dot{\gamma}$ may not exist. Using equations (3-7) - (3-11) one may now proceed to eliminate those costates which are variable in the Hamiltonian. Using (3-11)

$$\lambda_V = \frac{V}{g} (\lambda_h - \lambda_x \tan\gamma) \quad (3-12)$$

and hence

$$\dot{\lambda}_V = \frac{\dot{V}}{g} (\lambda_h - \lambda_x \tan\gamma) + \frac{V}{g} (\dot{\lambda}_h - \lambda_x \dot{\gamma} \sec^2\gamma) \quad (3-13)$$

substituting for λ_V from (3-12) in (3-8),

$$\dot{\lambda}_h + \frac{V}{W} (\lambda_h - \lambda_x \tan\gamma) \frac{\partial (T-D)}{\partial h} + \lambda_{\tilde{W}} \frac{\partial Q}{\partial h} = 0 \quad (3-14)$$

Using (3-13) in (3-7) and using equations (3-1) and (3-12), one obtains a second expression for $\dot{\lambda}_h$ as

$$\begin{aligned} \dot{\lambda}_h + \lambda_h \frac{g}{W} \left[\frac{(T-D)}{V} + \frac{\partial}{\partial V} (T-D) \right] \\ + \lambda_x \left[\frac{g}{V \cos\gamma} - \dot{\gamma} \sec^2\gamma - \frac{g \tan\gamma}{W} \left\{ \frac{(T-D)}{V} + \frac{\partial}{\partial V} (T-D) \right\} \right] \\ + \lambda_{\tilde{W}} \frac{g}{V} \frac{\partial Q}{\partial V} = 0 \end{aligned} \quad (3-15)$$

Equations (3-14) and (3-15) may now be used to obtain an expression for λ_h in terms of λ_x and $\lambda_{\tilde{W}}$.

$$\begin{aligned} \frac{\lambda_h}{W} \left[\frac{\partial}{\partial h} V(T-D) - \frac{g}{V} \frac{\partial}{\partial V} V(T-D) \right] \\ - \lambda_x \left[\tan\gamma \left\{ \frac{\partial}{\partial h} V(T-D) - \frac{g}{V} \frac{\partial}{\partial V} V(T-D) \right\} + \frac{g}{V \cos\gamma} - \dot{\gamma} \sec^2\gamma \right] \\ + \lambda_{\tilde{W}} \left[\frac{\partial Q}{\partial h} - \frac{g}{V} \frac{\partial Q}{\partial V} \right] = 0 \end{aligned} \quad (3-16)$$

The expressions (3-12) and (3-16) may be used for eliminating λ_V and λ_h in the Hamiltonian with the following result:

$$\begin{aligned} & \cos \gamma H \left\{ \left[\frac{\partial}{\partial h} - \frac{g}{V} \frac{\partial}{\partial V} \right] (V(T-D)) \right\} \\ & - \cos \gamma \lambda_{\tilde{W}} Q^2 \left\{ \left[\frac{\partial}{\partial h} - \frac{g}{V} \frac{\partial}{\partial V} \right] \left(\frac{V(T-D)}{Q} \right) \right\} \\ & - \lambda_x \left\{ V^2 \left[\frac{\partial}{\partial h} - \frac{g}{V} \frac{\partial}{\partial V} \right] \left((T-D) - \frac{(T-D)V}{\cos \gamma} \dot{\gamma} \right) \right\} = 0 \end{aligned} \quad (3-17)$$

Note that

$$\left\{ \frac{\partial}{\partial h} - \frac{g}{V} \frac{\partial}{\partial V} \right\} [\quad] = \frac{\partial}{\partial h} [\quad] \Big|_{E = \text{Constant}}$$

where $E = h + \frac{V^2}{2g}$, the specific energy.

In order to investigate the implications of this complicated expression, consider first the case of free final value of range x and fuel \tilde{W} . If the final values of these variables are left open, then the natural boundary conditions $\lambda_x = 0$ and $\lambda_{\tilde{W}} = 0$ apply and the optimization problem is a trade-off between final values of time t , altitude h and airspeed V , the maximum or minimum value of one of these variables or some function of these variables being sought without regard to range or fuel consumption. In equation (3-17), if the transversality condition for minimum time, $H = -1$, is imposed, the well-known energy-climb schedule is obtained.

One notes that, in this case, equation (3-17) can be satisfied either by $\cos \gamma = 0$, vertical flight, or by vanishing of the bracketed expression, viz., the partial derivative of specific excess power $V(T-D)$ with respect to altitude with specific energy held constant. Thus, the

solution of this, or any, h-V-t optimum problem is made up of vertical climbs, vertical dives and "energy climbs" pieced together in the proper order. Similar considerations apply if fuel expenditure rather than time is to be minimized. In this case $H = 0$, $\lambda_x = 0$ and $\lambda_{\tilde{W}} = 1$, and equation (3-17) yields the minimum-fuel climb path with fixed throttle in the V-h plane.

If range is to be maximized or minimized with final time and fuel unspecified, then $\lambda_x = \mp 1$ and $H = \lambda_{\tilde{W}} = 0$, and a first-order differential equation for path inclination emerges as follows:

$$\left\{ V^2 \left[\frac{\partial}{\partial h} - \frac{g}{V} \frac{\partial}{\partial V} \right] (T-D) - \frac{(T-D)V\dot{\gamma}}{\cos\gamma} \right\} = 0 \quad (3-18)$$

If one chooses $\lambda_x = -1$ and a fixed value of H (to be determined), with $\lambda_{\tilde{W}} = 0$, expression (3-17) is the Euler equation for maximizing range-to-climb with fixed final time. With $H = 0$, $\lambda_x = -1$ and a fixed value of $\lambda_{\tilde{W}}$, similarly, the maximum range to climb trajectory with fixed final value of fuel is obtained. It may be noted that the maximum-range-to-climb problem is ill-posed in that the range-to-climb for thrust greater than drag without time or fuel constraints does not have a maximum, or even an upper-bound. Further, fixed-throttle range-fuel trajectories are not of significant interest in practical situations. Hence, attention will be focused on the problem of maximizing the range-to-climb with a specified final time (fixed $H \neq 0$, $\lambda_x = -1$).

The system (3-1) - (3-3) and (3-18) generates a trajectory family for the range problem. The possibility of obtaining an analytical solution of the system for the case of thrust and drag as arbitrary functions of altitude and air speed is remote. However, using the

assumption of constant-density atmosphere, with thrust and drag dependent on airspeed only, one can obtain an analytical solution to this system (Ref. 50). The expression (3-18) can be rewritten as

$$\frac{\dot{\gamma}}{\cos\gamma} = \frac{V}{(T-D)} \left\{ \frac{\partial}{\partial h} - \frac{g}{V} \frac{\partial}{\partial V} \right\} (T-D) \quad (3-19)$$

In the following, several transformations of independent variable are carried out without attention to monotonicity requirements, the thought being to fit the solution segments obtained into families in due course. The temptation of range as independent variable will be avoided, however, in anticipation of purely-vertical-motion segments. In the interest of brevity we designate $\mu \equiv (T-D)/W$

$$\frac{1}{\cos\gamma} \frac{d\gamma}{dV} (-\sin\gamma + \mu) = \frac{V}{g\mu} \left\{ \frac{\partial}{\partial h} - \frac{g}{V} \frac{\partial}{\partial V} \right\} \mu \quad (3-20)$$

With altitude-dependence suppressed, the path angle γ is determined as the solution of the first-order differential equation

$$\frac{1}{\cos\gamma} \frac{d\gamma}{dV} (\sin\gamma - \mu) = \frac{d\mu}{dV} \frac{1}{\mu} \quad (3-21)$$

Further simplification is obtained by another change of independent variable, this time from V to μ

$$\frac{1}{\cos\gamma} \frac{d\gamma}{d\mu} (\sin\gamma - \mu) = \frac{1}{\mu} \quad (3-22)$$

If the rôles of independent and dependent variables are now regarded as reversed, this equation takes the form

$$\frac{d\mu}{d\gamma} + \frac{1}{\cos\gamma} \mu^2 - \mu \frac{\sin\gamma}{\cos\gamma} = 0 \quad (3-23)$$

which is the form of the Bernoulli differential equation

$$\frac{d\mu}{d\gamma} + f_1(\gamma) \mu^2 + f_2(\gamma) \mu^\beta = 0 \quad (3-24)$$

with $\beta = 1$. According to Kamke, (Ref. 51), this equation has the solution

$$\frac{1}{\mu} = E(\gamma) \int \frac{f_1(\gamma)}{E(\gamma)} d\gamma \quad (3-25)$$

where

$$E(\gamma) = e^{\int f_2 d\gamma} \quad (3-26)$$

with identification of f_1 and f_2 as

$$f_1(\gamma) = \frac{1}{\cos\gamma} \quad (3-27)$$

$$f_2(\gamma) = - \int \frac{\sin\gamma}{\cos\gamma} d\gamma \quad (3-28)$$

The solution (3-25) becomes as follows

$$E(\gamma) = e^{-\int \frac{\sin\gamma}{\cos\gamma} d\gamma} = e^{\ln\cos\gamma} = \cos\gamma \quad (3-29)$$

$$\frac{1}{\mu} = \cos\gamma \left[\int \frac{d\gamma}{\cos^2\gamma} + C \right] = \sin\gamma + C \cos\gamma \quad (3-30)$$

Before expressing this relationship in the form $\gamma = \gamma(\mu)$, we relate the integration constant C to equilibrium values of μ and γ corresponding to unaccelerated flight. Such values may be designated with a super-scribed bar:

$$\bar{\mu} = \sin\bar{\gamma} \quad (3-31)$$

$$C = \cot\bar{\gamma} \quad (3-32)$$

The solution may then be expressed as:

$$\sin\bar{\gamma} \sin\gamma + \cos\bar{\gamma} \cos\gamma = \frac{\bar{\mu}}{\mu} \quad (3-33)$$

or as

$$\gamma = \bar{\gamma} + \cos^{-1} \left[\frac{\bar{\mu}}{\mu} \right] \quad (3-34)$$

Here $\bar{\mu}$ is the value of μ in unaccelerated flight and

$$\bar{\gamma} = \sin^{-1} \bar{\mu} \quad (3-35)$$

In Figure 3.1, the solution (3-34) is illustrated for various values of $\bar{\mu}$. The range of angle γ has been restricted to $\pm 180^\circ$ in this plot.

With this solution at hand, the state histories can be generated. If the thrust is taken as zero, the state-Euler system produces the flattest-glide trajectory, flown with maximum lift-to-drag ratio, along with a family of transients to and from this point (Fig. 3.2). When a positive margin of thrust over drag exists, a family of oscillatory solutions is generated for various values of $\bar{\mu}$ as shown in Fig. 3.3. It may be noted in Fig. 3.3 that the innermost point corresponding to $\mu = .2$ in V - γ space corresponds to flight at $(T-D)_{\max}$, while along the outermost closed path, the flight path angle γ switches between $\pm 90^\circ$.

With the availability of the Euler solution (3-30) to the maximum-range problem with altitude dependence suppressed, one may proceed to obtain a similar solution to the more general Euler equation (3-17) using variation of parameters (Ref. 52). Equation (3-17) may be written as

$$\dot{\gamma} = -g \left\{ \frac{\cos \gamma}{\mu} \frac{\partial \mu}{\partial V} - \cos^2 \gamma \frac{H}{\lambda_x} \frac{1}{V^2 \mu} \frac{\partial (V\mu)}{\partial V} + \cos^2 \gamma \frac{\lambda \tilde{W}}{\lambda_x} \frac{Q^2}{V^2 \mu} \frac{\partial}{\partial V} \left[\frac{V\mu}{Q} \right] \right\} \quad (3-36)$$

As in equation (3-22), the independent variable is changed from time to airspeed resulting in

$$\begin{aligned} \frac{d\gamma}{dV} (\sin\gamma - \mu) = \frac{\cos\gamma}{\mu} \frac{d\mu}{dV} - \cos^2\gamma \frac{H}{\lambda_x} \frac{1}{V^2_\mu} \frac{d}{dV} (V_\mu) \\ + \cos^2\gamma \frac{\lambda_{\tilde{W}}}{\lambda_x} \frac{Q^2}{V^2_\mu} \frac{d}{dV} \left[\frac{V_\mu}{Q} \right] \end{aligned} \quad (3-37)$$

Rearranging, one obtains

$$\begin{aligned} \frac{d\gamma}{dV} (\sin\gamma - \mu) - \frac{\cos\gamma}{\mu} \frac{\partial\mu}{\partial V} = - \cos^2\gamma \frac{H}{\lambda_x} \frac{1}{V^2_\mu} \frac{d}{dV} (V_\mu) \\ + \cos^2\gamma \frac{\lambda_{\tilde{W}}}{\lambda_x} \frac{Q^2}{V^2_\mu} \frac{d}{dV} \left[\frac{V_\mu}{Q} \right] \end{aligned} \quad (3-38)$$

Equation (3-30) is the analytical solution to the differential equation (3-38) with H and $\lambda_{\tilde{W}}$ both zero. The expression (3-30) may be differentiated with respect to airspeed to obtain

$$- \frac{1}{\mu} \frac{\partial\mu}{\partial V} = (\cos\gamma - C \sin\gamma) \frac{d\gamma}{dV} + \frac{dC}{dV} \cos\gamma \quad (3-39)$$

Note that C is no longer a constant here, but a function of the independent variable V . Substituting for μ in (3-39) from (3-30)

$$\frac{1}{\mu} \frac{\partial\mu}{\partial V} = - \frac{[(\cos\gamma - C \sin\gamma) \frac{d\gamma}{dV} + \frac{dC}{dV} \cos\gamma]}{(\sin\gamma + C \cos\gamma)} \quad (3-40)$$

Using equation (3-40) in (3-38)

$$\begin{aligned} \frac{\cos^2\gamma}{\sin\gamma + C \cos\gamma} \frac{dC}{dV} = - \cos^2\gamma \frac{H}{\lambda_x} \frac{1}{V^2_\mu} \frac{d}{dV} (V_\mu) \\ + \cos^2\gamma \frac{\lambda_{\tilde{W}}}{\lambda_x} \frac{Q^2}{V^2_\mu} \frac{d}{dV} \left[\frac{V_\mu}{Q} \right] \end{aligned} \quad (3-41)$$

Since $\mu = \frac{1}{\sin\gamma + C \cos\gamma}$ from (3-30),

$$\begin{aligned} \cos^2\gamma \frac{dC}{dV} = \cos^2\gamma \left[-\frac{H}{\lambda_x} \left\{ \frac{1}{V_\mu^2} + \frac{1}{V_\mu^2} \frac{d\mu}{dV} \right\} \right. \\ \left. + \frac{\lambda_{\tilde{W}}}{\lambda_x} \left\{ \frac{Q}{V_\mu^2} + \frac{Q}{V_\mu^2} \frac{d\mu}{dV} - \frac{1}{V_\mu} \frac{dQ}{dV} \right\} \right] \end{aligned} \quad (3-42)$$

The quantities within the $\{ \}$ brackets can be identified as

$$-\frac{d}{dV} \left[\frac{1}{V_\mu} \right] = \frac{1}{V_\mu^2} + \frac{1}{V_\mu^2} \frac{d\mu}{dV} \quad (3-43)$$

and

$$-\frac{d}{dV} \left[\frac{Q}{V_\mu} \right] = -\frac{1}{V_\mu} \frac{dQ}{dV} + \frac{1}{V_\mu^2} \frac{d\mu}{dV} + \frac{Q}{V_\mu^2} \quad (3-44)$$

From which

$$\frac{dC}{dV} = \frac{H}{\lambda_x} \frac{d}{dV} \left[\frac{1}{V_\mu} \right] - \frac{\lambda_{\tilde{W}}}{\lambda_x} \frac{d}{dV} \left[\frac{Q}{V_\mu} \right] \quad (3-45)$$

Equation (3-45) is readily integrated to yield

$$C = \frac{H}{\lambda_x} \frac{1}{V_\mu} - \frac{\lambda_{\tilde{W}}}{\lambda_x} \frac{Q}{V_\mu} + C_1 \quad (3-46)$$

where C_1 is an arbitrary constant. Hence for the time-range-fuel problem, the solution with altitude-dependence suppressed is

$$\frac{1}{\mu} = \sin\gamma + \left(\frac{H}{\lambda_x V_\mu} - \frac{\lambda_{\tilde{W}}}{\lambda_x} \frac{Q}{V_\mu} + C_1 \right) \cos\gamma \quad (3-47)$$

To express the above result in the form $\gamma = \gamma(\mu)$, we need to relate the integration constant C_1 to equilibrium values of μ and γ corresponding to unaccelerated flight. Unlike the situation in the simpler problem, the interpretation of equation (3-47) is not straightforward.

From a practical viewpoint the time-range problem is of main interest since minimum-fuel problems with fixed throttle are rare. Fuel-range problem will not be discussed further in the present paper and in subsequent development the fuel multiplier $\lambda_{\bar{W}}$ will be taken as zero.

Investigation of equilibrium points with $\lambda_{\bar{W}} = 0$ results in a plot of the values of H/λ_x vs airspeed as shown in Fig. 3.4 for a parabolic (T-D) distribution illustrated in Fig. 3.5. In Fig. 3.4 three separate regimes can be identified. H/λ_x values to the left of the $(T-D)_{\max}$ velocity are positive while those between the $(T-D)_{\max}$ point and the $V(T-D)_{\max}$ point have a negative sign. All H/λ_x values to the right of the speed for $V(T-D)_{\max}$ are positive. Any of these values may be used to evaluate the arbitrary constant C_1 as follows.

As in (3-31)

$$\bar{\mu} = \sin \bar{\gamma} \quad (3-48)$$

$$\bar{V} = V \left| \text{Equilibrium value of } \frac{H}{\lambda_x} \right. \quad (3-49)$$

$$\cot \bar{\gamma} = \frac{H}{\lambda_x} \frac{1}{V \bar{\mu}} + C_1 \quad (3-50)$$

or

$$C_1 = \cot \bar{\gamma} - \frac{H}{\lambda_x} \frac{1}{V \bar{\mu}} \quad (3-51)$$

using (3-51) in (3-47)

$$\frac{1}{\mu} = \sin \gamma + \left[\frac{H}{\lambda_x} \left\{ \frac{1}{V \mu} - \frac{1}{V \bar{\mu}} \right\} + \cot \bar{\gamma} \right] \cos \bar{\gamma} \quad (3-52)$$

putting $\Delta \equiv \left[\frac{H}{\lambda_x} \left\{ \frac{1}{V_\mu} - \frac{1}{V_\mu^-} \right\} + \cot \bar{\gamma} \right]$ and using a well-known trigonometric identity,

$$\gamma = \tan^{-1} \left[\frac{1}{\Delta} \right] + \cos^{-1} \left[\frac{1}{\mu \sqrt{\Delta^2 + 1}} \right] \quad (3-53)$$

Equation (3-53) is the Euler solution to the time-range problem with altitude dependence of μ suppressed. In Figs. 3.6, 3.7 and 3.8, the analytical solution evaluated for representative H/λ_x values from each of the three regimes is shown. Fig. 3.6 and 3.7 indicate oscillatory solutions in the neighborhood of a stable equilibrium point. The similarity of these figures to Fig. 3.3 is striking. The solutions in Fig. 3.8 are non-oscillatory and bear some resemblance to Fig. 3.2.

Summarizing, one notes that the range problem has oscillatory solutions when a positive margin of thrust over drag exists. With zero thrust the solution obtained is the flattest glide with a family of transients to and from the maximum lift-to-drag point. For the time-range problem, values of H/λ_x to the left (low-speed end) of the $V(T-D)_{\max}$ point produce oscillatory solutions while, on the right of the $V(T-D)_{\max}$ point, a family of transients to and from the equilibrium point defined by the choice of H/λ_x is obtained.

SECTION 3.3

LEGENDRE-CLEBSCH NECESSARY CONDITION

From the Euler-Lagrange equations, with $\lambda_{\tilde{W}} = 0$

$$\frac{\partial H}{\partial \gamma} = -\lambda_v g \cos \gamma + \lambda_h V \cos \gamma - \lambda_x V \sin \gamma \quad (3-54)$$

and

$$\frac{\partial^2 H}{\partial \gamma^2} = (\lambda_V g - \lambda_h V) \sin \gamma - \lambda_x V \cos \gamma \quad (3-55)$$

Setting the left-hand side of equation (3-54) to zero as required for a stationary minimum of H leads to

$$\tan \gamma = \frac{\lambda_h V - \lambda_V g}{\lambda_x V} \quad \text{or} \quad \frac{\lambda_V g - \lambda_h V}{-\lambda_x V} \quad (3-56)$$

From (3-56), then

$$\sin \gamma = \frac{(\lambda_h V - \lambda_V g) \sigma}{\sqrt{(\lambda_h V - \lambda_V g)^2 + \lambda_x^2 V^2}} \quad (3-57)$$

and

$$\cos \gamma = \frac{\lambda_x V \sigma}{\sqrt{(\lambda_h V - \lambda_V g)^2 + \lambda_x^2 V^2}} \quad (3-58)$$

where $\sigma = \pm 1$

Using (3-57) and (3-58) in (3-55), it is possible to determine σ .

Next, one may employ the transversality conditions for the range problem. These lead to

$$\lambda_x = 1, \quad \frac{\partial^2 H}{\partial \gamma^2} > 0 \quad \text{if } \gamma \text{ lies in the second or third quadrant} \quad (3-59)$$

$$\lambda_x = -1, \quad \frac{\partial^2 H}{\partial \gamma^2} < 0 \quad \text{if } \gamma \text{ lies in the first or fourth quadrant} \quad (3-60)$$

viz, $\lambda_x = 1$ for range minimization and $\lambda_x = -1$ for range maximization.

From (3-59) it is clear that, with no restrictions on path-angle γ , the minimum-range-climb trajectory is that which maximizes the range in the negative direction, a result which is perhaps obvious. The implication is that, with no constraint on the final value of time or fuel, the "steepest-climb" problem does not possess a minimum or even a lower bound.

Attention is drawn to the solution to this problem given by Miele (Ref. 53) using the Green's theorem device. According to Ref. 53, the optimal trajectory for the "steepest climb" problem consists of a central path flown along the $(T-D)_{\max}$ locus in the airspeed-altitude chart with vertical climb/dive transitions at the ends to meet the boundary conditions, if they are off the $(T-D)_{\max}$ path. There is an important difference in vehicle modelling from that of the present work which should be noted as a key to resolving disparities between the character of optimal paths emerging: The analysis of Ref. 53 in essence replaces $\cos\gamma$ in equation (3-3) with unity so that the problem solved is maximum altitude in a given distance (arc length) rather than in a given range.

Consider, next, the imposition of limits on path-angle γ , say $-90^\circ \leq \gamma \leq 90^\circ$. In this case, since final time is unspecified, it is clear that by alternating between vertical-climb and vertical-dive paths, the range-to-climb can be made identically zero. This is a consequence of the intermediate vehicle modeling in which there is no limit to the path-angle rate.

It is of interest to examine vertical-flight sequences comprised of alternating up and down segments. Consider, for example, the case in which specified initial and final altitudes and velocities call for a net increase in specific energy. An initial vertical-flight transition, either up or down as appropriate, is performed to the neighborhood of the maximum of specific excess power (speed \tilde{V} in Fig. 3.9). Choosing a pair of reversal airspeeds V^* (below \tilde{V}) and V^{**} (above \tilde{V}), one constructs an alternating sequence of straight-up and straight-down trajectory segments.

In the case of net energy gain, both V^* and V^{**} should correspond to positive $\dot{E} = \frac{V(T-D)}{W}$. The relative duration of the segments can be adjusted so that the time-averaged speed is \tilde{V} . If V^* and V^{**} are chosen sufficiently close to \tilde{V} , the average energy rate can be made as close to the maximum value as one wishes. The motion during this alternating sequence is vertical and net-straight-up as long as the energy rates at V^* and V^{**} are positive. The limiting case of chattering at \tilde{V} corresponds to minimum-time as an auxiliary performance index, the primary one, "steepness", being independent of the parameters of the sequence. A final transient, straight up or straight down, is flown to meet the final specifications on speed and altitude. In the case of net energy loss specified, speeds V^* and V^{**} with negative energy rates should be chosen for the rectangular-wave construction of the path-angle history.

Returning to the maximum-range problem, it should be noted that the Legendre-Clebsch necessary condition is met in strengthened form for values of the path angle γ in the first or fourth quadrants. However, physical reasoning makes clear that a range-maximization problem without time or fuel constraints will not possess a proper maximum, or even an upper bound. In view of the above, the problem of interest is to maximize the range of climb from an initial (V,h) pair to a final (V,h) pair in a fixed time. This problem is of value in studies of the type reported in Ref.54 for a point-mass-modelled vehicle.

It may be noted that in the cases of time and/or fuel minimization problems with range open, the Legendre-Clebsch necessary condition is

met only in weak form along central arcs and, hence, these trajectories fall into the class of singular extremals.

SECTION 3.4

CONJUGATE-POINT TEST

The Legendre-Clebsch necessary condition is met with a margin for the time-range problem and hence the Euler solution (3-17) with $\lambda_{\tilde{W}} = 0$ furnishes a relative minimum for initial and terminal points sufficiently close together. For extremals of finite length, however, the task of ensuring that the second variation is non-negative for admissible neighboring paths leads to the accessory-minimum problem in the calculus of variations. This in essence boils down to a search for a system of admissible variations, not identically zero, which offer the most severe competition in the sense of minimizing the second variation. If a system of nonzero variations can be found which makes the second variation zero, then it is clear that a neighboring path is competitive and that the test extremal furnishes at best an improper minimum and at worst a merely stationary value (Ref. 55). The first value of the independent variable $x = x^* > x_0$ for which such a nontrivial system can be found defines a conjugate point.

Following the analysis of Ref. 55 for the Mayer problem, the rank of the matrix of variations of states and the multiplier corresponding to the state being minimized with respect to the initial values of costates is evaluated along the test extremal, viz.

The rank of

$$\begin{bmatrix}
 \frac{\partial x_2}{\partial \lambda_{10}} & \frac{\partial x_2}{\partial \lambda_{20}} & \cdots & \frac{\partial x_2}{\partial \lambda_{n0}} \\
 \cdot & & & \cdot \\
 \frac{\partial x_n}{\partial \lambda_{10}} & \frac{\partial x_n}{\partial \lambda_{20}} & \cdots & \frac{\partial x_n}{\partial \lambda_{n0}} \\
 \frac{\partial \lambda_1}{\partial \lambda_{10}} & \frac{\partial \lambda_1}{\partial \lambda_{20}} & \cdots & \frac{\partial \lambda_1}{\partial \lambda_{n0}}
 \end{bmatrix} \tag{3-61}$$

provides the criterion for the existence of a conjugate point. If the rank of the test matrix (3-61) drops at any point along the test extremal, it is indicative of the occurrence of a conjugate point.

For the time-range problem, if the independent variable is changed from time to range, the equations of motion become

$$h' = T \tan \gamma \tag{3-62}$$

$$V' = \frac{g(T-D)}{WV \cos \gamma} - \frac{g}{V} \tan \gamma \tag{3-63}$$

The optimal-control problem then is to maximize the final value of altitude 'h' for a specified range with time fixed. With the interpretation of H as the time multiplier, the test matrix (3-61) becomes

$$\begin{bmatrix} \frac{\partial V}{\partial \lambda_{h_0}} & \frac{\partial V}{\partial H_0} & \frac{\partial V}{\partial \gamma_0} \\ \frac{\partial t}{\partial \lambda_{h_0}} & \frac{\partial t}{\partial H_0} & \frac{\partial t}{\partial \gamma_0} \\ \frac{\partial \lambda_h}{\partial \lambda_{h_0}} & \frac{\partial \lambda_h}{\partial H_0} & \frac{\partial \lambda_h}{\partial \gamma_0} \end{bmatrix} = \begin{bmatrix} \frac{\partial V}{\partial \lambda_{h_0}} & \frac{\partial V}{\partial H_0} & \frac{\partial V}{\partial \gamma_0} \\ \frac{\partial t}{\partial \lambda_{h_0}} & \frac{\partial t}{\partial H_0} & \frac{\partial t}{\partial \gamma_0} \\ 1 & 0 & 0 \end{bmatrix} \quad (3-64)$$

Note that time appears in this problem as a state-like variable with

$$t' = \frac{1}{V \cos \gamma} \quad (3-65)$$

A prime on the variables denotes differentiation with respect to the range variable x .

From equation (3-64), the sign of

$$\frac{\partial V}{\partial \gamma_0} \cdot \frac{\partial t}{\partial H_0} - \frac{\partial V}{\partial H_0} \cdot \frac{\partial t}{\partial \gamma_0} \quad (3-66)$$

evaluated along the Euler solution determines the rank of the matrix (3-64). If the sign changes at any point on the time-range trajectory it is indicative of a conjugate point.

The Euler solution obtained for the time-range problem with altitude dependence of μ suppressed, may now be tested for conjugate points. In view of the particularly simple form of the conjugate-point test for this problem, it seems reasonable to attempt to obtain analytical approximations for the partial derivatives in equation (3-66).

Linearizing the equations of motion and the Euler equation (3-17) with range as the independent variable about an equilibrium point at a particular altitude, one obtains

$$\delta V' = a_0 \delta V - a_1 \delta \gamma \quad (3-67)$$

$$\delta t' = -a_2 \delta V + a_3 \delta \gamma \quad (3-68)$$

$$\delta \gamma' = a_4 \delta V - a_5 \delta \gamma + a_6 \delta H \quad (3-69)$$

Where:

$$a_0 = \frac{g}{WV \cos \gamma} \frac{\partial (T-D)}{\partial V} \quad (3-70)$$

$$a_1 = \frac{g}{V} \quad (3-71)$$

$$a_2 = \frac{1}{V^2 \cos \gamma} \quad (3-72)$$

$$a_3 = \frac{\sin \gamma}{V \cos^2 \gamma}$$

$$\begin{aligned} a_4 = & -\frac{\cos \gamma}{V^4} \frac{g}{\lambda_x} \frac{H}{\lambda_x} + \frac{\partial (T-D)}{\partial V} \frac{g}{V^2 (T-D)} \left[1 - \frac{\cos \gamma}{V} \frac{H}{\lambda_x} \right] \\ & + \frac{g}{V (T-D)^2} \left\{ \frac{\partial (T-D)}{\partial V} \right\}^2 \left[1 - \frac{\cos \gamma}{V} \frac{H}{\lambda_x} \right] \\ & + \frac{g}{V (T-D)} \frac{\partial^2 (T-D)}{\partial V^2} \left[\frac{\cos \gamma}{V} \frac{H}{\lambda_x} - 1 \right] \end{aligned} \quad (3-73)$$

$$a_5 = a_0 \quad (3-74)$$

$$a_6 = \frac{\cos \gamma}{V^3 (T-D)} \frac{g}{\lambda_x} \left[V \frac{\partial (T-D)}{\partial V} + (T-D) \right] \quad (3-75)$$

Equations (3-67), (3-68) and (3-69) constitute a linear, constant-coefficient system which can be put in the following form using Laplace transforms. (Initial conditions on δV and δt are zero.)

$$\frac{\delta V(s)}{\delta \gamma(0)} = \frac{-a_1}{s^2 + (a_1 a_4 - a_0 a_5)} \quad (3-76)$$

$$\frac{\delta V(s)}{\delta H(0)} = \frac{-a_1 a_6}{s[s^2 + (a_1 a_4 - a_0 a_5)]} \quad (3-77)$$

$$\frac{\delta t(s)}{\delta \gamma(0)} = - \frac{[(a_0 a_3 - a_1 a_2) - a_3 s]}{s[s^2 + (a_1 a_4 - a_0 a_5)]} \quad (3-78)$$

$$\frac{\delta t(s)}{\delta H(s)} = - \frac{-[(a_0 a_3 - a_1 a_2) - a_3 s] a_6}{s^2 [s^2 + (a_1 a_4 - a_0 a_5)]} \quad (3-79)$$

putting $\omega_n^2 = (a_1 a_4 - a_0 a_5)$ (3-80)

and

$$T = \frac{-a_3}{a_0 a_3 - a_1 a_2} \quad (3-81)$$

and cancelling out common constants in the numerator, one can bring eqs.

(3-76) - (3-79) to the form

$$\frac{\delta V(s)}{\delta \gamma(0)} = \frac{\omega_n^2}{s^2 + \omega_n^2} \quad (3-82)$$

$$\frac{\delta V(s)}{\delta H(0)} = \frac{\omega_n^2}{s(s^2 + \omega_n^2)} \quad (3-83)$$

$$\frac{\delta t(s)}{\delta \gamma(0)} = \frac{(1+Ts)\omega_n^2}{s(s^2 + \omega_n^2)} \quad (3-84)$$

$$\frac{\delta t(s)}{\delta H(0)} = \frac{(1+Ts)\omega_n^2}{s^2(s^2 + \omega_n^2)} \quad (3-85)$$

Equations (3-84) and (3-85) may be further simplified using the expression (3-82) and (3-83).

$$\frac{\delta t(s)}{\delta \gamma(0)} = \frac{\delta V(s)}{\delta H(0)} + T \frac{\delta V(s)}{\delta \gamma(0)} \quad (3-86)$$

$$\frac{\delta t(s)}{\delta H(0)} = \frac{\omega_n^2}{s^2(s^2 + \omega_n^2)} + T \frac{\delta V(s)}{\delta H(0)} \quad (3-87)$$

Equations (3-86) and (3-87) imply

$$\frac{\delta t(x)}{\delta \gamma_0} = \frac{\delta V(x)}{\delta H_0} + T \frac{\delta V(x)}{\delta \gamma_0} \quad (3-88)$$

$$\frac{\delta t(x)}{\delta H_0} = L^{-1} \left[\frac{\omega_n^2}{(s^2 + \omega_n^2)s^2} \right] + T \frac{\delta V(x)}{\delta H_0} \quad (3-89)$$

Using (3-88) and (3-89) in (3-66),

$$\frac{\partial V}{\partial \gamma_0} \cdot \frac{\partial t}{\partial H_0} - \frac{\partial V}{\partial H_0} \cdot \frac{\partial t}{\partial \gamma_0} = \frac{\delta V(x)}{\delta \gamma_0} L^{-1} \left[\frac{\omega_n^2}{s^2(s^2 + \omega_n^2)} \right] - \left\{ \frac{\delta V(x)}{\delta H_0} \right\}^2 \quad (3-90)$$

consequently, one needs to obtain the inverse transform of only three transfer functions, namely

$$\frac{\delta V(s)}{\delta \gamma_0}, \frac{\delta V(s)}{\delta H(0)}, \frac{\omega_n^2}{s^2(s^2 + \omega_n^2)}$$

when ω_n^2 is positive, the roots of the denominator polynomial are complex conjugates and

$$\frac{\partial V}{\partial \gamma_0} \cdot \frac{\partial t}{\partial H_0} - \frac{\partial V}{\partial H_0} \frac{\partial t}{\partial \gamma_0} = \omega_n x \sin(\omega_n x) + 2 \cos(\omega_n x) - 2 \quad (3-91)$$

The right-hand side of the (3-91), after being zero at $x = 0$, will subsequently become zero at

$$x = \frac{2\pi}{\omega_n} \quad (3-92)$$

implying that conjugate points will occur every full cycle of oscillatory solution. Hence, if the equilibrium point for the given H/λ_x is stable, i.e. it produces an oscillatory solution, a conjugate point will occur at the end of one full cycle of the oscillation. On the other hand, if ω_n^2 is negative, the roots are real and distinct, symmetric about the imaginary axis. In this case

$$\begin{aligned} \frac{\partial V}{\partial \gamma_0} \cdot \frac{\partial t}{\partial H_0} - \frac{\partial V}{\partial H_0} \frac{\partial t}{\partial \gamma_0} = \\ - x.d.\sinh(dx) + 2 \cosh(dx) - 2 \end{aligned} \quad (3-93)$$

where

$$d = \sqrt{|\omega_n^2|}$$

Expression (3-93) is zero only at $x = 0$. In this case, conjugate points do not occur. From (3-93), then, if the equilibrium point for the given H/λ_x is unstable, conjugate points will not occur.

The conjugate-point test is now applied to the three regimes of H/λ_x described earlier. As expected, for all values of H/λ_x to the left of $V(T-D)_{\max}$ point, conjugate points occur, indicating that the Euler solutions obtained with these values of H/λ_x do not afford a maximum to the time-range problem over long intervals. Euler solutions obtained with H/λ_x to the right of the $V(T-D)_{\max}$ point, on the other hand, satisfy the Legendre-Clebsch necessary conditions and Jacobi's necessary condition, and hence are optimal trajectories for the time-range problem.

SECTION 3.5

NUMERICAL SOLUTION OF THE TIME-RANGE PROBLEM

With the insight gained for the time-range problem with altitude dependence of thrust and drag suppressed, one may embark upon a numerical study of the more general case in which the aerodynamic coefficients are functions of Mach number and the thrust is Mach-altitude dependent. The data for a version of the F-4 aircraft with afterburner operative are used in this study. A cubic-spline representation (Ref. 44) is used to compute the values of zero-lift drag coefficient and the induced-drag coefficient. The drag coefficient is then computed as

$$C_D = C_{D_0}(M) + C_{D_{CL2}}(M) C_L^2 \quad (3-94)$$

where $C_L = \frac{W}{\frac{1}{2}\rho V^2 S}$ and C_{D_0} and $C_{D_{CL2}}$ are standard notation.

The drag is then obtained as the usual product of drag coefficient, dynamic pressure and the aircraft wing area. A cubic-spline lattice (Ref. 44) is used to compute the value of thrust at a given altitude and Mach number. Atmosphere density and speed of sound as functions of altitude are interpolated from standard-atmosphere tables using cubic splines. The system differential equations are integrated using a fifth-order Runge-Kutta-Verner method with variable step-size.

A plot of H/λ_x vs airspeed for equilibrium flight conditions corresponding to unaccelerated flight with specific energy, $E = h + \frac{v^2}{2g}$, frozen at 60,000 ft is shown in Fig. 3.10. The three regimes of H/λ_x identified earlier in this chapter can be seen in Fig. 3.10. Numerical

integration of the Euler equation with H/λ_x values picked from each of these regimes indicated that the solution for H/λ_x values to the left of $V(T-D)_{\max}$ are oscillatory. Numerical solution using H/λ_x to the right of $V(T-D)_{\max}$ point (high-speed end) are non-oscillatory and violent in character.

Next, a numerical conjugate-point test is set up based on a scheme suggested by Cicala (Ref. 56). In this scheme the partial derivatives with respect to λ_{i_0} required in the matrix (3-64) are calculated approximately in terms of difference quotients. Small increments in initial λ_i are employed in the evaluation of neighboring solutions of the original system of Euler equations. The conjugate-point test was carried out for various values of H/λ_x picked from Fig. 3.10. It was found, as expected, that only the non-oscillatory trajectories corresponding to H/λ_x values on the right of $V(T-D)_{\max}$ satisfy the no-conjugate-point condition. Oscillatory trajectories indicate the existence of a conjugate point after a cycle of oscillation.

From the foregoing, it is clear that the solution to time-range optimal-control problem are non-oscillatory and violently unstable in character. Within the permissible range of H/λ_x , as H/λ_x increases, the Euler solutions approach the energy-climb schedule in the (V,h) plane. Of particular interest in practical applications is that trajectory which terminates at the "dash-point" on the flight envelope, the maximum-level-flight-speed point. To determine the value of H/λ_x which will accomplish this, a plot of the locus of equilibrium points corresponding to unaccelerated flight at constant energy is made. Once this value of

H/λ_x is found, what remains to obtain the optimal trajectory is to determine the initial value of the control variable, γ , for a given set of initial conditions on altitude and airspeed.

In Fig. 3.11 the level-flight envelope for the F-4 aircraft is shown along with the energy-climb schedule. The discontinuity in the energy-climb schedule due to transonic drag rise may be noted (Ref. 41). The curve B is the locus of equilibrium points at each energy level corresponding to unaccelerated flight with the appropriate H/λ_x . The discontinuity due to transonic drag rise is again visible. An Euler solution for initial values of airspeed and altitude close to the equilibrium locus is also shown. To determine this trajectory, an iteration was undertaken on the initial value of the control variable, γ . With quadruple precision on the IBM-370/158, the initial path angle had to be determined to 13 significant digits. To illustrate the sensitivity of the Euler solution to the initial value of path angle γ , the last digit of γ_0 is perturbed in the positive and negative sense, with the trajectories 1 and 2 shown in Fig. 3.10 resulting.

A few more Euler solutions with initial conditions far removed from the equilibrium locus are shown in Fig. 3.12.

SECTION 3.6

DISCUSSION AND CONCLUSIONS

In this chapter, optimal flight in the vertical plane with a vehicle model intermediate in complexity between point-mass and energy

models was studied. Flight-path angle takes on the rôle of control variable in the model and range-open problems feature subarcs of vertical flight and singular subarcs as previously studied.

The minimum-range climb problem (the steepest climb of Ref. 53) has been found to have no minimum, not even a lower bound. In Ref. 53, the steepest-climb problem was studied using the Green's theorem device of Refs. 57 and 58. There is an important difference in vehicle modeling from that of the present chapter which should be noted as a key to resolving disparities between the character of optimal paths emerging. The analysis of Ref. 53 and 57 in essence replace $\cos\gamma$ in equation (3-3) with unity so that the problem solved is maximum altitude in a given distance (i.e. arc-length) rather than in a given range. This is a necessity with the linear-integral approach which can accommodate only problems of dimension two and a very special form of state equations. The solution to the distance-climb consists of a central path flown along a $(T-D)_{\max}$ locus in the V-h plane with vertical climb and dive transitions at the ends to meet specified boundary conditions.

From physical considerations it can be seen that when a positive margin of thrust over drag exists, the maximum-range climb trajectory without time or fuel constraints has neither a proper maximum nor an upper bound. In view of this fact major attention has been accorded to the time-range problem.

For the special case in which the thrust and drag depend only on airspeed, a plot of the ratio of time and range multipliers H/λ_x for equilibrium, corresponding to unaccelerated flight, revealed the

existence of three regimes. Positive values of H/λ_x on the low-speed side of $V(T-D)_{\max}$ and all negative values of H/λ_x were shown to yield oscillatory solutions. Although these meet the Legendre-Clebsch necessary conditions, they fail the conjugate-point test. Euler solutions with H/λ_x chosen to the right of the $V(T-D)_{\max}$ point satisfy both Legendre-Clebsch and Jacobi necessary conditions and are non-oscillatory in character. Depending on the nature of aircraft data, unstable equilibrium points may sometimes appear for certain H/λ_x values to the left of the airspeed corresponding to $V(T-D)_{\max}$, at certain energy levels. These normally have short duration and are not of major interest.

Numerical solution of the Euler equation and a numerical conjugate-point test for the F-4 aircraft data reinforced the conclusions arrived at in the analytical exercise.

From a practical viewpoint, the time-range trajectories which terminate at the "dash-point" on the level flight envelope are of particular interest. The multiplier ratio H/λ_x corresponding to this point is determined using the locus of equilibrium points at each energy level corresponding to unaccelerated flight. With this value of H/λ_x , the Euler solution for any (h,V) pair is obtained by iterating on the initial value of γ .

Euler solutions were obtained for various initial conditions. One observes that these tend to funnel rapidly into a certain corridor in the $V-h$ chart, in the vicinity of the equilibrium locus corresponding to unaccelerated flight. This feature of the solution family can be exploited in practical situations to simplify the computation of optimal trajectories.

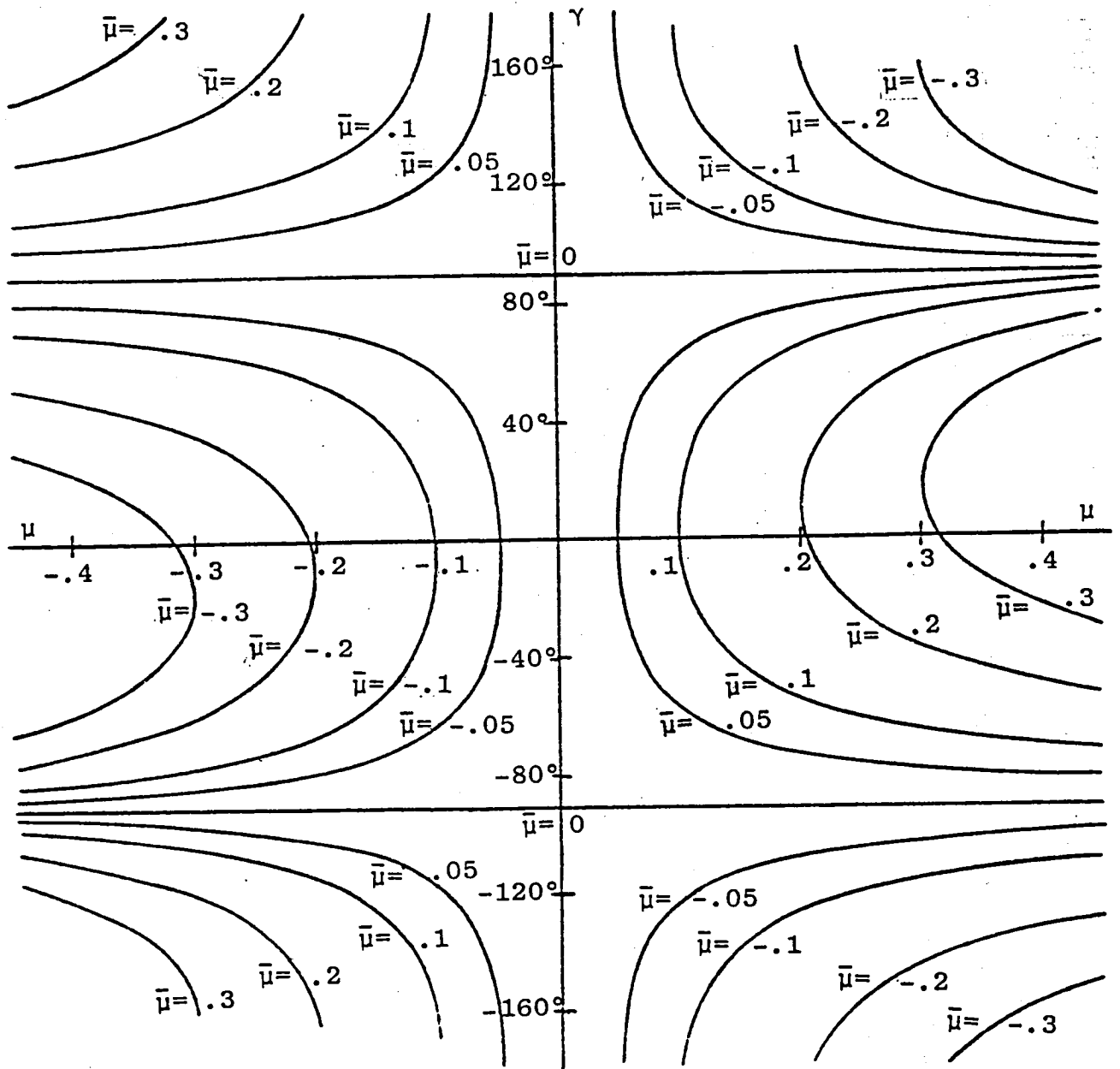
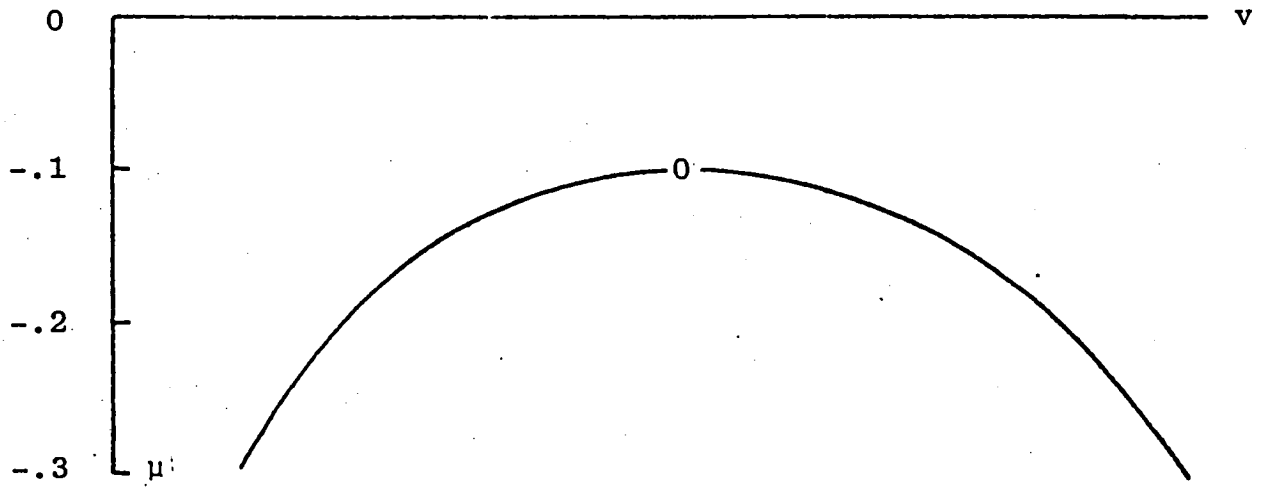


Fig. 3.1 Flight-Path Angle vs Acceleration variable for the Range Problem



Acceleration variable vs Airspeed

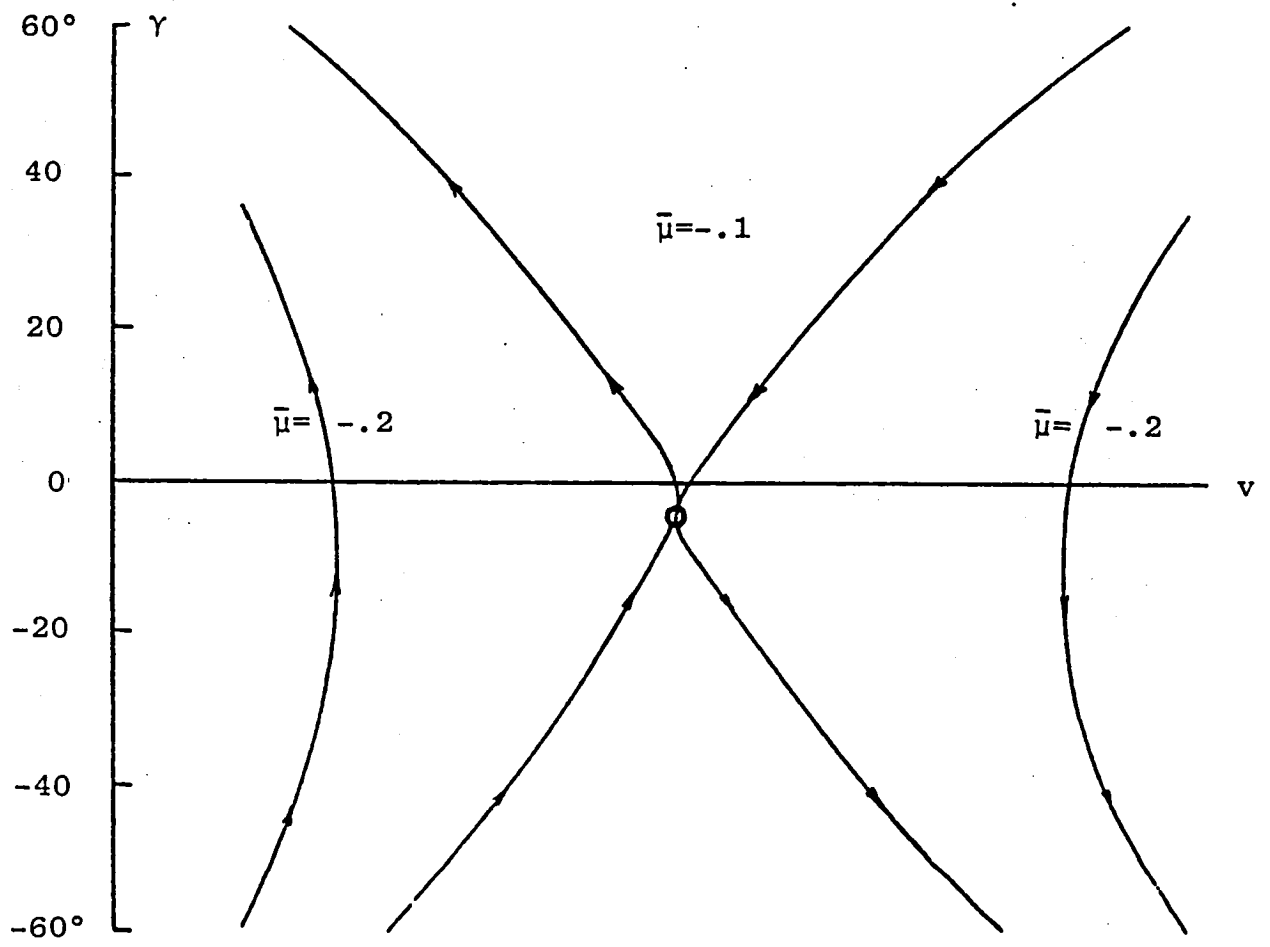
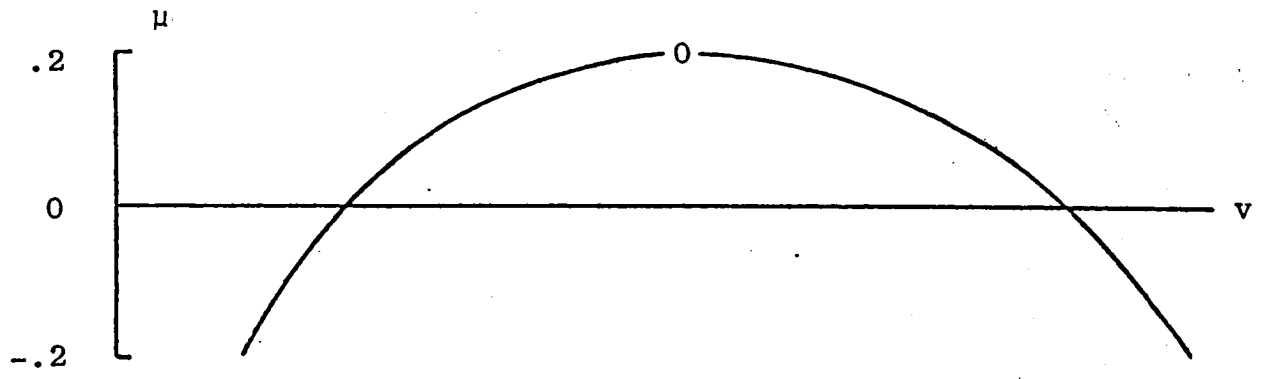


Fig. 3.2 Flight-Path Angle vs Airspeed in Gliding Flight for the Range Problem



Acceleration variable vs Airspeed

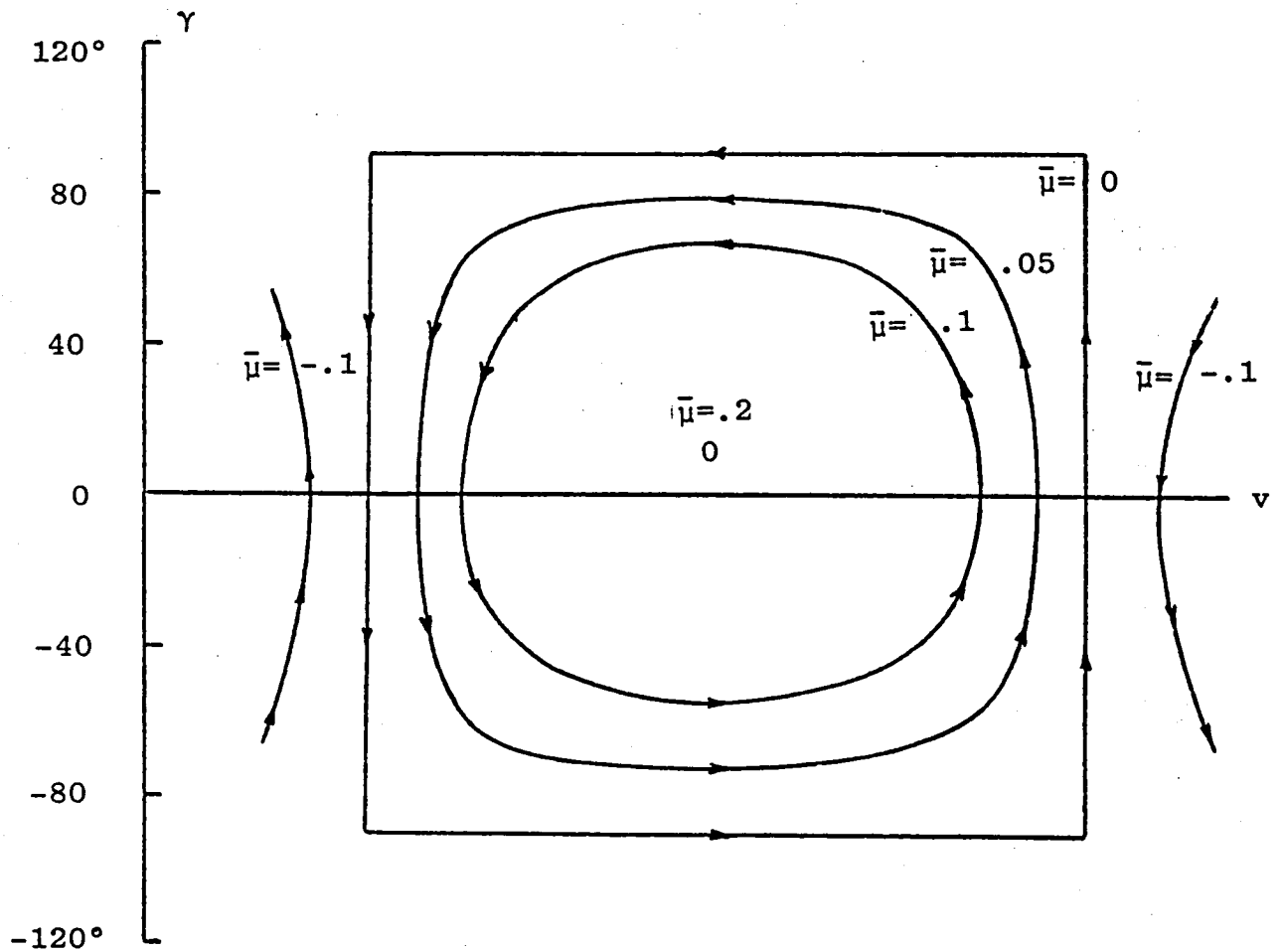


Fig. 3.3 Flight-Path Angle vs Airspeed in Powered Flight for the Range Problem

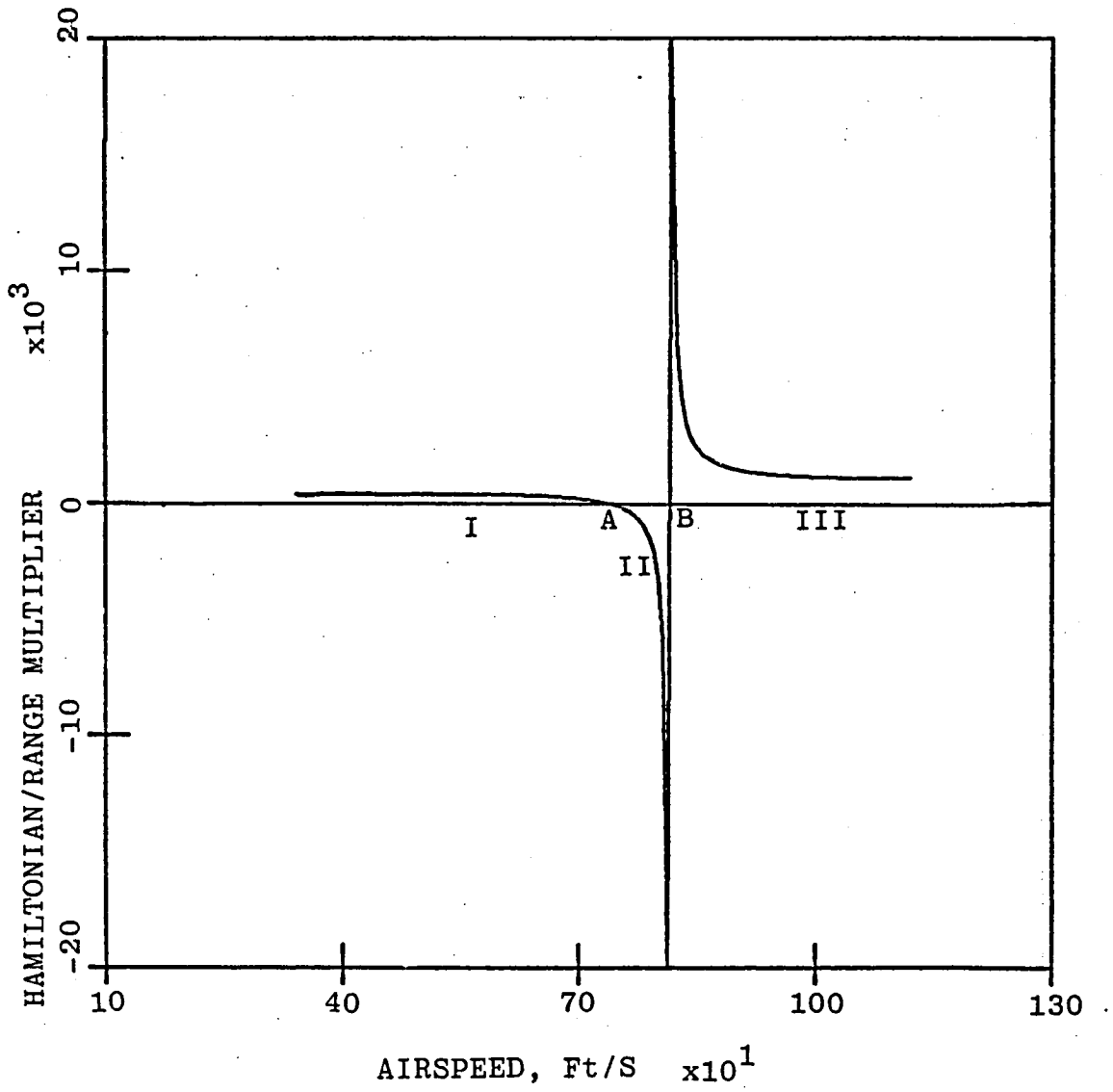


Fig. 3.4 H/λ_x vs Airspeed for Equilibrium Flight (Parabolic (T-D)/W distribution)

A : $(T-D)_{\max}$

B : $V(T-D)_{\max}$

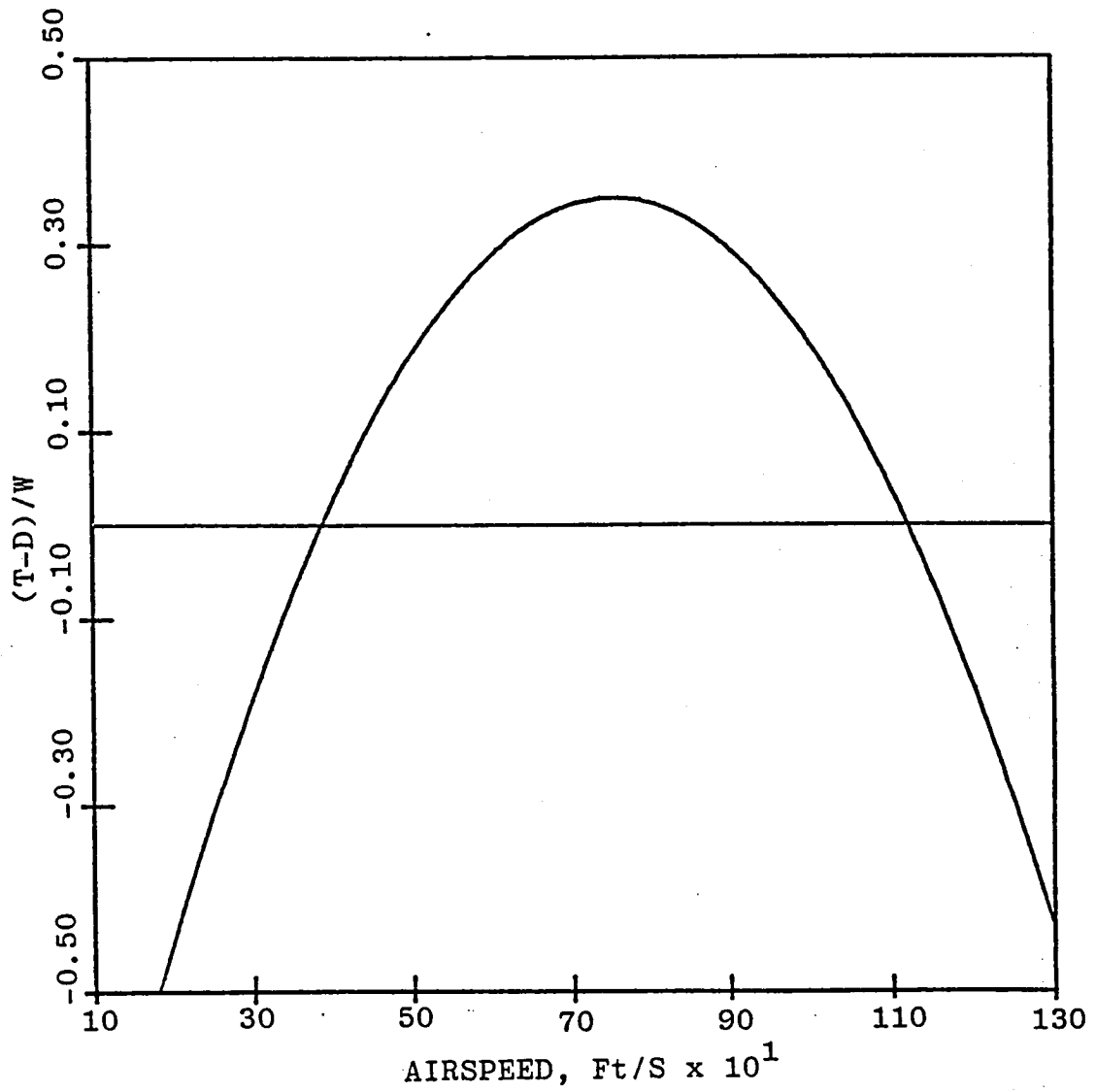


Fig. 3.5 $(T-D)/W$ vs Airspeed - A Typical Parabolic Distribution

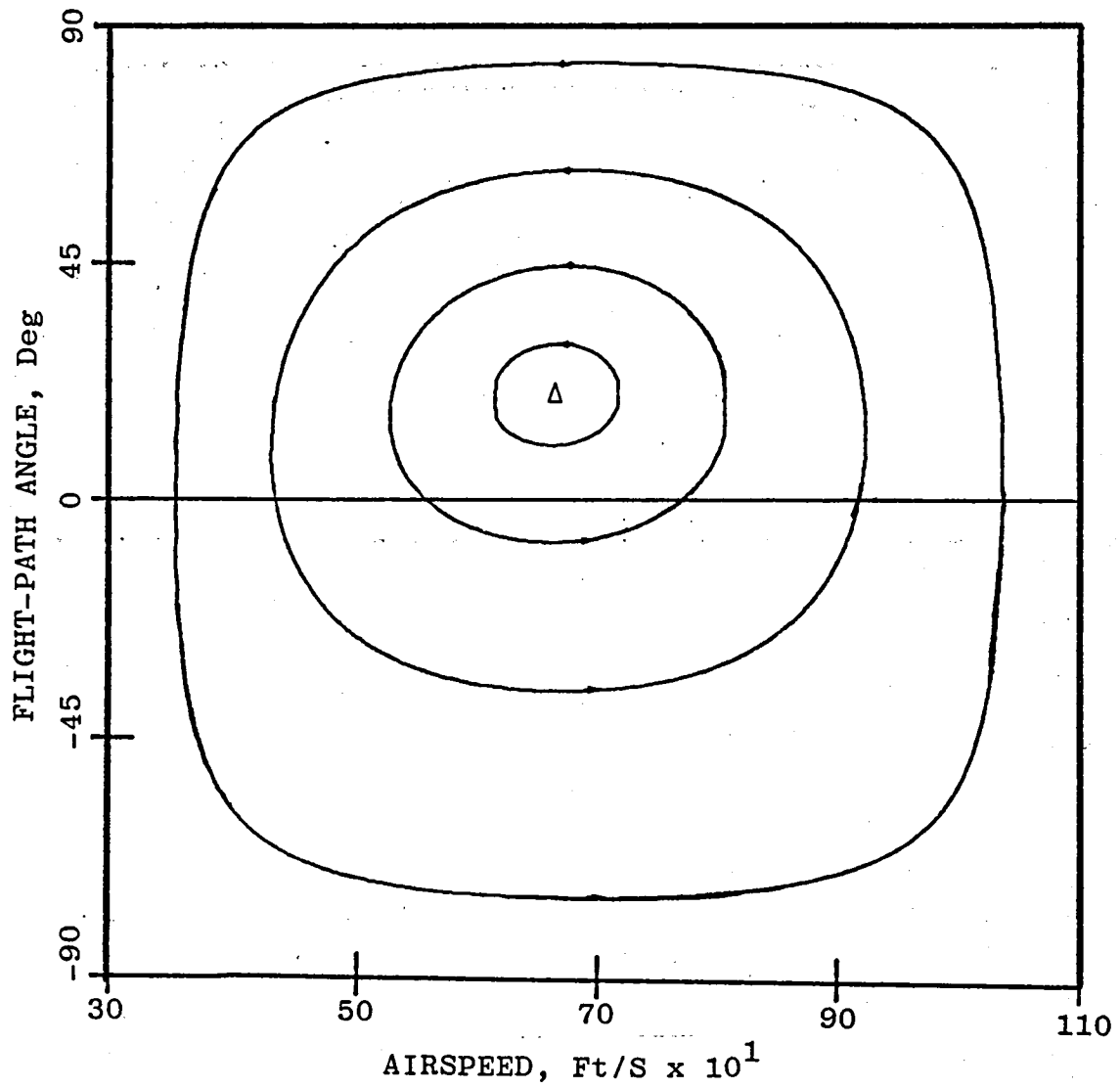


Fig. 3.6 Representative Analytical Solution for H/λ_x in the First Equilibrium Regime

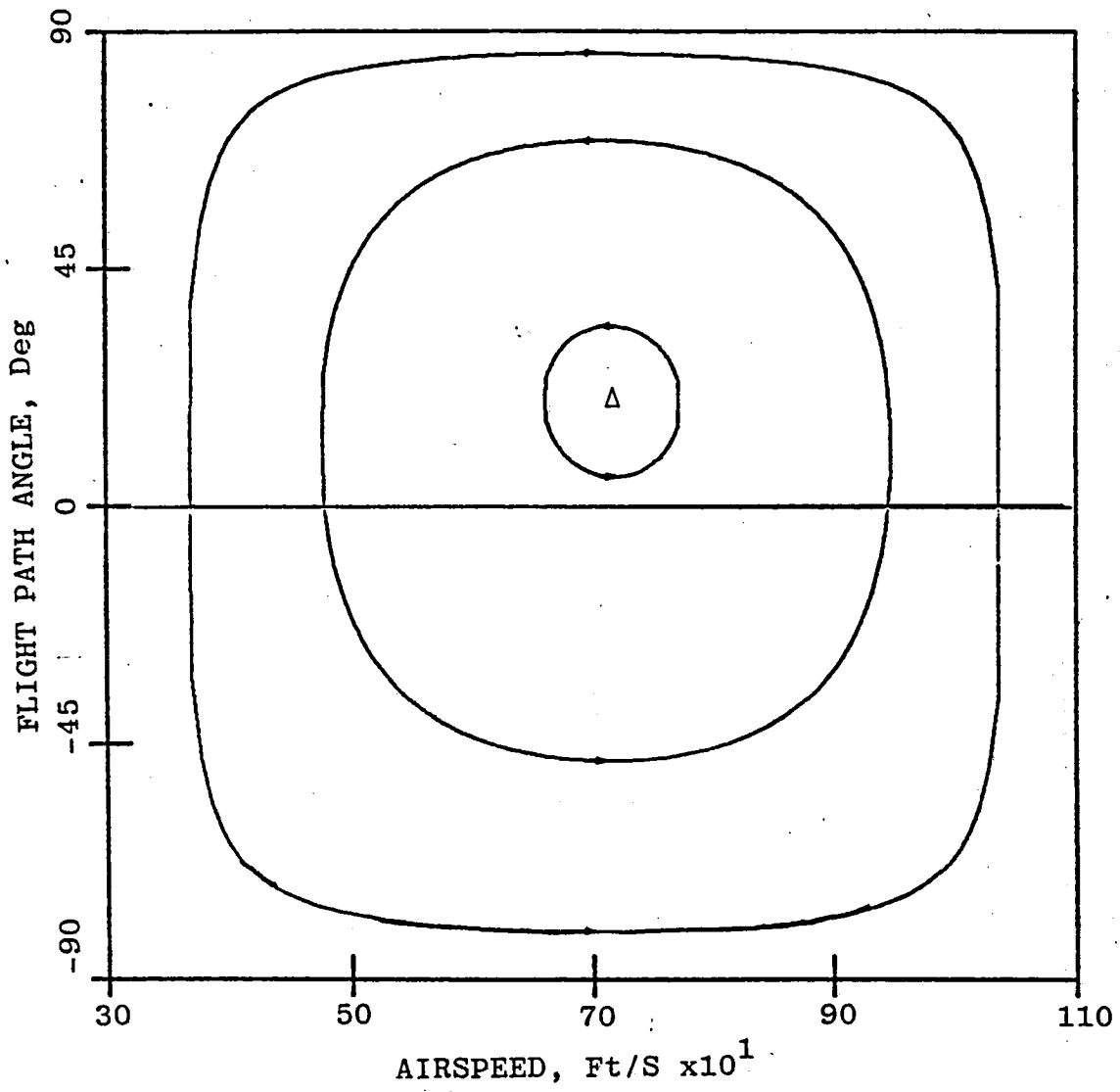


Fig. 3.7 . Representative Analytical Solution for H/λ_x in the Second Equilibrium Regime

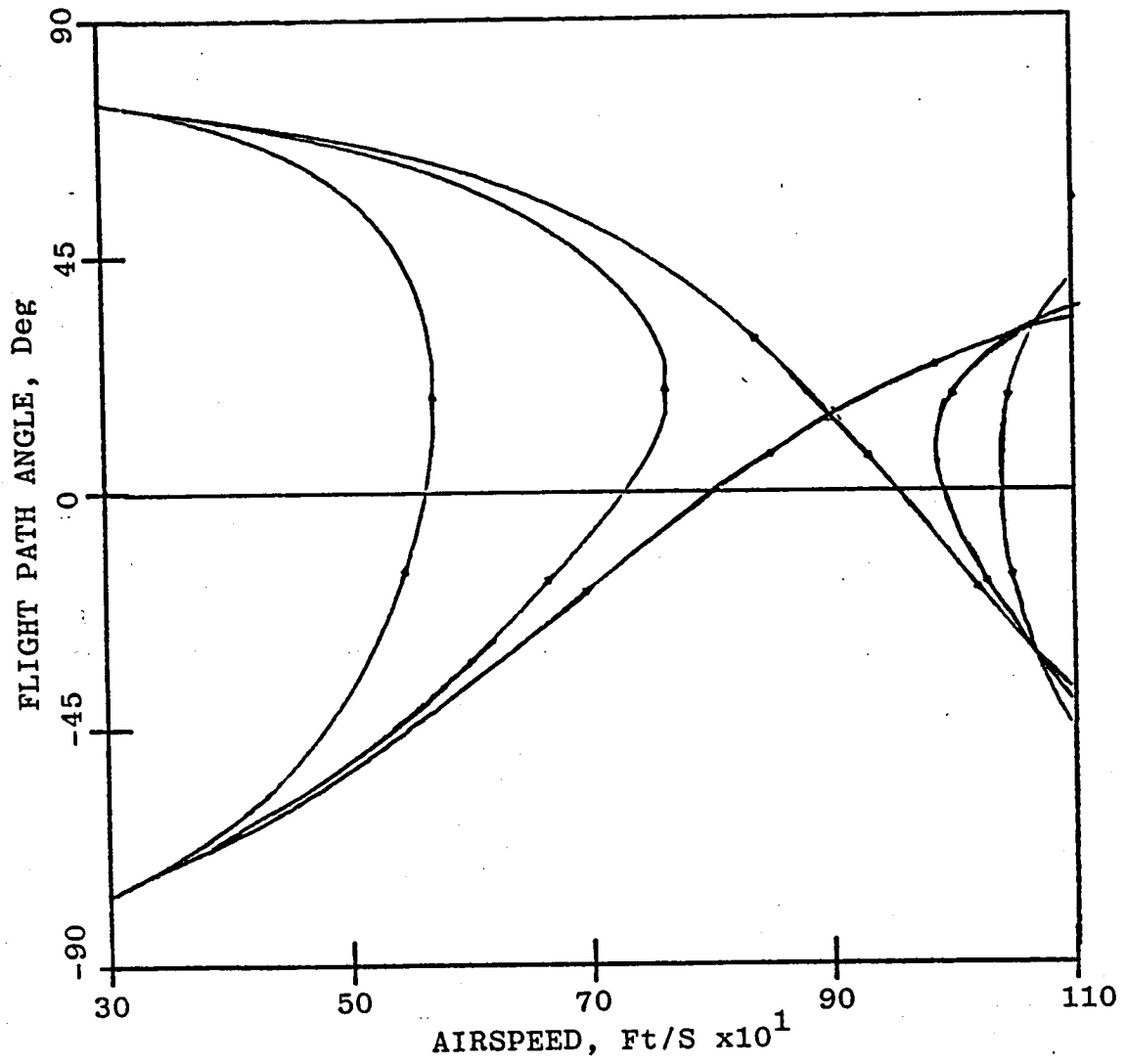


Fig. 3.8 Representative Analytical Solution for H/λ_x in the Third Equilibrium Regime

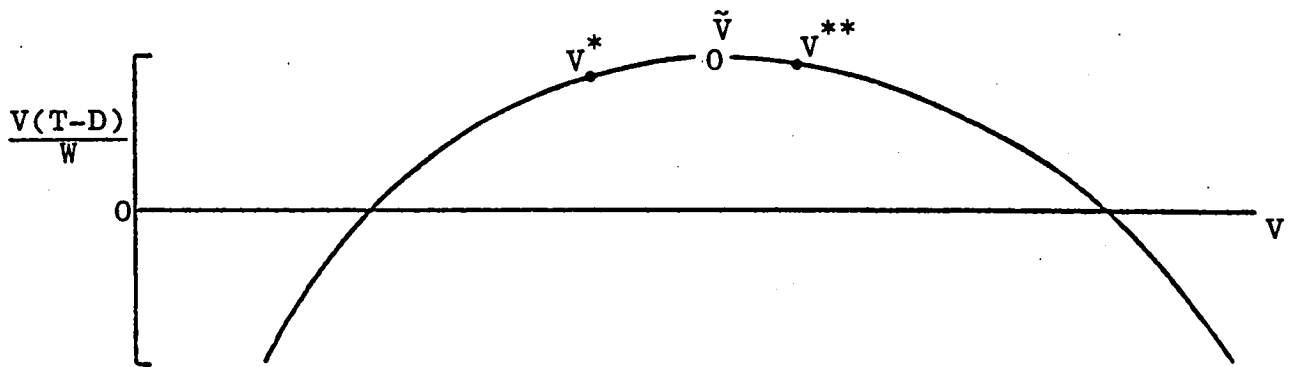


Fig. 3.9 A Parabolic distribution of Specific Excess Power vs Airspeed

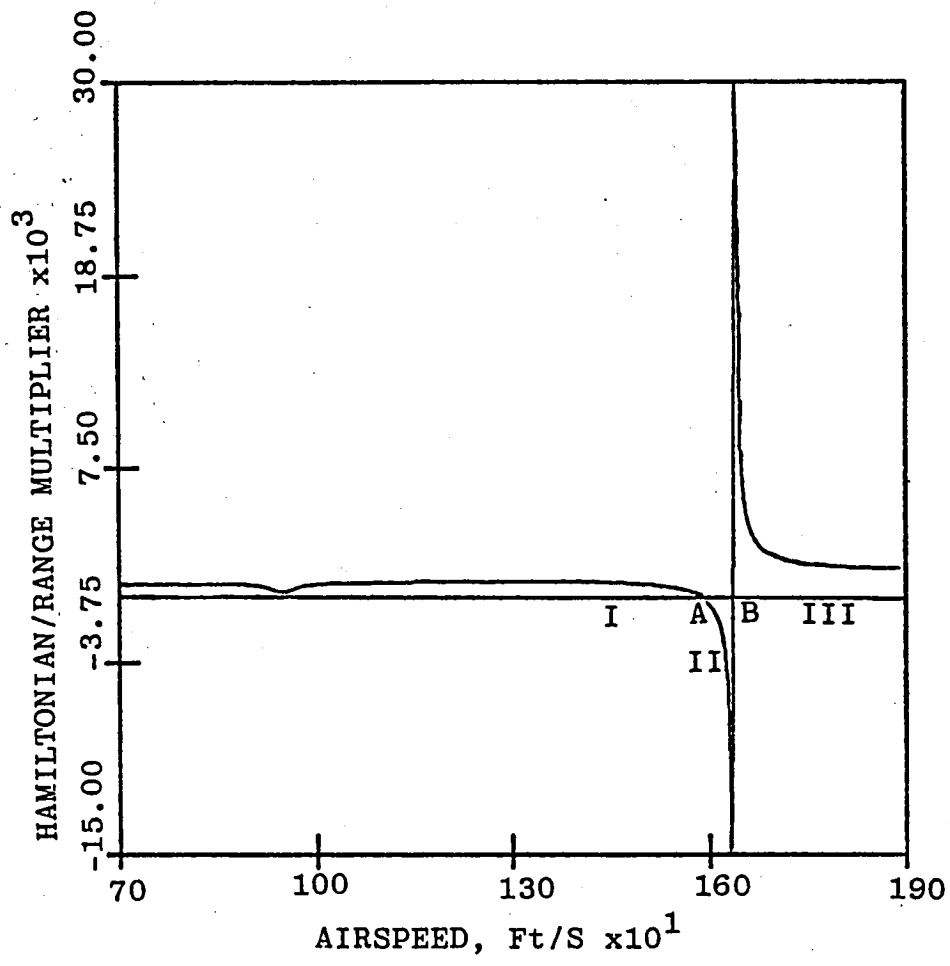


Fig. 3.10 H/λ_x vs Airspeed at Constant Specific Energy for F-4 Aircraft for Unaccelerated Flight

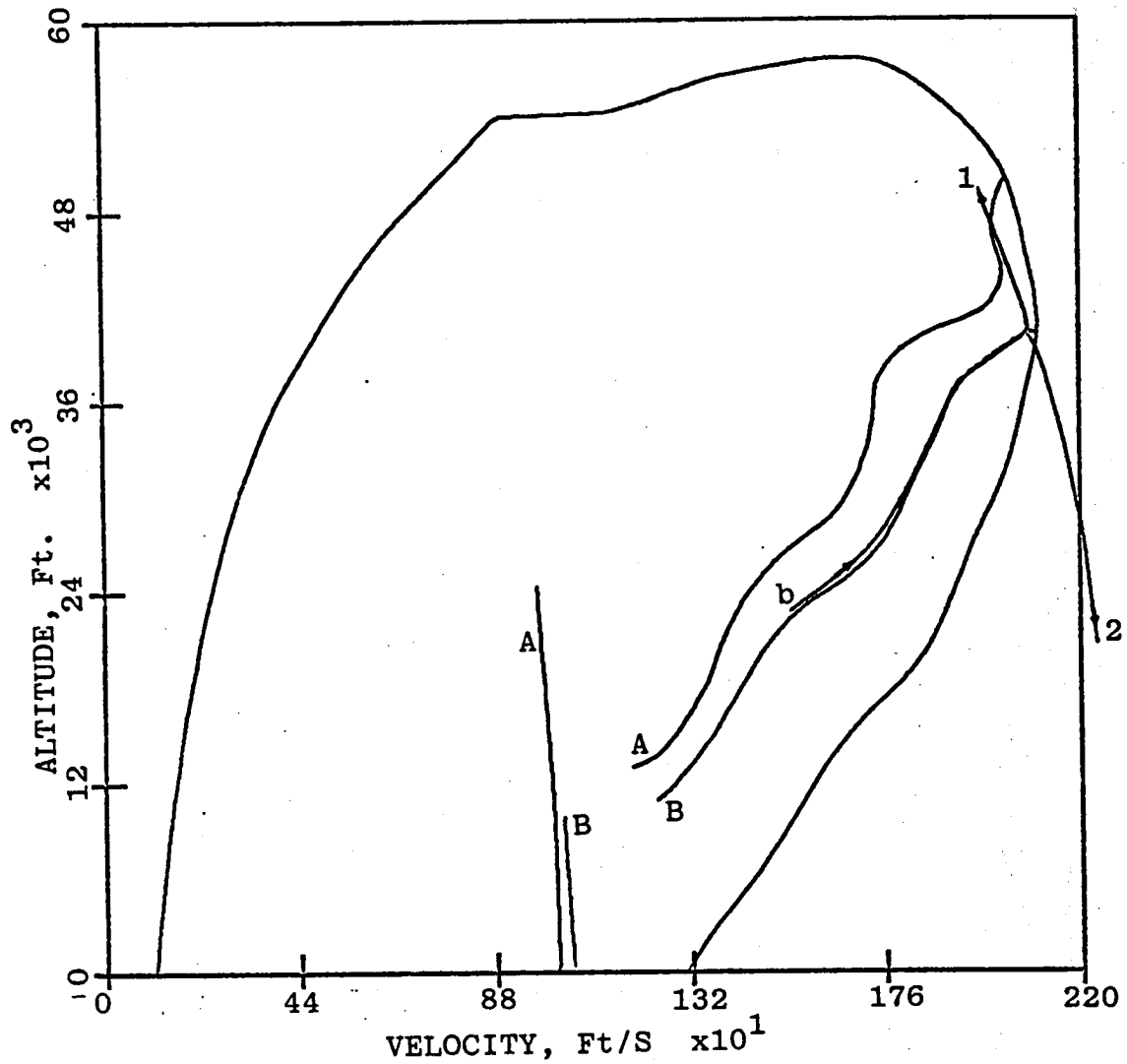


Fig. 3.11 Flight Envelope, Energy Climb Schedule, Equilibrium Locus and a Climb-Dash Euler Solution.

A : Energy Climb Schedule

B : Equilibrium Locus

b : Climb-Dash Euler Solution

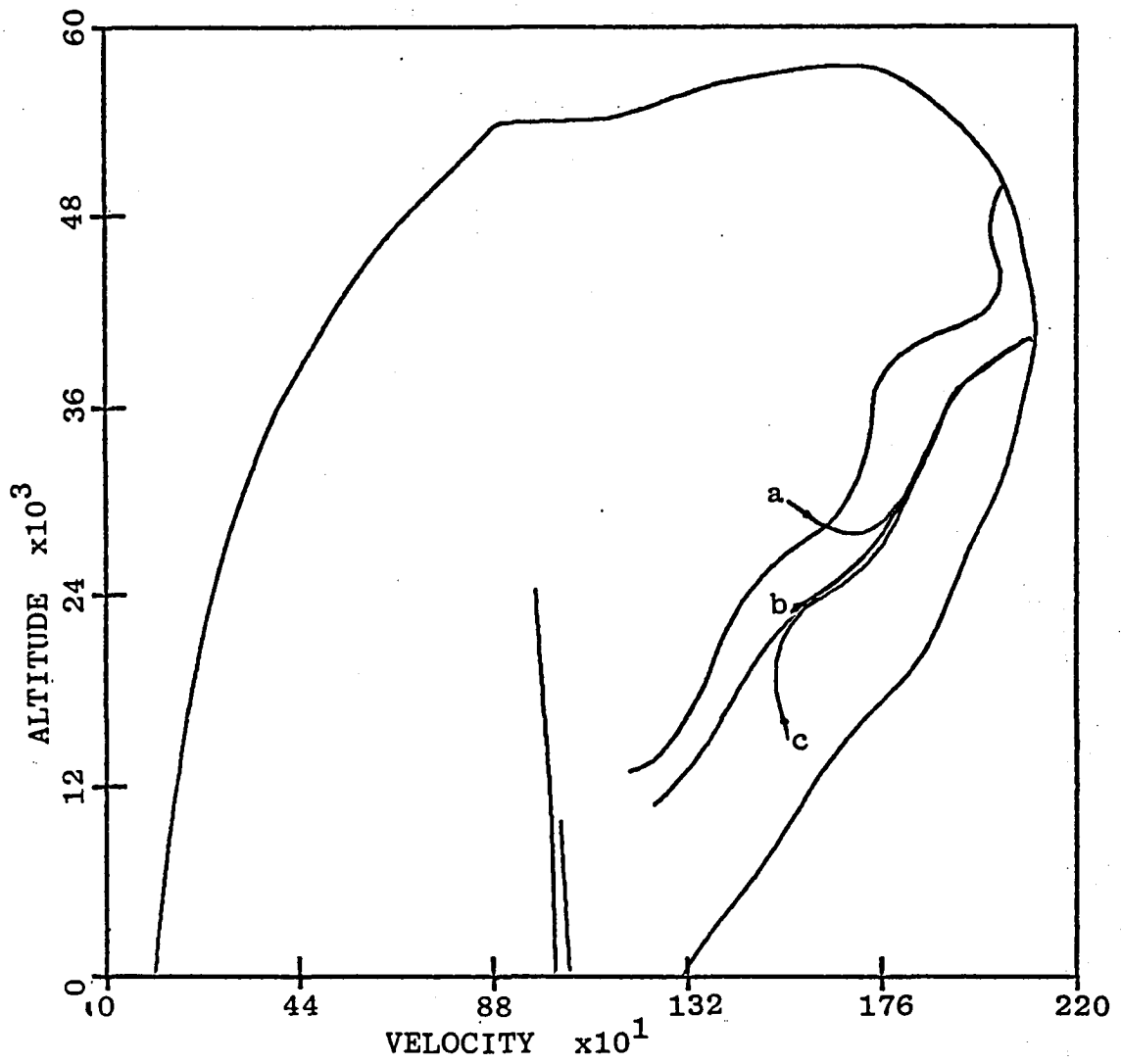


Fig. 3.12 Euler Solutions for the Climb-Dash Problem

a,b,c : Euler Solutions

CHAPTER 4

ENERGY STATE REVISITED

Henry J. Kelley

Eugene M. Cliff

Alan R. Weston

SECTION 4.1

PREFACE

Fritz Kaiser, a flight-test engineer at Messerschmitt, A. G., introduced the concept of "Gesamthöhe" ("resultant height") in connection with aircraft minimum-time climbs (Refs. 22 and 59). This is the sum of potential and kinetic energy per unit weight. Subsequently it has been referred to as "energy height" (Refs. 23 and 24) and "specific energy" (Ref. 60). Its use as a state variable in trajectory work is attractive because it is a "lower" variable than either altitude or velocity (Refs. 27, 61). Attempts to synthesize "slow" state variables are described in Refs. 25 and 61 in connection with singular-perturbation procedures. The present development attempts to synthesize both "fast" and "slow" variables for the minimum-time-to-climb problem along lines explored earlier in an appendix to Ref. 61. In the interest of brevity, familiarity on the part of the reader with the development of Ref. 25 is assumed in the following; however, knowledge of the relatively inaccessible Ref. 61 appendix is not. Minimum-time climbs in "energy" approximation are first reviewed and consideration given to choice of variables. A pair of variables which seem to offer attractive replacements for altitude and airspeed in singular-perturbation procedures is suggested. Use of the new variables in an energy-modelled climb-dash problem is illustrated.

SECTION 4.2

CLIMB EQUATIONS

The equations of motion for climbing flight are given in terms of conventional state variables, altitude, h , flight-path angle, γ , and velocity V , as

$$\dot{h} = V \sin\gamma \quad (4-1)$$

$$\dot{\gamma} = \frac{g}{V} \left(\frac{L}{W} - \cos\gamma \right) \quad (4-2)$$

$$\dot{V} = \frac{g(T-D)}{W} - g \sin\gamma \quad (4-3)$$

Here $T(h,V)$ is thrust, $D(h,V,L)$ drag, L lift and g the acceleration of gravity. An assumption of thrust-along-the-path has been incorporated.

SECTION 4.3

CHOICE OF VARIABLES

An essential feature of "energy" approximation is that drag be treated as a function of h and V only. This is consistent with approximation of $\sin\gamma$ and $\cos\gamma$ via expansion in powers of γ through first-order terms only and with deletion of the $\dot{\gamma}$ term as negligible—another feature essential to reduction in order. With these simplifications the system becomes

$$\dot{h} = V\gamma \quad (4-4)$$

$$\dot{V} = \frac{g(T-D)}{W} - g\gamma \quad (4-5)$$

where now $D(h,V,L)$ is evaluated for $L = W$.

Two new variables, ϕ and ψ , are to be introduced in place of h and V , ϕ to be "slow" and ψ "fast".

The equation of state for ϕ is

$$\begin{aligned} \dot{\phi} &= \frac{\partial \phi}{\partial h} \dot{h} + \frac{\partial \phi}{\partial V} \dot{V} \\ &= \frac{\partial \phi}{\partial V} \left[\frac{g(T-D)}{W} \right] + \left[V \frac{\partial \phi}{\partial h} - g \frac{\partial \phi}{\partial V} \right] \gamma \end{aligned} \quad (4-6)$$

If one insists that $\dot{\phi}$ be independent of the control-like variable, γ , then ϕ must satisfy the partial differential equation

$$V \frac{\partial \phi}{\partial h} - g \frac{\partial \phi}{\partial V} = 0 \quad (4-7)$$

This is satisfied by

$$\phi = h + \frac{V^2}{2g} \quad (4-8)$$

or by any once-differential function of this expression (Ref. 61). Thus $\phi = E$, specific energy, is "slow" in the sense specified.

It has been usual to adopt as the second state variable, ψ , either V (Ref. 27) or h (Ref. 25). Either is suitable for analysis of the "slow" motion, given by the single state equation

$$\dot{E} = \frac{V(T-D)}{W} \quad (4-9)$$

For minimum-time passage to higher energy levels, the right member of (4-9) is maximized with respect to V or h at constant E . The expression on the right of (4-9) is "specific excess power", P_s , of the flight-performance literature (e.g. Ref. 60) and simply p later in the present chapter. With a more general choice of $\psi(V,h)$, the maximization of (4-9) is done with

respect to this variable after V and h have been replaced by suitable functions of ϕ and ψ representing the inverse transformation. The resulting values of V , h and \dot{E} are the same, however.

The choice of $\psi(V,h)$ matters, however, in the determination of γ along the "slow-motion" (or "outer") solution, as γ must be such that $\dot{\psi} = 0$, in the procedure of Ref. 27. With the choice of $\psi = h$ as in Ref. 27, the approximation $\gamma = 0$ is obtained, while if $\psi = V$ is assumed, then

$$\gamma = \frac{(T-D)}{W} \quad (4-10)$$

which is, to linear approximation in γ , the path angle for unaccelerated climb. More generally the expression

$$\begin{aligned} \dot{\psi} &= \frac{\partial \psi}{\partial h} \dot{h} + \frac{\partial \psi}{\partial V} \dot{V} \\ &= \frac{\partial \psi}{\partial h} V\gamma + \frac{\partial \psi}{\partial V} \left[\frac{g(T-D)}{W} - g\gamma \right] = 0 \end{aligned} \quad (4-11)$$

is to be solved to obtain the zeroth-order "outer" approximation for γ . The choice

$$\psi = \left. \frac{\partial p}{\partial h} \right]_E \quad (4-12)$$

suggests itself for compatibility with the outer solution, because this quantity, and therefore its time derivative, is zero along the outer solution. Here

$$p \equiv \frac{V(T-D)}{W} \quad (4-13)$$

is "specific excess power", a known function of h and V . This choice of ψ is seen to generate zeroth-order γ consistent with (4-4) and (4-5) along

the outer solution.

Contours $\phi = E = \text{const.}$ and $\psi = \text{const.}$ are shown in Fig. 4.1 for the aircraft data of Ref. 41 (a version of the F-4). The contours of $\psi = \text{constant}$ indicate a breakdown of one-to-one mapping associated with jumps of the energy-climb path, $\psi = 0$, between ridges of $p(h,V)$ (Ref. 41); in fact, the mapping $(\phi, \psi) \rightarrow (h, V)$ is two-to-one and even three-to-one within the flight envelope. This local non-invertibility represents a less-than-ideal feature for a coordinate transformation; however, one does not actually have to transform to the new variable to exploit the concept.

Flight-path angle γ is shown as a function of $\phi = E$ in Fig. 4.2 for three choices of "fast" variable: h , V and ψ . Only the "outer" contributions are presented. Also presented is path angle γ for optimal climb with a point-mass model.

Experience is that the calculation of first- and higher-order composites is quite complex (Refs. 41, 42). Thus it makes sense to choose variables carefully so as to enhance the fidelity of the zeroth-order solution as far as possible.

SECTION 4.4

CLIMB-DASH PROBLEM

Consider as an application the climb-dash problem, in which a minimum-time trajectory to a remote value of x is sought, where x is down-range and, for small γ , is defined by

$$\dot{x} = V$$

(4-14)

The character of the solution is that of a combined climb-dash generally faster than an energy climb (Fig. 4.3) fairing into sustained flight at the high-speed point on the level-flight envelope. γ as a function of E is shown in Fig. 4.4 for the three choices of fast variable. Solutions of a corresponding point-mass-modelled problem for different aircraft data are studied in Ref. 41.

Fig. 4.1 Contours in the Altitude-Velocity Chart

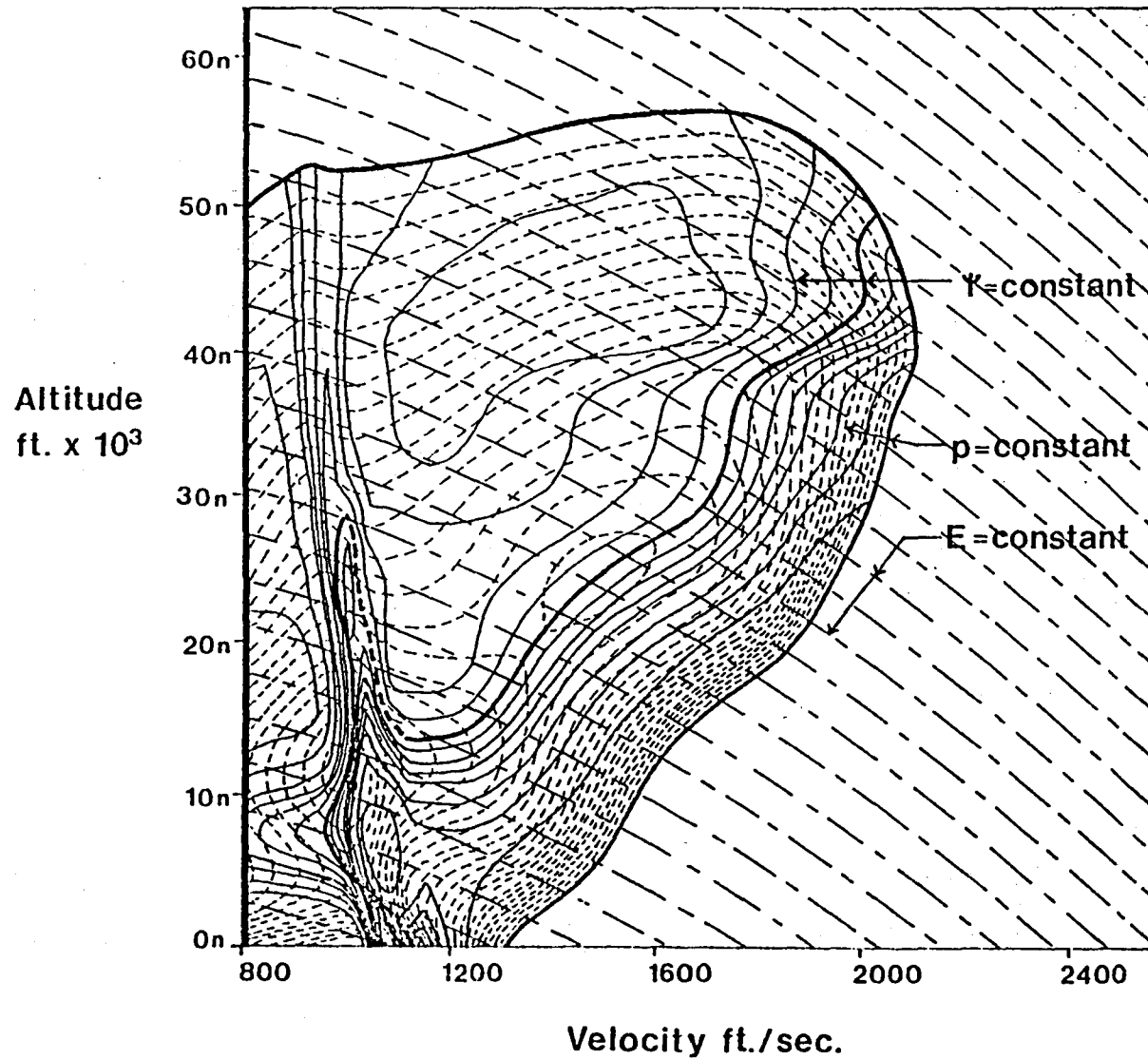


Fig. 4.2

δ vs. E - Energy Climb

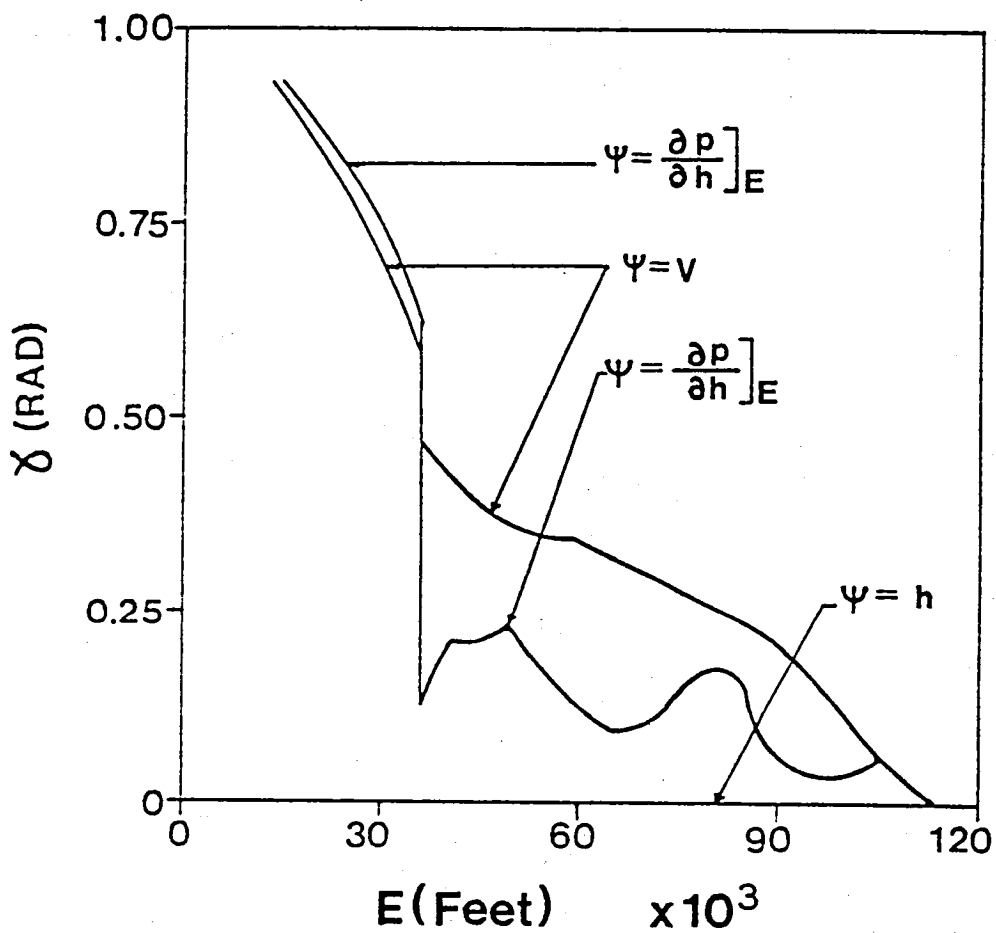


Fig. 4.3 **Altitude vs. Velocity - Climb-Dash**

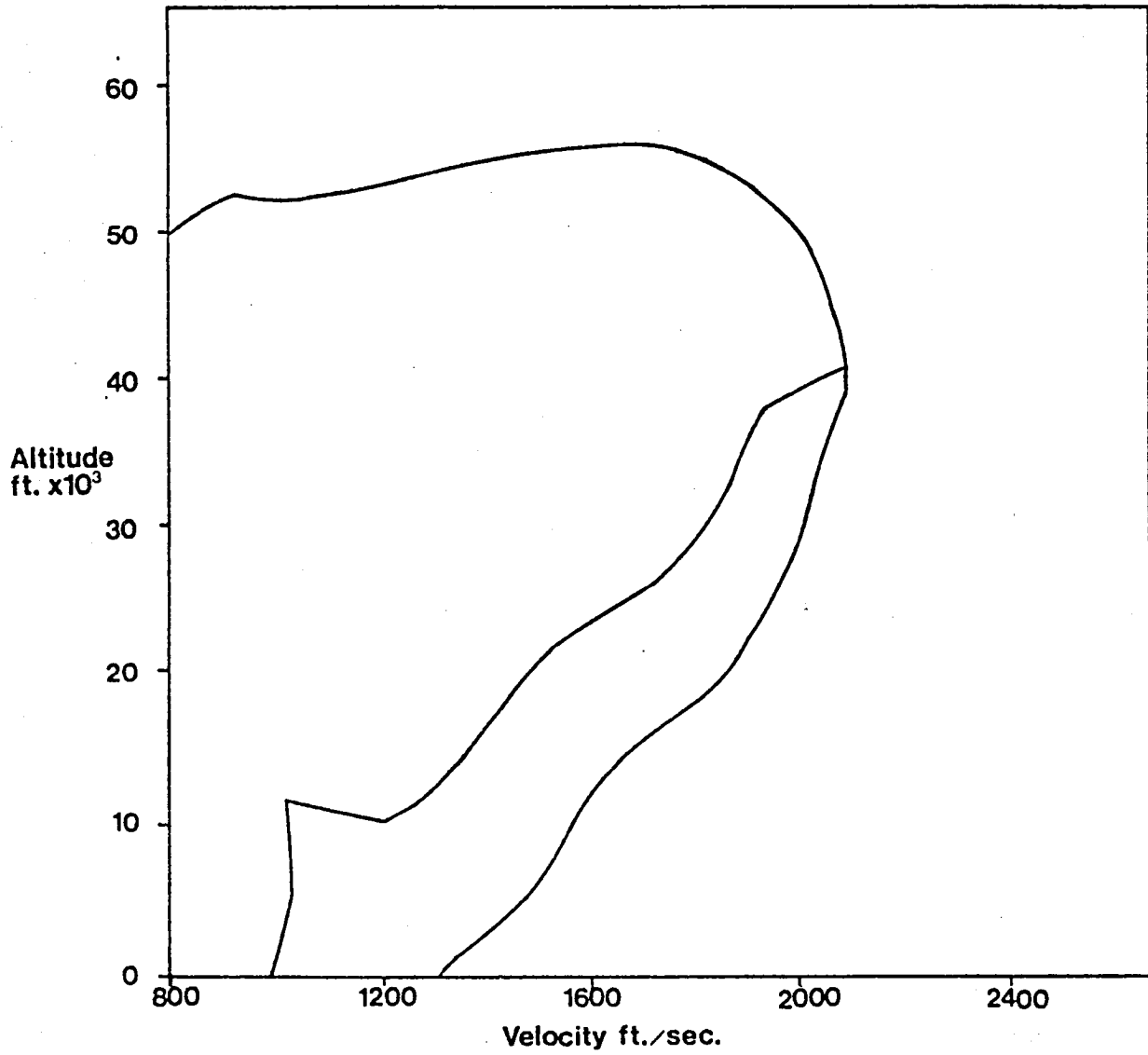
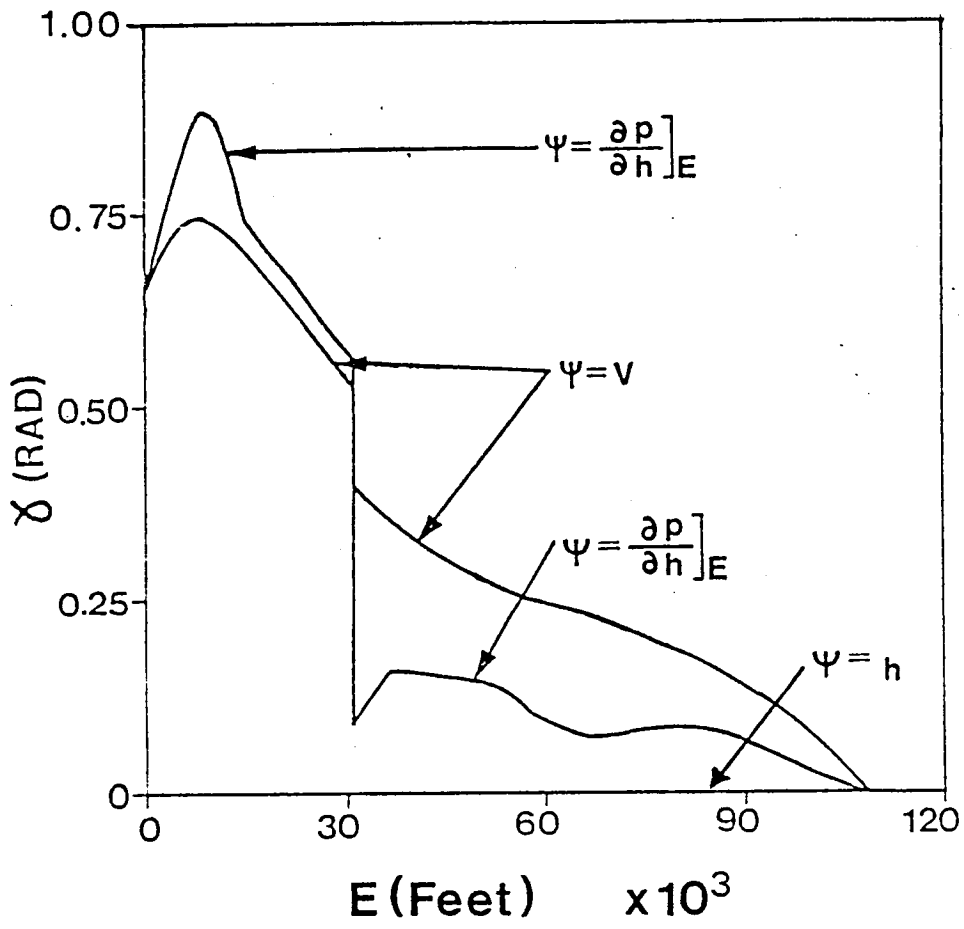


Fig. 4.4

δ vs. E - Climb-Dash



CHAPTER 5

CLASSICAL AND NEO-CLASSICAL CRUISE-DASH OPTIMIZATION

K. D. Bilimoria

E. M. Cliff

H. J. Kelley

SECTION 5.1

PREFACE

This chapter investigates the problem of determining an atmospheric flight-path between given end-points, that minimizes a linear combination of time and fuel. In the next section the trajectory-shaping problem will be formulated for a point-mass model and rectilinear cruise will be considered as an 'outer' solution when Newtonian dynamics are 'fast.' A subsequent section will discuss the resulting classical cruise-dash problem. In particular, it will be shown that nonconvexity in the fuel-flow vs air-speed graph has important consequences in optimum-cruise problems with time restrictions. Some computations will then be presented illustrating the sometime occurrence of time-shared operation between two altitude-airspeed combinations for optimal cruise-dash.

SECTION 5.2

PROBLEM FORMULATION

While this chapter is primarily concerned with classical cruise-dash analysis, it is appropriate to consider the connection between cruise-dash performance and the more general problem of flight-path optimization. For this purpose we begin with the point-mass model, albeit in a somewhat special form:

$$\epsilon^2 \ddot{h} = V \sin \gamma \quad (5-1)$$

$$\epsilon^2 \dot{\gamma} = (g/V) \left(\frac{(L + \epsilon_3 T \sin \alpha) \cos \mu}{(W - \epsilon_3 \tilde{W})} - \cos \gamma \right) \quad (5-2)$$

$$\epsilon^1 \dot{E} = \frac{(T-D)V + \epsilon_3 T V (\cos \alpha - 1)}{(W - \epsilon_3 \tilde{W})} \quad (5-3)$$

$$\epsilon^1 \dot{\chi} = \frac{g L \sin \mu}{V(W - \epsilon_3 \tilde{W}) \cos \gamma} \quad (5-4)$$

$$\dot{x} = V \cos \gamma \cos \chi \quad (5-5)$$

$$\dot{y} = V \cos \gamma \sin \chi \quad (5-6)$$

$$\dot{\tilde{W}} = Q \quad (5-7)$$

These are the equations for three-dimensional aircraft flight with zero side-force over a flat, non-rotating Earth. In these equations h is the altitude, γ the path-angle, E the energy per unit weight, χ the velocity-heading angle, x and y the Northerly and Easterly position components and \tilde{W} is the fuel used. The symbol V is to be regarded as a convenient shorthand for the quantity $[2g(E-h)]^{1/2}$, where g is the acceleration due to gravity. L and D denote the usual aerodynamic force components, lift and drag, respectively; W is the (initial) weight of the aircraft. T is the thrust and Q is the fuel-flow rate; each depends on a throttle parameter, η . The angle α is angle-of-attack, while μ is bank angle.

The parameters ϵ^1 and ϵ^2 are introduced as in Ref. 25 to motivate an order-reduction while ϵ_3 is convenient for imbedding certain complicating effects. In particular, with $\epsilon_3 = 0$ the model has constant aircraft weight and thrust along the path. Complications such as non-standard atmosphere or winds-aloft might be treated in the same manner in terms of ordinary perturbations.

In addition to the dynamical equations the system is subjected to certain other constraints of state/control - inequality type:

$$\beta_1 = (h - h_T) \geq 0 \quad (\text{terrain limit})$$

$$\beta_2 = (\bar{q} - q(E-h)) \geq 0 \quad (\text{dynamic pressure limit})$$

$$\beta_3 = (\bar{M} - M) \geq 0 \quad (\text{Mach limit})$$

$$\beta_4 = (\bar{n}W - C_L qS) \geq 0 \quad (\text{normal load-factor limit})$$

$$\beta_5 = (\bar{C}_L(M) - C_L) \geq 0 \quad (\text{aerodynamic limit})$$

In these constraints \bar{q} , \bar{M} , \bar{n} , \bar{C}_L are maximum allowable values of dynamic pressure, Mach number, normal load-factor and lift coefficient, respectively. The last is a specified function of Mach number. The path-optimization problem we wish to consider is:

Choose the controls C_L (or α), μ , and η so as to transfer the system from a given initial point $(h_0, \gamma_0, E_0, x_0, x_0, y_0)$ to a given final point $(h_f, \gamma_f, E_f, x_f, x_f, y_f)$ while minimizing a Mayer-type cost function

$$C = \mu_1 t_f + \mu_2 \bar{W} \quad (5-8)$$

The parameters μ_1 and μ_2 are specified so as to represent a trade-off between time and fuel. In particular, with $\mu_1 = 0$ and $\mu_2 > 0$ the problem is to minimize fuel while with $\mu_1 > 0$ and $\mu_2 = 0$ the problem is to minimize time. Note that the range is specified for this problem.

To 'solve' this optimization problem one proceeds to form the variational Hamiltonian and with the prejudice of foresight defines

$$H = H_1 + H_2 \quad (5-9)$$

$$H_1 = \lambda_x V \cos \gamma \cos \chi + \lambda_y V \cos \gamma \sin \chi + \lambda_{\tilde{W}} Q \quad (5-10)$$

$$H_2 = \lambda_h f_h + \lambda_\gamma f_\gamma + \lambda_E f_E + \lambda_\chi f_\chi \quad (5-11)$$

The terms such as f_h in H_2 are a shorthand for the right members of the respective dynamical equations.

One might now apply the Minimum Principle (Refs. 39 and 48) to this problem, deducing the state-Euler equations with appropriate boundary conditions. The result would be a two-point-boundary-value problem involving a fourteenth-order system of differential equations. While this may be solvable with modern computer software, its usefulness in on-board intercept guidance might, in the current state-of-the art, be questioned.

The interpolation parameters ϵ^1 and ϵ^2 separate the aircraft equations of motion into three time-scales involving 'fast', 'intermediate' and 'slow' state variables. The approach here, as in Ref. 25, is to begin by considering the problem for the reduced system with $\epsilon^1 = \epsilon^2 = \epsilon_3 = 0$. In this case the dynamical system involves only three state variables x , y , \tilde{W} (note that time is state-like since it appears in the performance index) and seven control variables h , γ , E , χ , μ , C_L and η . With $\epsilon^1 = \epsilon^2 = 0$ the first four system equations become constraints from which one deduces that

$$\mu = \gamma = 0 \quad (5-12)$$

$$L = W \quad (5-13)$$

$$T = D \quad (5-14)$$

Lift equals weight can be 'solved' for C_L given E and h , while thrust equals drag can then be 'solved' for η . With these explicit conditions the part of the Hamiltonian labelled H_2 is guaranteed to be zero. Hence,

the min-H operation amounts to selecting n , E , h and χ to minimize H_1 , subject to the inequality constraints, $\beta_i \geq 0$. Observe that with $\epsilon_3 = 0$ none of the state variables x , y or \tilde{W} appear on the right-hand side of a state equation so that the corresponding co-states λ_x , λ_y and $\lambda_{\tilde{W}}$ are constant in time.

Proceeding with the min-H operation one expresses the unknown co-states λ_x and λ_y in polar form as

$$\lambda_x = A \cos \Lambda \quad (5-15)$$

$$(A \geq 0)$$

$$\lambda_y = A \sin \Lambda \quad (5-17)$$

and rewrites the Hamiltonian as

$$H_1 = V A \cos(\chi - \Lambda) + \lambda_{\tilde{W}} Q \quad (5-17)$$

It is clear that the appropriate choice is $\Lambda = (\chi - \pi)$, where χ is selected so that the rectilinear path goes through the specified points (x_0, y_0) and (x_f, y_f) .

The terminal transversality condition requires (Refs. 39 and 48) that

$$H_1(t_f) = -\mu_1 \quad (5-18)$$

$$\lambda_{\tilde{W}}(t_f) = \mu_2 \quad (5-19)$$

from which one finds

$$A = \left[\mu_1 + \mu_2 Q(t_f) \right] / V(t_f) \quad (5-20)$$

so that

$$H_1 = - \left\{ \left[\mu_1 + \mu_2 Q(t_f) \right] / V(t_f) \right\} V + \mu_2 Q \quad (5-21)$$

One now defines constants λ_F (fuel) and λ_R (range) by

$$\lambda_F = \mu_2 \quad (5-22)$$

$$\lambda_R = \left[\mu_1 + \mu_2 Q(t_f) \right] / V(t_f) \quad (5-23)$$

and observes that the min-H operations can be interpreted as seeking a point (given by E, h and η) that minimizes the quantity

$$J = \lambda_F Q - \lambda_R V \quad (5-24)$$

subject to level-flight equilibrium constraints and the inequality constraints $\beta_i \geq 0$. This is a classical cruise-dash problem and will be examined in some detail. The approach taken here will be to solve this problem for specified λ_F and λ_R and compute the corresponding μ_1 and μ_2 from

$$\mu_1 = \lambda_R V - \lambda_F Q = - J_{\min} \quad (5-25)$$

$$\mu_2 = \lambda_F \quad (5-26)$$

SECTION 5.3

CRUISE-DASH ANALYSIS

The problem considered here is that of finding a point on or within the flight envelope, characterized by a speed V, an altitude h and a throttle-setting η , that minimizes the quantity

$$J = \lambda_F Q(\eta, h, V) - \lambda_R V \quad (5-27)$$

subject to the level-flight equilibrium constraints and inequality constraints $\beta_i \geq 0$.

The parameters λ_F and λ_R are specified constants and their relation to the parameters μ_1 and μ_2 in the dynamic performance index has been

described above. Recapitulating some of the previous discussion, one notes that for a given (h, V) pair the equation $L = W$ is to be solved for C_L . One then evaluates the corresponding drag $D(h, V, C_L)$ and then 'solves' for the throttle-setting η such that $T(\eta, h, V)$ equals the determined value for drag. If the throttle-setting that emerges is not admissible (e.g. drag greater than maximum available thrust), then one might set J equal to positive infinity and in this way interpret J to be a function of h and V .

To proceed with the analysis, note that the second term in the sum for J depends only on V and since

$$\min_{h, V} J(V, h) = \min_V \left[\min_h J(V, h) \right]$$

one is led to consider minimizing the fuel-flow over altitude for fixed V . Accordingly, define

$$Q^*(V) = \min_h \left[Q(\eta, h, V) \right] \quad (5-28)$$

and

$$J^*(V) = \lambda_F Q^*(V) - \lambda_R V \quad (5-29)$$

so that the cruise problem can be restated as seeking the speed V that minimizes the combination $(\lambda_F Q^*(V) - \lambda_R V)$. A method of characterizing solutions to this problem can be easily explained in geometrical terms set in the $(Q - V)$ plane. For fixed (non-negative) λ_F and λ_R , lines of constant $(\lambda_F Q - \lambda_R V)$ are as shown in Fig. 5.1 with values increasing as one moves upward (increasing Q) or to the left (decreasing V). If one superposes a graph of $Q^*(V)$, then it is seen that an optimal (V, Q) is a point of contact of the $Q^*(V)$ graph and that member of the constant

$(\lambda_F Q - \lambda_R V)$ family that separates the part of the plane containing the graph from the part of the plane containing no points on the graph. In optimization theory (Ref. 62) this is called a supporting hyperplane - in this case it is a line. From Fig. 5.1 it is also 'clear' that, if $Q^*(V)$ is smooth, then

$$\left(\frac{dQ^*}{dV} \right)_{V_0} = (\lambda_R / \lambda_F) \quad (5-30)$$

The necessity of this condition, under the smoothness assumption on $Q^*(V)$ can be established from the usual requirement that the first derivative of $J^*(V)$ must vanish at a minimizing V .

SECTION 5.4

COMPUTATIONS AND RESULTS

A computational study of cruise-dash optimization was carried out, using data for a twin-engined high-performance military aircraft. The aerodynamic and propulsive modelling is presented in Section 5.5. Only the aerodynamic limit (defined by $\bar{C}_L(M)$) was considered in this study, and the terrain limit was sea-level.

The $Q^*(V)$ graphs obtained from a one-dimensional minimization over altitude are presented in Figs. 5.2 and 5.3. Details of the numerical procedures used to calculate $Q^*(V)$ are included in Section 5.6. Figs. 5.4 and 5.5 include the graphs of optimal altitude and throttle-setting that emerge from the min- Q operation over altitude. As described in Section 5.5, η equals zero corresponds to zero thrust, η equals unity to military thrust and η equals two implies full afterburning thrust. The most interesting features of the $Q^*(V)$ graph are its regions of

nonconvexity. These imply that the tangency condition (5-30) is not sufficient for optimality. In other words, a tangent line need not be a 'supporting' line (see Fig. 5.6 which shows three candidates marked X, Y and Z).

We now consider the problem of characterizing the minimizing V in terms of the parameter $\lambda_{FR}(= \lambda_F/\lambda_R)$. Cruise-dash points are computed for values of λ_{FR} ranging from 0 ft/lb to 10^6 ft/lb, thus covering the entire spectrum from the high-speed point to the minimum-fuel-flow point respectively (Fig. 5.7). It is observed that the locus of optimal operating points has several discontinuities, and that the jumps in velocities are closely related to the nonconvexities in the $Q^*(V)$ graph. As an illustration, consider the behavior of the cruise-dash locus, starting at the fixed-range minimum-fuel point ($h = 46,510$ ft, $V = 775$ fps) with $\lambda_{FR} = 1000$ ft/lb. As λ_{FR} decreases, the emphasis on velocity (range) in the performance index increases while the importance of fuel-flow decreases. Fig. 5.8 presents the level-flight envelope along with loci of constant fuel-flow for unaccelerated level-flight. From these contours one might expect that as λ_{FR} decreases, the cruise-dash altitude and velocity would both increase. The cruise-dash locus does in fact follow this trend, with velocity and altitude both increasing until λ_{FR} reaches 319.36 ft/lb. At this value, the cruise-dash point abruptly jumps from ($h = 48,535$ ft, $V = 864$ fps) to ($h = 67,179$ ft, $V = 1075$ fps). The explanation for this behavior can be found in Fig. 5.6 which shows a region of the $Q^*(V)$ curve. It can be seen that $Q^*(V)$ exhibits nonconvex behavior in the range 864 fps $< V < 1075$ fps, so that a 'supporting' line will not touch the curve for any velocity in this region. Therefore, there can be no cruise-dash

points in this velocity range, thus explaining the gap in the cruise-dash locus.

The $Q^*(V)$ graph (Figs. 5.4 and 5.5) has several regions of nonconvexity and thus the locus of optimal operating points characterized by λ_{FR} has several gaps (see Fig. 5.7). Note that there is a one-to-one correspondence between nonconvexities in the (Q,V) plane and discontinuities of the cruise-dash locus in the (h, V) plane, both labelled A through E in Figs. 5.2, 5.3 and 5.7.

There is another interesting consequence of the nonconvexity of the function $Q^*(V)$. Consider the question of minimum-fuel transport for the kinematic model ($\epsilon_1 = \epsilon_2 = 0$) with specified average speed. The classical-cruise exercise is to seek the altitude h_0 and throttle-setting η_0 that minimizes $Q(\eta, h, V_0)$ with V_0 specified. Note that this will produce fuel-flow $Q^*(V_0)$. If V_0 is in a region of nonconvexity of $Q^*(V)$ then one could do better by flying at speeds V_1 and V_2 (see Fig. 5.9) with time at each apportioned so as to average V_0 . Fig. 5.10 shows the fuel savings as a function of velocity.

One could even achieve constant average speed V_0 by 'chattering' (Ref. 63) between V_1 and V_2 . (Note that for the reduced model the graph of the function $Q^*(V)$ traces out the boundary of the hodograph figure). The simplest and most frequently occurring type of time-shared operation would seem to feature a single transition between two (h, V) points. The order of the sequence is ambiguous in zeroth-order asymptotic approximation. More complex time-sharing (possible 'chattering') may correspond to oscillatory cruise-dash in optimal flight with a point-mass vehicle model (Refs. 64 and 65).

SECTION 5.5

MODELLING

5.5.1 Atmosphere

Air density (slugs/ft³) and sonic velocity (ft/sec) are supplied in tabular form as functions of altitude (feet). The sonic velocity and the natural logarithm of the air density are interpolated as cubic-spline functions of altitude (Ref. 44). The acceleration due to gravity (ft/sec²) is a specified constant.

5.5.2 Aerodynamics

The aircraft drag coefficient C_D is computed as a parabolic function of lift coefficient C_L with polar parameters C_{D_0} and $C_{D_{CL^2}}$, both of which are supplied in tabular form as functions of Mach number. The maximum lift coefficient \bar{C}_L is also specified as a function of Mach number. C_{D_0} , $C_{D_{CL^2}}$, and \bar{C}_L are interpolated as cubic-spline functions of Mach number. This is shown for C_{D_0} and $C_{D_{CL^2}}$ in Figs. 5.11 - 5.12. The aircraft weight (lbs) and aerodynamic reference area (ft²) are specified constants.

5.5.3 Propulsion

Two sets of thrust (lbs) and fuel-flow (lbs/hr) tables are available as functions of Mach number and altitude (feet). One set corresponds to military (maximum non-afterburning) operation, and the other represents operation with full afterburner. The afterburning thrust and fuel-flow data are presented in Figs. 5.13 - 5.14. Interpolation of these tables

between (h, M) points is done by using cubic-spline lattices (Ref. 44).

Interpolation between military and afterburning is linear as is partial-throttle military. One introduces a throttle parameter, η , such that operation at military power corresponds to throttle-setting $\eta = 1$, and throttle-setting $\eta = 2$ gives full afterburner operation. $\eta = 0$ is a zero-thrust setting. Thrust and fuel-flow values (for a given altitude and Mach number) are known only for three throttle-settings, $\eta = 0, 1, 2$. A linear variation in throttle is assumed between $\eta = 0, 1$ and $\eta = 1, 2$, hence given a value of thrust, the throttle-setting can be computed by linear interpolation. Note that this is not truly an assumption; indeed it only serves to define the throttle parameter η . However, one now assumes that fuel-flow also varies in a sectionally-linear way with η . Thus, the specific fuel consumption is independent of throttle for idle-to-military settings and the incremental specific fuel consumption in afterburning operation is also independent of throttle. Given that we only have propulsive data at three throttle-settings, a sectionally-linear model is reasonable. However, the results obtained may well be influenced by this type of modelling. Finally, note that the 'data' at $\eta = 0$ is taken as $T = Q = 0$.

SECTION 5.6

COMPUTATION OF $Q^*(V)$

By definition,

$$Q^*(V) = \min_h [Q(\eta, h, V)]$$

Given a (h, V) pair, the thrust T and throttle-setting η can be computed by making use of $L = W$ and $T = D$ as described in the section on Cruise-Dash Analysis. Since the values of fuel-flow are known for three throttle-settings ($\eta = 0, 1, 2$), one can evaluate $Q(\eta, h, V)$ by linear interpolation.

$Q^*(V_0)$ is found by performing a one-dimensional search over altitude for a given velocity V_0 . A coarse grid is set up ranging from 0 to 80,000 feet with increments of 5000 feet. The fuel-flow $Q(\eta, h, V_0)$ is evaluated at each altitude grid point (with fixed velocity V_0). The minimizing altitude (h_1) is then picked out by direct comparison of fuel-flow values. Another search is carried out over a range of 10,000 feet centered at altitude h_1 , with a grid size of 500 feet. A refined estimate of the minimizing altitude (h_2) is obtained by comparing values of fuel-flow. Finally, a golden-section search is performed over the 1,000 ft interval centered at h_2 , with an accuracy of 0.1 foot. It was observed from plots of $Q(\eta, h, V_0)$ vs h that $Q(\eta, h, V_0)$ satisfies the unimodality requirement near the minimum; hence the golden-section search is successful.

The minimizing altitude obtained from the golden-section search is h_0 and the corresponding throttle-setting is η_0 . Thus, one finds that

$$\begin{aligned} Q^*(V_0) &= \min_h [Q(\eta, h, V_0)] \\ &= Q(\eta_0, h_0, V_0) \end{aligned}$$

In this manner, $Q^*(V)$ can be computed for any given velocity.

SECTION 5.7

CONCLUSIONS

The classical problem of selecting an altitude, velocity and throttle-setting to minimize a linear combination of fuel-flow and (negative) range-rate has been considered as an 'outer' solution of a dynamic path-optimization problem, when Newtonian dynamics are modelled as 'fast'. This classical cruise-dash problem has a family of solutions where each member depends on the relative emphasis placed on time and fuel. Computations performed for a particular high-performance aircraft show that the locus of optimal operating points has several breaks, each corresponding to a nonconvexity in the $Q^*(V)$ curve. Consequently, certain velocity regions are non-optimal for cruise-dash operation.

If a time constraint forces operation at an average velocity in such a region, time-shared operation is more fuel-efficient than classical (steady-state) cruise. This behavior may have an interpretation as a simple sequence of operation at two (h, V) points or, possibly, as 'chattering', corresponding to oscillatory cruise-dash in point-mass modelling.

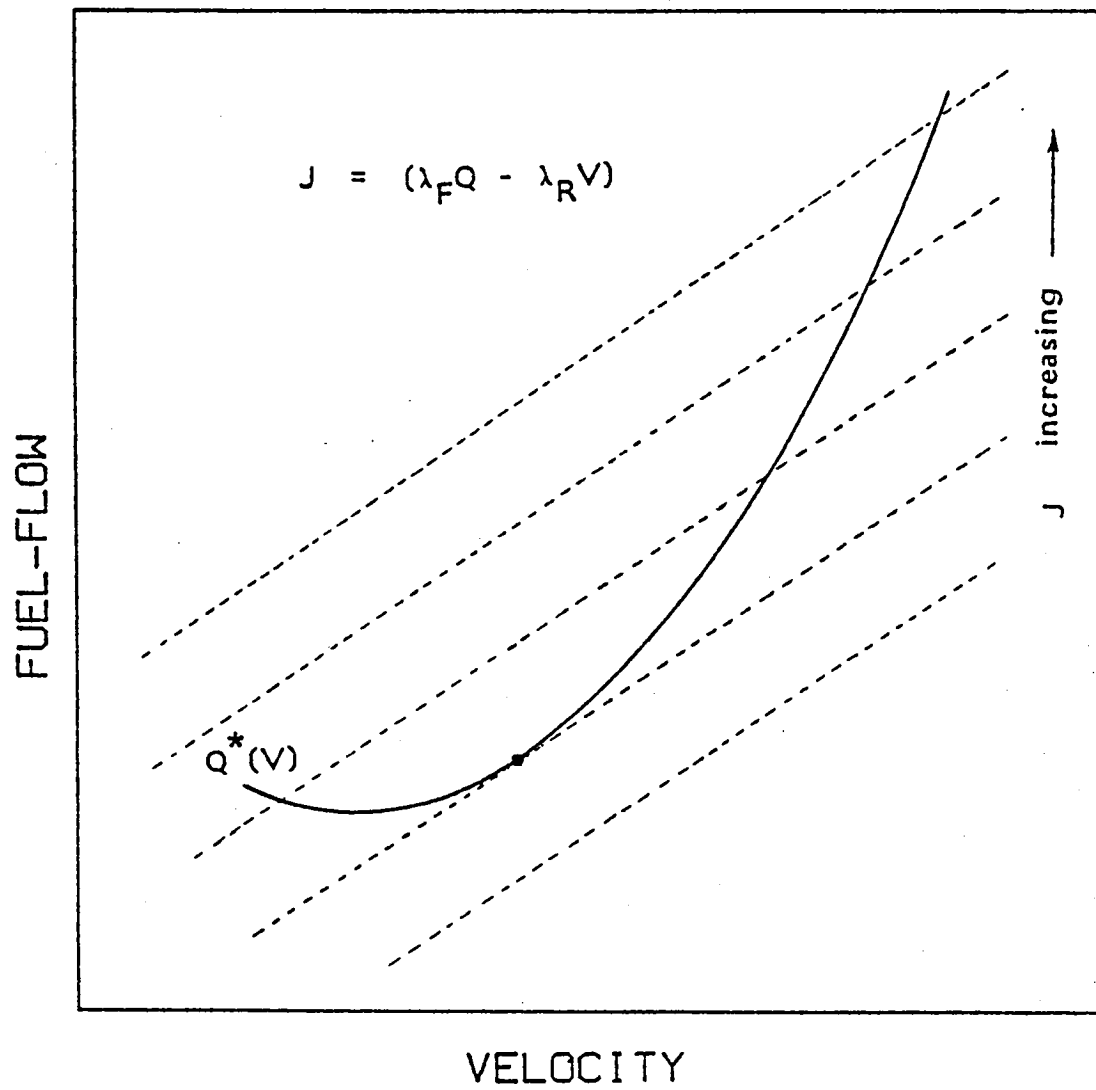


Fig. 5.1 Lines of constant $J = (\lambda_F Q - \lambda_R V)$ and $Q^*(V)$

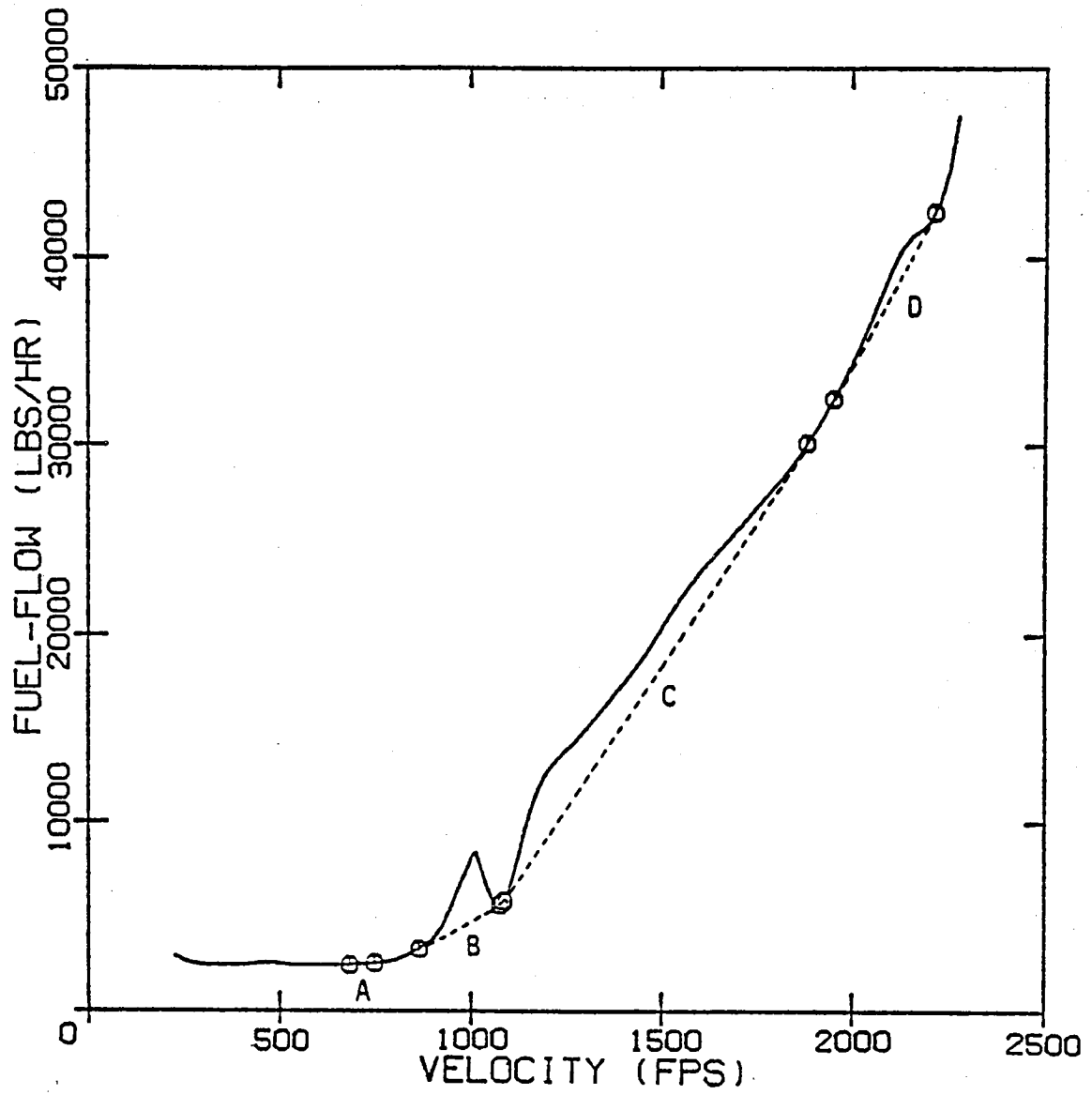


Fig. 5.2 Minimum Fuel-flow $Q^*(V)$ vs Velocity

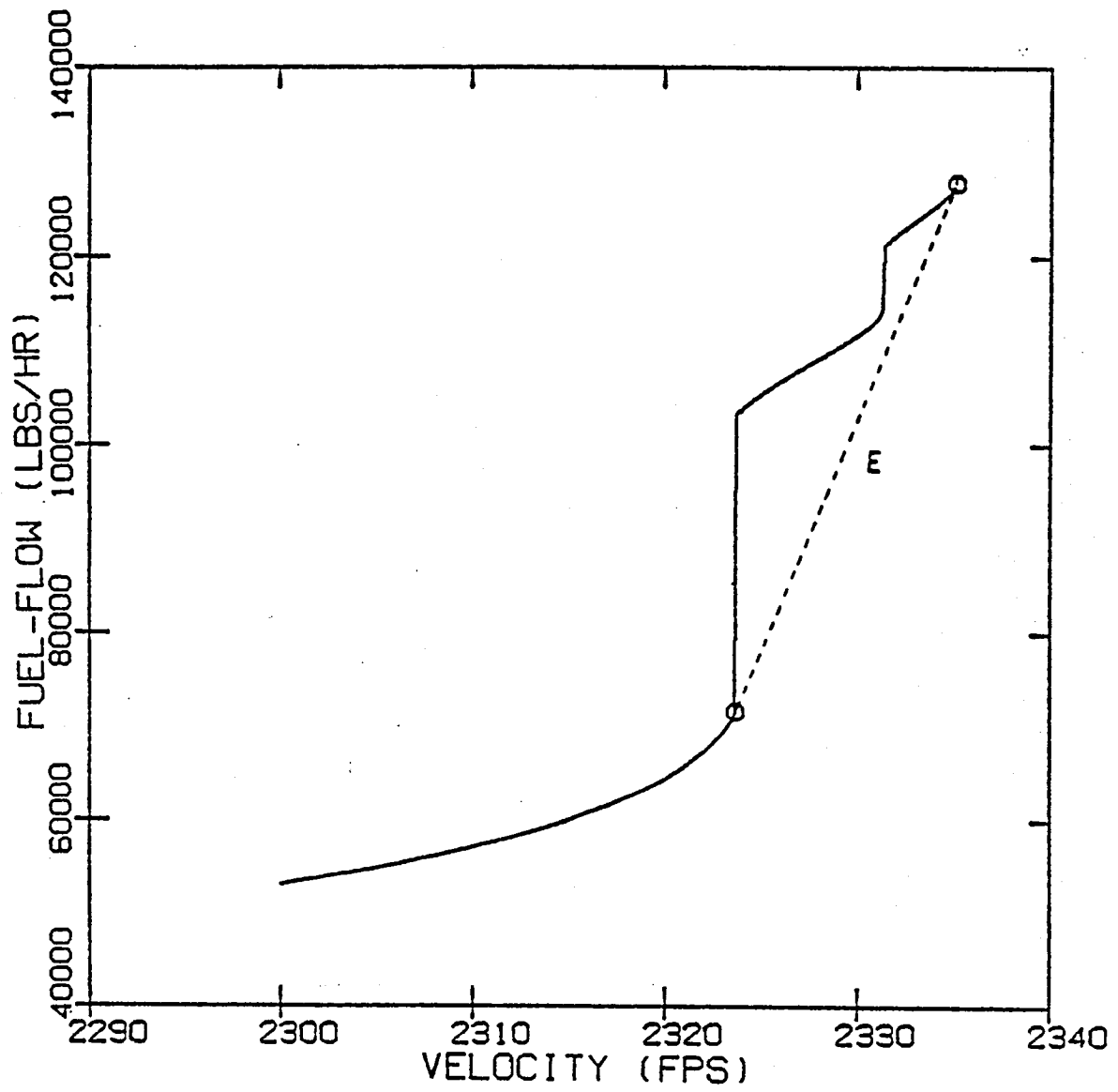


Fig. 5.3 Minimum Fuel-flow $Q^*(V)$ vs Velocity (high-speed region)

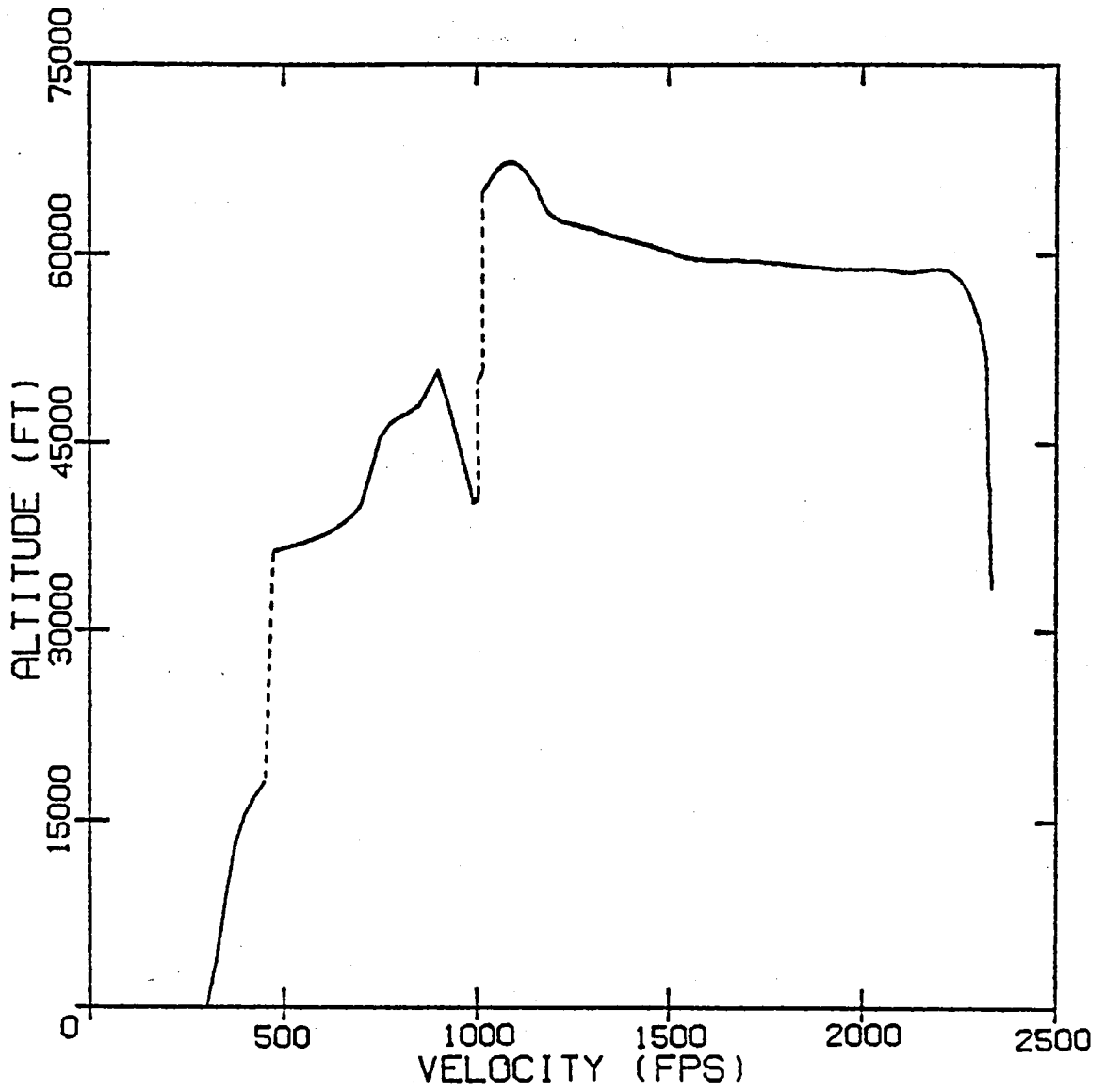


Fig. 5.4 Fuel-minimizing altitude h_0 vs Velocity

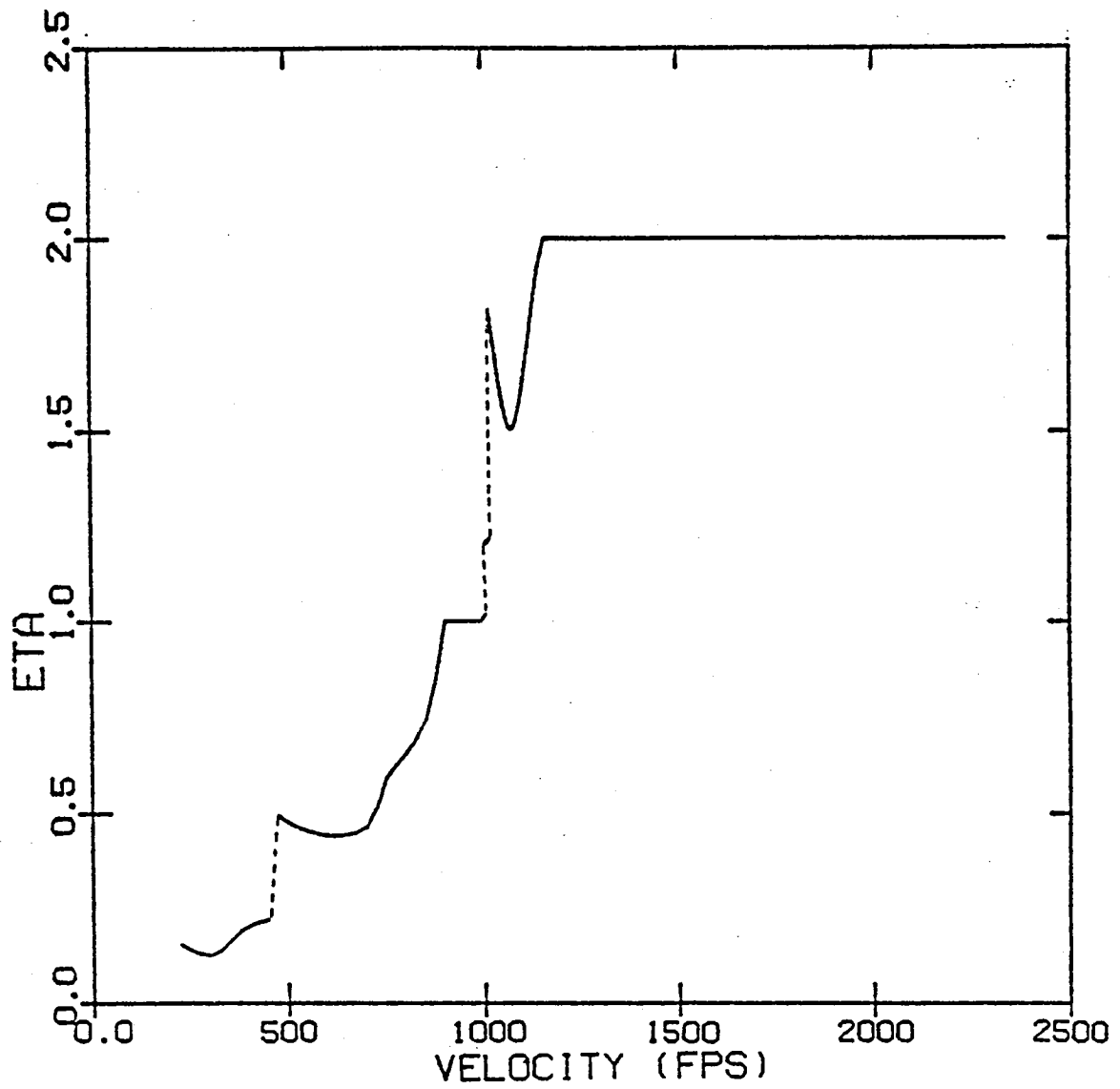


Fig. 5.5 Fuel-minimizing throttle-setting η_0 vs Velocity

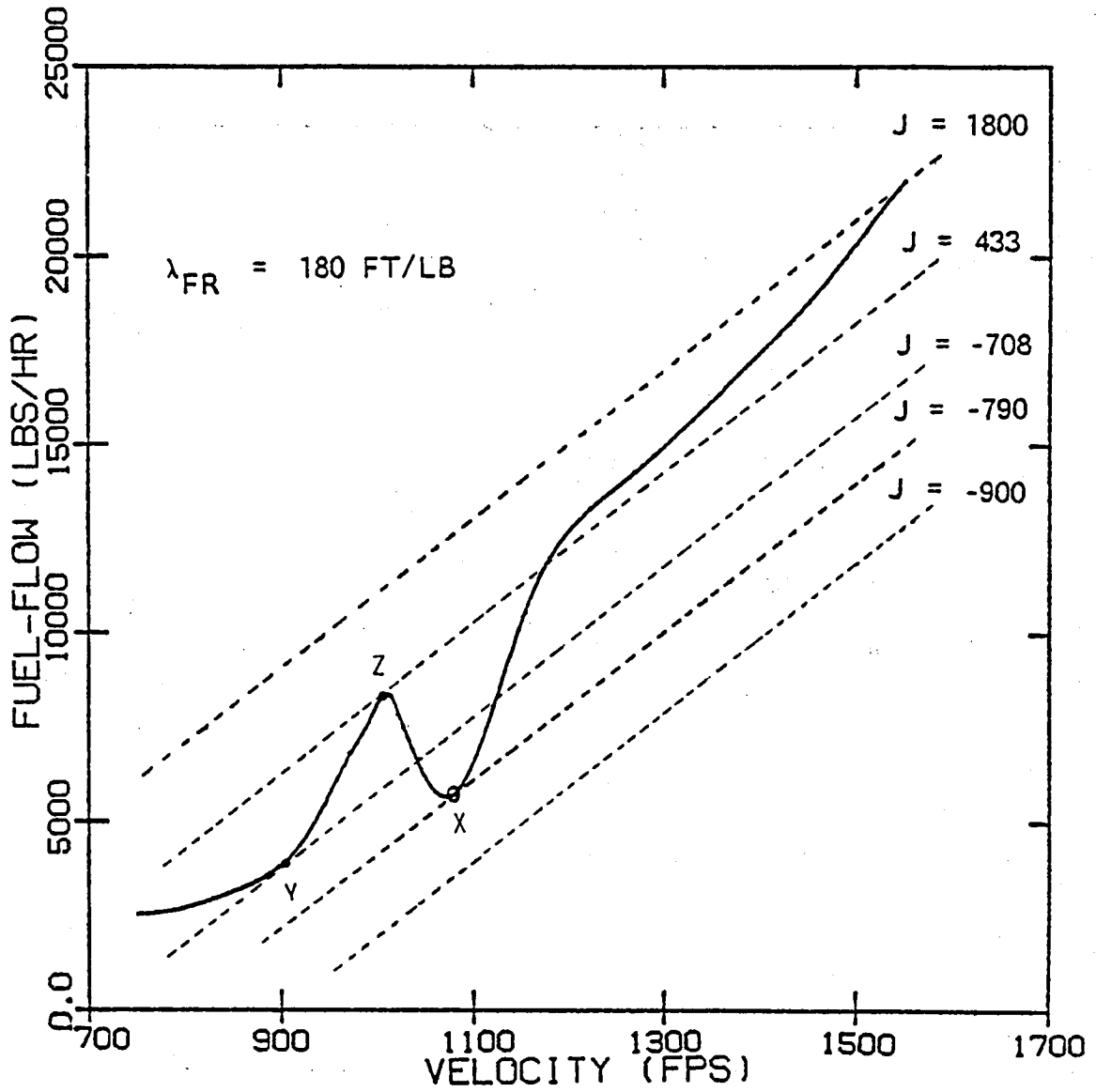


Fig. 5.6 Candidate minima of $J = (\lambda_F Q - \lambda_R V)$

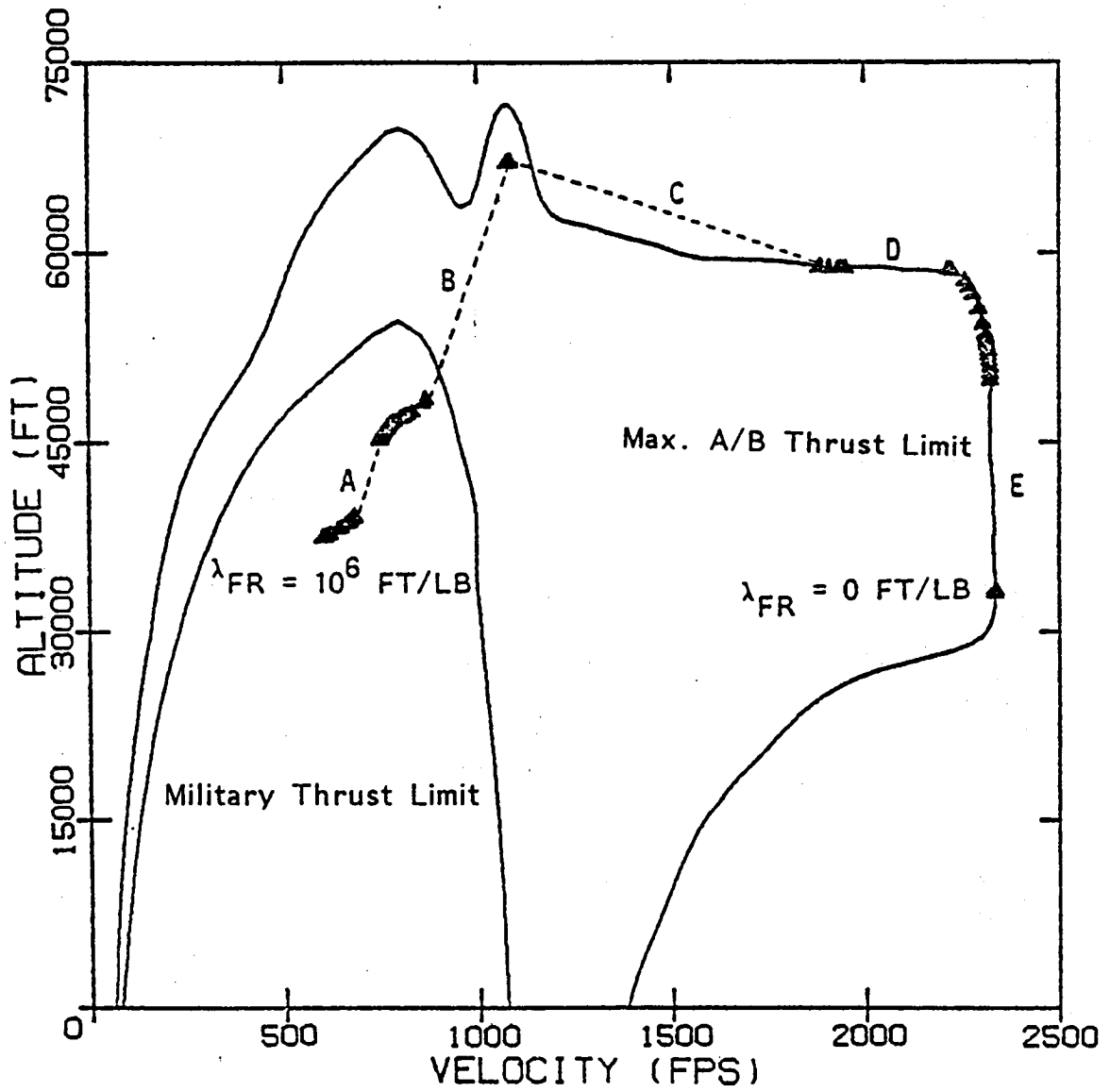


Fig. 5.7 Cruise-Dash points and flight envelopes in the (h,V) plane

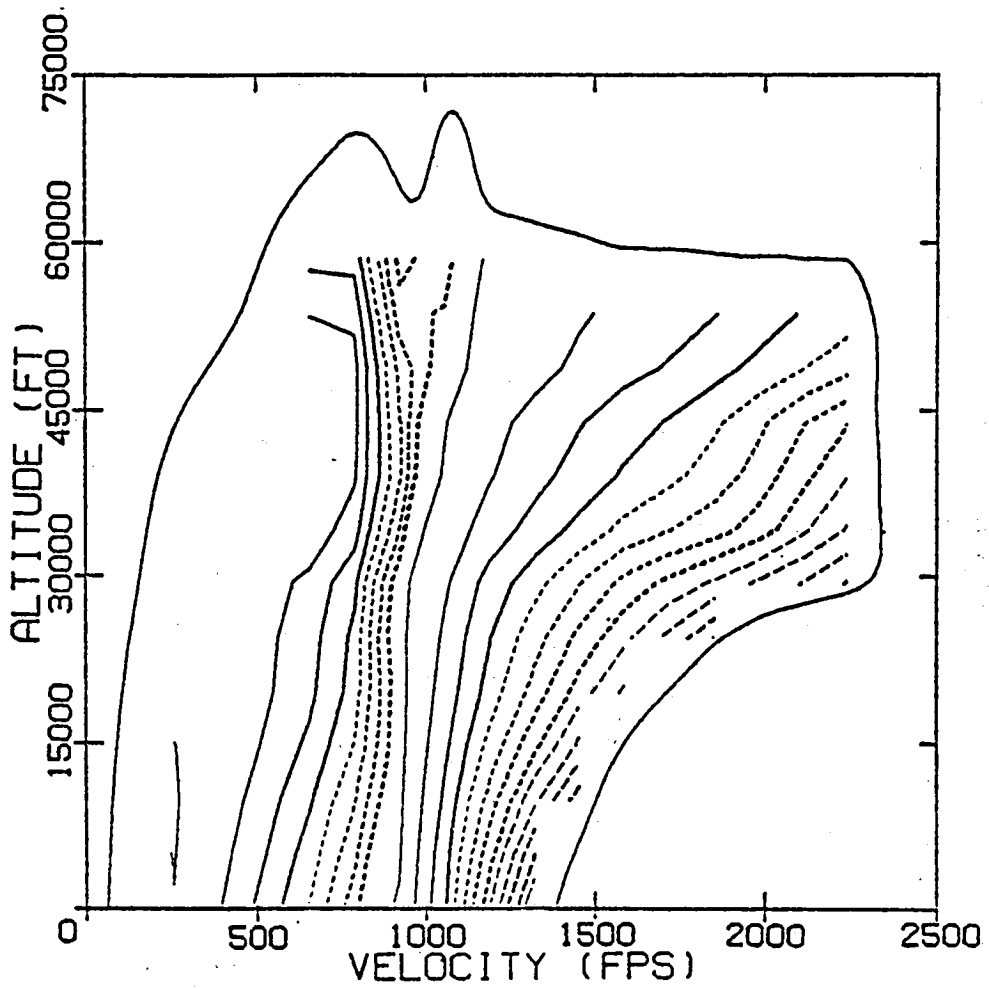


Fig. 5.8 Constant fuel-flow contours for level unaccelerated flight

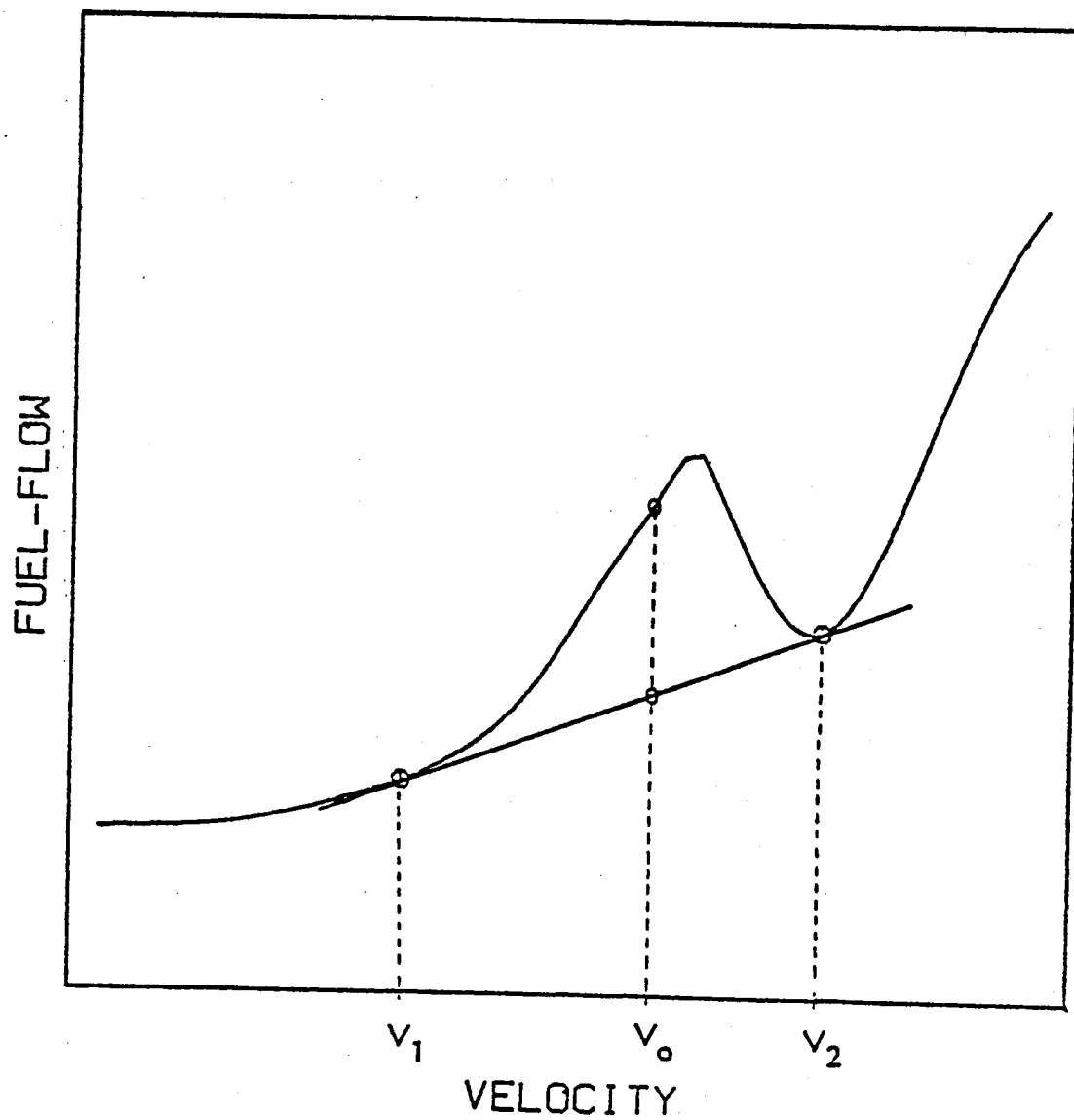


Fig. 5.9 A non-convex region of $Q^*(V)$ vs Velocity

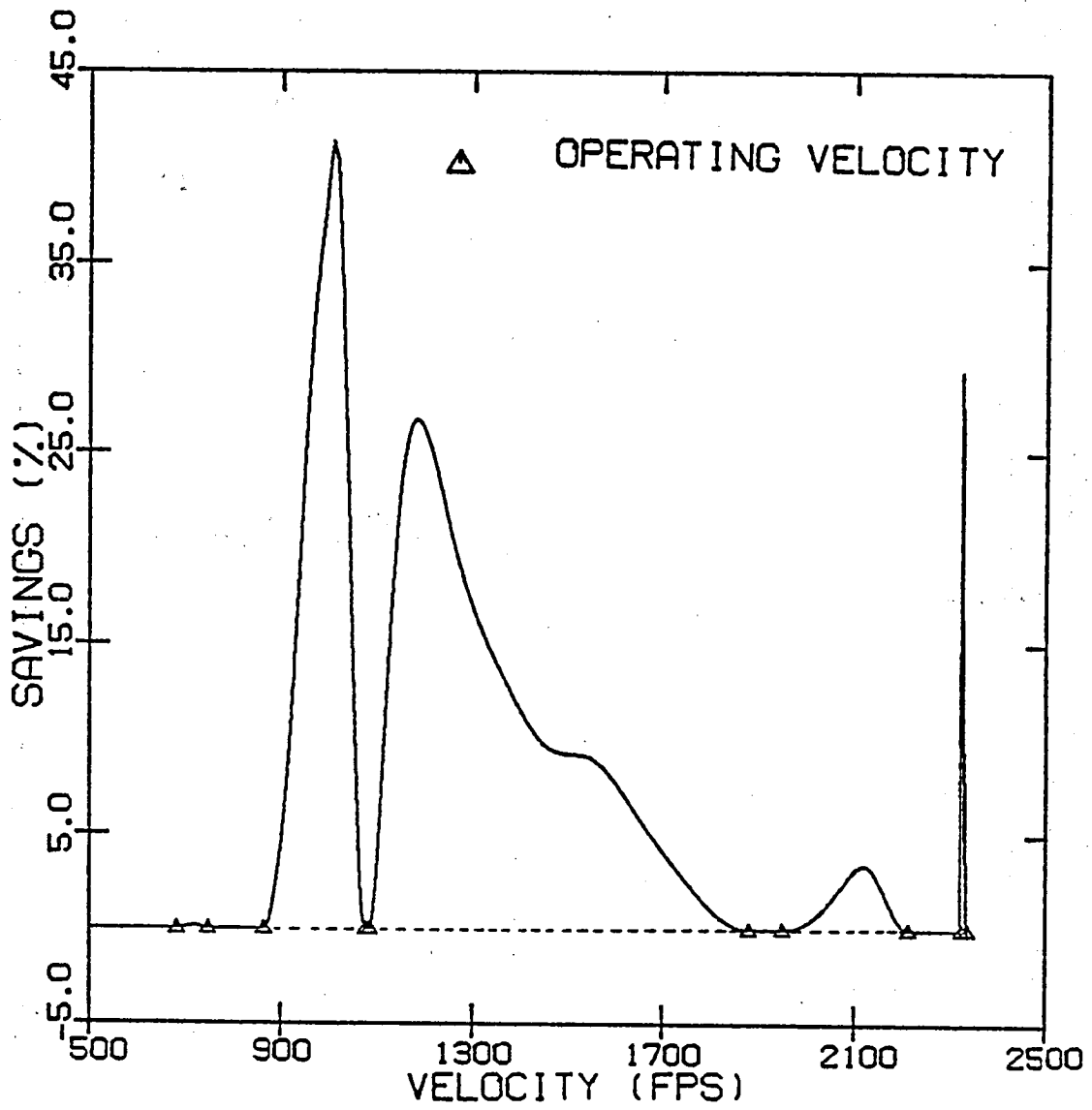


Fig. 5.10 Fuel savings for time-shared operation

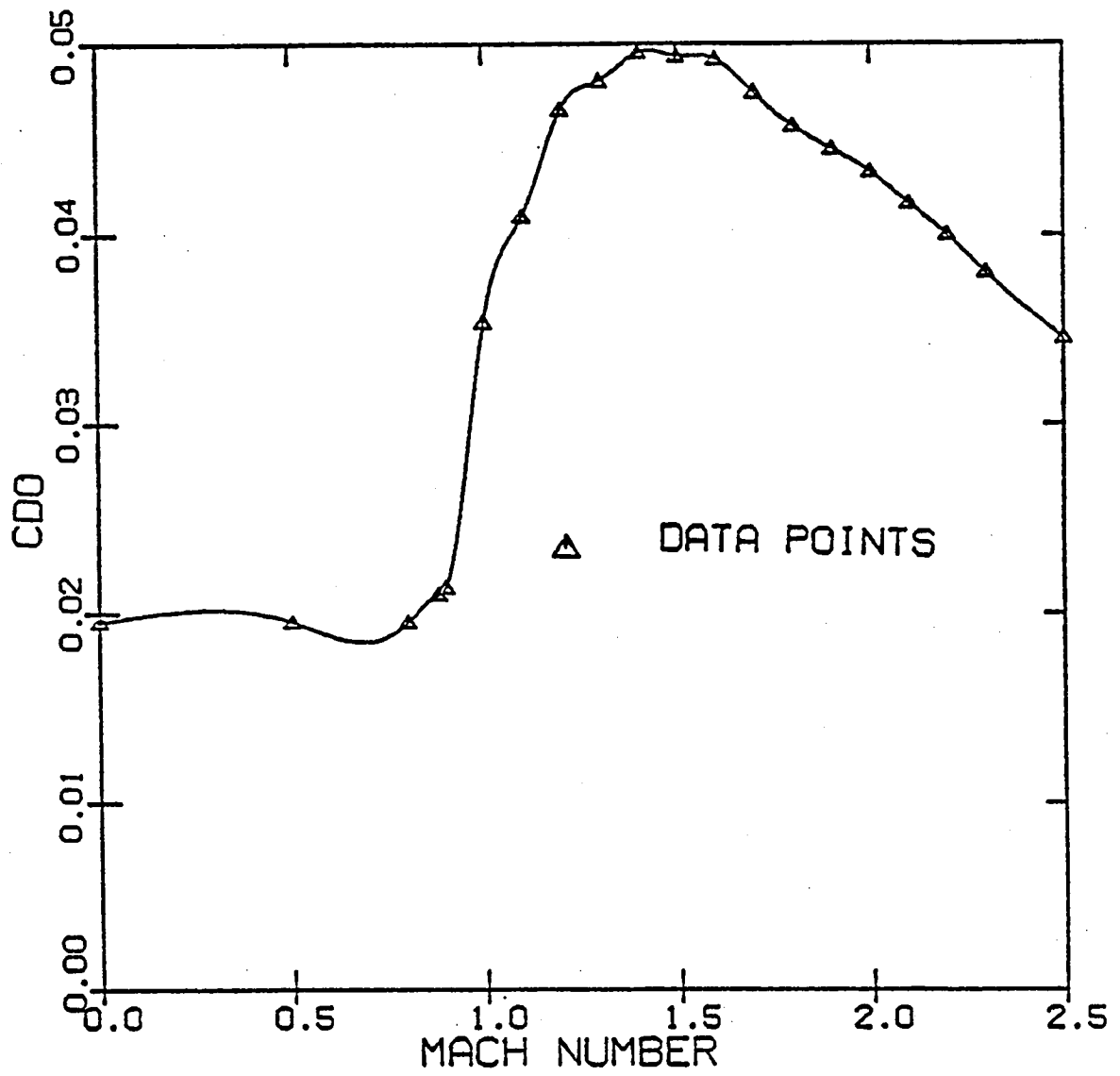


Fig. 5.11 Zero-lift drag coefficient C_{D_0} vs Mach number

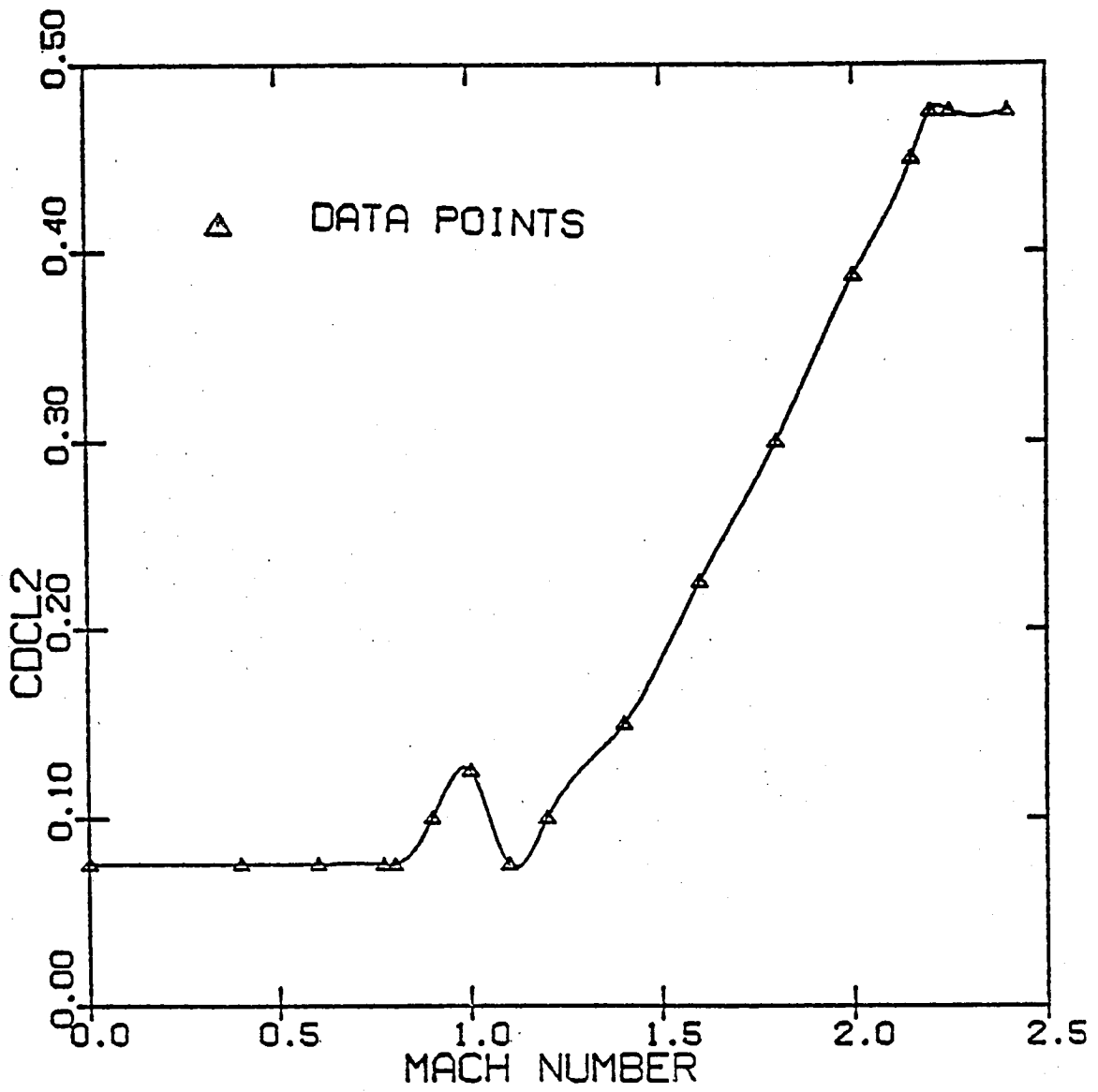


Fig. 5.12 Induced drag coefficient $C_{D_{CL2}}$ vs Mach number

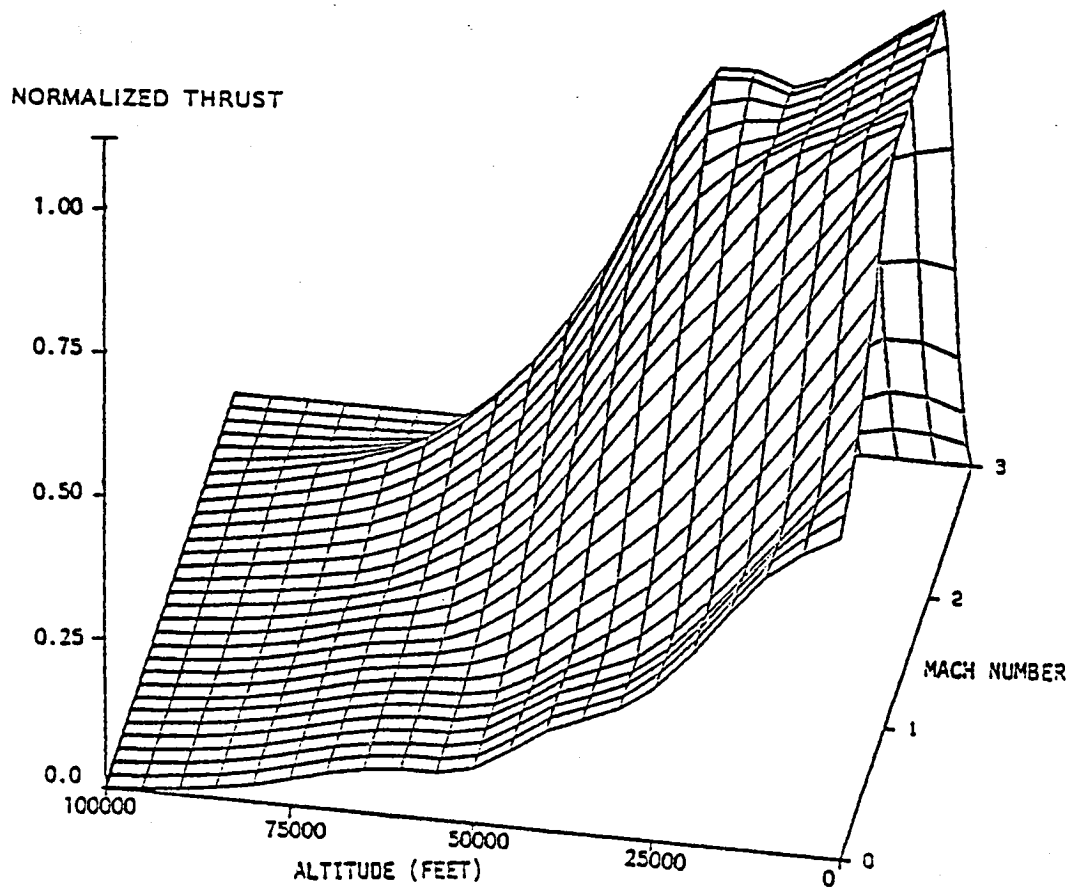


Fig. 5.13 Maximum afterburning thrust vs Mach number and altitude

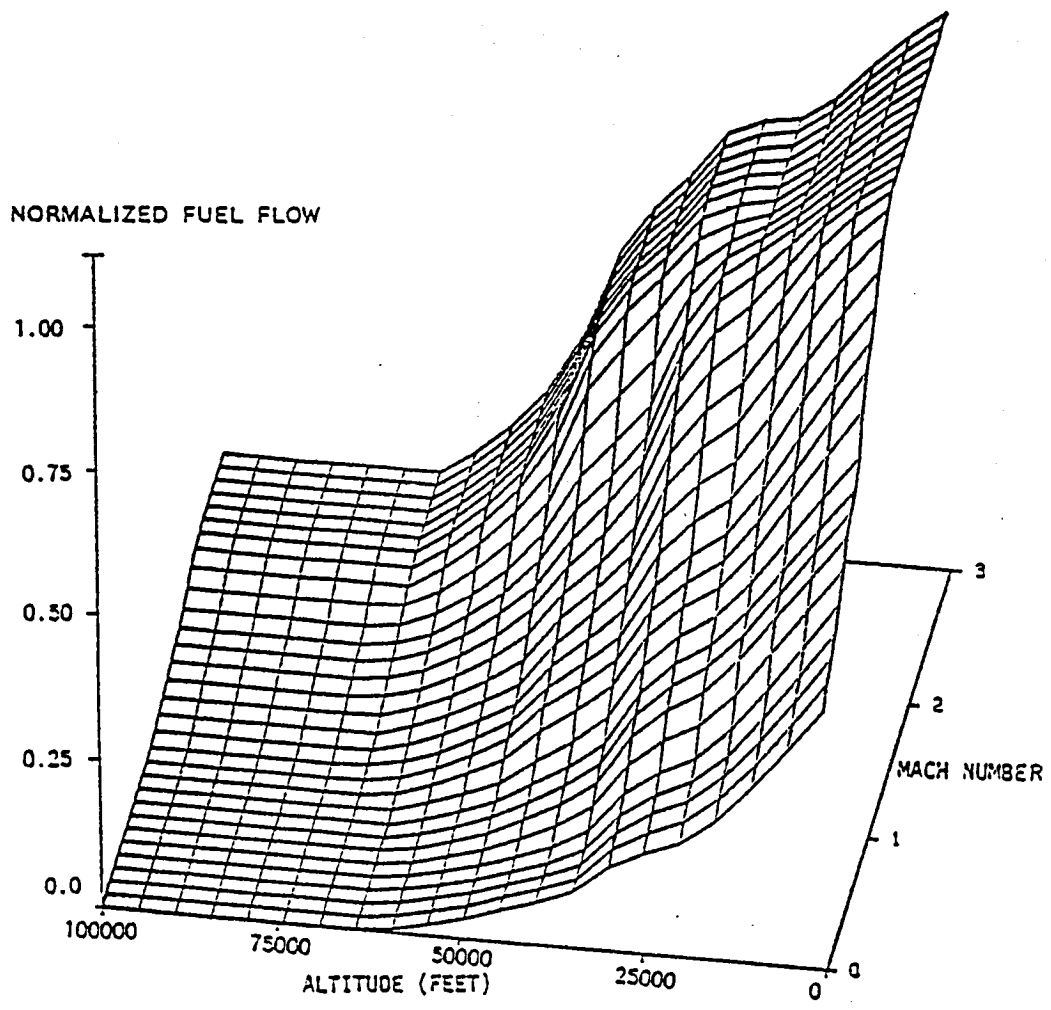


Fig. 5.14 Maximum afterburning fuel-flow vs Mach number and altitude

APPENDIX A

ENERGY-MODELLED CLIMB AND CLIMB-DASH - THE KAISER TECHNIQUE

Sandra R. Merritt

Eugene M. Cliff

Henry J. Kelley

SECTION A-1

PREFACE

Energy modelling of aircraft flight had its origin in the 1944 Messerschmitt A. G. report listed as Ref. 22; it was perhaps the most important analytical development in flight performance to come out of WWII. The object of the present paper is to review the Kaiser report in the context of later developments and to attempt to recreate the main results, especially the intriguing "distance-climb" trajectories.

Reference 22 is Part 1 of a report on climb problems; it deals with the minimum-time-to-climb case. Parts 2, 3 and 4, which were to be concerned with other climb problems, were never issued. Nonetheless some "distance-climb" results found their way into a figure of Part 1 and, although analysis is missing, it is interesting to speculate on these data in the light of optimal climb-dash results obtained by current methods.

In the following, Kaiser's "resultant-height" concept is reviewed along with his calculations for the Me. 262 and some results of an attempt to recreate them presented. It should be noted that a variational formulation of a related problem (minimum-fuel) had been given a year earlier by Alexander Lippisch, using the same physical modelling approximation, but no solution had been sought (Ref. 66).

SECTION A.2

QUASI-STEADY CLIMB ANALYSIS AND CORRECTIONS

With a point-mass-model and symmetric flight assumed, the governing equations of motion are

$$\dot{h} = V \sin\gamma \quad (A-1)$$

$$\dot{V} = g [(T-D)/W - \sin\gamma] \quad (A-2)$$

$$\dot{\gamma} = (g/V)(L/W - \cos\gamma) \quad (A-3)$$

Here, geometric altitude, h , velocity, V , and flight-path angle, γ , are the conventional state variables, g is the acceleration of gravity, T thrust, D drag, L lift, and W weight. The left-hand members of the equations are the derivatives with respect to time, time differentiation being denoted by a superscribed dot as usual. The symbols adopted are those of the "modern" flight-performance literature.

Traditional quasi-steady approach to climb performance, specifically maximum rate-of-climb, focuses entirely on potential energy increase. The so-called specific excess power $P_s = V(T-D)/W$ is maximized at each altitude by choice of airspeed V . That is, for a given altitude, a velocity is chosen to maximize P_s , without regard to kinetic energy changes. For low-performance aircraft this is a good approximation, since the change in kinetic energy is generally small. For high-performance jet aircraft, however, the velocity change must be accounted for; even for purely subsonic flight the effect is appreciable. Note that the analysis produces a climb schedule in the form $V(h)$: i.e.

at each altitude there is a best velocity.

The technology of the WWII period included various correction factors to adjust the steady-state results to account for acceleration effects. Since V changes with time, we have that

$$\dot{V} = (dV/dh) \dot{h} = (dV/dh) V \sin\gamma \quad (A-4)$$

Combining equations (A-4) and (A-2),

$$(T-D) - W \sin\gamma [1+(V/g)dV/dh] = 0 \quad (A-5)$$

Rearranging the terms equation (A-5) becomes,

$$\sin\gamma = [(T-D)/W] / [1+(V/g)dV/dh] \quad (A-6)$$

After multiplying both sides of equation (A-6) by V , one may identify the right-hand side of equation (A-1) with the right-hand side of equation (A-6): therefore, the "corrected" rate of climb becomes,

$$\dot{h} = V \sin\gamma = [(T-D)V/W] / [1+(V/g)dV/dh] \quad (A-7)$$

Hence $1/[1+(V/g)dV/dh]$ is the correction factor to adjust for the change in speed. It is important to note that whereas the analysis provides a correction due to velocity change the optimization was done ignoring the change.

SECTION A-3

RESULTANT HEIGHT AND ENERGY MODELLING

Kaiser presented a then-new concept of "Gesamthöhe" (resultant height) subsequently called "energy height" and "specific energy" (Refs. 23 and 24). This is the altitude where "the potential energy of

the aircraft would be equal to the sum of its potential and kinetic energy at height h and speed V' (Ref. 22). At a given energy height the potential and kinetic energies are regarded as easily and rapidly interchangeable in this approximation.

It is readily shown that the resultant-height variable h_{res}
 $= h + V^2/2g$ satisfies the differential equation

$$\dot{h}_{res} = V(T-D)/W \quad (A-8)$$

which may be thought of as replacing both equations (A-1) and (A-2). By small- γ assumption ($\cos \gamma \approx 1$) and deletion of the $\dot{\gamma}$ term in (A-3) the drag is approximated as the drag for level flight, $L = W$, and is a function of h and V only, $D(h,V)$. Note that the right-hand side of (A-8) is the specific excess power, P_s . In modern terminology \dot{h}_{res} is the specific energy rate; Kaiser used the symbol w_u (unaccelerated climb rate).

Kaiser's scheme was to "reach a certain height and end speed as quickly as possible" (Ref. 22). The velocity-altitude path is chosen so as to maximize the time derivative of h_{res} at each value of h_{res} . Altitude-speed transitions along constant- h_{res} curves are imagined as occurring instantly, if necessary, and without dissipation of energy. Thus, h_{res} is "slow" and γ and h at constant h_{res} are "fast", in the language of singular perturbations (Refs. 25, 41, 43).

Speeds for optimum climb were obtained graphically in Ref. 22. This was done by first plotting contours of equal specific excess power in a V - h chart. Such a chart with superimposed constant- h_{res} contours is sometimes called a "Kaiser diagram" (Ref. 67). Optimum climb speeds

then lie at the points where "the tangents to the curves of resultant height and to the w_u line have the same direction" (Ref. 22). Kaiser's representation of these results for the Me. 262 are reproduced in Fig. A-1, with certain features omitted for clarity. A cubic-spline-lattice representation, with coefficients selected to fit Kaiser's data, was used to generate a family of curves to approximate Kaiser's P_s curves. The P_s curves generated are shown in Fig. A.1 against a background of constant h_{res} contours. Also shown is Kaiser's approximation to the best climb schedule comprising two straight-line segments.

In the present re-creation of Kaiser's calculations the P_s curves in spline-lattice approximation do not match Kaiser's data exactly but are reasonably close. The climb trajectory also disagrees slightly since it was obtained from the same spline-lattice fit.

Kaiser's climb schedule for the Me. 262 "condensed for display in the cockpit" (Ref. 22), was as follows,

Altitude (km)	True Airspeed (km/hr)
2	500
6	550
10	650

The airspeeds given are 25 - 50 km/hr faster than for quasi-steady maximum-rate-of-climb scheduling.

Note that flight along the optimum-speed curve requires a slightly longer time to reach a desired height than does climb with classical maximum-rate-of-climb. However, the additional speed realized can be

converted into height.

SECTION A.4

ENERGY INTERCHANGE

The essence of energy approximation is order reduction. The order of the original system, Eqs. (A-1) - (A-3), is reduced from three to one for the "slow" motion or "outer" solution; the state variable is h_{res} , "resultant height" or "energy height" or "specific energy." The "fast" motion of h , γ transition at constant h_{res} is a "boundary layer." The motions are not patched together but spliced in a Vasiléva composite (Ref. 25). That Kaiser well understood the concept of fast and slow motions taking place concurrently in a composite approximation is clear from the following passage from Ref. 22: "For example after reaching a definite resultant height the speed is to be increased by pushing the nose down. Now the pilot begins to do this earlier by the length of time required to bring it into effect. During this time the aircraft further increases its resultant height without variation with w_u . Here the paradox is presented that the resultant height increases in spite of the downward motion of the aircraft. The desired resultant height is thus reached at the same moment as it would be without increasing the speed."

SECTION A.5

CLIMB-DASH

Kaiser was also concerned with the problem of optimum range. For a given resultant height one might find the value of altitude which maximizes the weighed sum $P_s(h,V) + \lambda_x V$, where λ_x is an arbitrary constant; this procedure produces a family of trajectories with λ_x as a parameter. If $\lambda_x = 0$, the minimum-time-to-climb profile is generated. When $\lambda_x > 0$ one begins to place some "weight" on the velocity factor, hence range-rate is now receiving some emphasis.

Kaiser's analysis of optimum range was to be presented in Part 2, which never appeared. He did, however, illustrate his range findings on the h-V plot presented in Part 1 (Fig. A.2). It is conjectured that Kaiser may have used the weighing scheme just stated to find his "distance climbs" by placing varying importance on the velocity term. Therefore, the greater the range desired, the larger λ_x used. Using the data produced by the spline-lattice representation of P_s and solving the equations numerically with various constant λ_x values, curves were generated (Fig. A.3) and compared to Kaiser's. The results obtained seem to agree with our conjecture as to Kaiser's method of optimum range calculations.

If a family of optimal time-energy-range solutions is sought in energy approximation from the Euler system (Ref. 25) with resultant height (specific energy) and range on the same time scale, the curves given in Fig. A.4 are obtained. These are seen to bear a resemblance

to the constant-weighting-factor curves of Fig. A.3 and to Kaiser's family of Fig. A.2. The modern formulation requires that altitude be chosen so as to

$$h^{\text{opt}} = \arg. \max_h [\lambda_E \text{PS}(h, V) + \lambda_R V] \quad (\text{A-9})$$

at fixed h_{res} . The terms λ_E and λ_R are the co-states of optimal control theory and in general vary along the trajectory. With $\lambda_R = 0$ the time-varying nature of λ_E does not affect the maximization operation in equation (A-9) (as long as $\lambda_E > 0$). However, when $\lambda_R > 0$, the time-varying nature of λ_E effectively produces a variable weight [$\lambda_X = \lambda_R/\lambda_E$] in Kaiser's formulation.

SECTION A.6

CONCLUSIONS

Kaiser's resultant-height method was the forerunner of the singular-perturbation approach to aircraft flight performance. The computational results and procedures are, accordingly, of more than historical interest in the context of optimal-flight methodology.

POSTSCRIPT

Recently MBB has kindly assisted the writers in making contact with Fritz Kaiser. Herr Kaiser explains that his "Gesamthöhe" idea was suggested by kinetic-energy corrections to climb measurements developed earlier (Ref. 68). With regard to the Lippisch work: "I hear from you for the first time that he (Lippisch) too was occupied with

this problem. It is true we worked in the same firm but within different departments, which were shielded against each other by highly secret classification." In connection with the projected Parts 2, 3 and 4 of his report, he explains that "I did not carry out these works as my first report met no interest at all." About the distance-climb calculations: "In the meantime, in February 1944, the great air raid to Augsburg and the factories took place, which among others, destroyed my working papers and which forced the flight-test department to move to Lager Lechfeld. There too, I had to change four times the destroyed offices. The parameters drawn in sheet 8 for the distance climbing are the result of (destroyed) preparatory works. However, I cannot explain them any more."

Fig. A.1 ME. 262 MINIMUM - TIME CLIMB (KAISER)

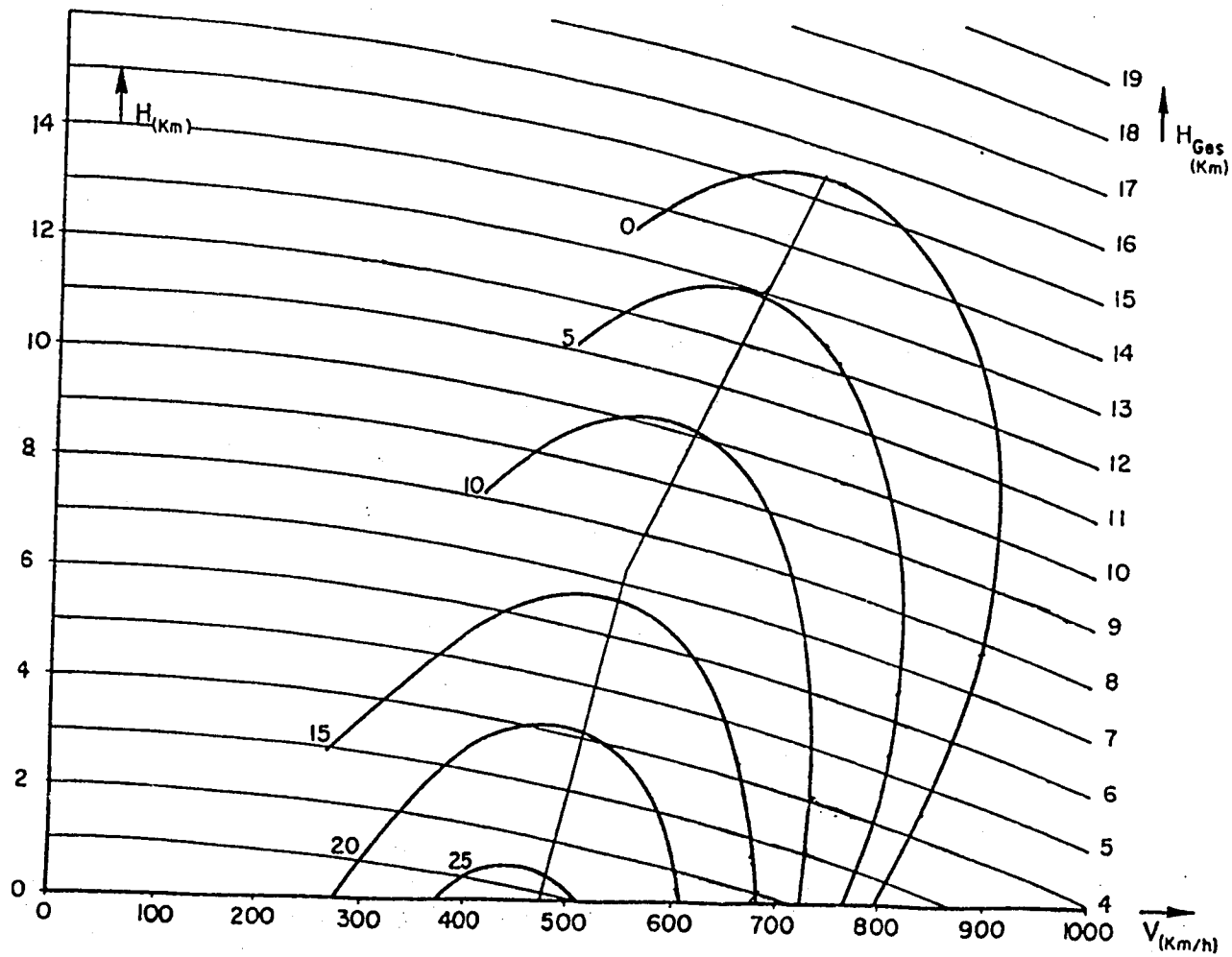


Fig. A.2 HE. 262 DISTANCE - CLIMB (KAISER)

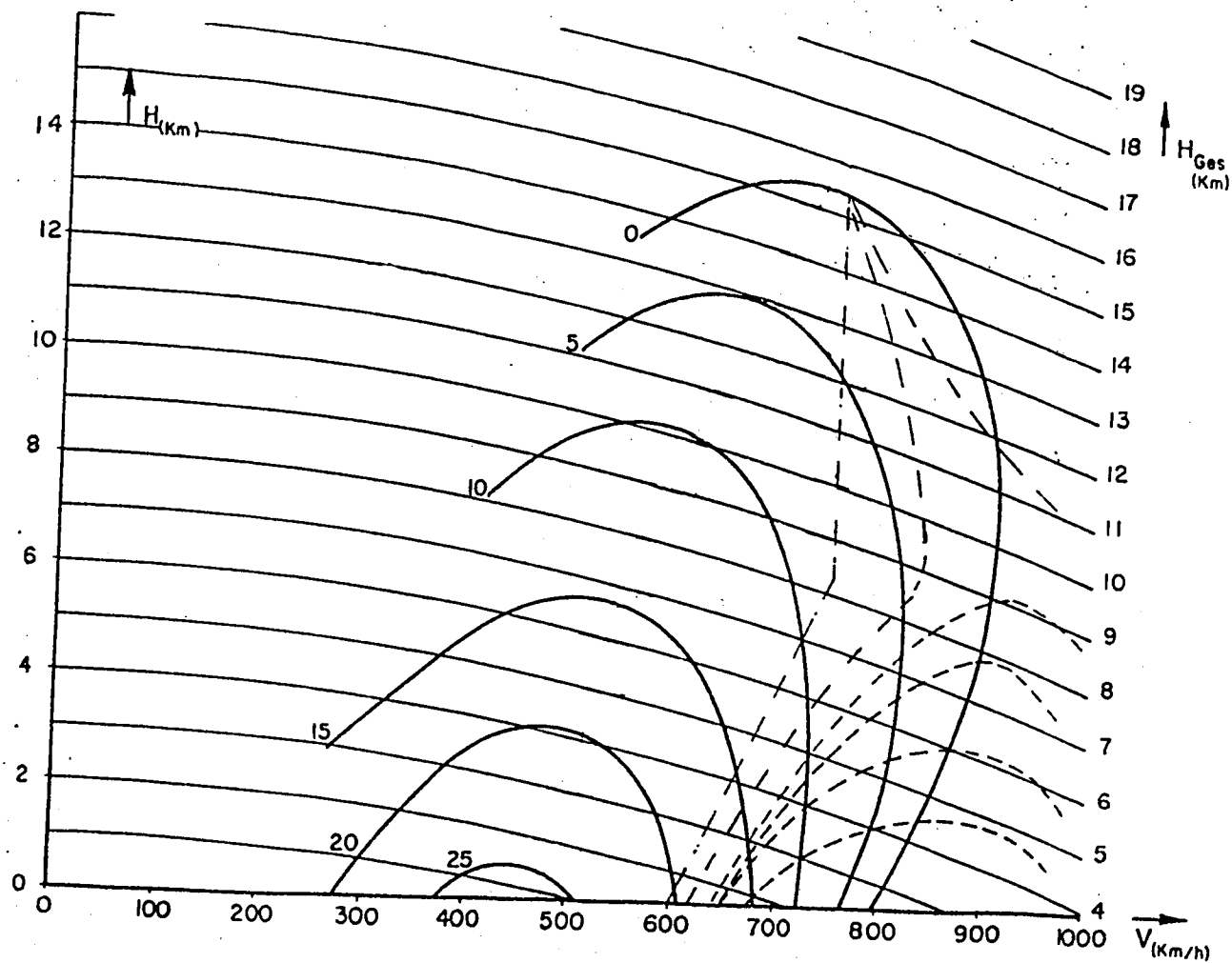


Fig. A.3 ME. 262 DISTANCE - CLIMB FAMILY (CONSTANT MULTIPLIER)

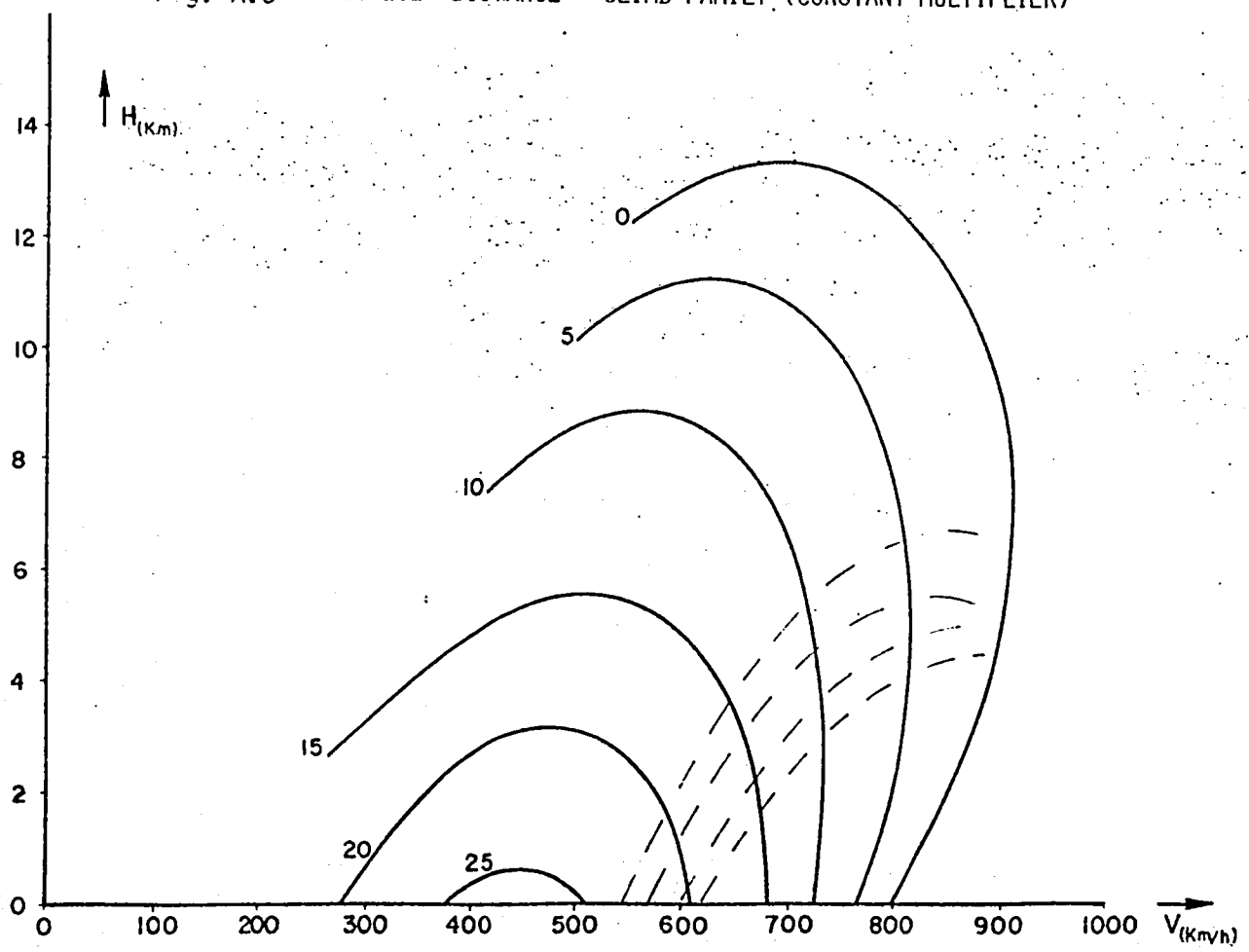
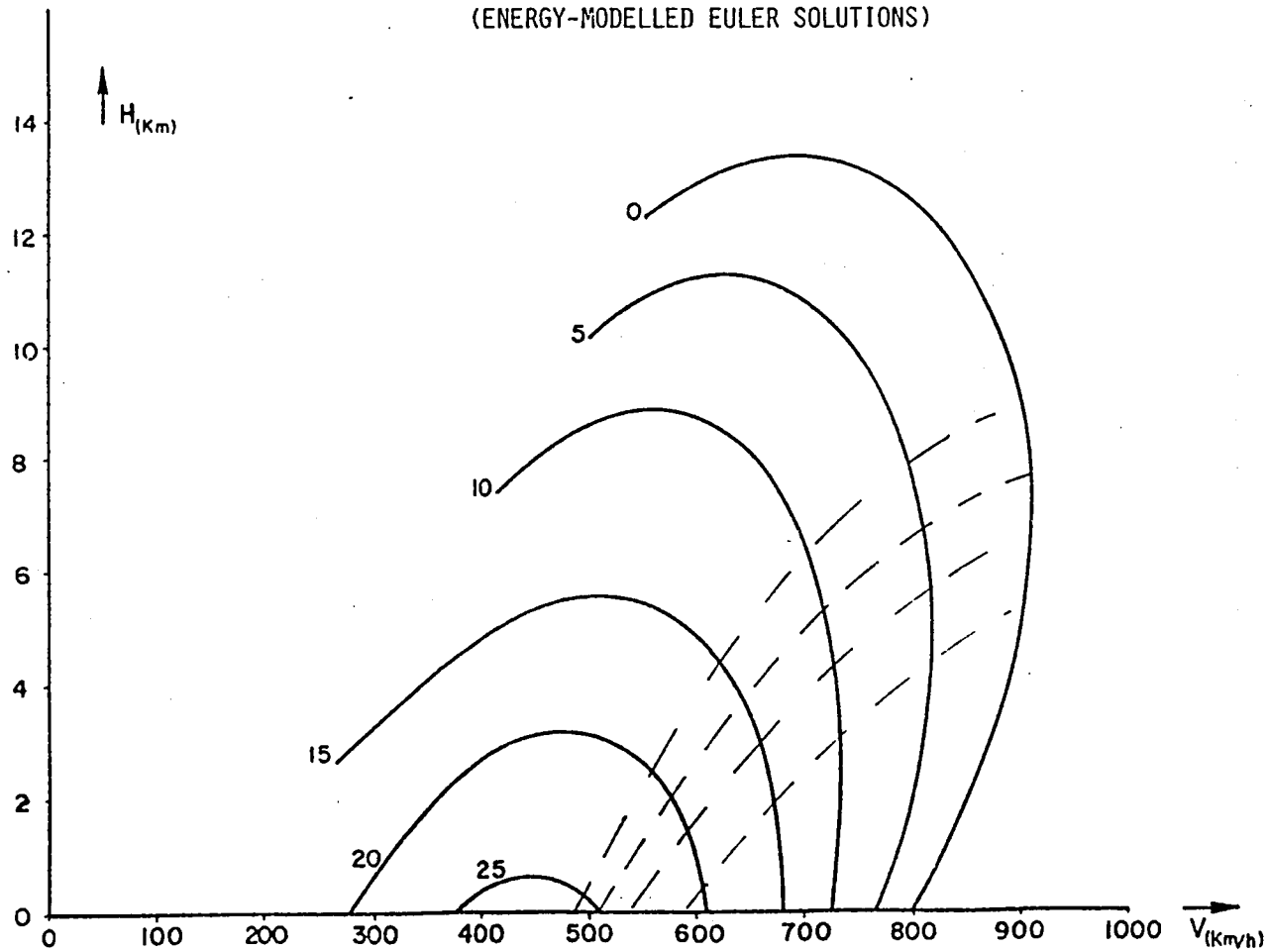


Fig. A.4 ME. 262 CLIMB - DASH FAMILY
(ENERGY-MODELLED EULER SOLUTIONS)



APPENDIX B

SINGULAR OPTIMAL CONTROL AND THE
IDENTICALLY NON-REGULAR PROBLEM
IN THE CALCULUS OF VARIATIONS

P. K. A. Menon

H. J. Kelley

E. M. Cliff

SECTION B.1

PREFACE

In optimal-control problems featuring scalar control appearing linearly in the system differential equations, singular subarcs can sometimes arise. Along singular subarcs which are minimizing, the Generalized Legendre-Clebsch necessary condition should hold (Refs. 69 and 70). A class of such optimal-control problems can be recast as identically non-regular problems in the classical Calculus of Variations if the dimension is low. Specifically, this transformation appears feasible if there are at most two-non-ignorable state variables and one control variable. In general, the procedure involves a change in the independent variable under appropriate smoothness and monotonicity assumptions. (The phrase "Classical Calculus of Variations" employed here refers to unconstrained problems, i.e., not to Lagrange-Mayer-Bolza problems.)

For this class of problems, Mancill (Ref. 58) has obtained conditions for a minimizing singular arc. In this research, Mancill made use of Green's theorem on line integrals to establish conditions for a strong relative minimum. Miele (Refs. 57, 71) used the Green's theorem approach for problems with control bounds, extended the technique to handle isoperimetric constraints and carried out applications to several flight problems. Goh (Ref. 72) examined the singular Bolza problem and noted the connection between Miele's work and the identically non-regular

problem in the Calculus of Variations.

This appendix deals with an evaluation of Mancill's 1950 work and its relation to the Generalized Legendre-Clebsch necessary condition. A critique on the nature of transversality conditions for this class of problems is presented. Three illustrative examples are also given.

SECTION B.2

IDENTICALLY NON-REGULAR PROBLEM

The identically non-regular problem with fixed endpoints in the Calculus of Variations (Refs. 58 and 73) is the minimization of an integral of the form

$$J = \int_{t_1}^{t_2} [P(t,x) + Q(t,x)\dot{x}]dt \quad (B-1)$$

with

$$x(t_1) = x_1 \text{ and } x(t_2) = x_2 \quad (B-2)$$

Note that

$$[P(t,x) + Q(t,x)\dot{x}]_{xx} = 0 \quad (B-3)$$

It is known that the Euler's equation for this problem is either an identity or a finite equation (Refs. 73, 74 and 75). If it is an identity, the integral is independent of the path joining two fixed points and no proper minimum exists. On the other hand, if it is a finite equation, the Euler's equation is satisfied only along certain paths which in general do not pass through the specified end points.

These functionals are sometimes called "degenerate" because the Euler equation for such functionals is not a differential equation, but a finite equation without any derivatives of the unknown function (Ref. 76).

Two theorems by Mancill (Ref. 58) give necessary and sufficient conditions for a strong local minimum in these problems. These are presented in the following.

Theorem 1. If E_{12} is of class D' and minimizes the integral J in the class of admissible curves joining 1 and 2, where $P(t,x)$ and $Q(t,x)$ are of class C^{2n} in a closed region R of (x,t) space, then

$$\begin{aligned} \frac{\partial^{2n-1} P}{\partial x^{2n-1}} &= \frac{\partial^{2n-1} Q}{\partial t \partial x^{2n-2}}, \\ \frac{\partial^{2n} P}{\partial x^{2n}} &\geq \frac{\partial^{2n} Q}{\partial t \partial x^{2n-1}}, \end{aligned} \tag{I}$$

if $\frac{\partial^k P}{\partial x^k} = \frac{\partial^k Q}{\partial t \partial x^{k-1}}$, $k = 1, 2, 3, \dots, 2n-2$, along arcs interior to R , including all isolated points in common with the boundary of R :

$$\frac{\partial^r P}{\partial x^r} \geq \frac{\partial^r Q}{\partial t \partial x^{r-1}} \tag{I_B}$$

if $\frac{\partial^k P}{\partial x^k} = \frac{\partial^k Q}{\partial t \partial x^{k-1}}$, $k = 1, 2, 3, \dots, r-1$, along arcs in common with the boundary of R .

Let (I') and (I'_B) represent conditions (I) and (I_B) respectively with the inequalities \geq replaced by the strict inequality $>$. This is a familiar notation in the classical Calculus of Variations and it will be employed in this work.

The first part of (I) with $n = 1$, is the Euler's necessary condition for this problem. The inequality in (I) with $n = 1$, is derived from the

second variation. For $n > 1$ the conditions (I) are obtained from higher variations.

Theorem 2. If $P(t,x)$ and $Q(t,x)$ are of class C^{2n} in R and the conditions (I') and (I'_B) are satisfied along an admissible curve E_{12} joining 1 and 2, then E_{12} furnishes a strong proper relative minimum for the integral J in the class of admissible curves joining 1 and 2.

It is implied in Theorem 2 that the Euler equation is not an identity. This Theorem is proved using Green's theorem on line integrals. Mancill has given two additional theorems on the necessary and sufficient conditions for the identically non-regular problem with variable end points. However, the interpretation of these in the light of modern optimal-control theory indicates their inapplicability owing to the violation of the smoothness assumption essential to the results in Mancill's work. A detailed discussion of this is presented in Section B.6.

At this point, it is perhaps interesting to compare the results obtained by Mancill with those of Miele (Refs. 57, 71). The first part of condition (I) in Theorem 1 with $n = 1$ is termed the "fundamental function" $\omega(t,x)$ in Miele's work. The inequality in (I) appears as a specification on the direction of traverse along the extremal. Similarly, the condition (I'_B) of Mancill also appears in Miele's work as a specification on the direction of traverse along the boundary of the admissible region, applicable whenever the arcs interior to the admissible region are non-optimal.

SECTION B.3

THE PROBLEM IN AN OPTIMAL-CONTROL FORMAT

With a short development it will be shown that with $n = 1$, the inequality in (I) is the Generalized Legendre-Clebsch necessary condition for $q = 1$.

Consider the optimal control problem

$$\text{Min} \int_{t_0}^{t_f} [P(t,x) + Q(t,x)u]dt \quad (\text{B-4})$$

subject to the differential constraint $\dot{x} = u$. It is apparent that this problem is equivalent to the identically non-regular problem in the Calculus of Variations. Note that the control u is unbounded.

To proceed via the "modern" approach one defines the variational Hamiltonian

$$H(\lambda,x,t,u) = P(t,x) + Q(t,x)u + \lambda u \quad (\text{B-5})$$

and forms the adjoint equation

$$\dot{\lambda} = -P_x - Q_x u \quad (\text{B-6})$$

From the expression (B-5) for H , one has that along a singular subarc

$$H_u = Q(t,x(t)) + \lambda(t) = 0 \quad (\text{B-7})$$

Differentiating this with respect to time, substituting $\dot{x} = u$ and using (B-6) for λ , one finds

$$\frac{d}{dt} [H_u] = Q_t(t,x) - P_x(t,x) \quad (B-8)$$

Differentiating with respect to time again, while using $\dot{x} = u$, leads to

$$\frac{d^2}{dt^2} [H_u] = Q_{tt} - P_{xt} + (Q_{tx} - P_{xx})u \quad (B-9)$$

Hence the Generalized Legendre-Clebsch necessary condition for first-order singular arc is

$$\frac{\partial}{\partial u} \left\{ \frac{d^2}{dt^2} [H_u] \right\} = Q_{tx} - P_{xx} \leq 0 \quad (B-10)$$

that is

$$P_{xx} \geq Q_{tx} \quad (B-11)$$

The inequality (B-11) is the same as that in condition (I) of Ref. 58.

One notes that the inequality (I) of Mancill for $n > 1$ is not equivalent to the Generalized Legendre-Clebsch necessary condition but is something more general. (See Example 1b to follow.)

SECTION B.4

TRANSFORMATION TO CANONICAL FORM

To investigate the situations in which specified boundary conditions are off the path defined by the conditions (I), and the variable-endpoint problem, a transformation approach discussed in Ref. 77 is next employed. The identically non-regular problem is first brought into the Mayer format:

$$\dot{y} = P(t,x) + Q(t,x)u \quad (B-12)$$

$$\dot{x} = u \quad (B-13)$$

with $t_1, t_2, x(t_1) = x_1, x(t_2) = x_2$ specified. A minimum of $y(t_2)$ is sought with $y(t_1) = 0$.

Next, a transformation of state variables will be performed so that the state system has a special form. The new state variables are z and x and the system is to have the control variable u appearing in only one of the state equations, the one for x .

The system is

$$\dot{z} = P(t,x) + \frac{\partial R(t,x)}{\partial t} \quad (\text{B-14})$$

$$\dot{x} = u \quad (\text{B-15})$$

and the choice of z leading to it is

$$z = y + R(t,x) \quad (\text{B-16})$$

where

$$R(t,x) = - \int^x Q(t,\xi) dJ \quad (\text{B-17})$$

(Refs. 69, 77). The end conditions are $t_1, t_2, x(t_1) = x_1, x(t_2) = x_2$ specified as before. The initial value of z is $z(t_1) = R(t_1, x_1)$ and a minimum of $z(t_2)$ is sought.

Since there are no bounds on the control u , it can behave impulsively and $x(t)$ can jump. If the equation (B-15) is discarded and a solution sought in the class of functions $x(t)$ piecewise-continuous, x becomes control-like (Refs. 69, 77). At points $t_1 < t < t_2$, x minimizes the right member of equation (B-14).

$$x = \text{Arg min}_x [P(t,x) + \frac{\partial R}{\partial t}(t,x)] \quad (\text{B-18})$$

possibly exhibiting jump discontinuities in the interior of the interval

depending on the nature of the time dependence of equation (B-14). The variable x will generally jump at the initial and final times to satisfy the end conditions unless the value emerging from expression (B-18) happens fortuitously to satisfy them.

The situation with endpoint freedom is interesting. Consider for example, t_1 and t_2 fixed as before, but $x(t_2)$ unspecified. To minimize $y(t_2)$, x should jump at the final time t_2 to the value

$$x(t_2) = \text{Arg max}_x R(t_2, x) \quad (\text{B-19})$$

This seems to be the nearest thing to a transversality condition that one can have with x control-like.

SECTION B.5

ILLUSTRATIVE EXAMPLES

To convey an impression of Mancill's work, three examples are given in the following.

(1) Two elementary examples

(a)

$$\text{Min} \int_{t_0}^{t_f} x^2 dt, \text{ subject to } \dot{x} = u$$

$x(t_0) = x_0$ and $x(t_f) = x_f$ specified.

Since there are no bounds on the control, the differential constraint is inactive. Hence, the problem in classical Calculus of Variations format is

$$\text{Min } \int_{t_0}^{t_f} x^2 dt \quad (\text{B-20})$$

With the identification of

$$P(t,x) \equiv x^2 \quad (\text{B-21})$$

$$Q(t,x) \equiv 0 \quad (\text{B-22})$$

The necessary conditions of Ref. 58 become,

$$2x = 0 \quad (\text{B-23})$$

and

$$2 \geq 0 \quad (\text{B-24})$$

The sufficient condition

$$2 > 0 \quad (\text{B-25})$$

is met in the strengthened form along the arc $x = 0$ and hence, the trajectory $x = 0$ affords a strong relative minimum. The result (B-25) was obtained in Ref. 69 via the Generalized Legendre-Clebsch necessary condition. If the initial and final conditions are off the $x = 0$ path, jumps in x are required at the end points. Such motions have no effect on the performance index.

The next example is chosen to illustrate the necessary conditions of Mancill for $n > 1$.

$$(b) \quad \text{Min } \int_{t_0}^{t_f} x^4 dt, \text{ subject to } \dot{x} = u$$

The conditions $x(t_0) = x_0$ and $x(t_f) = x_f$ specified. Since there are no bounds on the control variable, the problem in the Calculus of Variations format is

$$\text{Min} \int_{t_0}^{t_f} x^4 dt \quad (\text{B-26})$$

The necessary conditions for a minimum are

$$4x^3 = 0 \quad (\text{B-27})$$

Hence $x = 0$ is the extremal. Further,

$$12x^2 = 0 \quad (\text{B-28})$$

$$24x = 0 \quad (\text{B-29})$$

$$24 \geq 0 \quad (\text{B-30})$$

Note that the sufficient condition (I') in Theorem I, (B-30) with strengthened inequality, is met for $n = 4$. Just as in the previous example, jumps in x must be permitted at the endpoints if the specified conditions are off the $x = 0$ path.

(2) Minimum-time aircraft climb

Following Miele (Ref. 57), a model of aircraft in symmetric flight under the assumptions of constant weight and thrust, T , and drag D , functions of altitude, h , and airspeed, V , only, is:

$$\dot{V} = g \left[\left\{ \frac{T-D}{W} \right\} - \sin \gamma \right] \quad (\text{B-31})$$

$$\dot{h} = V \sin \gamma \quad (\text{B-32})$$

Differential equations for range rate and fuel-flow rate have been dropped from the system, since they are ignorable in this problem. The optimal-control problem is the minimization of time required to fly from an initial (V,h) pair to a final (V,h) pair, viz.

$$\text{Min} \int_{(V_i, h_i)}^{(V_f, h_f)} dt \quad (\text{B-33})$$

Changing the independent variable from time to altitude,

$$v' = \frac{dV}{dh} = \frac{g(T-D)}{W V \sin \gamma} - \frac{g}{V} \quad (\text{B-34})$$

$$\text{Min} \int_{(V_i, h_i)}^{(V_f, h_f)} \frac{dh}{V \sin \gamma} \quad (\text{B-35})$$

Substituting next for $\sin \gamma$ in (B-35) from (B-34), the problem in the classical Calculus-of-Variations format is

$$\text{Min} \int_{(V_i, h_i)}^{(V_f, h_f)} \left[\frac{W}{V(T-D)} + \frac{W V'}{g(T-D)} \right] dh \quad (\text{B-36})$$

In this development, the monotonicity of the altitude variable has been tacitly assumed. If desired, $\sin \gamma$ may be constrained by defining an admissible region in the V-h space as suggested in Ref. 71, however, this falls outside the Mancill model. Employing conditions (I) in Theorem 1, the necessary conditions for a minimum for arcs interior to the admissible region, are

$$\frac{\partial}{\partial V} \left\{ \frac{W}{g(T-D)} \right\} = \frac{\partial}{\partial h} \left\{ \frac{W}{V(T-D)} \right\} \quad (\text{B-37})$$

$$\frac{\partial^2}{\partial V^2} \left\{ \frac{W}{g(T-D)} \right\} \geq \frac{\partial^2}{\partial h \partial V} \left\{ \frac{W}{V(T-D)} \right\} \quad (\text{B-38})$$

The expressions (B-37) and (B-38) may be put in the following form

$$\left. \begin{array}{l} \frac{\partial^2 [V(T-D)]}{\partial h} \\ E = \text{Constant} \end{array} \right| = 0 \quad (\text{B-39})$$

$$\left. \begin{array}{l} \frac{\partial^2 [V(T-D)]}{\partial h^2} \\ E = \text{Constant} \end{array} \right| \leq 0 \quad (\text{B-40})$$

The necessary condition for a strong relative minimum, then, is

$$\left. \begin{array}{l} \frac{\partial^2 [V(T-D)]}{\partial h^2} \\ E = \text{Constant} \end{array} \right| \leq 0 \quad (\text{B-41})$$

This result was obtained in Ref. 69 using the Generalized Legendre-Clebsch necessary condition. The expression (B-39) corresponds to stationary points of excess power $V(T-D)$ along contours of constant energy $E \equiv h + V^2/2g$. Inequality (B-41) implies that the stationary points of excess power along constant-energy contours must be maxima, a result in accord with engineering intuition.

If the endpoints are off the path defined by (B-39), jumps in air-speed and altitude must be permitted to meet the boundary condition. With bounds on control, on the other hand, operation at one of the control limits is indicated.

SECTION B.6

SMOOTHNESS DIFFICULTIES AND THEIR IMPACT

In Ref. 58, and in classical Calculus-of-Variations treatments generally (e.g. Refs. 73-75), the function $x(t)$, which appears along with its derivative, $\dot{x}(t)$, as an argument of the integrand, is assumed to possess a first derivative which is at least piecewise continuous. The various theorems of Ref. 58 do not apply to discontinuous solutions of the type examined in the preceding sections. In the classical setting one would say that no minimum exists in the class of admissible functions, but only a lower bound. Indeed the classical treatment (Refs. 73-75) focuses entirely on the degenerate case in which the integral is independent of the path.

One is faced with the choice between extending the theory to admissible $x(t)$ piecewise continuous, or the introduction of bounds on the control $u(t)$. Unfortunately Mancill did neither and produced an array of results of seemingly enormous power (e.g., sufficiency by strengthening inequalities), which are in fact of extremely limited applicability because of their smoothness hypotheses. An unwelcome complication of the Mancill theory is the incorporation of state-inequality constraints, a relic of his earlier work on this special type of problem (Ref. 78), which does not alleviate the smoothness difficulties.

Treatment of variational problems with $x(t)$ piecewise continuous only has been given by V. F. Krotov (Ref. 79). (See also Petrov, Ref. 76.) Bounded-control problems approached by Green's Theorem have been studied

by Miele (Refs. 57, 71).

SECTION B.7

CONCLUDING REMARKS

Mancill's two Theorems given in the present work are of interest and seem to have been ahead of their time. For the narrow class of problems considered by Mancill, the inequality (I) with $n = 1$ is equivalent to the generalized Legendre-Clebsch condition. Perhaps equally important was Mancill's introduction of the Green's Theorem device for the study of problems of small dimension.

REFERENCES

1. Pastrick, H. L., Seltzer, S. M., Warren, M. E., "Guidance Laws for Short-Range Tactical Missiles," Journal of Guidance and Control, 1981, Vol. 4, No. 2, pp. 98-108.
2. Häussermann, W., "Developments in the Field of Automatic Guidance and Control of Rockets," Journal of Guidance and Control, 1981, Vol. 4, No. 2, pp. 225-239.
3. Anderson, G. M., "Comparison of Optimal Control and Differential Game Intercept Missile Guidance Laws," Journal of Guidance and Control, 1981, Vol. 4, No. 2, pp. 109-115.
4. Sridhar, B., Gupta, N. K., "Missile Guidance Laws based on Singular Perturbation Methodology," Journal of Guidance and Control, 1980, Vol. 3, No. 2, pp. 158-165.
5. Stengel, R. F., Miller, G. E., "Flight Tests of a Microprocessor Control System," Journal of Guidance and Control, 1980, Vol. 3, No. 6, pp. 494-500.
6. Burrows, J. W., "Fuel Optimal Trajectory Computation," Journal of Aircraft, 1982, Vol. 19, No. 4, pp. 324-329.
7. Sorenson, J. A., Waters, M. H., "Generation of Optimal Vertical Profiles for an Advanced Flight Management System," NASA CR 165674, March 1981.
8. Erzberger, H., Lee, H., "Constrained Optimum Trajectories with Specified Range," Journal of Guidance and Control, 1980, Vol. 3, No. 1, pp. 78-85.
9. Chakravarty, A., Vagners, J., "Application of Singular Perturbation Theory to On-Board Aircraft Optimization," AIAA Paper 81-0019.
10. Gracey, C., Price, D., "Altitude/Path-Angle Transitions in Fuel Optimal Problems for Transport Aircraft," Paper presented at the ACC Conference, June 1983, San Francisco, CA.
11. Erzberger, H., McLean, J. D., "Fuel Conservative Guidance System for Powered Aircraft," Journal of Guidance and Control, 1981, Vol. 4, No. 3, pp. 253-261.
12. Beser, J., "Approach Guidance Logic for Tilt Rotor Aircraft," Journal of Guidance and Control, 1979, Vol. 2, No. 6, pp. 528-535.
13. Merrick, V. K., Gerdes, R. M., "Design and Piloted Simulation of a VTOL Flight Control System," Journal of Guidance and Control, 1978, Vol. 1, No. 3, pp. 209-215.
14. Urnes, J. M., Hess, R. K., Moomaw, R. F., Huff, R. W., "Hdot Automatic Carrier Landing System for Approach Control in Turbulence," Journal of Guidance and Control, 1981, Vol. 4, No. 2, pp. 177-183.

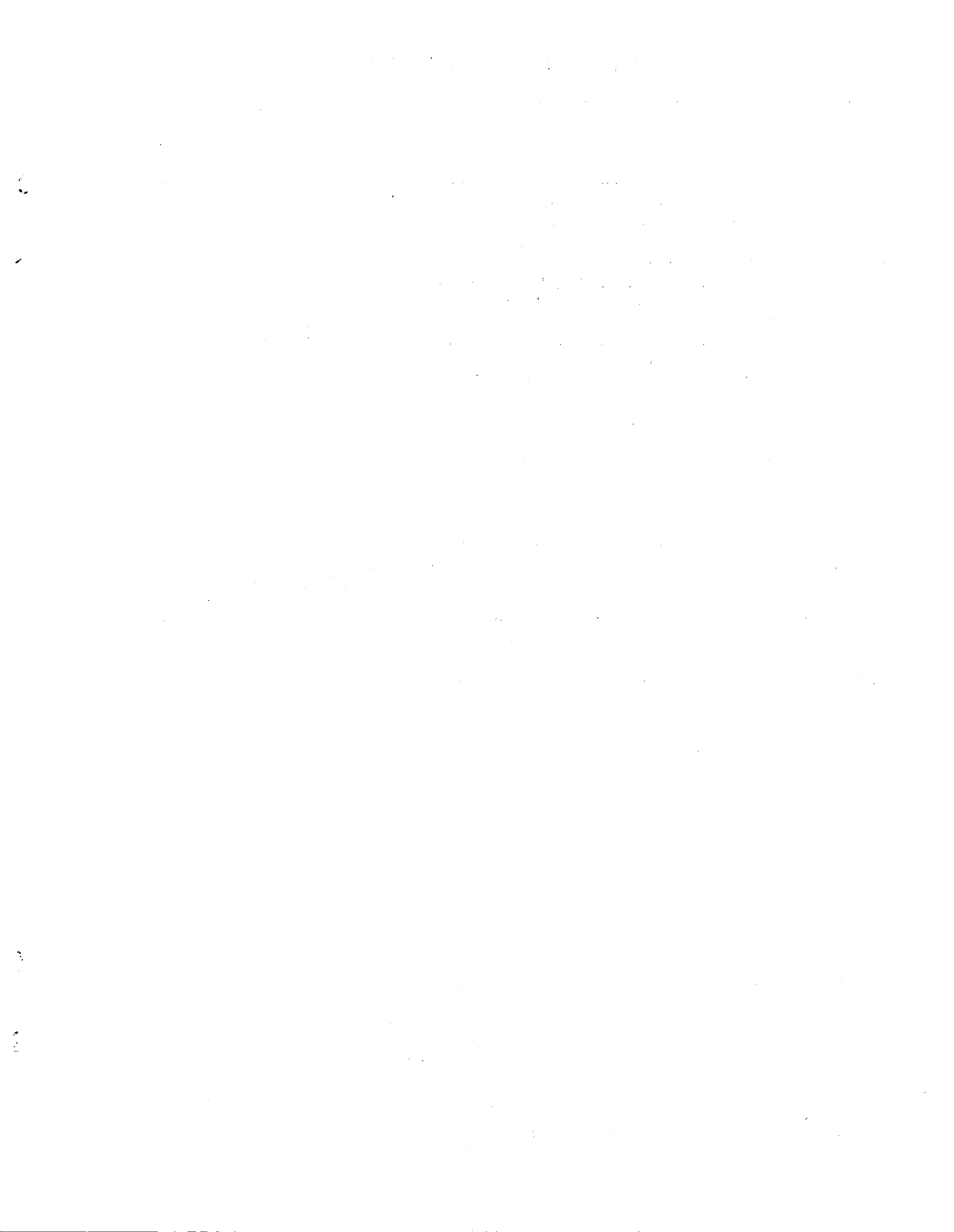
15. McGee, A. L., Paulk, C. H., Steck, S. M., Merz, A. W., "Evaluation of the Navigation Performance of Shipboard VTOL Guidance Systems," Journal of Guidance and Control, 1981, Vol. 4, No. 4, pp. 433-446.
16. Osder, S., "DC-9-80 Digital Flight Guidance System Monitoring Techniques," Journal of Guidance and Control, 1981, Vol. 4, No. 1, pp. 41-49.
17. Uehara, S., Stewart, M. J., Wood, L. J., "Minimum Time Loop Maneuvers of Jet Aircraft," Journal of Aircraft, 1978, Vol. 15, pp. 449-455.
18. Shinar, J., Merari, A., Blank, D., Medinah, E. M., "Analysis of the Optimal Turning Maneuvers in the Vertical Plane," Journal of Guidance and Control, 1980, Vol. 3, No. 1, pp. 69-77.
19. Well, K. H., Faber, B., Berger, E., "Optimization of Tactical Aircraft Maneuvers Utilizing High Angles of Attack," Journal of Guidance and Control, 1982, Vol. 5, No. 2, pp. 124-130.
20. Kelley, H. J., Well, K. H., "An Approach to Intercept Calculations," Preprint Volume, 1980 American Control Conference, San Francisco, June 22-24, 1983.
21. Wasow, W., Asymptotic Expansions for Ordinary Differential Equations, Wiley/Interscience, New York.
22. Kaiser, F., "Der Steigflug mit Strahlflugzeugen-Teil I, Bahngeschwindigkeit für besten Steigens." Versuchsbericht 262-02-L44, Messerschmitt A. G., Augsburg, 1944. Translated as British Ministry of Supply RPT/TIB, Translation GDC/15/148T.
23. Lush, K. J., "A Review of the Problem of Choosing a Climb Technique with Proposals for a New Climb Technique for High Performance Aircraft," Aero. Res. Council Rept. Memo. 2557, 1951.
24. Rutowski, E. S., "Energy Approach to the General Aircraft Performance Problem," J. Aero. Sci., 1954, (21), 187-189.
25. Kelley, H. J., "Aircraft Maneuver Optimization by Reduced Order Approximation." In C.T. Leondes (Ed.), Control and Dynamic Systems, Vol. 10, 1973, Academic Press, New York.
26. Breakwell, J. V., "Optimal Flight-Path-Angle Transitions in Minimum-Time Airplane Climbs," Journal of Aircraft, 1977, Vol. 14, pp. 782-786.
27. Bryson, A. E., Desai, A., Hoffman, K., "Energy State Approximation in Performance Optimization of Supersonic Aircraft," Journal of Aircraft, 1969, Vol. 6, pp. 481-488.
28. Kelley, H. J., "Guidance Theory and Extremal Fields," IRE Transactions on Automatic Control, 1962, Vol. 7, No. 5, pp. 75-82.
29. Kelley, H. J., "An Optimal Guidance Approximation Theory," IEEE Transactions on Automatic Control, 1964, Vol. 9, No. 4, pp. 375-380.

30. Breakwell, J. V., Speyer, J. L., Bryson, A. E., "Optimization and Control of Nonlinear Systems using the Second Variation," Journal of SIAM Control, 1963, Vol. 1, No. 2, pp. 193-223.
31. Powers, W. F., "A Method for Comparing Trajectories in Optimum Linear Perturbation Guidance Schemes," AIAA Journal, 1968, Vol. 6, No. 12, pp. 2451-2452.
32. Powers, W. F., "Techniques for Improved Convergence in Neighboring Optimum Guidance," AIAA Journal, 1970, Vol. 8, No. 12, pp. 2235-2341.
33. Pesch, H. J., "Numerische Berechnung Optimaler Flugbahn Koerrekturen in Echtzeit-Rechnung," Dissertation, Technische Universität München, 1978.
34. Pesch, H. J., "Neighboring Optimum Guidance of Space Shuttle Orbiter Type Vehicle," Journal of Guidance and Control, 1980, Vol. 3, No. 5, pp. 386-392.
35. Speyer, J. L., Bryson, A. E., "A Neighboring Optimum Feedback Law Based on Estimated Time-to-go with Application to Re-entry Flight Paths," AIAA Journal, 1968, Vol. 6, No. 5, pp. 769-776.
36. Wood, L. J., "Perturbation Guidance for Minimum Time Flight Paths of Spacecraft," AIAA Paper 72-915.
37. Hart, J. D., "A Comparison of Low-Thrust Guidance Techniques," Ph.D. Dissertation, University of Texas at Austin, 1971.
38. Pontryagin, L. S., Boltyanskii, V. G., Gamkrelidze, R. V., Mischchenko, E. F., The Mathematical Theory of Optimal Processes, John Wiley, New York, 1962.
39. Leitmann, G., An Introduction to Optimal Control, McGraw-Hill, New York, 1966.
40. Tihonov, A. N., "Systems of Differential Equations Containing Small Parameters in the Derivatives," Matematicheskii Sbornik 31, (1952).
41. Weston, A. R., Cliff, E. M., Kelley, H. J., "Altitude Transitions in Energy Climbs," Automatica, Vol. 19, No. 2, 1983.
42. Ardema, M. D., "Solution of the Minimum-Time-to-Climb by Matched Asymptotic Expansions," AIAA Journal, 1976.
43. Kelley, H. J., Cliff, E. M., Weston, A. R., "Energy State Revisited," AIAA Atmospheric Flight Mechanics Conference, Gatlinburg, Tennessee, August 17-19, 1983.
44. Mummolo, F. and Lefton, L., "Cubic Splines and Cubic Spline Lattices for Digital Computation," Analytical Mechanical Associates, Inc. Report No. 72-28, July 1972, revision dated December 1974.
45. Keller, H. B., Numerical Methods for Two-Point Boundary-Value Problems, Blaisdell, London, 1968.

46. Keller, H. B., "Numerical Solution of Two-Point Boundary Value Problems," SIAM, 1976.
47. Bulirsch, R., "Die Mehrzielmethode zur numerischen Lösung von Nicht-linearen Randwertproblemen und Aufgaben der optimalen Steuerung," Vortrag im Lehrgang Flugbahnoptimierung der Carl-Cranz Gesellschaft, V. October 1971.
48. Bryson, A. E. and Ho, Y.-C., Applied Optimal Control, Jun/Blaisdell, Waltham, Mass., 1975.
49. Cline, A. K., "Scalar- and Planar- Valued Curve Fitting Using Splines under Tension," Communications of the ACM, April 1974.
50. Kelley, H. J., "An Investigation by Variational Methods of Flight Paths for Optimum Performance," Sc. D. Dissertation, New York University, May 1958.
51. Kamke, E., Differentialgleichungen Lösungsmethoden und Lösungen, Band 1, Gewöhnliche Differentialgleichungen, Third edition, Chelsea Publishing Company, New York, 1948.
52. Boyce, W. E. and Diprima, R. C., Elementary Differential Equations and Boundary-Value Problems, Third edition, John Wiley and Sons, New York, 1977.
53. Miele, A., "General Solutions of Optimum Problems in Nonstationary Flight," NACA TM-1388, October 1955.
54. Weston, A. R., Cliff, E. M. and Kelley, H. J., "On-Board Near-Optimal Climb-Dash Energy Management," American Control Conference, San Francisco, CA, June 22-24, 1983.
55. Kelley, H. J. and Moyer, G. H., "Computational Jacobi-Test Procedure," Proceedings of the JUREMA Workshop on Current Trends in Control, Dubrovnik, Yugoslavia, June 29-30, 1984.
56. Cicala, P., An Engineering Approach to the Calculus of Variations, Levrotto-Bella, Torino, Italy, 1957.
57. Miele, A., "Problemi di Minimo Tempo nel Volo Non-stazionario degli Aeroplani," Atti della Accademia delle Scienze di Torino, Vol. 85, 1950-51, pp. 41-42.
58. Mancill, J. D., "Identically Non-Regular Problems in the Calculus of Variations," Mathematica Y Fisica Teorica, (Universidad Nacional Del Tucumán, República Argentina), Vol. 7, No. 2, June 1950.
59. Merritt, S. R., Cliff, E. M. and Kelley, H. J., "Energy-Modelled Climb and Climb-Dash - The Kaiser Technique," Ninth IFAC World Congress, Budapest, Hungary, July 2-6, 1984.

60. Boyd, J. R., Christie, T. P. and Gibson, J. E., "Energy Maneuverability," Armament Laboratory Report, APGC-TR-66-4, Vols. I and II, Eglin AFB, 1966.
61. Kelley, H. J., "State-Variable Selection and Singular Perturbations," in Singular Perturbations: Order Reduction in Control System Design, P. V. Kokotovic and W. R. Perkins, Editors, ASME, June 1972.
62. Luenberger, D. G., Optimization by Vector Space Methods, J. Wiley, 1969, pp. 131-133.
63. Marchal, C., "Chattering Arcs and Chattering Controls," Journal of Optimization Theory and Applications, Vol. 11, 1973, pp. 441-468.
64. Gilbert, E. G. and Parsons, M. G., "Periodic Control and the Optimality of Aircraft Cruise," Journal of Aircraft, Vol. 13, October 1976, pp. 828-830.
65. Houlihan, S. C., Cliff, E. M. and Kelley, H. J., "A Study of Chattering Cruise," Journal of Aircraft, Vol. 19, February 1982, pp. 119-124.
66. Lippisch, A., "Flugmechanische Beziehungen der Flugzeuge mit Strahltrieb." Forschungsbericht Nr. 1791, Deutsche Luftfahrtforschung, May 29, 1943. Translated as F-TS-685 RE, Air Material Command, Wright Field, Ohio, 1946.
67. Behrbohm, H., "Brachystochrone Flugbahnen im Raum bei zietlich veränderlichen Fluggewicht." Jahrbuch 1954 der Wissenschaftlichen Gesellschaft für Luftfahrt, Vieweg, Braunschweig.
68. Kaiser, F., "Einfluss der Zusammendrückbarkeit der Luft auf die Messung von Geschwindigkeit und Polare." Technische Berichte Bd. 10, Nr. 6.
69. Kelley, H. J., Kopp, R. E. and Moyer, G. H., "Singular Extremals," in Topics in Optimization, Ed. G. Leitmann, Chapter 3, Academic Press, New York, 1967.
70. Bell, D. J. and Jacobson, D. H., Singular Optimal Control Problems, Academic Press, New York, 1975.
71. Miele, A., "Extremization of Linear Integrals by Green's Theorem," in Optimization Techniques, Ed. G. Leitmann, Chapter 3, Academic Press, New York, 1962.
72. Goh, B. S., "The Second Variation for the Singular Problem," SIAM Journal of Control, Vol. 4, 1966, pp. 309-325.
73. Bolza, O., Lectures on the Calculus of Variations, G. E. Stechert and Co., New York, 1904.
74. Leitmann, G., The Calculus of Variations and Optimal Control, Plenum Press, New York, 1981.
75. Courant, R., "Calculus of Variations and Supplementary Notes and Exercises," Institute for Mathematics and Mechanics, New York University, 1945-46.

76. Petrov, I. P., Variational Methods in Optimum Control Theory, Academic Press, New York, 1968.
77. Kelley, H. J., "A Transformation Approach to Singular Subarcs in Optimal Trajectory and Control Problems," SIAM Journal of Control, Vol. 2, 1964, pp. 234-240.
78. Mancill, J. D., "Unilateral Variations with Variable Endpoints," American Journal of Mathematics, Vol. LXIX, 1947, pp. 121-138.
79. Krotov, V. F., "The Principal Problem of the Calculus of Variations for the Simplest Functional on a Set of Discontinuous Functions," Soviet Mathematics Doklady, Vol. 2, 1961, pp. 231-234.



1. Report No. NASA CR-172508		2. Government Accession No.		3. Recipient's Catalog No.	
4. Title and Subtitle Optimal Symmetric Flight Studies				5. Report Date February 1985	
				6. Performing Organization Code	
7. Author(s) A.R. Weston, P.K.A. Menon, K.D. Bilimoria, E.M. Cliff and H.J. Kelley				8. Performing Organization Report No.	
				10. Work Unit No.	
9. Performing Organization Name and Address Virginia Polytechnic Institute and State University Aerospace and Ocean Engineering Department Blacksburg, VA 24060				11. Contract or Grant No. NAG-1-203	
				13. Type of Report and Period Covered CONTRACTOR REPORT	
12. Sponsoring Agency Name and Address National Aeronautics and Space Administration Washington, DC 20546				14. Sponsoring Agency Code 505-34-03-02	
15. Supplementary Notes Langley Technical Monitor: Christopher Gracey Interim Report					
16. Abstract Several topics in optimal symmetric flight of airbreathing vehicles are examined. In one study, an approximation scheme designed for onboard real-time energy management of climb-dash is developed and calculations for a high-performance aircraft presented. In another, a vehicle model intermediate in complexity between energy and point-mass models is explored and some quirks in optimal-flight characteristics peculiar to the model uncovered. In yet another study, energy-modelling procedures are re-examined with a view to stretching the range of validity of zeroth-order approximation by special choice of state variables. In a final study, time-fuel tradeoffs in cruise-dash are examined for the consequences of nonconvexities appearing in the classical steady cruise-dash model. Two appendices provide retrospective looks at two early publications on energy modelling and related optimal-control theory.					
17. Key Words (Suggested by Author(s)) Optimal Control Flight Mechanics Reduced-Order Modelling Symmetric Flight			18. Distribution Statement Unclassified - Unlimited Subject Category 08		
19. Security Classif. (of this report) Unclassified		20. Security Classif. (of this page) Unclassified		21. No. of Pages 227	22. Price A11

